

Springer Theses

Recognizing Outstanding Ph.D. Research

David J. Liptrot

Group 2 Mediated Dehydrocoupling

 Springer

Springer Theses

Recognizing Outstanding Ph.D. Research

Aims and Scope

The series “Springer Theses” brings together a selection of the very best Ph.D. theses from around the world and across the physical sciences. Nominated and endorsed by two recognized specialists, each published volume has been selected for its scientific excellence and the high impact of its contents for the pertinent field of research. For greater accessibility to non-specialists, the published versions include an extended introduction, as well as a foreword by the student’s supervisor explaining the special relevance of the work for the field. As a whole, the series will provide a valuable resource both for newcomers to the research fields described, and for other scientists seeking detailed background information on special questions. Finally, it provides an accredited documentation of the valuable contributions made by today’s younger generation of scientists.

Theses are accepted into the series by invited nomination only and must fulfill all of the following criteria

- They must be written in good English.
- The topic should fall within the confines of Chemistry, Physics, Earth Sciences, Engineering and related interdisciplinary fields such as Materials, Nanoscience, Chemical Engineering, Complex Systems and Biophysics.
- The work reported in the thesis must represent a significant scientific advance.
- If the thesis includes previously published material, permission to reproduce this must be gained from the respective copyright holder.
- They must have been examined and passed during the 12 months prior to nomination.
- Each thesis should include a foreword by the supervisor outlining the significance of its content.
- The theses should have a clearly defined structure including an introduction accessible to scientists not expert in that particular field.

More information about this series at <http://www.springer.com/series/8790>

David J. Liptrot

Group 2 Mediated Dehydrocoupling

Doctoral Thesis accepted by
the University of Bath, UK

Author

Dr. David J. Liptrot
Department of Chemistry
University of Bath
Bath
UK

Supervisor

Prof. Michael S. Hill
Department of Chemistry
University of Bath
Bath
UK

ISSN 2190-5053

Springer Theses

ISBN 978-3-319-21035-3

DOI 10.1007/978-3-319-21036-0

ISSN 2190-5061 (electronic)

ISBN 978-3-319-21036-0 (eBook)

Library of Congress Control Number: 2015944441

Springer Cham Heidelberg New York Dordrecht London

© Springer International Publishing Switzerland 2016

This work is subject to copyright. All rights are reserved by the Publisher, whether the whole or part of the material is concerned, specifically the rights of translation, reprinting, reuse of illustrations, recitation, broadcasting, reproduction on microfilms or in any other physical way, and transmission or information storage and retrieval, electronic adaptation, computer software, or by similar or dissimilar methodology now known or hereafter developed.

The use of general descriptive names, registered names, trademarks, service marks, etc. in this publication does not imply, even in the absence of a specific statement, that such names are exempt from the relevant protective laws and regulations and therefore free for general use.

The publisher, the authors and the editors are safe to assume that the advice and information in this book are believed to be true and accurate at the date of publication. Neither the publisher nor the authors or the editors give a warranty, express or implied, with respect to the material contained herein or for any errors or omissions that may have been made.

Printed on acid-free paper

Springer International Publishing AG Switzerland is part of Springer Science+Business Media
(www.springer.com)

Parts of this thesis have been published in the following journal articles:

1. *Hetero-dehydrocoupling of Silanes and Amines by Heavier Alkaline Earth Catalysis*. (Chapter 3)
M. S. Hill, D. J. Liptrot, D. J. MacDougall, M. F. Mahon and T. P. Robinson; *Chemical Science*; 2013, **4**, 4212.
2. *Accessing the Single-Electron Manifold: Magnesium-mediated Hydrogen Release from Silane*. (Chapter 5)
D. J. Liptrot, M. S. Hill and M. F. Mahon; *Angewandte Chemie International Edition*; 2014, **53**, 6224.
3. *High Nuclearity Heterobimetallic s-block Hydrides via σ -bond Metathesis*. (Chapter 2)
D. J. Liptrot, M. S. Hill and M. F. Mahon; *Chemistry—A European Journal*; 2014, **20**, 9871

Supervisor's Foreword

It provides me with enormous satisfaction and pleasure to see the doctoral thesis of my former student, Dr. David Liptrot, included as part of the Springer Theses series. The thesis is rooted in some world class synthetic inorganic chemistry and describes the development of heavier alkaline earth reagents to effect catalytic dehydrocoupling reactions in which valuable new E-E' bonds may be formed by elimination of H₂ from E-H and E'-H precursor molecules.

With global sales in excess of US\$ 3 trillion, more than 95 % of all manufactured products rely on the chemical industry. Although a consequently enormous consumer of energy, accounting for 30 % of the worldwide industrial demand, this voracious appetite may be mitigated through the implementation of solid- (heterogeneous) or solution-based (homogeneous) catalysts. Many such systems, however, are derived from the reactivity of precious metals such as platinum, palladium, rhodium and iridium. For example, the largest global industrial homogeneous catalytic process, the hydroformylation of alkenes, produces seven million tonnes of commodity aldehydes or alcohols per annum but requires the use of rhodium catalysts. Palladium catalysis is of similarly crucial importance in pharmaceutical and agricultural chemistry for the construction of carbon-carbon bonds. Palladium and the other 'platinum group' metals are, however, scarce and particularly sensitive to potential supply restrictions. These issues are well recognised and in the European Union, for example, a sustainable basis for the entire life-cycle of minerals and metals has been identified as a primary ambition by 2050. In response, more earth abundant first row transition elements such as iron and cobalt have attracted significant recent international attention as catalysts. Although the heavier alkaline earths, particularly magnesium and calcium, respectively, the sixth and third most lithospherically abundant metals, are similarly attractive candidates for development, well-defined examples of their use in catalysis were non-existent until the last decade.

It is against this backdrop that David conducted the research described in his Ph.D. thesis. He joined my research group at the University of Bath in 2011, having completed a remarkably successful period as an undergraduate during which he secured a series of national awards, and made an immediate impact

in discovering routes to several spectacular bimetallic hydride species. Such derivatives are key catalytic intermediates during dehydrocoupling reactions mediated by the heavier alkaline earths. David not only discovered and developed several examples of this class of reaction during his Ph.D. but, through a series of detailed, inventive and nuanced mechanistic analyses, was also able to fully delineate the roles of the group 2 centres during catalytic turnover. More generally, and of even greater significance, he has started to devise a series of ground rules with which to predict the facility for sigma bond metathesis of an entire group of the periodic table. I am convinced that the growing international interest in the chemistry of these elements will ensure that David's research will be recognised as a seminal contribution in years to come.

David's Ph.D. thesis is outstanding by every metric. It comprises excellent science, provides an effortless and enjoyable read and is beautifully presented. It was my privilege to act as his doctoral advisor and to count him as a collaborator, confidante and friend. I am convinced that he will continue to thrive as he moves on to bigger and (even) better things as a Lindemann Fellow at the University of California, Davis and I wish him all the very best for the future.

Bath
June 2015

Prof. Michael S. Hill

Abstract

Whilst Group 2 elements continue to emerge from their obscurity, with a plethora of heterofunctionalisation thus described, such extensive investigations into cross metathesis remain limited.

Described herein is an extensive investigation into a variety of factors which contribute to the understanding of the complexity of the mechanistic surface upon which Group 2 mediated catalytic cross- and stoichiometric σ -bond-metatheses sit.

An initial study of the synthetic potential of σ -bond metathesis yielded a range of unprecedented and structurally fascinating compounds-mixed metal amidoalkyls and amidohydrides of Groups 1 and 2. Subsequently, a pair of variables in Group 2 mediated dehydrocoupling was investigated:

- (a) The effect of congeneric variation upon Group 2 (magnesium, calcium and strontium) mediated dehydrocoupling of amines and silanes, most notably indicating the significance of ancillary ligation, solution molecularity and pre-catalyst activation mechanisms.
- (b) The effect of variation in hydridic coupling partner on the dehydrocoupling of a range of amines with 9-BBN, pinacol(borane) and diphenylsilane mediated by a β -diketiminato supported magnesium centre, most notably indicating the profound effect of coupling partner Lewis acidity and contingent variations in catalyst molecularity and rate determining step.

Finally, an investigation into the introduction of unprecedented steps in Group 2 catalysis is reported herein. Specifically, the activity of the stable radical TEMPO is investigated for its propensity to induce single electron transfer upon labile, reactive ligands around magnesium and the ability for its anionic analogue to undergo σ -bond metathesis

Acknowledgments

I must concede that if the first time one of the wealth of people who deserve my gratitude hears of it is via this section then I have failed as a friend and colleague. Nevertheless, my career thus far in chemistry has been blessed by its diversity, quality and volume of other chemists with whom I have shared my life, lab, drinks or just the odd chat.

The foremost and deepest gratitude must be extended to my supervisor, Mike Hill, who has had the patience to allow me my space but the prescience to press me when necessary. I could not wish for a better supervisor, nor a truer friend, I'll miss the 5 coffees a day more than anything.

Yet groups are not simply supervisors—they are the people who bring that philosophy of life and science to day to day lab work, and in the Hill group I have been particularly fortunate. Particular thanks must go to Cath, Mat, Merle, Dawkins, Dug and Ben—doing it without you would have been a pale imitation.

Beyond the group there are a plethora of people at Bath who contribute to an environment which is both scientifically and otherwise beautiful. John Lowe's patience and support with regard to NMR is frankly incredible and Mary paedogogy is the stuff of legends. I could not have wished for two more caring or brilliant teachers. Thanks must also go to Gabi Kociok-Köhn and Anneke Lubben for other analytical assistance.

My thanks must also, inevitably, go to my family. Your input made me who I am, this thesis, know it or not, is a result of that input.

And finally, my thanks go to Sarah. The final year of my Ph.D. has been rendered immeasurably more enjoyable, thanks to you.

Contents

1	Introduction	1
1.1	Group 2	1
1.2	Redox-Inactive Lanthanide-Mediated Catalysis	3
1.3	Group 2-Mediated Catalysis	4
1.3.1	Group 2-Mediated Hydroamination	5
1.3.2	Further Group 2-Mediated Heterofunctionalisations	15
1.3.3	Synthesis and Reactivity of Molecular Group 2 Hydrides	17
1.3.4	Synthesis and Reactivity of Magnesium(I) Species	21
1.3.5	Group 2-Mediated Cross-Metathesis and Dehydrocoupling	21
1.3.6	Alternative Mechanisms in Group 2-Mediated Reactivity	24
1.4	Mechanistic Considerations in Redox-Inactive Dehydrocouplings	28
1.5	Aims of This Project	34
	References	35
2	Group 1-Group 2 Bimetallic Alkyls and Hydrides	41
2.1	Introduction	41
2.2	s-Block Mixed Metal Amidoalkyls	43
2.3	s-Block Mixed Metal Hydrides	51
2.4	Experimental Data	57
	References	60
3	Silicon–Nitrogen Dehydrocoupling	63
3.1	Introduction	63
3.2	Catalytic Scope	64
3.3	Stoichiometric Studies	68
3.4	Kinetic Analyses	74
3.4.1	Catalyst Initiation	75
3.4.2	Order of Reactants for Magnesium	78
3.4.3	Order of Reactants for Calcium	80
3.4.4	Order of Reactants for Strontium	81
3.4.5	Eyring and Arrhenius Analyses for IIa–c	83

3.5	Alternative Ligands in Magnesium-Mediated σ -Bond Metathesis . . .	88
3.6	Tin-Nitrogen Coupling	90
3.7	Experimental	97
	References	100
4	Boron–Nitrogen Dehydrocoupling.	103
4.1	Introduction	103
4.2	Catalytic B–N Dehydrocoupling	104
4.3	Catalytic Scope.	104
4.4	Stoichiometric Studies	108
4.5	Kinetic Analyses.	114
4.5.1	Order of Reactants for 9-BBN	115
4.5.2	Order of Reactants for Pinacol(Borane).	117
4.5.3	Order of Reactants for Diphenylsilane.	117
4.5.4	Eyring and Arrhenius Analyses for 9-BBN, Pinacolborane and Diphenylsilane	119
4.6	Experimental	125
	References	128
5	Single Electron Transfer Steps in Group 2 Catalysis.	131
5.1	Introduction	131
5.2	Stoichiometric Reactivity of TEMPO with Magnesium Species	132
5.3	Catalytic TEMPO Induced Silane Dehydrogenation	136
5.4	Reactivity of TEMPO with Calcium and Strontium Amides	138
5.5	Experimental Details	141
	References	144
6	Summary	147
7	Future Work	149
7.1	Chapter 2	149
7.2	Chapter 3	149
7.3	Chapter 5	150
	Appendix A: General Experimental Procedures	151
	Appendix B: Literature Compounds Described Herein	155
	Appendix C: Novel Compounds Described Herein	159

Abbreviations

9-BBN	9-Borabicyclo(3.3.1)nonane
br.	Broad NMR resonance
CatBH	Catechol(borane)
Cp	Cyclopentadienyl
Cp*	Pentamethylcyclopentadienyl
Dipp	2,6-Di- <i>iso</i> -propylaniline
DOSY	Diffusion Ordered Spectroscopy
<i>i</i> Pr	<i>Is</i> o-propyl
L	Supporting ligand
<i>n</i> Bu	<i>n</i> -butyl
NHC	N-heterocyclic carbene
NMR	Nuclear Magnetic Resonance
ORTEP	Oak Ridge Thermal Ellipsoid Plot
Ph	Phenyl
PinBH	Pinacol(borane)
RDS	Rate determining step
<i>t</i> Bu	<i>Tertiary</i> -butyl
TEMPO	2,2,6,6-tetramethyl-1-piperidinyloxy
THF	Tetrahydrofuran
ΔG^\ddagger	Gibb's Free Energy of Activation
ΔH^\ddagger	Enthalpy of Activation
ΔS^\ddagger	Entropy of Activation

Chapter 1

Introduction

1.1 Group 2

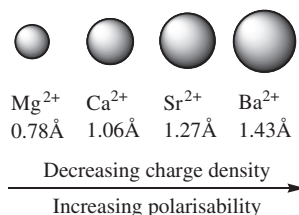
The transition metals are well known for their extensive catalytic chemistry (e.g. Pd, Ru, Ir) and a vast range of transformations are accessible utilising these elements. Furthermore the exploration of their catalytic chemistry is assisted by a well-defined coordination chemistry, variability of oxidation state and consistency in mechanistic steps which underpin predictable catalysis. The metals of Group 2, on the other hand, have been notable stoichiometric reagents for more than a century in the form of magnesium Grignard reagents as well as Lewis acid catalysts. Until recently, however, very little exploration had been undertaken into both the coordination chemistry of the heavier congeners (Ca, Sr and Ba) and the catalytic ability of these species.

Many of the Group 2 metals are notable for their high relative abundance in the Earth's crust [1] and, hence, low cost and their environmentally benign nature. This suggests that a catalytic framework based on these metals could be sustainable, economical and green. The chemistry of the Group 2 metals is marked by their extremely stable +2 oxidation state, with some notable exceptions [2, 3]. This redox inactivity precludes chemistry reminiscent of the transition metals, which relies upon oxidation state variation for bond activation.

Although all of the heavier Group 2 congeners have a strong propensity to form their respective M^{2+} ions with a $d0$ electronic configuration, marked variations in the ionic radii of the ions is observed as the group is descended, with a concurrent increase in polarisability and electropositivity (Fig. 1.1).

This has profound consequences upon the nature of metal ligand bonding for Group 2, with a degree of covalency accessible for magnesium which is precluded for its heavier congeners, the bonding of which is dominated by non-directional ionic interactions. These bonding characteristics represent a challenge for accessing well defined, heteroleptic heavier Group 2 complexes owing to their propensity to undergo Schlenk-type equilibria as summarised in Scheme 1.1.

Fig. 1.1 The variation in, and consequences thereof, of the ionic radii of Group 2 M^{2+} ions [4]



Redistribution of heteroleptic complexes often yields metal centres ligated by two large, stabilising ligands. Consequently, approaches to spectator ligands for Group 2 have focused on polydentate monoanionic frameworks encompassing hard donor sites and significant steric bulk to assist in kinetic stability and suppress the Schlenk-like redistribution summarised in Scheme 1.1. Stabilising ligands include β -diketiminates (**Ia-g**) [5–10], borates (**VII**) [11, 12], (bisimino)acenaphthenes [13], bisimidazolinates (**VI**) [14], aminotropiminates [15, 16], triazenides [17] and anilido-imines (**Va-c**) [18]. Whilst an alternative approach has relied upon the use of homoleptic Group 2 complexes including those incorporating bulky amides (**IIa-d**, **IIIa-d**) [19, 20] and alkyls (**IVa-d**) [21, 22]. A range of well-known ligands relevant to this work are summarised in Fig. 1.2.



Scheme 1.1 The Schlenk-type redistribution to which Group 2 M^{2+} complexes are prone

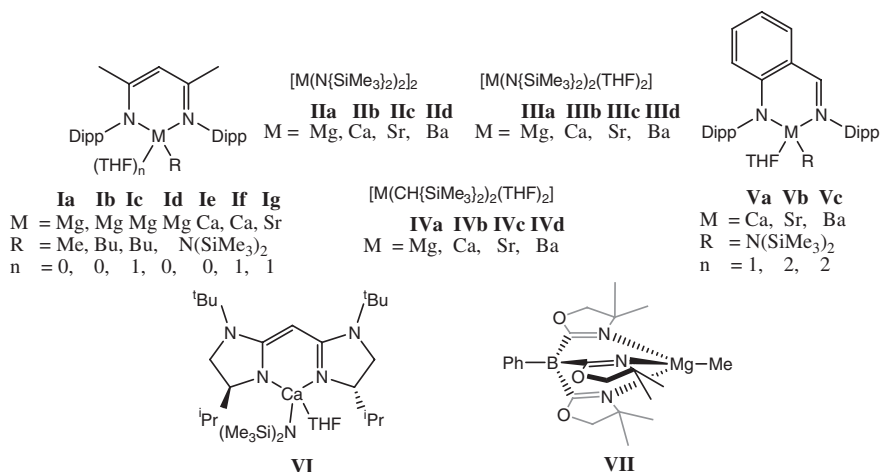


Fig. 1.2 A range of pre-catalysts utilised in Group 2-mediated catalysis, of relevance to this work

1.2 Redox-Inactive Lanthanide-Mediated Catalysis

The M^{2+} state of Group 2 elements has a d^0 electronic configuration and analogies can, thus, be drawn with trivalent, redox inactive, d^0 lanthanide complexes of the form L_2MX (L = spectator ligands, X = reactive group). Reactivity of the lanthanides is marked by two principal mechanistic steps, σ -bond metathesis and insertion, which occur without any alteration to the oxidation state of the metal. These steps are summarised in Scheme 1.2 and were initially exploited in the ground-breaking work of Marks et al. [23].

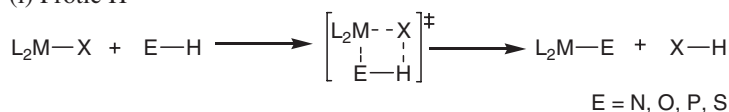
Protonolysis of the form shown in Scheme 1.2a(i) yields, in the case of an amine N–H bond, lanthanide amides of the form L_2MNR_2 [24]. Exploitation of these species in insertion as shown in Scheme 1.2b initially yielded a variety of stoichiometric heterofunctionalisations of unsaturated bonds. Alkenes, by dint of their unpolarised nature, showed a sluggish hydroamination reliant upon polarization of the C=C double bond by the M–X fragment. In contrast, more polarised bonds such as aldehydes, ketones or imines showed far more rapid, selective heterofunctionalisation [25–30]. In contrast, Scheme 1.2a(ii) shows the case wherein the E–H bond is polarised with a greater electron density localised upon the hydrogen, as in silanes and boranes, in which case σ -bond metathesis yields a metal hydride, L_2MH and an E–X bond.

Beyond these initial stoichiometric reports, work by Marks et al. has exploited such fundamental steps in catalysis, yielding two redox-inactive catalytic cycles as shown in Fig. 1.3 [23, 31].

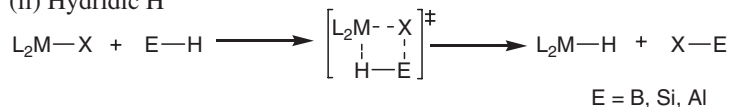
The divergence in these catalytic cycles occurs as a result of the polarization of the E–H bond. As noted in Scheme 1.2a, whilst E–H protic bonds undergo a

(a) σ -bond metathesis

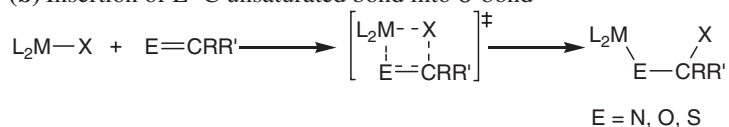
(i) Protic H



(ii) Hydridic H



(b) Insertion of E=C unsaturated bond into σ -bond



Scheme 1.2 The key steps in trivalent lanthanide mediated catalysis put forward by Marks et al.: **a** σ -bond metathesis with a (i) protic E–H bond (ii) hydridic E–H bond, **b** the insertion of an unsaturated bond into an L_n –X σ -bond

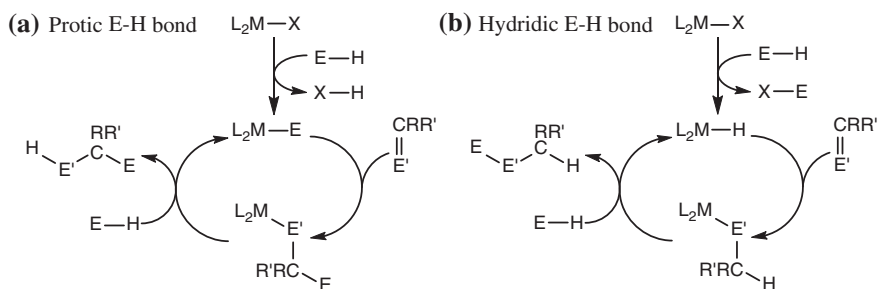


Fig. 1.3 The catalytic cycles predicated upon the steps summarised in Scheme 1.2. **a** The addition of an E–H fragment to a C=E' moiety with polarization of the E–H bond yielding a protic hydrogen; **b** the addition of an E–H fragment to a C=E' unsaturated moiety with polarization of the E–H bond yielding a hydridic hydrogen

protonolysis to yield an M–E fragment, hydridic E–H bonds undergo a σ -bond metathesis to yield a M–H fragment. In the case of Fig. 1.3a, the former case is in operation wherein the M–E fragment undergoes an insertion of the unsaturated bond yielding a species of the form $L_2MEC(E)RR'$ which can subsequently undergo protonolysis with another equivalent of the E–H bond to yield, typically the anti-Markovnikov, product and another M–E fragment allowing turnover. In contrast, when the E–H bond is hydridic (Fig. 1.3b), the metal hydride L_2MH is active for the insertion, yielding the intermediate $L_2MEC(H)RR'$ which undergoes a σ -bond metathesis with the E–H fragment to yield the active L_2MH species and Markovnikov addition product.

Exploitation of these cycles has yielded a wide variety of heterofunctionalisation reactions operant upon unsaturated moieties mediated by L_2MX species, including hydroamination, hydroboration, hydrophosphination and hydroalkoxylation of alkenes alongside polymerization of olefins [30–59].

1.3 Group 2-Mediated Catalysis

As noted, analogies in the electronic structure and bonding of the Group 2 M^{2+} and lanthanide M^{3+} ions have been drawn, and, inspired by the extensive catalytic chemistry of the trivalent lanthanides, Group 2 mediated catalysis has emerged as a burgeoning field over the last decade. Although Group 2 mediated Lewis acid catalysis has also undergone a renaissance, such reactivity is of limited relevance to this work and, thus, will not be discussed further [60].

Initial work focused upon the viability of the protonolysis step, as shown in Scheme 1.2a(i), on Group 2 reagents in order to yield catalytically relevant Group 2 species. Indeed, the activity of Group 2 amides and alkyls with alcohols, pyrroles, terminal alkynes, phosphines and C–H acidic heterocycles has been shown to yield alkoxide [61–63], pyrrolide [64], acetylide [65–68], phosphide [69–72]



Scheme 1.3 The protonolysis of a protic E–H bond by Group 2 hexamethyldisilazides, yielding a new E–M bond and a hexamethyldisilazane (M = Mg, Ca, Sr, Ba)

and carbanion [73] fragments bound to a Group 2 centre alongside the respective protonated fragment; in the case of metal hexamethyldisilazides (**IIa-d**) this is an amine, as summarised in Scheme 1.3.

With this protonolysis in hand, work by Westerhausen et al. indicated that Group 2 phosphides such as $[M\{P(\text{SiMe}_3)_2\}_2(\text{THF})_4]$ (M = Ca, Sr, Ba) readily metallophosphinated 1,4-diphenylbutadiyne. Furthermore these compounds, and their amide analogues **IIa-d** readily added across the C–N bond in benzonitrile [68, 74–78]. Further evidence for the ability of Group 2 complexes to mediate insertion chemistry was provided by the styrene polymerization activity shown by the Group 2 benzyl complexes reported by Harder, such as $[M(\text{DMAT})_2(\text{THF})_2]$ (M = Ca, Sr, DMAT = 2-dimethylamino-2-trimethylsilylbenzyl) [79–82].

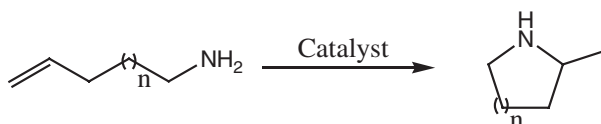
As a result of these promising stoichiometric reactions, initial reports of Group-2-mediated catalysis centred on the heterofunctionalisation of unsaturated C=C and C=E moieties, similar to the earlier reports of lanthanide mediated catalysis.

1.3.1 Group 2-Mediated Hydroamination

The Hill group initially reported the intramolecular hydroamination of alkenes and alkynes by Chisholm's β -diketiminato calcium complex **If** as summarised in Scheme 1.4 [83].

Subsequently, this reactivity was found to be mediated by a much wider range of Group 2 catalysts including **Ia-g** [5, 6, 9], **IIa-d**, and **IIIa-d** [19, 20]. Extensive mechanistic investigation into both the homoleptic Group 2 bisamides **IIa-d**, **IIIa-d** alongside the bisalkyls **IVa-d** [21, 22] and β -diketiminato ligated magnesium, calcium and strontium centres **Ia-g** [5, 6, 9] has been subsequently undertaken by the Hill group.

This reaction was found to give access to a wide range of nitrogen-containing heterocycles, including 5- and 6-membered rings in near quantitative yields under mild conditions. 7-membered rings are also accessible but only with specific



Scheme 1.4 The Group 2-catalysed intramolecular hydroamination of alkenes reported by the Hill group

precatalysts and in moderate yields and in all cases cyclisations are effected in concordance with Baldwin's rules [84]. Both alkenes and alkynes consistently yielded the expected isomers [6, 9].

A number of less in-depth studies by Hill and Roesky with triazenide and aminotropimate ligands respectively, suggested two very different congeneric effects on rate. The Hill group reported that strontium may catalyse the reaction more rapidly than calcium [17] while the Roesky group reported the opposite trend. Further studies with these ligands were, however, not undertaken [15, 16]. Owing to the increasing rate of redistribution down Group 2, studies with heteroleptic barium complexes of these forms proved fruitless. The Hill group reported a series of stable heteroleptic tris(imidazolin-2-ylidene-1-yl)borate Group 2 silylamides allowing comparison to barium. These species, however, proved to be ineffectual hydroamination catalysts owing to their propensity to cleave the B–N bonds in the ligand [85].

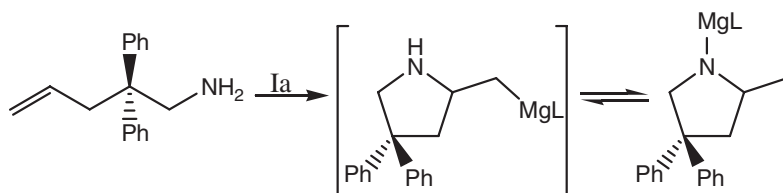
Substitution around the aminoalkene was generally found to decrease the rate of reaction, and terminal mono- or disubstitution often prevented the reaction completely. Furthermore, geminal substitution was found to be beneficial to the reaction rate and this was attributed to the reduction of conformational freedom these groups induce resulting in the species being confined to more reactive conformations—the Thorpe-Ingold effect [86]. Furthermore, synthesis of 5-membered rings proceeded faster than 6-membered rings which, in turn proceeded faster than the far more problematic 7-membered rings [5, 6, 9].

Consideration of the basicity of the β -diketiminato Group 2 metal amides **Id-f** indicated that entry into the catalytic cycle occurs via protonolysis yielding hexamethyldisilazane. This step was found to be reversible and a dynamic equilibrium observed for both congeners which appear to be monomeric. On the other hand for alkyl analogues such as **Ia-c** the protonolysis is, unsurprisingly, irreversible. These investigations yielded a range of soluble and stable Group 2 metal amides which form exergonically, and could be subjected to both NMR and crystallographic characterisation, indicating the viability of a Group 2 metal amide intermediate in these hydroamination reactions [5, 6].

Attempts to isolate the metal bound N-heterocyclic product were subsequently undertaken, and a ligated magnesium amide was characterised by NMR spectroscopy as shown in Scheme 1.5. Although further NMR analysis suggested an intermediate magnesium alkyl as shown, this rapidly converts via inter- or intramolecular tautomerisation to the far more stable metal amide. Nevertheless these observations were suggestive of an insertion step analogous to that seen for the lanthanides (Fig. 1.3a) and are consistent with the mechanism proposed for these reactions as shown in Scheme 1.5 [5].

Deuteration studies confirmed this as well as ruling out any further proton migration steps on the N-heterocyclic product [5].

Kinetic analysis, initially undertaken with **Ia** and **If**, indicated a marked dependence of the rate of reaction on the identity of the Group 2 metal centre. Calcium-catalysed intramolecular hydroamination was markedly faster than that catalysed by magnesium. Further studies focussed on magnesium owing to the



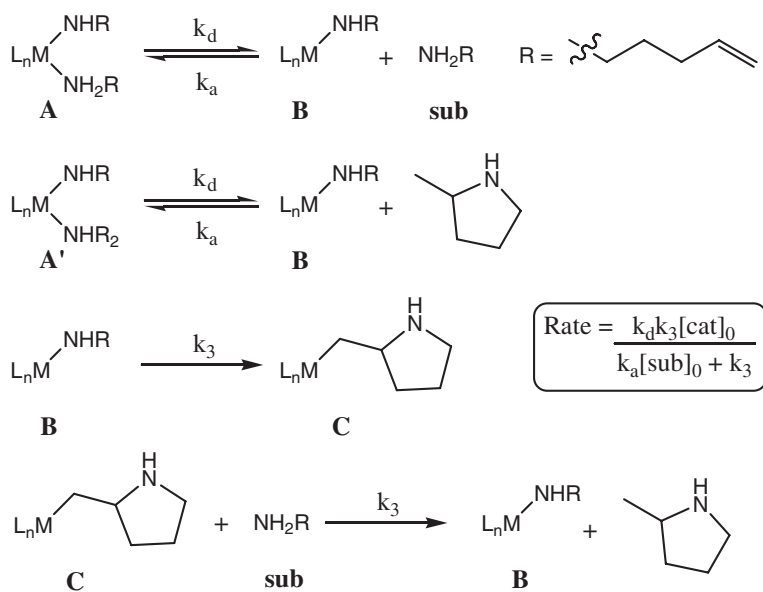
Scheme 1.5 The route to the β -diketiminato magnesium amide via an unisolated magnesium alkyl suggested by NMR analysis

accessibility of **Ia** which undergoes an irreversible initiation yielding the active catalyst and inert methane [5].

The reaction was found to be first order with respect to [pre-catalyst], suggesting the reaction occurs with a monomeric catalytic centre in solution. Alongside this, a first order rate relationship to aminoalkene concentration was observed [5].

Beyond this, the mechanism is significantly more complicated. A range of proposed equilibria involving complexation and decomplexation of both the substrate and product amines, alongside the protonolysis and insertion steps yielded a rate law as shown in Scheme 1.6 [5].

These data yielded a pair of catalytic manifolds involving (i) irreversible, (ii) reversible catalyst initiation which are shown in Fig. 1.4. This is consistent with the elementary steps proposed by Marks in lanthanide catalysis (Fig. 1.3) and



Scheme 1.6 The model for hydroamination catalysis mediated by **Id-f** proposed by the Hill group

reaction was proposed to be an equilibrium between the precatalyst **If** and the dimeric β -diketiminato calcium amide formed by the protonolysis of the aminoalkene precursor. With irreversible initiation, however, the resting state was proposed to be simply the dimeric β -diketiminato magnesium amide of the form shown in Fig. 1.4 [5].

A subsequent preparation by the group of Roesky gave access to the β -diketiminato strontium amide **Ig** [7] and the Hill group investigated this in comparison to the aforementioned magnesium and calcium analogues. In this case, the rate was found to be intermediate between that of calcium and magnesium although closer to the much higher calcium rate than the magnesium. In concordance with the higher propensity for heavier Group 2 metals to undergo Schlenk-type equilibria, this species was extremely prone to redistribution, precluding any investigation over 50 °C [9]. Although the Hill group previously noted similar results for the β -diketiminato calcium amide these redistribution processes were far slower and only became apparent at higher temperatures [5].

With this species in hand, Arrhenius and Eyring analyses comparing the solvated β -diketiminato supported metal amides of calcium and strontium **If** and **Ig** were undertaken by the Hill group. These suggested a trend which reflects the variation in rate with a decreased free energy of activation, ΔG^\ddagger for the calcium congener. Of significant note, however, between calcium and strontium the entropy of activation, ΔS^\ddagger value had a significant shift to a less negative value. This large shift was counterbalanced by a similar magnitude shift in the enthalpy of activation, ΔH^\ddagger value and reflects the complicated interplay of effects which define Group 2 catalytic rates [9].

Furthermore, access to the unsolvated β -diketiminato calcium amide **Ie** allowed a direct comparison of the effect of donor solvents on these reactions. The presence of THF in the reaction mixture was found to both decrease the rate of reaction and, through Arrhenius and Eyring analyses, increase the free energy of activation, ΔG^\ddagger . This increase is in fact in contrast to the observed activation energy which is actually larger for the unsolvated species, and the Hill group attribute this to the drastic shift of the ΔS^\ddagger to a less negative value on moving to the unsolvated species [9].

Studies centred on the Group 2 bisamides both as the unsolvated compounds **IIa-d** and THF adducts **IIIa-d** alongside the bisalkyls **IVa-d**, were also undertaken. Owing to their homoleptic nature and ease of synthesis, direct comparison of all the congeners from magnesium to barium was possible [9].

Most notably, barium, in the form of any of the precatalysts **IId**, **IIIId** and **IVd**, once again proved to be an ineffective catalyst for intramolecular hydroamination resulting in a maximum of two turnovers followed by the formation of an unidentified, insoluble and inactive product. The Hill group postulated this to be a result of the very large, diffuse nature of the barium centre which is insufficiently polarising to activate the C=C bond leading to an increased relative rate of deactivating side reactions. Furthermore, the magnesium precatalysts **IIa**, **IIIa** and **IVa** were found to have very low activity and as such further investigation into these was hampered by the long reaction times precluding any comparable evidence.

Nevertheless, the rate dependence on metal was found to follow a similar trend to that observed for the β -diketiminato supported species **Ia-g**, with an order of $\text{Ca} > \text{Sr} \gg \text{Mg}$ [9].

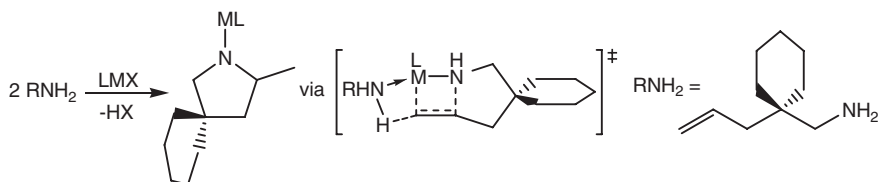
As with the reactions catalysed by β -diketiminato-supported precatalysts, the metal amides were shown to undergo a reversible protonolysis in the presence of amine. Of note, however, was the fact that protonolysis only appears to proceed once and at any one time each metal centre continued to be ligated by one hexamethyldisilazide ligand and one substrate amide ligand, in equilibrium with the amine complexed parent diamides structurally related to **IIa** and **IIc**. Although analysis of the NMR spectrum was suggestive of a dimeric metal centre, the complexity of the NMR spectra precluded the Hill group from making anything more than tentative comments along these lines [9].

Once again, in common with the β -diketiminato magnesium complexes, protonolysis by the Group 2 alkyls **IVb** and **IVc** was found to be irreversible. Furthermore, the extremely reactive alkyl substituents were both observed to undergo protonolysis yielding the metal bisamide, although the Hill group do not assign a particular molecularity to this species. This increase in reactive sites yields a very active system and, as a result of the very rapid conversion of aminoalkene by these species, further detailed kinetic investigations were practically precluded. Notable also was the propensity of the metal alkyls to undergo decomposition at even slightly elevated temperatures obviating attempts to perform Arrhenius or Eyring analyses [9].

Further credence to the suggestion of a dimeric active catalyst with the metal bisamides **IIa** and **IIc** was given by the kinetic analysis performed by the Hill group which suggested a second order dependence on catalyst loading for these unsolvated species. In contrast, the metal bisamide THF adducts **IIIa** and **IIIc** were found to have a first order rate dependence on catalyst loading, in conformity with the β -diketiminato supported metal centres. The latter observation was tentatively attributed to the THF molecules cleaving the catalyst dimers to yield monomeric, THF-supported catalytic centres [9].

Arrhenius and Eyring analyses of reactions indicated a marked dependence on the identity of the metal for activation energy and free energy of activation values. More notable variations were deduced for the activation entropies (ΔS^\ddagger), with strontium amides providing consistently less negative values than calcium with a proportionate effect on free energy of activation. This entropy dominated free energy change of activation is a common theme for Group 2 catalysis. Entropy of activation values were decreased by utilising the THF adduct precatalysts. The observed entropic effect was attributed primarily to the larger size and more deformable coordination geometry of the Sr^{2+} cation, and its consequent ability to form a less well-ordered transition state [9].

With the THF adducted amides **IIIa-c** and free amides **IIa-c** in hand an analysis of the effects of donor solvents was also undertaken by the Hill group. Of interest was the contrast to the β -diketiminato supported species (vide supra) as in this case THF adducts resulted in an increased rate of reaction, contrary to the observations for **Ie** and **Ic**. Furthermore, at high catalyst loadings of Group 2 amides **IIa-c**



Scheme 1.7 The two-substrate 6-membered transition state put forward by the Hill group to account for the observed kinetic isotope effect

deviations were observed from the initial second order dependence on catalyst loading. This resulted in a tailing off of the rate dependence on [catalyst] which was attributed to catalyst aggregation in solution. The presence of THF precluded this by occupying coordination sites on the metal centres [9].

Although NMR investigations suggested a mechanism with many features in common with the β -diketiminato supported system, a number of notable deviations were observed. Once again, the reaction was found to have a first order dependence on aminoalkene concentration. A moderate kinetic isotope effect for *N*-deuteration was observed and, by analogy to the previous investigations into the lanthanides, the Hill group postulated a modification to the previously suggested transition state in which a concerted C–N bond formation/protonolysis step occurs via a 6-membered two-substrate transition state as shown in Scheme 1.7 [9].

With this in mind the Hill group performed a more in depth analysis and, by analogy with Michaelis-Menten type enzyme kinetics, postulated a new rate law, which accounted for this refined transition state and inhibition by species such as THF. This new rate law is shown in below [9].

$$\text{rate} = \frac{k[\text{catalyst}]_0[\text{amine}]_t}{[\text{amine}]_0 + K_I[\text{inhibitor}]} \quad \text{where } K_I = \frac{k_d}{k_a}$$

This model is valid for both the β -diketiminato supported and THF adduct metal amides, but fails to take into account the second order dependence on catalyst loading observed for the THF-free bisamides **IIa-c**. The Hill group note that this rather complicated situation, alongside its contrast to other literature reports [87] is indicative of the complexity of Group 2 catalysis and a warning against over-generalisation [9].

Beyond these extensive investigations into intramolecular hydroamination, a number of the more entropically demanding Group 2-catalysed intermolecular hydroaminations have since been reported. Most notably, the Hill group has performed extensive studies into Group 2 bisamide **IIa-d** and bisalkyl **IVa-d** catalysts in this reaction [88, 89] while the group of Sarazin has more recently investigated the anilido imine supported Group 2 metals **Va-c** [18]. The generalised catalytic scheme for these transformations is summarised in Fig. 1.5.

Access to the catalytic manifold generally occurs via protonolysis of the pre-catalyst as shown. The regioselectivity of the initial addition is defined by the orientation of partial charges in the polarised transition state and hence the inherent

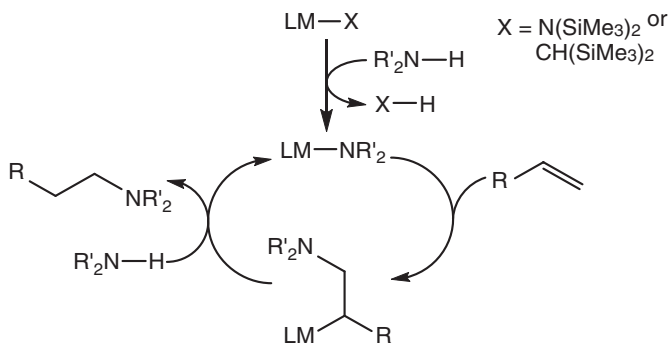
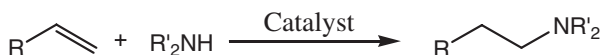


Fig. 1.5 The generalised mechanism for Group 2 mediated intermolecular hydroamination of activated alkenes



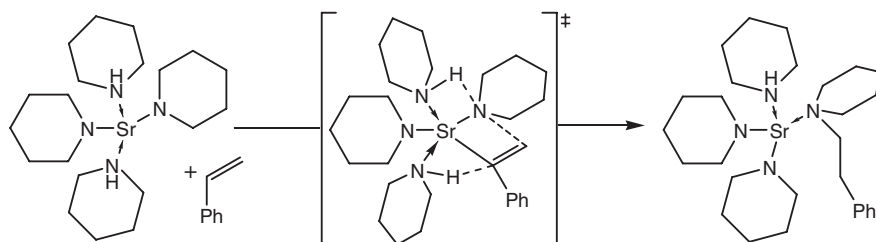
Scheme 1.8 The intermolecular hydroamination of styrene

polarity of the unsaturated substrate and metal-amide bond. Formation of the final, anti-Markovnikov, product and return to the uninserted catalytic amide intermediate occurs via a protonolysis of another equivalent of N–H bond.

In general, the Ca- and Sr-catalysed intermolecular hydroaminations of styrene and its derivatives, alongside isoprene and diphenylacetylene proceed in moderate to good yields at ambient to mild conditions. Viable coupling partners include a wide range of cyclic and acyclic mono- and disubstituted amines as shown in Scheme 1.8 [18, 88].

The Hill group went on to perform an extensive kinetic analysis of the reaction. Initial rate analysis showed that for the Group 2 bisamides **IIa-d**, and di-*n*-butyl-magnesium the rate dependence on catalyst was of the order $\text{Sr} > \text{Ca} \gg \text{Ba} > \text{Mg}$ as predicted by a computational assessment [89]. As a result of the extremely slow rate of conversion by both barium and magnesium precatalysts, no further analysis of these species was undertaken. This slow rate was attributed to, in the former case, the inability of the diffuse barium centre to sufficiently polarise the C=C bond, and in the latter due to the reduced polarising ability of the far less polar Mg–N bond [88, 89].

Once again, entry into the catalytic cycle was deduced to occur via deprotonation of an initial equivalent of amine and, in the case of the Group 2 amides, this product is in equilibrium with the parent precatalyst and amine. As for the intramolecular reactions the metal alkyls **IVb-c** allow irreversible deprotonation of the amine coupling partner and as such yield both faster and broader reactivity [88].



Scheme 1.9 The putative transition state for the intermolecular hydroamination of styrene put forward by the Hill group

Subsequent investigation by the Hill group gave rise to a rate law for the intermolecular hydroamination of alkenes, as shown below.

$$\text{rate} = k[\text{amine}]^1[\text{alkene}]^1[\text{catalyst}]^2$$

Once again, the second order rate dependence on [catalyst] was suggested to implicate a dimeric metal centre. Kinetic isotope studies were conducted and yielded values for *N*-deuteroamines similar to those observed for the intramolecular hydroamination of aminoalkenes. These data were interpreted to suggest once again, a concerted C–N bond forming protonolysis step takes place, and a putative transition state was presented as shown in Scheme 1.9, for strontium [88].

Arrhenius and Eyring analyses were undertaken and once again counterintuitive activation energies were observed. In spite of the increased rate of the catalysis by strontium centres, this reaction had a higher activation energy than the corresponding calcium catalyst. Eyring analysis however, yielded values for ΔG^\ddagger which were more in concert with the rate dependence and these were attributed to the far less negative ΔS^\ddagger values for the strontium system. This consistent dominance of entropic effects in reaction rates is notable [88].

The Sarazin group subsequently reported a range of Group 2 precatalysts supported by anilido-imines (**Va-c**) and tetradentate phenoxyaminoether ligands, which were analysed for their intermolecular hydroamination activity. Notably, with the lighter congeners the trend was consistent with that observed for the metal bisamides, to wit $\text{Mg} < \text{Ca} < \text{Sr}$. The heaviest congener analysed, barium, however was found to have the highest activity and consequently fastest reaction rates in contrast to the computational analysis performed by the Hill group suggesting a rate order of $\text{Sr} > \text{Ca} \gg \text{Ba} > \text{Mg}$ [23]. Kinetic analysis suggested a rate law similar to that proposed by the Hill group for the metal bisamides, although the likely monomeric constitution of the active catalyst, as a consequence of ligation, yielded a first order dependence on [catalyst], as shown below.

$$\text{rate} = k[\text{amine}]^1[\text{alkene}]^1[\text{catalyst}]^1$$

Furthermore, a kinetic isotope effect study gave a value similar to that seen by the Hill group for intramolecular hydroamination, leading the Sarazin group to once again postulate a 6-membered transition state involving concerted C–N bond formation and protonolysis [18].

Finally, the study by the Sarazin group allowed a direct comparison of a range of ligand systems; the aforementioned anilido imines **Va-c**, phenolates and the β -diketiminato complexes **Ia-d** initially investigated by the Hill group. In cases where a direct comparison can be made, the β -diketiminates are consistently faster however in all cases the phenolate complexes are the least able to catalyse this reaction. Finally, the barium anilido imine, **Vc** shows the highest activity of any reported species in catalysing this transformation. This once again reiterates the large effects of ligands on Group 2 catalysis alongside the interplay between stabilisation of complexes and loss of reactivity [18].

In the case of simple homoleptic precatalysts the trend generally followed is as follows: Sr > Ca > Mg > Ba [9]. When ligation becomes a factor the trend is more complicated and variation based on ligand systems is observed. In the case of the Hill group's investigations into β -diketiminates the trend was observed to follow that of Ca > Sr \gg Mg [5, 9]. Further extensive investigations into the effects of congeneric variation and ligation have been undertaken by the Sarazin group. Whilst the aminophenolate complexes derived from 2-[(1,4,7,10-tetraoxa-13-azacyclopentadecan-13-yl)methyl]-4,6-di-tert-butylphenoxy ligated Group 2 centres show a similar trend in reactivity to that seen for β -diketiminates [90], anilido-imines (**Va-c**) showed a contrasting order: Ba > Sr > Ca for intermolecular hydroamination [18] whilst intramolecular hydroamination once again reflected the trend initially described by the Hill group [91]. These variations may be rooted in the reactions proceeding by different mechanisms, although this is contradicted by the consistent rate laws, and more likely reflects significant and hitherto unconsidered ligand effects. Nevertheless these observations suggest further investigation is necessary to adequately explain and predict the effect of metal centre size and charge density on the rate of hydroamination and, most likely, other Group 2-catalysed reactions.

On the basis of their extensive investigations the Hill group have attempted to summarise the fundamental rate defining effects in Group 2-catalysed hydroamination. They put forth that the rate, defined by the activation barrier height toward rate determining C=C insertion is a result of both the polarity of the M-N bond, and hence its ability to polarise the C=C bond and the polarisability of the metal dication. This latter consideration defines the ability of the substrates to rearrange towards N-C and M-C bond formation. Finally, they attribute the high activity of the strontium-based systems to be a result of entropic effects as the large dication allows a looser arrangement of the substrates in the coordination sphere of the metal [9].

The Sarazin group sought to extend this summary in order to account for their observations, particularly; the contrasting, or complementary trends in congeneric effects on reactivity in concert with ligand effects. The Hill group suggested that the inability of barium to competently catalyse intramolecular hydroamination was a result of the diffuse Ba²⁺ ion being unable to sufficiently polarize the C=C double bond [9]. The Sarazin group, however, observed that barium was a competent catalyst and in fact the most able congener when ligated by an anilidoimine in the case of intermolecular hydroamination [18]. Although suggesting this contrasting

result required a more nuanced explanation than that provided by an argument of simple polarizing ability, they drew short of making any in-depth argument of their own. They further noted that denticity played a key role in catalytic ability with lower chelating or donating ability of a ligand yielding an increase in activity, an effect also obvious in the comparative results for the series of β -diketiminato supported precatalysts **Ia-g**, versus the homoleptic amides **IIa-d**. They attributed this result to being indicative of both steric congestion of the transition state, the unproductive occupation of coordination sites essential for catalysis and a reflection of the effect of coordination number upon the electron deficiency at the metal centre which, in the case of polydentate ligands, is reduced thus reducing the metal's ability to polarize the alkene [90].

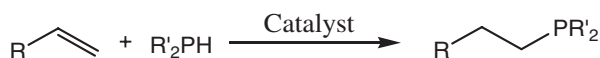
Subsequently, the groups of Harder [92] and Ward [14, 93, 94] reported attempts to yield an asymmetric hydroamination of alkenes utilising a range of chiral ligands such as **VI** shown in Fig. 1.2. Enantiomeric excesses were modest and this is proposed to be a result of the Schlenk type equilibria summarised in Scheme 1.1.

1.3.2 Further Group 2-Mediated Heterofunctionalisations

Subsequent to these initial reports, a wide range of both protic E–H and C=E bonds have been reported as viable substrates for heterofunctionalisation reactions. The Hill group has reported the catalytic intermolecular hydrophosphination of alkenes utilising the β -diketiminato calcium complex **If** as shown in Scheme 1.10 [95].

Subsequently Westerhausen and co-workers extended the scope of this reaction to alkynes utilising a homoleptic calcium phosphanide precatalyst [96]. More recently, the Sarazin group reported the hydrophosphination of alkenes catalysed by heteroleptic calcium, strontium and barium amides of both the aforementioned anilidoimines **Va-c**, and further with their set of phenoxyimines. The order of reactivity was found to be Ca < Sr < Ba mirroring that observed for hydroamination. Furthermore a ligand effect was observed with the phenoxides and anilidoimines showing higher activity than their analogous β -diketiminato species [18, 91]. Moving beyond activation of P(III)–H bonds, the Sarazin group reported the hydrophosphonylation of ketones and aldehydes mediated by **IIIb-d** [97].

The scope of these reactions has been further expanded to unsaturated substrates beyond alkenes, alkynes and ketones. Extensive reports of carbodiimide heterofunctionalisation have been made, initially by the Hill group who reported hydrophosphination [98] and hydroamination, [99] utilising **If** as well as **IIb-d**



Scheme 1.10 The hydrophosphination of alkenes

and **IIIb-d**. The latter transformation has been further explored by the group of Nembenna who investigated the effect of NHC ligation on the reaction, utilising the precatalyst **IIa** and its adduct with $[(\text{HCN}\{t\text{Bu}\})_2\text{C}:]$. This group noted a slight improvement in activity for the NHC supported species, over the parent **IIa**, for reactivity under solvent free conditions. They did not, however, provide any rationale for this observation [100].

Subsequent work in the Hill group has yielded further metalloamination and metallophosphination reactions utilising the heavier Group 2 homoleptic amides **IIa-c** [101]. Finally, inspired by the ready deprotonation of terminal alkynes mediated by Group 2 amides, hydroacylenation of carbodiimides has been extensively investigated by the Hill group mediated by **IIIa-c** [102].

Extension of this reactivity to isocyanates has proved more challenging. An initial report of isocyanate trimerisation was made by Harder et al. [103], a report which was expanded upon by Wei and co-workers who recently extended this reactivity to a tris(pyrrolyl)magnesium precatalyst [104]. Reactivity with isocyanates has been further expanded to catalytic hydroamination of isocyanates by the Hill group yielding substituted ureas [105] alongside a report of hydrophosphorylation from Westerhausen with phosphines [106] and phosphine oxides [107] but little further work has been reported.

The extension of this reactivity to cycles contingent upon the intermediacy of metal hydrides (Fig. 1.3b) has been more limited. An initial report of hydrosilylation of activated alkenes with range of calcium and strontium benzyl complexes of the form $[\text{M}(\text{DMAT})_2(\text{THF})_2]$ ($\text{M} = \text{Ca}, \text{Sr}$, $\text{DMAT} = 2\text{-dimethylamino-2-trimethylsilylbenzyl}$) was made by the Harder group. Notably, regioselectivity was contingent upon metal identity and solvent, with a more polar solvent yielding a terminal silane. This led the authors to postulate the possibility of two, contrasting catalytic cycles, one consistent with that proposed for lanthanide catalysis (Fig. 1.3b) and one which implicated a metal silyl formed via the deprotonation of silane by an incipient metal hydride (Fig. 1.6a, b respectively) [108].

Attempts to extend this reactivity to an asymmetric regime in the hydrosilylation of styrene utilising **VI** were broadly unsuccessful, with enantiomeric excesses

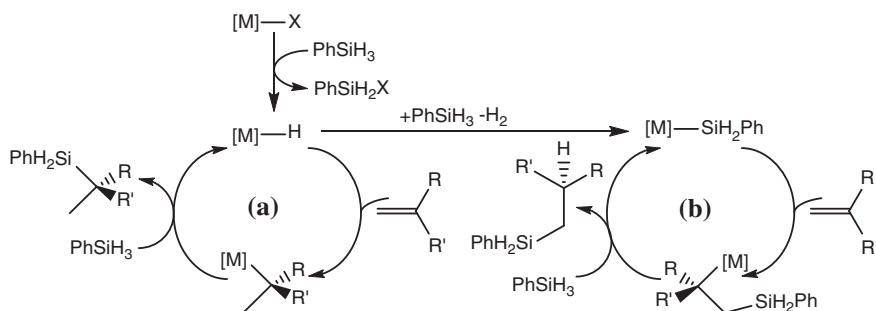


Fig. 1.6 The solvent dependent catalytic cycles proposed by Harder and co-workers for the hydrosilylation of alkenes

below 5 [92]. Okuda and co-workers extended this reactivity to a homoleptic calcium silyl, $[\text{Ca}(\text{SiPh}_3)_2(\text{THF})_4]$, which was found to mediate the hydrosilylation of α -phenyl- and α -methylstyrene with triphenylsilane showing regioselectivity reflecting the intermediacy of a calcium silyl as postulated by Harder, lending further credence to this alternative mechanistic hypothesis [109].

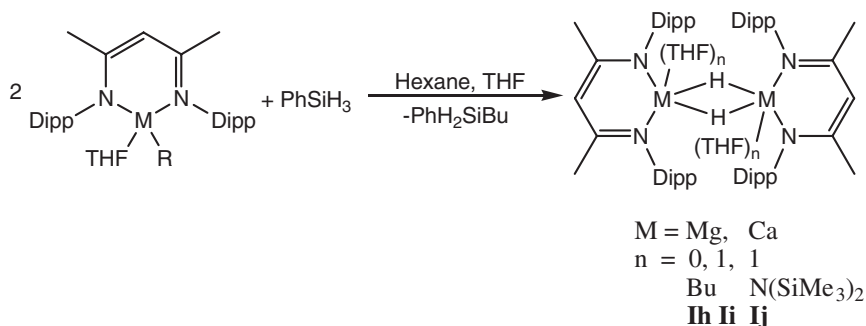
The Harder group then turned their attention to hydroboration of diphenylethylene with catecholborane utilising a range of organocalcium catalysts (**II**, **II**, and $[\text{Ca}(\text{DMAT})_2(\text{THF})_2]$). Once again, reactivity which contrasted with that previously observed for the lanthanides was noted—instead of the expected $\text{Ph}_2\text{CHCH}_2\text{OBCat}$ (Ph_2CHCH_2) $_3\text{B}$ was produced. This activity was attributed to a calcium-hydride mediated decomposition of the catecholborane, yielding BH_3 which spontaneously hydroborated the diphenylethylene and side-product analysis gave credence to this hypothesis [110].

1.3.3 Synthesis and Reactivity of Molecular Group 2 Hydrides

Complementary to these initial reports which implicated Group 2 metal hydrides in catalysis, albeit giving unexpected reactivity via a plethora of side reactions, was a focus upon the synthesis of well-defined, structurally characterised Group 2 hydrides as summarised in Scheme 1.11.

Initial work came in the form of the seminal report of a β -diketiminato supported calcium hydride by the Harder group, which relied upon a σ -bond metathesis pathway [111]. Subsequent work from Jones and co-workers yielded a variety of β -diketiminato supported magnesium hydrides [112, 113], and this σ -bond metathesis route utilising phenylsilane has now yielded a variety of higher magnesium hydrides reported by the Hill [114] and Harder groups [115].

In contrast to the initial reports of extensive side reactivity in catalysis which implicated Group 2 metal hydrides (*vide supra*), an exploration of the activity of



Scheme 1.11 The general approach to β -diketiminato supported Group 2 metal-hydrides exploited by the Harder and Jones groups

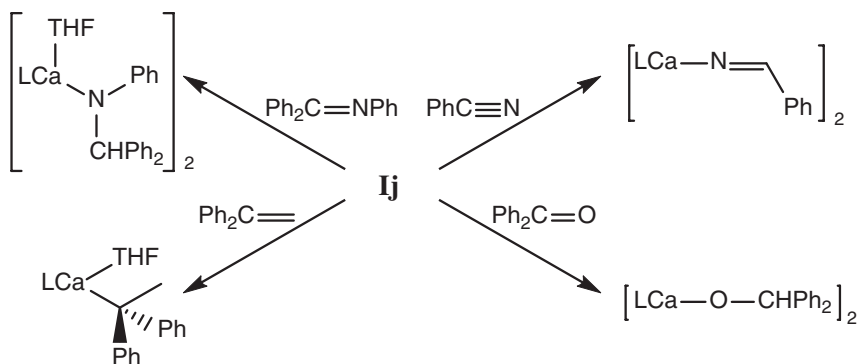
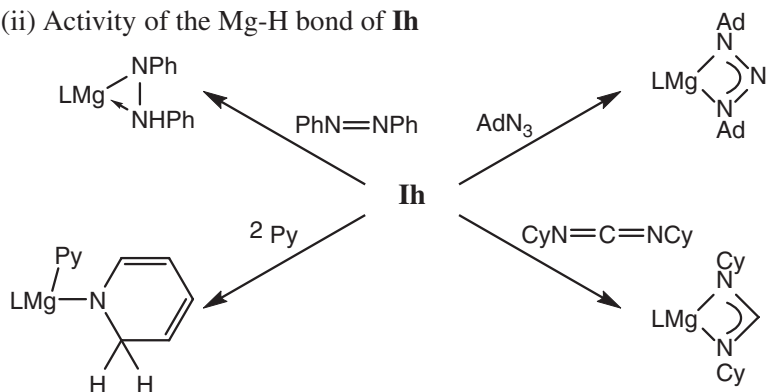
(i) Activity of the Ca-H bond of **Ij**(ii) Activity of the Mg-H bond of **Ih**

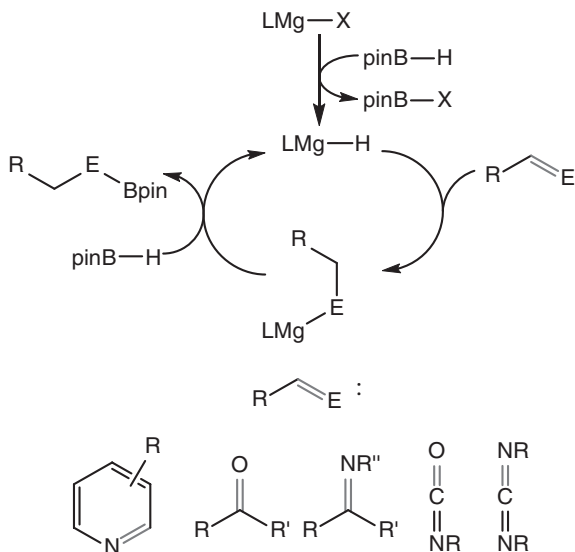
Fig. 1.7 The well-defined reactivity of β -diketiminate supported Group 2 hydrides **Ij** and **Ih** as described by the groups of Harder, Jones and Hill

Harder's calcium complex, **Ij**, showed well-defined and predictable stoichiometric reactivity. This is summarised in Fig. 1.7 alongside that of its unsolvated lighter congener reported by Jones and co-workers, **Ih** [116–122].

Indeed, subsequent to these stoichiometric reports, a variety of well-defined hydroboration reactions of unsaturated moieties mediated by Group 2 hydrides have been reported. These rely upon pinacolborane as a source of the B–H fragment and appear to follow the mechanism previously observed for lanthanide-hydride mediated reductions, as summarised in Fig. 1.8.

Initial work in this field was undertaken by the Hill group who, noting that the magnesium hydride **Ih** could stoichiometrically dearomatise pyridines

Fig. 1.8 The β -diketiminato supported magnesium hydride mediated hydroboration of C=E bonds reported extensively upon by the Hill group



(vide supra), reported a catalytic hydroboration of these cyclic masked imines [123]. The Harder group extended this reactivity to a di- β -diketiminato dimagnesium system, although noted no significant effect from the shift to this precatalyst [124]. More recently, the Hill group has reported hydroboration of ketones by the β -diketiminato ligated magnesium butyl precatalyst **1b** which yields boronate esters [125].

The Hill group have extended this reactivity to the dihydroboration of nitriles, yielding aminodi(boranes) for a wide variety of nitrile substrates [126]. In this case, an extensive kinetic study indicated a complex mechanistic energy surface upon which the pathway, most notably the rate determining step in the catalysis, was contingent upon a subtle interplay between the Lewis basicity and polarization of the nitrile fragment, as summarised in Fig. 1.9.

In order to extend this reactivity to more challenging substrates, specifically carbon dioxide, the Hill group turned to activation of the magnesium and calcium hydrides **1h-j** via the strongly Lewis acidic tris(pentafluorophenyl)boron which, in the latter case, yielded a structurally characterised β -diketiminato supported calcium borohydride [127]. These activated catalyst systems were competent for the exquisitely selective reduction of CO_2 to the methanol analogue, PinBOME as summarised in Scheme 1.12.

Although this initial report contained limited mechanistic study, the increased activity of these species mirrors similar effects of tris(pentafluorophenyl)boron upon a range of lanthanide hydrides reported by Piers and coworkers [128].

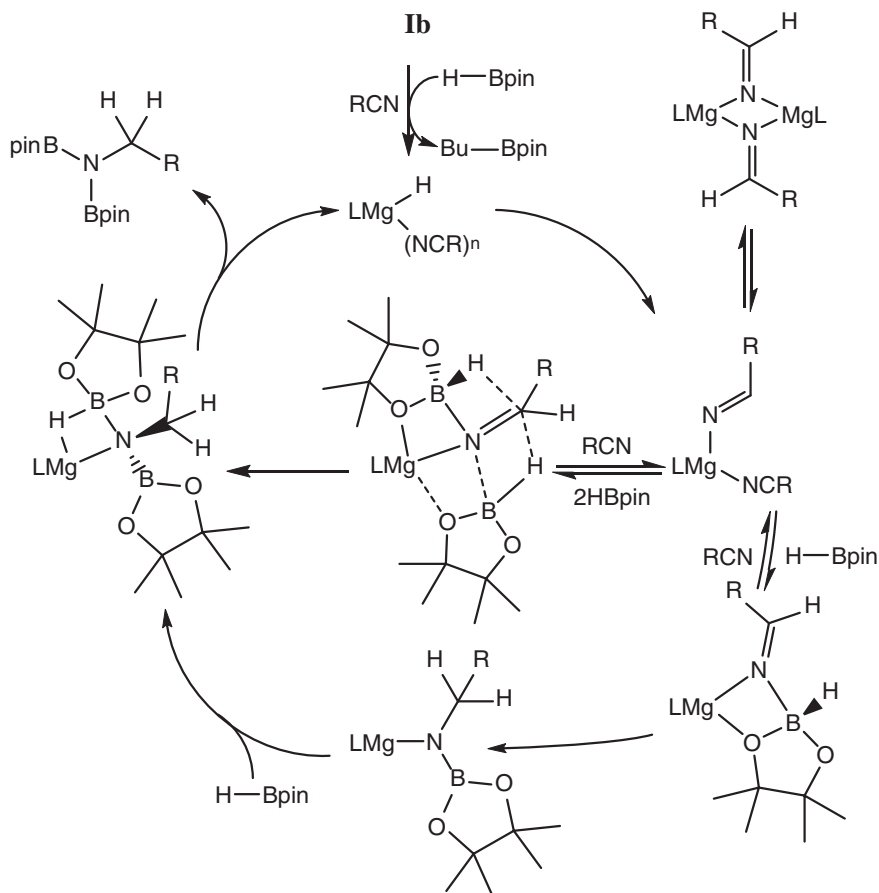
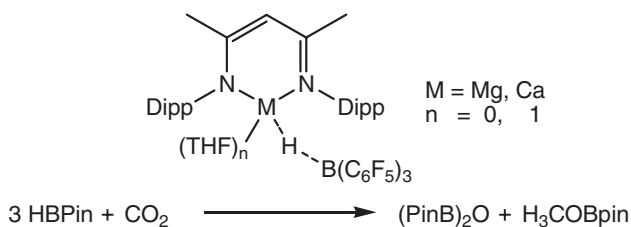


Fig. 1.9 The complex mechanistic surface upon which **Ib** mediated dihydroboration of nitriles was suggested to operate by the Hill group



Scheme 1.12 The exquisitely selective hydroboration of carbon dioxide to a methanol equivalent mediated by a Lewis acid-activated β -diketiminato supported Group 2 hydride

1.3.4 Synthesis and Reactivity of Magnesium(I) Species

Alongside these extensive investigations into Group 2 hydride mediated reductions, a separate class of magnesium based reducing agent has also been reported. As noted, only limited reports of well-defined Group 2 complexes deviating from a +2 oxidation state exist. Most notable are the range of bulky β -diketiminato, guanidinate and diazabutadienediide supported magnesium(I) dimers initially reported by Jones and co-workers, which were synthesized via reduction of the relevant magnesium(II) iodides utilising sodium or potassium, as summarised in Scheme 1.13 [2, 112, 113].

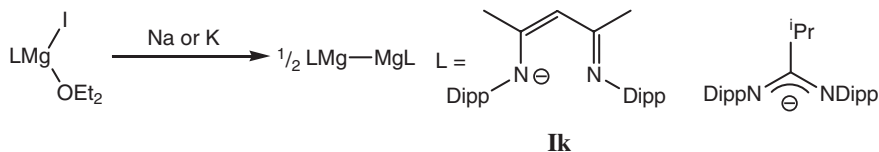
Work from Stasch has extended this to a diiminophosphinate supported magnesium(I) dimer, synthesized by a Mg(I)–Mg(II) redox reaction as summarised in Scheme 1.14 [129].

The reactivity of these species as reducing agents has thus been extensively explored by Jones and co-workers and is summarised in Fig. 1.10.

As shown, reduction of unsaturated organic fragments by these species shows complementary reactivity to that of Group 2-hydride mediated reductions and is thought to occur via, in the case of the dimer, a concerted $2e^-$ reduction ($1e^-$ per metal centre) [130]. These species are confined to stoichiometric reductions as synthesis of the magnesium(I) dimer under catalytic conditions is unlikely [121, 131, 132].

1.3.5 Group 2-Mediated Cross-Metathesis and Dehydrocoupling

As shown extensive studies into the insertion chemistry of Group 2 metal centres have now been undertaken. In contrast, little investigation into the σ -bond metathesis steps that underpin not only access to the insertion manifold, but



Scheme 1.13 The approach to a series of Mg(I) dimers supported by bulky ligands utilised by Jones and co-workers to describe the first set of species in this class



Scheme 1.14 The remarkable Mg(II)/Mg(I) redox reaction exploited by Stasch to yield a new class of bulky-ligand supported Mg(I) dimers

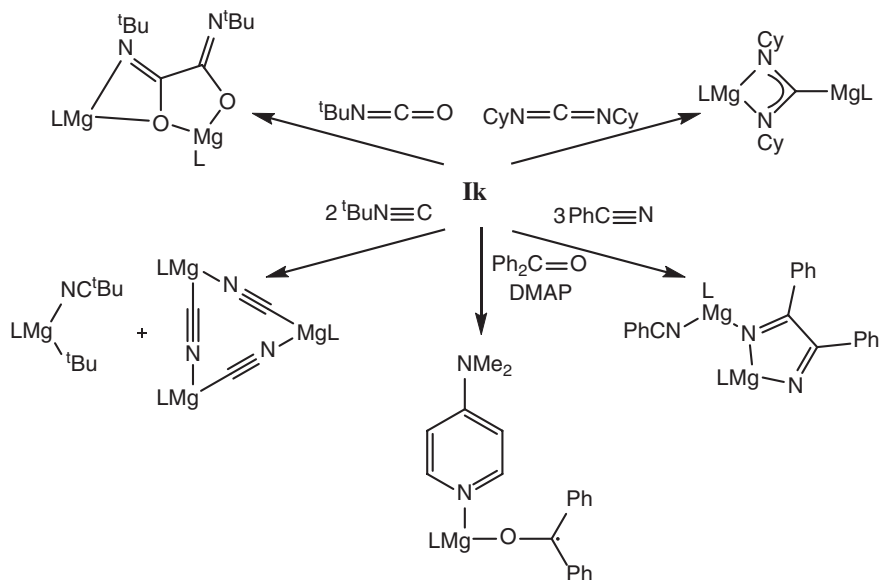


Fig. 1.10 The reaction of the β -diketiminate supported Mg(I) dimer with a variety of unsaturated organic fragments described by Jones and co-workers

also formation of the final product of insertion reactions has been performed. Furthermore, a reaction manifold entirely predicated on σ -bond metathesis can be proposed in the form of cross metathesis. Such a manifold is shown in Scheme 1.15.

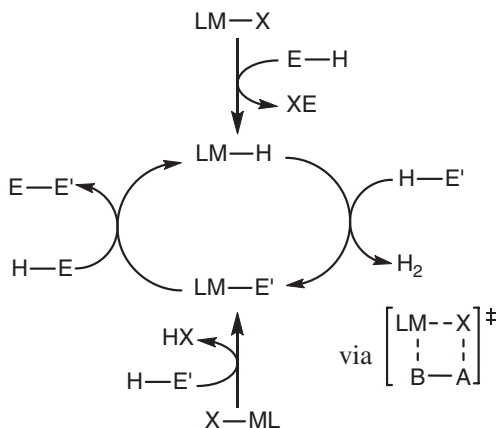
While a limited number of Group 2-mediated cross metatheses have been reported, these are limited to reactions between $E'-H$ protic and $E-H$ hydridic moieties yielding $E-E'$ bonds and hydrogen in dehydrocouplings. Harder et al. reported a Si-C dehydrocoupling between a silane and terminal alkyne which proceeded in a catalytic fashion, alongside an initial report of Si-N dehydrocoupling between a range of silanes and amines [133].

Recently, Sadow et al. have performed a more in-depth investigation into a dehydrocoupling between silanes and amines mediated by the trisoxazolinylborate magnesium precatalyst **VII** [12]. This reaction is postulated to occur via the manifold shown in Scheme 1.15 and allows access to a range of silanes in excellent yields. Kinetic analysis yielded a rate law as shown below [12].

$$\text{rate} = k[\text{amine}]^0[\text{silane}]^1[\text{catalyst}]^1$$

A large, negative entropy of activation (ΔS^\ddagger) value was also determined, which was interpreted to represent a highly ordered transition state with catalyst and silane involved in the rate determining step. Kinetic isotope studies employing deuterated silane provided a small normal kinetic isotope effect ($k_H/k_D = 1.0(2)$) indicating the concerted 4-membered transition state which is proposed above

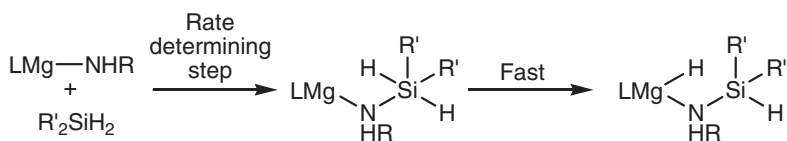
Scheme 1.15 The simplified proposed mechanism for Group-2-catalysed dehydrogenative cross metathesis



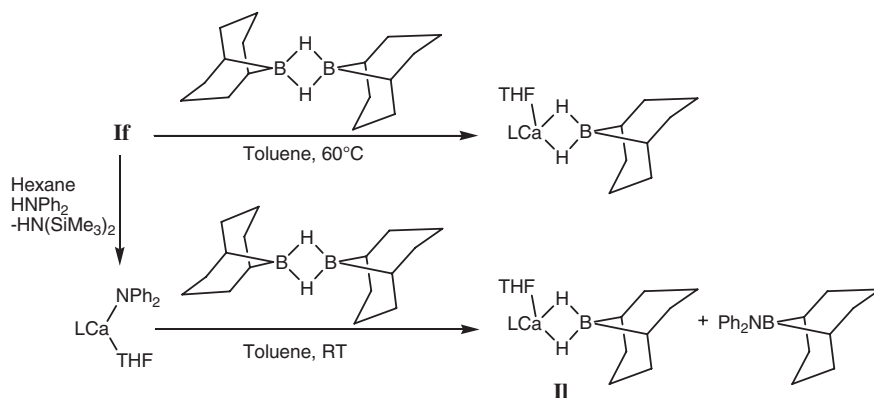
with limited Si-H bond cleavage in the transition state. Finally, a Hammett plot with a moderate positive slope was thought to suggest a transition state involving a five-coordinate silicon centre owing to the stabilising effect of electron withdrawing substituents on this species and to favour a limited degree of Si-H cleavage in the transition state, as such electron-withdrawing aryl substituents would disfavour hydride transfer to magnesium. Hence, Sadow postulated nucleophilic attack of the magnesium amide on silane as the rate determining step followed by a rapid hydride transfer reminiscent of β -hydride elimination to yield the product neutral silazane complexed to the metal centre as shown in Scheme 1.16 [12].

Further divergent reactivity has been described by Hill et al. with regards to phosphine oxides. Diarylphosphine oxides undergo both reduction and dehydrocoupling in the presence of phenylsilane mediated by **If** and **IVb**, to yield both the mixed P(III)-P(V) compound $\text{Ph}_2\text{P}(\text{O})\text{PPh}_2$ and its fully reduced counterpart Ph_2PPPh_2 . However, triarylphosphine oxides also show P-P coupling, which is postulated to occur via a P-C σ -bond metathesis. This latter observation suggests that not only X-H bonds but X-E bonds may be viable partners for cross metathesis [134].

The Hill group also reported a B-N bond formation between β -diketiminato calcium amide **If** and 9-BBN in which the resultant hydride was intercepted by a second equivalent of 9-BBN, to form a metal borohydride with no catalytic turnover observed [135].



Scheme 1.16 The proposed mechanism of silicon-nitrogen dehydrocoupling put forward by the Sadow group



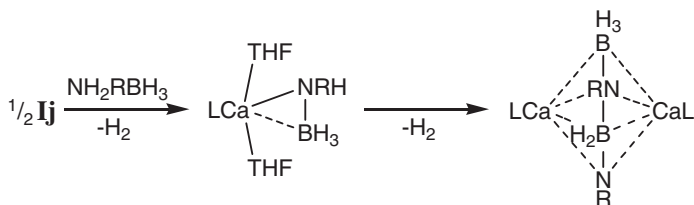
Scheme 1.17 The reaction of **If** and its diphenylamide derivative with 9-BBN showing a σ -bond metathesis N–B bond forming step described by Hill and co-workers

As shown in Scheme 1.17, the reaction of a Group 2 amide with 9-BBN yields a B–N bond forming step which, the Hill group proposed, occurred via a σ -bond metathesis to yield a metal hydride (**Ij**) which was subsequently intercepted by an equivalent of 9-BBN yielding a metal borohydride (**II**).

1.3.6 Alternative Mechanisms in Group 2-Mediated Reactivity

In contrast to these limited results in boron-nitrogen cross-coupling, investigations into the dehydrocoupling of amine-boranes, molecules wherein the N–H and B–H moieties are both contained, has been explored more extensively. A wide range of transition metal mediated reactions have been reported but almost all rely upon redox-active steps and thus will not be further discussed [136–138].

Harder and co-workers initially reported the hydrogen release reactivity of the parent ammonia-borane with their soluble calcium hydride, **Ij**, and further expanded this work to the bulky monosubstituted $\text{DippNH}_2\text{BH}_3$ with both this calcium hydride, **Ij**, and the β -diketiminato supported magnesium amide **Id**. Subsequent work from the Hill group interrogated, initially, hydrogen release from the disubstituted Me_2NHBH_3 with a range of Group 2 complexes and then extended this work to both pyrrolidine-borane and di-*iso*-propylamine-borane, as well as investigating the reactivity of a range of Group 3 amides. The Harder group went on to investigate the reactivity of monosubstituted amine-boranes with a more complex bimetallic β -diketiminato supported magnesium system. Finally, Jones and co-workers reported the reactivity of a β -diketiminato supported Mg(I) dimer, **Ik**, with ammonia-borane which yielded a set of soluble β -diketiminato supported magnesium(II) amidoboranes although no hydrogen release was investigated.



Scheme 1.18 The dehydrogenative coupling of ammonia-borane and methylamine-borane mediated by **Ij** to yield a coupled diaminodiborane dianion reported by Harder and co-workers. (R = H, Me)

Harder and co-workers' report of the reactivity of the β -diketiminato calcium hydride, **Ij**, with ammonia-borane yielded, initially, the ligated calcium amidoborane which, upon gentle heating, resulted in a B–N coupling, yielding a $[\text{NH}-\text{BH}_2-\text{NH}-\text{BH}_3]^{2-}$ dianion, bridging two β -diketiminato supported calcium centres, as summarised in Scheme 1.18 [139].

Similar reactivity, albeit at a slightly elevated temperature, was observed for the methylamine-borane and a further investigation into the far more sterically encumbered $\text{DippNH}_2\text{BH}_3$ yielded a deprotonated iminoborane coordinated to a β -diketiminato supported calcium centre, in contrast to this result, the lighter congener, utilising **Id**, yielded a di(amino)borane of the form $[\text{DippNHBHNHDipp}]$, under analogous conditions (Scheme 1.19) [140].

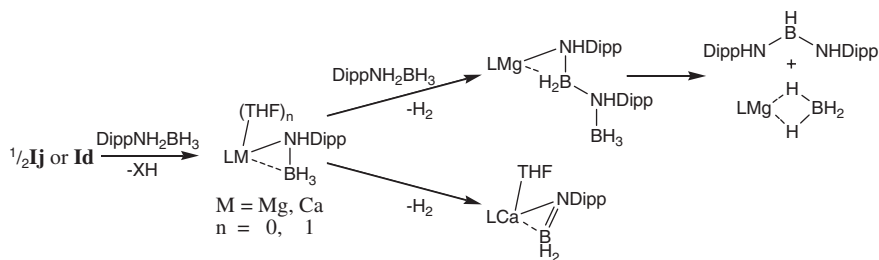
In spite of these results suggesting the possibility of a more complex mechanistic pathway being accessible to amine-boranes, the Harder group postulated a mechanism which was predominantly reliant on metal-mediated σ -bond metathesis preceded by the Hill group's initial report of B–N coupling via an analogous pathway for the coupling of the diphenylamide anion to 9-BBN.

Subsequent extensive catalytic and stoichiometric B–N dehydrocoupling was investigated by the Hill group in the dehydrogenative dimerisation of dimethylamine-borane catalysed by a range of Group 2 precatalysts (**Ib** and **If**) (Scheme 1.20).

Extensive stoichiometric investigations yielded not only amidoborane fragments bound to Group 2 centres, but also magnesium complexes of the B–N coupled anion $[\text{NMe}_2-\text{BH}_2-\text{NMe}_2-\text{BH}_3]^-$ as summarised in Fig. 1.11.

Although this reaction, and these intermediates could be accounted for by a σ -bond metathesis only pathway, further extensive NMR investigations coupled with these crystallographic investigations led this group to postulate an alternative catalytic manifold as shown in Fig. 1.12.

In this mechanism an initial protonolysis yields a metal-amidoborane which undergoes a β -hydride elimination to yield a metal-hydride and imidoborane fragment. This unsaturated fragment, which is isoelectronic to a C=C bond, then undergoes an insertion into an M–N bond of a metal-amidoborane. This process is analogous to the aforementioned C=E heterofunctionalisations and provides a coupled metal-diaminodiborane which undergoes a subsequent δ -hydride



Scheme 1.19 Congeneric variations in the dehydrogenation of $\text{DippNH}_2\text{BH}_3$ by \mathbf{Ij} or \mathbf{Id}



Scheme 1.20 The dehydrogenative dimerisation of dimethylamine-borane extensively investigated by the Hill group

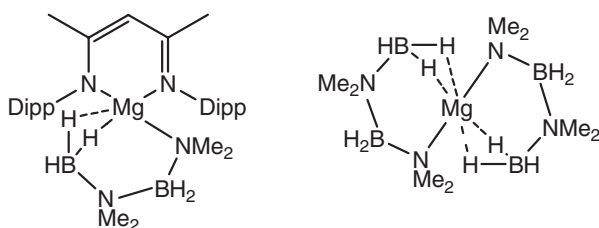


Fig. 1.11 The crystallographically-characterised magnesium complexes of a coupled diaminodiborane anion proposed by the Hill group, to represent an intermediate in the Group 2 mediated dehydrogenative dimerisation of dimethylamine-borane

elimination to yield the observed product and a metal hydride. As such this reaction involves an intramolecular B–N cross coupling to yield an initial π -bond and a subsequent B–N σ -bond and represents a hybrid of both the cross metathesis and insertion pathways [141].

Although extension of this work to pyrrolidine-borane indicated a generality to this mechanism, moving to the far bulkier secondary amine-borane, di-*iso*-propylamine-borane, yielded only the respective iminoborane, even under catalytic conditions as shown in Scheme 1.21.

It was postulated that dehydrogenation of the parent di-*iso*-propylamine-borane in a manner analogous to the mechanism proposed for the dimerisation of dimethylamine-borane, yielded an iminoborane fragment which, owing to its more extreme steric demands, was unable to undergo an insertion into the metal-aminoborane to yield B–N coupling. Under NMR conditions quantitative production of ${}^1\text{Pr}_2\text{N}=\text{BH}_2$ was accessible and this was considered to provide further evidence for the complex catalytic cycle initially proposed (Fig. 1.12) [142].

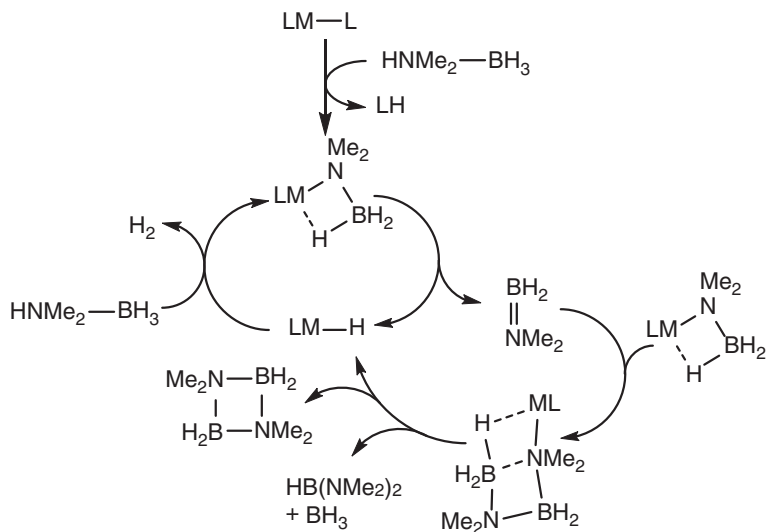


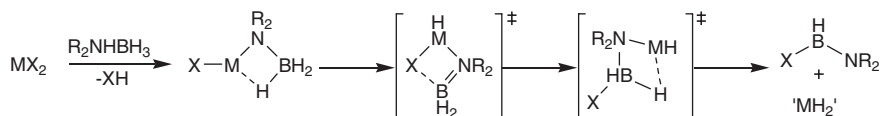
Fig. 1.12 The proposed mechanism of the Group-2-catalyzed dehydrocoupling of dimethylamine-borane



Scheme 1.21 The dehydrogenation of ${}^i\text{Pr}_2\text{NHBH}_3$ yielding an imidoborane incapable of dimerisation, and dihydrogen

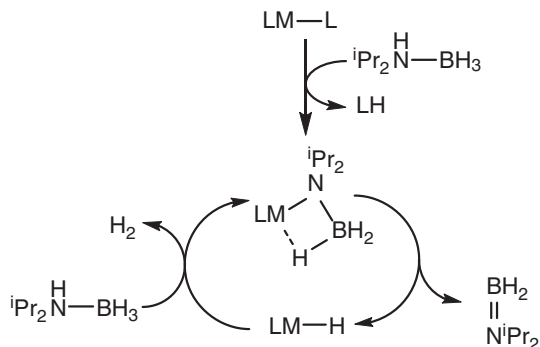
Further evidence for the intermediacy of such an unsaturated fragment was provided by a subsequent report from the Hill group who noted the interception of a postulated in situ generated imidoborane by an M–X bond yielding variously an unsymmetrical diamineborane or aminoalkylborane in the case of **IIIc** and **IVc** respectively. In each case an equivalent of ‘MH₂’ was also formed which, in the case of amines, could be intercepted dehydrogenatively to yield amides and render the synthesis of diamineboranes catalytic in alkaline earth dication utilising **IIIa** and **IIIb** as precatalysts (Scheme 1.22) [143] (Fig. 1.13).

Most remarkable in this chemistry was the rate-dependence of dehydrocoupling upon metal identity. In contrast to the more nuanced approach required in interpreting the rate dependence of Group 2-mediated hydroamination upon metal identity, amine-borane dehydrocoupling was found to be consistently contingent upon metal charge-density, with an increase charge-density (Ba > Sr > Ca > Mg) yielding increasingly efficient dehydrocoupling. Further credence for this hypothesis was put forward by the Hill group who noted that the even greater charge density of the Sc³⁺ ion provided catalytic efficiency well in excess of that of the magnesium dication [144].



Scheme 1.22 The insertion chemistry of an in situ generated iminoborane fragment into M–X bonds ($X = R_2N, (Me_3Si)_2CH$) yielding unsymmetrically substituted boranes and catalytically viable Group 2 hydrides

Fig. 1.13 The mechanism for di-*iso*-propylamine-borane dehydrogenation, proposed by the Hill group to indicate the viability of the mechanistic postulate summarised in Fig. 1.12



1.4 Mechanistic Considerations in Redox-Inactive Dehydrocouplings

In spite of the relative lacuna of investigation into Group 2 mediated cross-metathesis and its component mechanistic step, σ -bond metathesis, such reactivity has garnered extensive interest for other parts of the periodic table. Indeed, such interest has yielded a variety of in-depth reviews, most recently by Waterman [145]. Furthermore, cross-metathesis mediated dehydrocoupling has been extensively studied for the transition metals. In such cases, the reactivity is most commonly mediated by redox-active processes such as oxidative insertion and reductive elimination [146, 147]. Owing to the preclusion of such steps for Group 2 mediated catalysis, these reactions will not be further discussed.

Beyond such redox active catalytic processes, dehydrocoupling reactivity occurring via redox inactive steps has also been the subject of much investigation. Such investigations have suggested a more nuanced mechanistic surface whereupon a variety of element–element bond forming mechanisms are operant beyond the simple σ -bond metathesis characteristic of both lanthanide and, hitherto, Group 2 mediated reactivity.

Harrod and co-workers initially reported the polymerization of disubstituted silanes mediated by Cp_2TiR_2 and further reported the polymerization of germanes [148, 149]. Tilley and co-workers expanded on this, extending the reactivity to a range of group 4 metallocenes, and, through extensive and elegant mechanistic

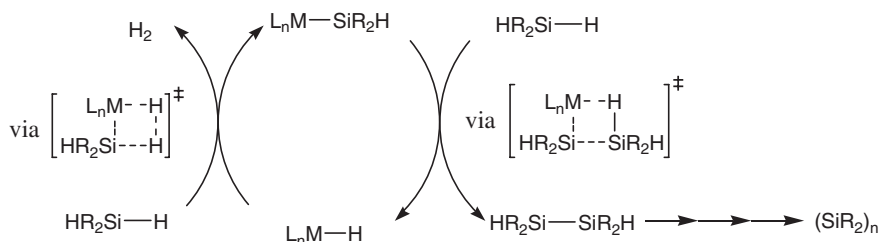


Fig. 1.14 The initial mechanistic report of σ -bond metathesis made by Tilley and co-workers with reference to the polymerisation of diarylsilanes to yield poly(silanes) and hydrogen ($M = \text{Ti}, \text{Zr}, \text{Hf}$)

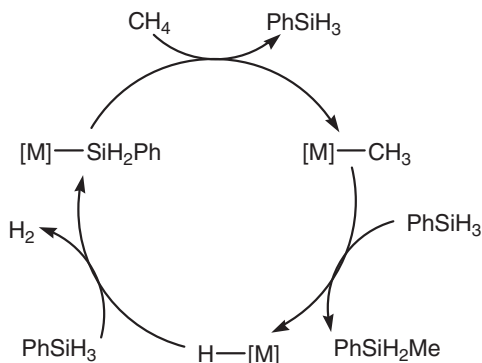
studies implicated a 4-centred concerted reaction between a metal hydride and Si–H bond [150], the first mechanistic report of a dehydrocoupling via σ -bond metathesis (Fig. 1.14) [151, 152].

Following this initial report of silane homo-dehydrocoupling, group 4 metallocenes with reactive alkyl and hydride substituents were found to provide far more general heterodehydrocoupling reactivity for a variety of p-block pairings, including Si–H/O–H, Si–H/N–H, B–H/N–H and Sn–H/Te–H dehydrocoupling. Initial analysis suggested that these cross-metatheses once again occurred via σ -bond metathesis steps, suggesting the potential for generality of this reactivity for group 4 metallocenes [153, 154]. Further Si–H/N–H dehydrocoupling has since been reported, alongside a report utilising a magnesium precatalyst as reported by Sadow and co-workers which was subject to some noteworthy mechanistic nuances (*vide supra*). The Cui group has further reported a dehydrocoupling of these elements mediated by a redox-inactive NHC supported Group 3 centre, utilising an $[(\text{HCN}\{2,6\text{-}i\text{Pr}_2\text{C}_6\text{H}_3\})_2\text{C}]\text{Y}(\text{N}\{\text{SiMe}_3\}_2)_3$ precatalyst [155]. Most recently, the Crimmin group have reported the extension of such reactivity to the coupling of alanes with amines mediated by the simple yttrium amide, $[\text{Y}(\text{N}\{\text{SiMe}_3\}_2)_3]$ [156].

Extension of this reactivity to less acidic E–H bonds has proved more challenging, with limited reports of Si–H/C–H dehydrocoupling. An initial, elegant study from the Tilley group achieved the striking result of dehydrogenative silylation of methane, albeit at 150 bar and 80 °C over the course of days. This fascinating result was proposed to be a result of a purely σ -bond metathesis pathway, albeit via a scandium silyl-mediated deprotonation of methane reminiscent of the reactivity proposed by Harder for Group 2 mediated hydrosilylation of alkenes (*vide supra*), as summarised in Fig. 1.15 [157].

Building on this initial result, Hou and co-workers were able to dehydrogenatively silylate the privileged directed-*ortho*-metallation substrate, anisole alongside a range of derivatives, under far less forcing conditions. This transformation relied upon a scandium half-sandwich complex of the form $[(\text{C}_5\text{Me}_4\text{SiMe}_2\text{N}t\text{Bu})\text{Sc}(\text{CH}_2\text{SiMe}_3)(\text{THF})]$ and was judged to occur via the generalised catalytic manifold proposed in Scheme 1.15 [158]. The extension of such reactivity to the

Fig. 1.15 The mechanism for dehydrogenative methane silylation proposed by Tilley and co-workers for a scandium half-sandwich complex



ylide, Ph_3PCH_2 , was investigated by Crimmin and co-workers who noted a key metal dependence in the reaction. Whilst $[\text{Y}(\text{N}\{\text{SiMe}_3\}_2)_3]$ competently dehydrocoupled phenylsilane with this ylide, to yield $\text{Ph}_3\text{PC}(\text{H})\text{Si}(\text{H})_2\text{Ph}$ both **IIIb** and $[\text{M}(\text{N}\{\text{SiMe}_3\}_2)]$ ($\text{M} = \text{Li}, \text{Na}, \text{K}$) were unable to do so. These workers went on to extensively investigate the possible mechanism of this reactivity and settled upon a Si–H/C–H σ -bond metathesis operant directly upon the ylide $-\text{CH}_2$ fragment [159].

Subsequent to their initial reports, Harrod and co-workers went on to describe the titanocene(III) mediated dehydrocoupling of phosphines with silanes. This reaction was once again proposed to occur via an all- σ -bond metathesis pathway, although the authors were unable to discern between Si–H or P–H protonolysis implicating a titanocene-silyl or -phosphide intermediate respectively [160]. Waterman and co-workers went on to explore similar reactivity with a trisamidoamine supported zirconium complex which was found to be active for both Si–H/P–H and Ge–H/P–H dehydrocoupling. In this case, although the group invoked a purely σ -bond metathesis mediated pathway, ligand activation by the intermediate LZrH yielded a cyclometallated species which was judged to mediate the P–H deprotonation to yield an intermediate zirconium phosphide (vide infra) [161].

Building upon their report of Si–H/P–H heterodehydrocoupling, the Waterman group subsequently reported a P–H homodehydrocoupling, once again mediated by their trisamidoamine zirconium(IV) complex [162]. A mechanism contingent upon a purely σ -bond metathesis manifold, albeit with ligand involvement being necessary, was again proposed (Fig. 1.16).

Subsequent work extended this reactivity to intramolecular and cascade reactivity of diphosphines [163]. Further credence for the importance of the ligand involvement was given in a comparative study performed by this group into zirconocene mediated P–H homodehydrocoupling which found the majority of zirconocene(IV) precatalysts to be inactive, with the exception of a $[\text{Cp}^*_2\text{ZrH}_3]^-$ complex, initially studied by Stephan and co-workers, appearing to follow an alternative mechanistic pathway (vide infra) [164]. P–H homodehydrocoupling was then expanded to include p-block elements by the work of Wright and co-workers

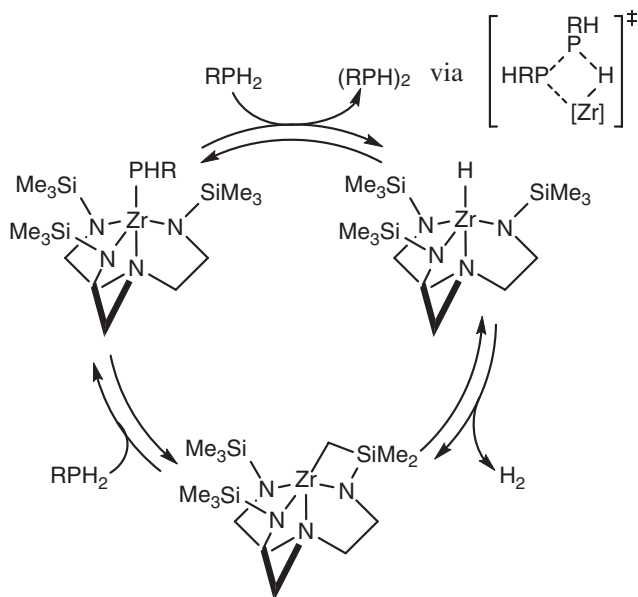


Fig. 1.16 The trisamidoamine-zirconium(IV) mediated dehydrocoupling of phosphines proposed, by Waterman and co-workers, proposed to occur via a σ -bond metathesis mechanism

who found $\text{Cp}^*_2\text{SnCl}_2$ to be a competent catalyst for the dehydrocoupling of primary phosphines to both diphosphanes and, via a further dehydrocoupling, *cyclo*-tetraphosphines [165].

The Waterman group subsequently turned their attention to the homodehydrocoupling of the heavier Group 15 congeners. The mechanistic landscape for arsine dehydrocoupling begins to show more nuanced behaviour. Once again exploiting their zirconium(IV) trisamidoamine complex, diphenylarsine was readily dehydrocoupled to yield $\text{Ph}_2\text{AsAsPh}_2$ and this group attributed such reactivity to the mechanism previously proposed for both Si–H/P–H hetero- and P–H homo-dehydrocoupling (Fig. 1.16) [145]. In contrast, the move to primary arsines yielded divergent results. The very bulky 2,6-dimesitylphenylarsine (dmpAsH_2) yielded the multiply-bonded dimer $\text{dmpAs}=\text{Asdmp}$ while its less sterically demanding counterpart MesAsH_2 yielded *cyclo*-(MesAs)₄. Detailed mechanistic investigations, including deuteration and trapping experiments with Me_3P implicated the intermediacy of an arsinidene fragment of the form RAs : which undergoes spontaneous dimer- or tetramerisation. The formation of this fragment was postulated to occur via an α -arsinidene elimination, which also yielded a LZrH intermediate rendering the reaction catalytic (Fig. 1.17) [166].

Such a mechanistic implication has limited precedent in heavier main group dehydrocoupling mediated by redox-inactive catalysis. Work by Tilley and co-workers upon zirconocene(IV) mediated dehydrogenative stannane coupling was initially thought to occur via a σ -bond metathesis pathway, analogous to that

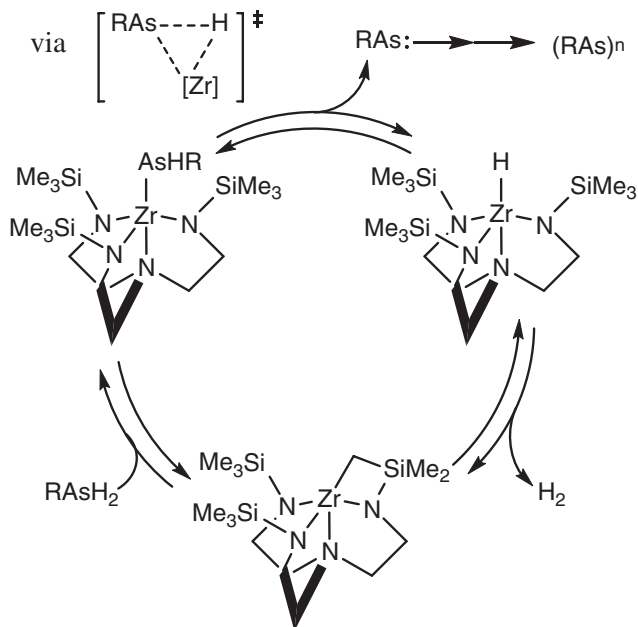


Fig. 1.17 The trisamidoamine-zirconium(IV) mediated dehydrocoupling of primary arsines proposed, by Waterman and co-workers, to occur via a α -arsinidene elimination mechanism

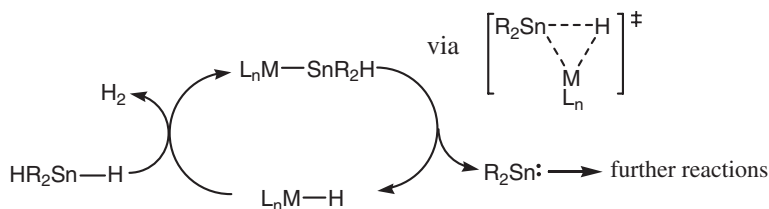


Fig. 1.18 The α -stannylene elimination mechanism for metallocene mediated dehydrocoupling of stannanes to yield poly(stannanes) and dihydrogen proposed by Tilley and co-workers

proposed for the poly(silane) congeners [167]. Subsequent mechanistic investigations on both an isolated d0 hafnium hydrostannyl complex and the catalytic dehydrocoupling of stannanes mediated by a hafnocene(IV) complex implicated an α -stannylene elimination as shown in Fig. 1.18 [168].

Notably, a hafnium(IV) triphenylstannyl complex showed analogous reactivity yielding a distannane and hafnium(IV) phenyl complex via an aryl migration, implying that redox inactive cross-metatheses beyond dehydrocoupling may implicate such an α -elimination pathway [169].

Such reactivity has also been observed by Tilley and Waterman for the heaviest Group 15 congener investigated, antimony. Both MesSbH_2 and dmpSbH_2

underwent dehydrocoupling in the presence of a hafnocene(IV) complex to yield the analogous products as observed for arsenic (*vide supra*). Extensive kinetic analysis by these authors allowed them to once again implicate α -stibinidene elimination in such reactivity [170].

Whilst a large variety of precatalysts have been suggested to mediate P–H homodehydrocoupling via a σ -bond only cross metathesis pathway, work by Stephan and co-workers has implicated alternative reactive intermediates in such reactivity mediated by titanium(IV) half-sandwich complexes alongside zirconocene(IV) derivatives [164, 171]. In these cases oligomerisation of primary phosphines yielded a variety of $(RP)_n$ compounds, with n showing a marked dependence on the nature, most notably the steric demands, of R; substituted phenyl substituents tend towards $n = 5$ while the more demanding naphthyl derivatives yield tetramers [172, 173]. The precatalysts in each of these reactions were possessed of at least 2 reactive ligand fragments and analysis of the ^{31}P NMR spectrum indicated the intermediacy of a zirconium phosphinidene, as shown in Fig. 1.19 [171].

One final mechanistic class for dehydrocoupling mediated by redox inactive catalysts has recently been described by the Stephan group. The use of highly electrophilic phosphonium cations of the form $[(\text{C}_6\text{F}_5)_3\text{PF}][\text{B}(\text{C}_6\text{F}_5)_4]$ has allowed not only dehydrocoupling of a wide range of protic E–H bonds with silanes (with Si–H/N–H, S–H and O–H being described) but also transfer hydrogenation from such systems. Extensive experimental and computational investigations allowed this group to propose a mechanism for such dehydrocouplings which is summarised in Fig. 1.20 [174].

This mechanism is reminiscent of FLP chemistry, with the highly electrophilic phosphorus centre interacting with the silane Si–H bond to render the silane amenable to nucleophilic attack. This step yields an ammonium cation in the presence

Fig. 1.19 The proposed mechanism for $[\text{Cp}^*_2\text{ZrH}_3]^-$ mediated dehydrocoupling of mono-substituted phosphines put forward by Stephan and co-workers implicating a zirconium-phosphinidene intermediate

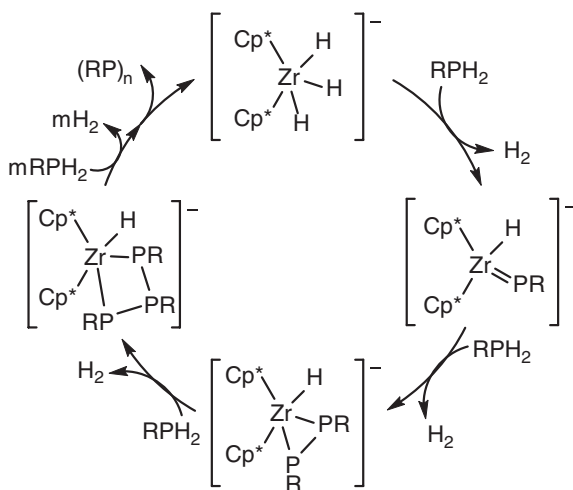
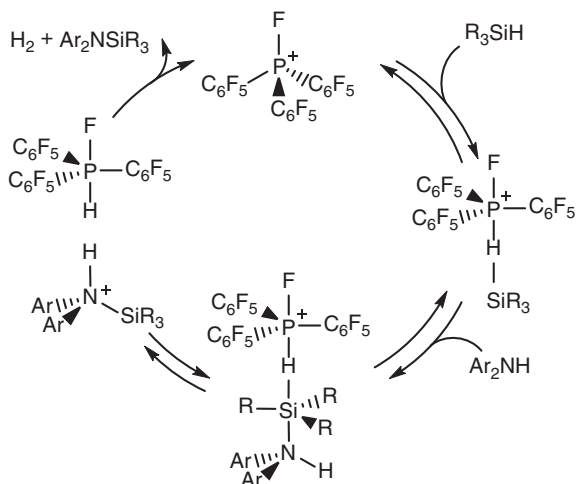


Fig. 1.20 The mechanistic proposal for electrophilic phosphonium cation mediated silicon-nitrogen dehydrocoupling proposed by Stephan and co-workers



of an acidic P(V)–H bond, the interaction of which yields the product silylamine, dihydrogen and reforms the electrophilic phosphonium cation upon which the reactivity is contingent.

1.5 Aims of This Project

As shown, extensive mechanistic investigations into the synthetic utility and mechanistic nuances of Group 2 mediated hydroamination have been undertaken. Furthermore, a plethora of redox-inactive dehydrocoupling mechanisms have been described for many elements other than Group 2. As a result, the aims of this thesis are to investigate the synthetic utility of σ -bond metathesis with Group 2 complexes, to extend the understanding of Group 2 mediated dehydrocoupling and to advance the state of Group 2 mediated reactivity by coupling σ -bond metathesis to hitherto unprecedented steps in catalysis. These investigations will rely upon a combination of synthetic and mechanistic investigations utilising crystallographic determination of solid state structure, NMR analysis of solution structure and kinetic investigations to yield mechanistic insight.

Chapter 2 of this thesis explores the structure in the solid-state and solution of a series of mixed metal Group 1-Group 2 amidoalkyls of the form $[\text{M}(\text{N}\{\text{SiMe}_3\}_2)_2\text{MgBu}]$ ($\text{M} = \text{Li}$ (**1**), Na (**2**), K (**3**)). Subsequent investigation of the reactivity of these species with phenylsilane yield an intractable white solid, a structurally unprecedented heterododecametallic octaamide decahydride of the form $[\text{Na}_6\text{Mg}_6\{\text{N}(\text{SiMe}_3)_2\}_8\text{H}_{10}]$ (**5**), and a more simple bridged bimetallic diamido hydride dimer of the form $[\text{K}\{\text{N}(\text{SiMe}_3)_2\}_2\text{MgH}]_2$ (**4**) respectively. The solid state and solution structures of these latter species were thus investigated.

Chapter 3 contains an in-depth exploration of silicon-nitrogen dehydrocoupling mediated by a set of Group 2 bis(amide) precatalysts, $[M(N\{SiMe_3\}_2)_2]_2$ ($M = Mg, Ca, Sr$. **IIa-c**). A scope study indicated rapid dehydrocoupling gives insight into both steric and electronic effects in this reaction, whilst a number of stoichiometric reactions give insight into the mechanism of this reaction. Finally, an extensive kinetic study on the dehydrocoupling of diethylamine and diphenylsilane highlights intriguing congeneric variations down Group 2. Further explored is a preliminary investigation into tin-nitrogen coupling which is found to yield distannanes via a protonolysis of the incipient stannylamine and can be rendered catalytic in amine.

Chapter 4 investigates the effect of hydridic coupling partner upon silicon-nitrogen and, boron-nitrogen dehydrocoupling mediated by the well defined β -diketiminato supported magnesium centre, **Ib**. An initial scope study suggests a rapid and efficacious route to aminoboranes and further indicates significant effects when varying both the hydridic partner from pinacol(borane) to 9-BBN and a range of phenylsilanes alongside a range of amines. A stoichiometric study indicates these variations in hydridic partner yield distinctly different reaction pathways and an extensive kinetic study provides further support for this, as well as revealing putative reaction mechanisms.

Chapter 5 explores the addition of single electron transfer steps to Group 2 mediated catalytic cycles. An initial stoichiometric study into the activity of the stable radical TEMPO upon a range of magnesium alkyl and hydride species (dibutylmagnesium, **Ib** and **Ih**) indicates SET activity which yields radical coupling of metal bound fragments and, notably, structurally characterised TEMPOxide anions bound to magnesium. The activity of silanes upon magnesium TEMPOxides is then shown to yield TEMPO silyl ethers and incipient metal hydrides via σ -bond metathesis, allowing access to a dehydrogenative coupling manifold, the first report of SET steps in Group 2 mediated catalysis. Finally, an initial structural study into the “chameleonic” nature of TEMPO versus TEMPOxide ligands yields the first report of a metal-bound mixed valence oxygen species which, via ligand non-innocence shows potential spin delocalization.

References

1. A. Yaroshevsky, *Geochem. Int.* **44**, 48 (2006)
2. S.P. Green, C. Jones, A. Stasch, *Science*, **318**, 1754 (2007); M. Westerhausen, *Angew. Chem. Int. Ed.* **47**, 2185 (2008)
3. S. Krieck, H. Görls, L. Yu, M. Reiher, M. Westerhausen, *J. Am. Chem. Soc.* **131**, 2977 (2009)
4. R.D. Shannon, *Acta Crystallogr. Sect. A* **32**, 751 (1976)
5. M.H. Chisholm, J. Gallucci, K. Phomphrai, *Chem. Commun.* **48** (2003); M.H. Chisholm, J.C. Gallucci, K. Phomphrai, *Inorg. Chem.* **43**, 6717 (2004)
6. S. Sarish, S. Nembenna, S. Nagendran, H.W. Roesky, A. Pal, R. Herbst-Irmer, A. Ringe, J. Magull, *Inorg. Chem.* **47**, 5971 (2008)
7. A.G.M. Barrett, I.J. Casely, M.R. Crimmin, M.S. Hill, J.R. Lachs, M.F. Mahon, P.A. Procopiou, *Inorg. Chem.* **48**, 4445 (2009)

8. M.R. Crimmin, M. Arrowsmith, A.G.M. Barrett, I.J. Casely, M.S. Hill, P.A. Procopiu, *J. Am. Chem. Soc.* **131**, 9670 (2009)
9. M. Arrowsmith, M.R. Crimmin, A.G.M. Barrett, M.S. Hill, G. Kociok-Köhn, P.A. Procopiu, *Organometallics* **30**, 1493 (2011)
10. C. Jones, S.J. Bonyhady, S. Nembenna, A. Stasch, *Eur. J. Inorg. Chem.* 2596 (2012)
11. J.F. Dunne, J. Su, A. Ellern, A.D. Sadow, *Organometallics* **27**, 2399 (2008)
12. J.F. Dunne, S.R. Neal, J. Engelkemier, A. Ellern, A.D. Sadow, *J. Am. Chem. Soc.* **133**, 16782 (2011)
13. M. Arrowsmith, M.S. Hill, G. Kociok-Köhn, *Organometallics* **30**, 1291 (2011)
14. J.S. Wixey, B.D. Ward, *Dalton Trans.* **40**, 7693 (2011)
15. S. Datta, P.W. Roesky, S. Blechert, *Organometallics* **26**, 4392 (2007)
16. S. Datta, M.T. Gamer, P.W. Roesky, *Organometallics* **27**, 1207 (2008)
17. A.G.M. Barrett, M.R. Crimmin, M.S. Hill, P.B. Hitchcock, G. Kociok-Köhn, P.A. Procopiu, *Inorg. Chem.* **47**, 7366 (2008)
18. B. Liu, T. Roisnel, J.-F. Carpentier, Y. Sarazin, *Angew. Chem. Int. Ed.* **51**, 4943 (2012)
19. B.A. Vaartstra, J.C. Huffman, W.E. Streib, K.G. Caulton, *Inorg. Chem.* **30**, 121 (1991)
20. M. Westerhausen, M. Hartmann, N. Makropoulos, B. Wieneke, M. Wieneke, W. Schwarz, D. Stalke, *Z. Naturforsch. B: Chem. Sci.* **53**, 117 (1998)
21. M.R. Crimmin, A.G.M. Barrett, M.S. Hill, D.J. MacDougall, M.F. Mahon, P.A. Procopiu, *Chem. Eur. J.* **14**, 11292 (2008)
22. M. Arrowsmith, M.S. Hill, G. Kociok-Köhn, *Organometallics* **29**, 4203 (2010)
23. S. Hong, T.J. Marks, *Acc. Chem. Res.* **37**, 673 (2004); A. Molander, J.A.C. Romero, *Chem. Rev.* **102**, 2161 (2002)
24. R. Anwander, *Lanthanide Amides* (Springer, Berlin, 1996)
25. J. Barluenga, F. Aznar, R. Liz, R. Rodes, *J. Chem. Soc. Perkin Trans.* 2732 (1980)
26. P.J. Walsh, A.M. Baranger, R.G. Bergman, *J. Am. Chem. Soc.* **114**, 1708 (1992)
27. D.R. Coulson, *Tetrahedron Lett.* **12**, 429 (1971)
28. A.L. Casalnuovo, J.C. Calabrese, D. Milstein, *J. Am. Chem. Soc.* **110**, 6738 (1988)
29. J.J. Brunet, D. Neibecker, K. Philippot, *Tetrahedron Lett.* **34**, 3877 (1993)
30. Y.W. Li, T.J. Marks, *Organometallics* **15**, 3770 (1996)
31. M.R. Gagné, T.J. Marks, *J. Am. Chem. Soc.* **111**, 4108 (1989)
32. S.W. Hong, S. Tian, M.V. Metz, T.J. Marks, *J. Am. Chem. Soc.* **125**, 14768 (2003)
33. S.D. Wobser, C.J. Stephenson, M. Delferro, T.J. Marks, *Organometallics* **32**, 1317 (2013)
34. B.D. Stubbert, T.J. Marks, *J. Am. Chem. Soc.* **129**, 4253 (2007)
35. X.H. Yu, S. Seo, T.J. Marks, *J. Am. Chem. Soc.* **129**, 7244 (2007)
36. A. Dzudza, T.J. Marks, *Org. Lett.* **11**, 1523 (2009)
37. P.W. Roesky, U. Denninger, C.L. Stern, T.J. Marks, *Organometallics* **16**, 4486 (1997)
38. A. Motta, I.L. Fragala, T.J. Marks, *Organometallics* **24**, 4995 (2005)
39. A.M. Kawaoka, M.R. Douglass, T.J. Marks, *Organometallics* **22**, 4630 (2003)
40. S.Y. Seo, X.H. Yu, T.J. Marks, *J. Am. Chem. Soc.* **131**, 263 (2009)
41. S. Hong, A.M. Kawaoka, T.J. Marks, *J. Am. Chem. Soc.* **125**, 15878 (2003)
42. M.R. Douglass, C.L. Stern, T.J. Marks, *J. Am. Chem. Soc.* **123**, 10221 (2001)
43. C.J. Weiss, S.D. Wobser, T.J. Marks, *Organometallics* **29**, 6308 (2010)
44. A. Dzudza, T.J. Marks, *J. Org. Chem.* **73**, 4004 (2008)
45. S. Seo, T.J. Marks, *Chem. Eur. J.* **16**, 5148 (2010)
46. C.J. Weiss, T.J. Marks, *Dalton Trans.* **39**, 6576 (2010)
47. A.M. Seyam, B.D. Stubbert, T.R. Jensen, J.J. O'Donnell, C.L. Stern, T.J. Marks, *Inorg. Chim. Acta* **357**, 4029 (2004)
48. A. Motta, I.L. Fragala, T.J. Marks, *Organometallics* **25**, 5533 (2006)
49. V.M. Arredondo, S. Tian, F.E. McDonald, T.J. Marks, *J. Am. Chem. Soc.* **121**, 3633 (1999)
50. Y.W. Li, T.J. Marks, *J. Am. Chem. Soc.* **120**, 1757 (1998)
51. J.S. Ryu, T.J. Marks, F.E. McDonald, *J. Org. Chem.* **2004**, 69 (1038)
52. A.M. Kawaoka, T.J. Marks, *J. Am. Chem. Soc.* **127**, 6311 (2005)

53. J.S. Ryu, G.Y. Li, T.J. Marks, *J. Am. Chem. Soc.* **125**, 12584 (2003)
54. X.H. Yu, T.J. Marks, *Organometallics* **26**, 365 (2007)
55. L. Jia, X.M. Yang, A.M. Seyam, I.D.L. Albert, P.F. Fu, S.T. Yang, T.J. Marks, *J. Am. Chem. Soc.* **118**, 7900 (1996)
56. S. Seo, X.H. Yu, T.J. Marks, *Tetrahedron Lett.* **2013**, 54 (1828)
57. G. Jeske, H. Lauke, H. Mauermann, H. Schumann, T.J. Marks, *J. Am. Chem. Soc.* **107**, 8111 (1985)
58. G. Jeske, H. Lauke, H. Mauermann, P.N. Swepston, H. Schumann, T.J. Marks, *J. Am. Chem. Soc.* **107**, 8091 (1985)
59. A.S. Dudnik, V.L. Weidner, A. Motta, M. Delferro, T.J. Marks, *Nat. Chem.* (2014). doi:[10.1038/nchem.2087](https://doi.org/10.1038/nchem.2087)
60. J.-M. Begouin, M. Niggemann, *Chem. Eur. J.* **19**, 8030 (2013)
61. M. Westerhausen, S. Schneiderbauer, A.N. Kneifel, Y. Soltl, P. Mayer, H. Nöth, Z.Y. Zhong, P.J. Dijkstra, J. Feijen, *Eur. J. Inorg. Chem.* 3432 (2003)
62. Y. Sarazin, R.H. Howard, D.L. Hughes, S.M. Humphrey, M. Bochmann, *Dalton Trans.* 340 (2006)
63. M.G. Davidson, C.T. O'Hara, M.D. Jones, C.G. Keir, M.F. Mahon, G. Kociok-Köhn, *Inorg. Chem.* **46**, 7686 (2007)
64. W. Vargas, K. Ruhlandt-Senge. *Eur. J. Inorg. Chem.* 3472 (2003)
65. D.J. Burke, T.P. Hanusa, *Organometallics* **15**, 4971 (1996)
66. D.C. Green, U. Englich, K. Ruhlandt-Senge, *J. Chem. Ed.* **38**, 354 (1999)
67. A.G.M. Barrett, M.R. Crimmin, M.S. Hill, P.B. Hitchcock, S.L. Lomas, M.F. Mahon, P.A. Procopiu, K. Suntharalingam, *Organometallics* **27**, 6300 (2008)
68. M. Westerhausen, M.H. Digeser, M. Krofta, N. Wiberg, H. Nöth, J. Knizek, W. Ponikwar, T. Seifert, *Eur. J. Inorg. Chem.* 743 (1999)
69. A.G. Avent, M.R. Crimmin, M.S. Hill, P.B. Hitchcock, *Organometallics* **24**, 1184 (2005)
70. M. Westerhausen, M.H. Digeser, B. Wieneke, H. Nöth, J. Knizek, *Eur. J. Inorg. Chem.* 517 (1998)
71. M. Westerhausen, C. Birg, M. Krofta, P. Mayer, T. Seifert, H. Nöth, A. Pfitzner, T. Nilges, H.J. Deiseroth, *Z. Anorg. Allg. Chem.* **626**, 1073 (2000)
72. M. Westerhausen, M.H. Digeser, H. Nöth, J. Knizek, *Z. Anorg. Allg. Chem.* **624**, 215 (1998)
73. S.E. Baillie, V.L. Blair, T.D. Bradley, W. Clegg, J. Cowan, R.W. Harrington, A. Hernan. R. Kennedy, Z. Livingstone, E. Hevia, *Chem. Sci.* **4**, 1895 (2013)
74. M. Westerhausen, M.H. Digeser, W. Schwarz, *Inorg. Chem.* **36**, 521 (1997)
75. M. Westerhausen, M.H. Digeser, H. Nöth, W. Ponikwar, T. Seifert, K. Polborn, *Inorg. Chem.* **38**, 3207 (1999)
76. M. Westerhausen, M.H. Digeser, C. Guckel, H. Nöth, J. Knizek, W. Ponikwar, *Organometallics* **18**, 2491 (1999)
77. M. Westerhausen, H.D. Hausen, W. Schwarz, *Z. Anorg. Allg. Chem.* **618**, 121 (1992)
78. M. Westerhausen, H.D. Hausen, *Z. Anorg. Allg. Chem.* **615**, 27 (1992)
79. A. Weeber, S. Harder, H.H. Brintzinger, K. Knoll, *Organometallics* **19**, 1325 (2000)
80. F. Feil, S. Harder, *Organometallics* **19**, 5010 (2000)
81. F. Feil, S. Harder, *Organometallics* **20**, 4616 (2001)
82. S. Harder, F. Feil, A. Weeber, *Organometallics* **2001**, 20 (1044)
83. M.R. Crimmin, I.J. Casely, M.S. Hill, *J. Am. Chem. Soc.* **127**, 2042 (2005)
84. J.E. Baldwin, *J. Chem. Soc. Commun.* 734 (1976)
85. M. Arrowsmith, M.S. Hill, G. Kociok-Köhn, *Organometallics* **28**, 1730 (2009)
86. M.E. Jung, G. Piizzi, *Chem. Rev.* **105**, 1735 (2005)
87. X. Zhang, T.J. Emge, K.C. Hultzs, *Organometallics* **29**, 5871 (2010)
88. C. Brinkmann, A.G.M. Barrett, M.S. Hill, P.A. Procopiu, *J. Am. Chem. Soc.* **134**, 2193 (2012)
89. A.G.M. Barrett, C. Brinkmann, M.R. Crimmin, M.S. Hill, P. Hunt, P.A. Procopiu, *J. Am. Chem. Soc.* **131**, 12906 (2009)

90. B. Liu, T. Roisnel, J.-F. Carpentier, Y. Sarazin, *Chem. Eur. J.* **19**, 2784 (2013)
91. B. Liu, T. Roisnel, J.-F. Carpentier, Y. Sarazin, *Chem. Eur. J.* **19**, 13445 (2013)
92. F. Buch, S. Harder, *Z. Naturforsch. B: Chem. Sci.* **63**, 169 (2008)
93. J.S. Wixey, B.D. Ward, *Chem. Commun.* **47**, 5449 (2011)
94. T.D. Nixon, B.D. Ward, *Chem. Commun.* **48**, 11790 (2012)
95. M.R. Crimmin, A.G.M. Barrett, M.S. Hill, P.B. Hitchcock, P.A. Procopiou, *Organometallics* **26**, 2953 (2007)
96. T.M.A. Görls, M. Westerhausen, *Inorg. Chem. Commun.* **11**, 1419 (2008)
97. B. Liu, J.-F. Carpentier, Y. Sarazin, *Chem. Eur. J.* **18**, 13259 (2012)
98. M.R. Crimmin, A.G.M. Barrett, M.S. Hill, P.B. Hitchcock, P.A. Procopiou, *Organometallics* **27**, 497 (2008)
99. J.R. Lachs, A.G.M. Barrett, M.R. Crimmin, G. Kociok-Köhn, M.S. Hill, M.F. Mahon, P.A. Procopiou, *Eur. J. Inorg. Chem.* 4173 (2008)
100. A. Baishya, M.K. Barman, T. Peddarao, S. Nembenna, *J. Organomet. Chem.* **769**, 112 (2014)
101. A.G.M. Barrett, M.R. Crimmin, M.S. Hill, P.B. Hitchcock, S.L. Lomas, M.F. Mahon, P.A. Procopiou, *Dalton Trans.* **39**, 7393 (2010)
102. M. Arrowsmith, M.R. Crimmin, M.S. Hill, S.L. Lomas, M.S. Heng, P.B. Hitchcock, G. Kociok-Köhn, *Dalton Trans.* **43**, 14249 (2014)
103. L. Orzechowski, S. Harder, *Organometallics* **26**, 2144 (2007)
104. Q. Liu, Z. Guo, H. Han, H. Tong, X. Wei, *Polyhedron* **85**, 15 (2015)
105. A.G.M. Barrett, T.C. Boorman, M.R. Crimmin, M.S. Hill, G. Kociok-Köhn, P.A. Procopiou, *Chem. Commun.* 5206 (2008)
106. T.M.A. Al, K. Palfi, L.A. Yu, R. Kretschmer, K. Wimmer, R. Fischer, H. Görls, M. Reiher, M. Westerhausen, *J. Organomet. Chem.* **696**, 216 (2011)
107. S. Härling, J. Greiser, T.M.A. Al-Shboul, H. Görls, S. Kriek, M. Westerhausen, *Aus. J. Chem.* **66**, 1264 (2013)
108. F. Buch, H. Brettar, S. Harder, *Angew. Chem. Int. Ed.* **45**, 2741 (2006)
109. V. Leich, T.P. Spaniol, L. Maron, J. Okuda, *Chem. Commun.* **50**, 2311 (2014)
110. S. Harder, J. Spielmann, *J. Organomet. Chem.* **698**, 7 (2012)
111. S. Harder, J. Brettar, *Angew. Chem. Int. Ed.* **45**, 3474 (2006)
112. S.P. Green, C. Jones, A. Stasch, *Angew. Chem. Int. Ed.* **47**, 9079 (2008)
113. S.J. Bonyhady, C. Jones, S. Nembenna, A. Stasch, A.J. Edwards, G.J. McIntyre, *Chem. Eur. J.* **16**, 938 (2010)
114. M. Arrowsmith, M.S. Hill, D.J. MacDougall, M.F. Mahon, *Angew. Chem. Int. Ed.* **48**, 4013 (2009)
115. S. Harder, J. Spielmann, J. Intemann, H. Bandmann, *Angew. Chem.* **123**, 4242 (2011); J. Intemann, J. Spielmann, P. Sirsch, S. Harder, *Chem. Eur. J.* **19**, 8478 (2013)
116. S. Harder, *Chem. Rev.* **110**, 3852 (2010)
117. J. Spielmann, S. Harder, *Chem. Eur. J.* **13**, 8928 (2007)
118. S. Harder, *Chem. Commun.* **48**, 11165 (2012)
119. J. Spielmann, S. Harder, *Eur. J. Inorg. Chem.* 1480 (2008)
120. J. Spielmann, G. Jansen, H. Bandmann, S. Harder, *Angew. Chem. Int. Ed.* **47**, 6290 (2008)
121. S.J. Bonyhady, S.P. Green, C. Jones, S. Nembenna, A. Stasch, *Angew. Chem. Int. Ed.* **48**, 2973 (2009)
122. M.S. Hill, D.J. MacDougall, M.F. Mahon, *Dalton Trans.* **39**, 11129 (2010)
123. M. Arrowsmith, M.S. Hill, T. Hadlington, G. Kociok-Köhn, C. Weetman, *Organometallics* **30**, 5556 (2011)
124. J. Intemann, M. Lutz, S. Harder, *Organometallics* (2014). doi:[10.1021/om500469h](https://doi.org/10.1021/om500469h)
125. M. Arrowsmith, T.J. Hadlington, M.S. Hill, G. Kociok-Köhn, *Chem. Commun.* **48**, 4567–4569 (2012)
126. C.E. Weetman, M.D. Anker, M. Arrowsmith, M.S. Hill, D.J. Liptrot, M.F. Mahon, G. Kociok-Köhn, *Chem. Sci.*, submitted

127. M.D. Anker, M. Arrowsmith, P. Bellham, M.S. Hill, G. Kociok-Köhn, D.J. Liptrot, M.F. Mahon, C. Weetman, *Chem. Sci.* **5**, 2826 (2014)
128. A. Berkefeld, W.E. Piers, M. Parvez, L. Castro, L. Maron, O. Eisenstein, *Chem. Sci.* **4**, 2152 (2013)
129. A. Stasch, *Angew. Chem. Int. Ed.* **38**, 10200 (2014)
130. C.E. Kefalidis, A. Stasch, C. Jones, L. Maron, *Chem. Commun.* **50**, 12318 (2014)
131. M.T. Ma, A. Stasch, C. Jones, *Chem. Eur. J.* **18**, 10669 (2012)
132. C. Jones, L. McDyre, D.M. Murphy, A. Stasch, *Chem. Commun.* **46**, 1511 (2010)
133. F. Buch, S. Harder, *Organometallics* **26**, 5132 (2007)
134. M.S. Hill, M.F. Mahon, T.P. Robinson, *Chem. Commun.* **46**, 2498 (2010)
135. A.G.M. Barrett, M.R. Crimmin, M.S. Hill, P.B. Hitchcock, P.A. Procopiou, *Organometallics* **26**, 4076 (2007)
136. A. Staubitz, A.P.M. Robertson, M.E. Sloan, I. Manners, *Chem. Rev.* **110**, 4023 (2010)
137. E.M. Leitao, T. Jurca, I. Manners, *Nat. Chem.* **5**, 817 (2013)
138. R. Waterman, *Chem. Soc. Rev.* **42**, 5629 (2013)
139. J. Spielmann, G. Jansen, H. Bandmann, S. Harder, *Angew. Chem. Int. Ed.* **47**, 6290 (2008); J. Spielmann, D.F.J. Piesik, S. Harder, *Chem. Eur. J.* **16**, 8307 (2010); J. Spielmann, S. Harder, *Dalton Trans.* **40**, 8314 (2011)
140. J. Spielmann, S. Harder, *J. Am. Chem. Soc.* **131**, 5064 (2009); J. Spielmann, M. Bolte, S. Harder, *Chem. Commun.* 6934 (2009)
141. C. Jones, S.J. Bonyhady, S. Nembenna, A. Stasch, *Eur. J. Inorg. Chem.* 2596 (2012)
142. M.S. Hill, M. Hodgson, D.J. Liptrot, M.F. Mahon, *Dalton Trans.* **40**, 7783 (2011)
143. P. Bellham, M.S. Hill, D.J. Liptrot, D.J. MacDougall, M.F. Mahon, *Chem. Commun.* **47**, 9060 (2011); P. Bellham, M. S. Hill, G. Kociok-Köhn, D.J. Liptrot, *Dalton Trans.* **42**, 737 (2013); P. Bellham, M. S. Hill, G. Kociok-Köhn, D.J. Liptrot, *Chem. Commun.* **49**, 1960 (2013)
144. M.S. Hill, G. Kociok-Köhn, T.P. Robinson, *Chem. Commun.* **46**, 7587 (2010)
145. R. Waterman, *Organometallics* **32**, 7249 (2013)
146. T.J. Clark, K. Lee, I. Manners, *Chem. Eur. J.* **12**, 8634 (2006)
147. R.J. Less, R.L. Melen, D.S. Wright, *RSC Adv.* **2**, 2191 (2012)
148. C. Aitken, J.F. Harrod, E. Samuel, *J. Organomet. Chem.* **279**, C11 (1985)
149. J.F. Harrod, Y. Mu, E. Samuel, *Polyhedron* **10**, 1239–1245 (1991)
150. J.Y. Corey, *Adv. Organomet. Chem.* **51**, 1 (2004)
151. T.D. Tilley, *Acc. Chem. Res.* **26**, 22 (1993)
152. J.Y. Corey, *Chem. Rev.* **111**, 863 (2011)
153. J.F. Harrod, Y. Mu, E. Samuel, *Polyhedron* **10**, 1239 (1991)
154. F. Gauvin, J.F. Harrod, H.G. Woo, *Adv. Organomet. Chem.* **42**, 363 (1998)
155. W. Xie, H. Hu, C. Cui, *Angew. Chem. Int. Ed.* **51**, 11141 (2012)
156. A.E. Nako, S.J. Gates, N. Schadel, A.J.P. White, M.R. Crimmin, *Chem. Commun.* **50**, 9536 (2014)
157. A.D. Sadow, T.D. Tilley, *J. Am. Chem. Soc.* **127**, 643 (2004)
158. J. Oyamada, M. Nishiura, Z. Hou, *Angew. Chem. Int. Ed.* **50**, 10720 (2011)
159. A.E. Nako, A.J.P. White, M.R. Crimmin, *Chem. Sci.* **4**, 691 (2013)
160. R. Shu, L. Hao, J.F. Harrod, H. Woo, E. Samuel, *J. Am. Chem. Soc.* **120**, 12988 (1998)
161. A.J. Roering, S.N. MacMillan, J.M. Tanski, R. Waterman, *Inorg. Chem.* **46**, 6855 (2007)
162. R. Waterman, *Organometallics* **26**, 2492 (2007)
163. M.B. Ghebream, T. Shalumova, J.M. Tanski, R. Waterman, *Polyhedron* **29**, 42 (2010)
164. M.B. Ghebream, D.K. Newsham, R. Waterman, *Dalton Trans.* **40**, 7683 (2011)
165. V. Naseri, R.J. Less, R.E. Mulvey, M. McPartlin, D.S. Wright, *Chem. Commun.* **46**, 5000 (2010); K.A. Erickson, L.S.H. Dixon, D.S. Wright, R. Waterman, *Inorg. Chim. Acta* **422**, 141 (2014)
166. A.J. Roering, J.J. Davidson, S.N. MacMillan, J.M. Tanski, R. Waterman, *Dalton Trans.* 4488 (2008)

167. T. Imori, V. Lu, H. Cai, T.D. Tilley, *J. Am. Chem. Soc.* **117**, 9931 (1995)
168. N.R. Neale, T.D. Tilley, *J. Am. Chem. Soc.* **124**, 3802 (2002)
169. N.R. Neale, T.D. Tilley, *J. Am. Chem. Soc.* **127**, 14745 (2005)
170. R. Waterman, T.D. Tilley, *Angew. Chem. Int. Ed.* **45**, 2926 (2006)
171. M.C. Fermin, D.W. Stephan, *J. Am. Chem. Soc.* **117**, 12645 (1995)
172. N. Etkin, M.C. Fermin, D.W. Stephan, *J. Am. Chem. Soc.* **119**, 2954 (1997)
173. J.D. Masuda, A.J. Hoskin, T.W. Graham, C. Beddie, M.C. Fermin, N. Etkin, D.W. Stephan, *Chem. Eur. J.* **12**, 8696 (2006)
174. M. Pérez, C.B. Caputo, R. Dobrovetsky, D.W. Stephan, *Proc. Nat. Acad. Sci.* **111**, 10917 (2014)

Chapter 2

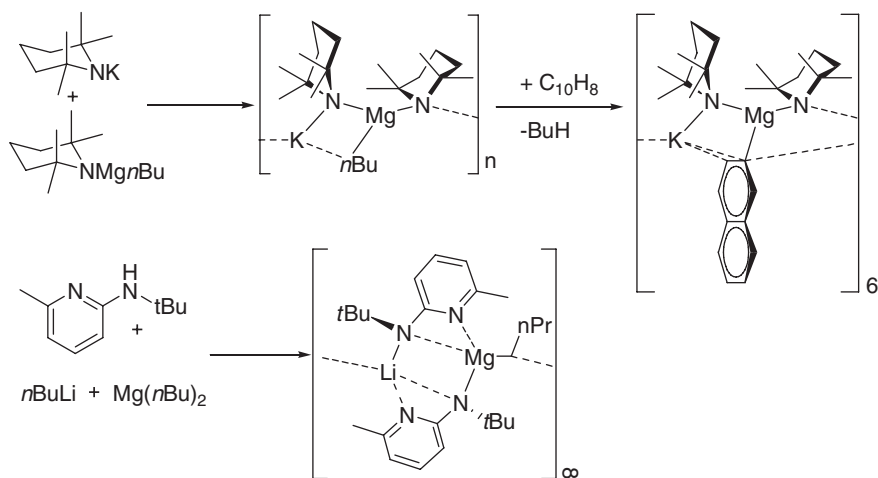
Group 1-Group 2 Bimetallic Alkyls and Hydrides

2.1 Introduction

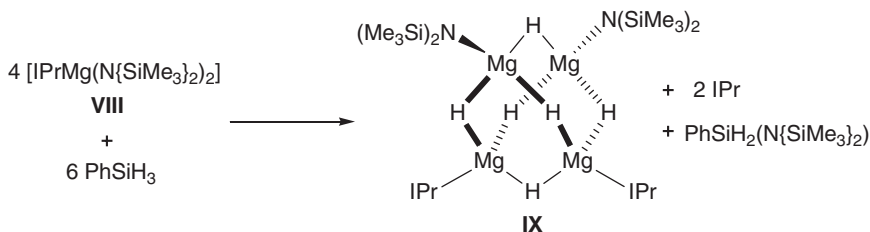
Main group heterobimetallic compounds are extremely common and encompass a variety of simple salts and cluster types. The interactions that dominate the coordination chemistry of the s-block metals in particular have yielded a huge variety of heterobimetallic complexes. These generally contain elements of the alkali- and alkaline earth-metals, or both, bridged by alkoxide, amide or halide ligands [1, 2].

The extension of this motif to more reactive carbanion and hydride ligands however is less common. Carbanion containing mixed Group 1-Group 2 heterobimetallics are dominated by metallocycle anion bridges, with a far more limited number of alkyl-, and aryl-terminated species reported, as shown in Scheme 2.1 [3, 4].

The structures of the early main group metal hydrides are dominated by saline species of the form MH_n (Group 1; $n = 1$, Group 2; $n = 2$) [5] wherein ionic or bridging structures yield extended networks. Recently, however, a variety of molecular Group 2 hydrides have been structurally characterised, spurred on by investigations into the postulated intermediacy of these species in a variety of H-C [6], Si-N [7], Si-O [8] and B-N [9] bond forming reactions. The lighter congeners of the saline s-block hydrides have, in spite of their structure, been identified as potential hydrogen storage materials as a result of their relatively high hydrogen weight percentages (LiH; 12.7 % [10], MgH_2 ; 7.6 % [11]). Utilisation of these species in this application is, however, hindered by their large lattice energies relative to the bulk metals, which require impractically high hydrogen release temperatures (LiH; 858 kJ mol^{-1} , MgH_2 ; 2791 kJ mol^{-1}). Recent calculations regarding magnesium hydride have suggested a reduction in cluster size of $(MgH_2)_n$ ($n < 19$) can lower these temperatures [12]. As a result, a variety of higher magnesium hydride clusters have been synthesised utilising a molecular approach; generally relying upon the reaction of organometallic complexes bearing reactive metal bound substituents with phenylsilane. The Hill group reported the first hydride-rich magnesium cluster, $[(IPr)_2Mg_4H_6\{N(SiMe_3)_2\}_2]$ ($IPr = ((HCN\{2,6-iPr_2C_6H_3\})_2C:) (IX)$) supported by bulky amides and N-heterocyclic carbene ligands with a magnesium to hydride ratio of 1:1.5 (Scheme 2.2) [13].



Scheme 2.1 Previously reported synthetic routes and crystallographically defined structures of heterobimetallic s-block clusters with alkyl or aryl substituents



Scheme 2.2 The synthetic route reliant upon σ -bond metathesis utilised by the Hill group to yield their record-breaking magnesium hydride cluster, IX

Subsequent work from the group of Harder has shown the utility of β -diketiminate ligands in the formation of higher magnesium hydrides yielding $[(\text{PARA})_3\text{Mg}_8\text{H}_{10}]$ ($\text{PARA} = 1,4\text{-C}_6\text{H}_4\{2,6\text{-}i\text{Pr}_2\text{C}_6\text{H}_3\text{NC}(\text{Me})\text{C}(\text{H})\text{C}(\text{Me})\text{N}\}_2$) [14] and $[\{\text{NN}(\text{MgH})_2\}_2]$ ($\text{NN} = \{2,6\text{-}i\text{Pr}_2\text{C}_6\text{H}_3\text{NC}(\text{Me})\text{C}(\text{H})\text{C}(\text{Me})\text{N}\}_2$) [15].

In contrast to this burgeoning body of work in Group 2 metal hydrides, structurally characterised molecular hydrides of Group 1 have proved more elusive (Fig. 2.1). Alongside the remarkable “superaggregate” $[(\text{tBuOLi})_{16}(\text{LiH})_{17}]$ [16], generated photolytically, only a relatively small number of molecular Group 1 hydrides have been synthesised by the rational application of a silane derivative to a reactive metal precursor. These are the bulky phosphinoamide (XI) and pyrazolate supported clusters described by Stasch [17, 18]. Instead, prior work in the field of Group 1 hydrides has been dominated by mixed metal “ate” structures, most notably the ‘inverse crowns’ $[\text{M}_2\text{Mg}_2(\text{Ni-Pr}_2)_4(\mu\text{-H})_2(\text{toluene})_2]$ ($\text{M} = \text{Na}$ (Xa), K (Xc)) [19, 20] reported by Mulvey and co-workers which are thought

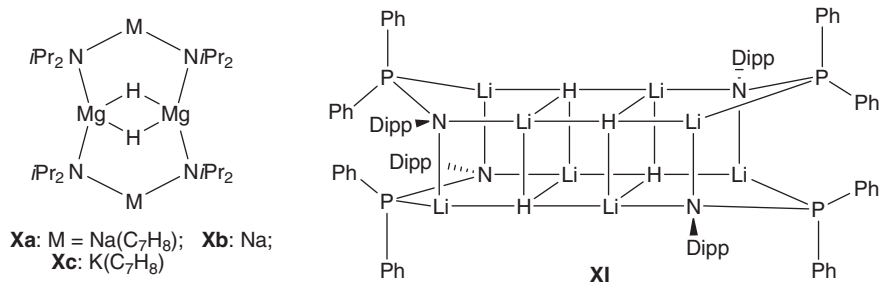
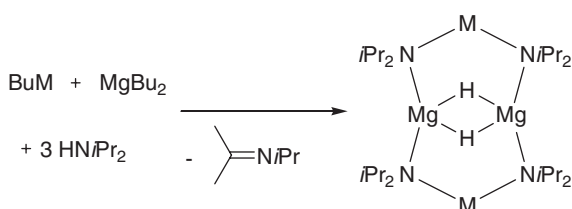


Fig. 2.1 The crystallographically defined structures of a heterobimetallic and homometallic *s*-block hydride cluster

Scheme 2.3 The proposed synthetic route to **Xa-c** via a β -hydride elimination

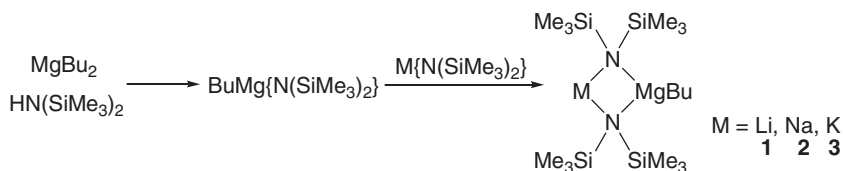


to form via a serendipitous β -hydride elimination from the Ni-Pr₂ ligands of the bimetallic trisamides [M(μ -NiPr₂)₂Mg(NiPr₂)], synthesized in situ, as shown in Scheme 2.3 [20].

2.2 *s*-Block Mixed Metal Amidoalkyls

Extensive work by Mulvey and co-workers has demonstrated the enhanced reactivity of heterobimetallic *s*-block amides of the form [M(μ -NR₂)₂M'(NR₂)] (M = Group 1 metal; M' = Group 2 metal) in a variety of contexts [1]. Seeking to capitalise on this foundation, an alternative synthetic approach to heterobimetallic hydrides may be envisaged based on mixed *s*-block amidoalkyls of the form [M{N(SiMe₃)₂}₂MgBu], [M = Li (**1**), Na (**2**), K (**3**)]. The bulky hexamethyldisilazide ligand was selected for both its relevance in catalysis and its steric characteristics while the reactive alkyl group is anticipated to allow selective reactivity with phenylsilane.

Compounds **1-3** were readily synthesised at room temperature via the 1:1 reaction of [BuMg{N(SiMe₃)₂}], synthesised in situ by the reaction of an equimolar mixture of di-butylmagnesium and hexamethyldisilazane, and subsequent addition of the relevant [M{N(SiMe₃)₂}] complex in toluene (Scheme 2.4). Crystallisation from the reaction mixture at -34 °C yielded the desired compounds suitable for single crystal X-ray diffraction analysis.



Scheme 2.4 The synthetic approach to heterobimetallic s-block amidoalkyls utilised in this work yielding **1–3** (M = Li, Na, K respectively)

Table 2.1 The unit cell parameters for complexes **1–3**

	1	2	3
$a/\text{\AA}$	9.2930(1)	9.3020(2)	9.2520(2)
$b/\text{\AA}$	20.3790(4)	20.6500(4)	20.5140(4)
$c/\text{\AA}$	13.8580(3)	13.9670(3)	14.6960(3)
$\alpha/^\circ$	90	90	90
$\beta/^\circ$	98.2550(10)	96.493(1)	93.112(1)
$\gamma/^\circ$	90	90	90

Compounds **1–3**, when isolated under similar conditions crystallise in the $P2_1/n$ space group and show only a very limited variation in unit cell dimensions. A slightly greater variation in β (Table 2.1) is however indicative of notable variations in the deduced crystal structures.

Compound **1** appears to crystallise as a 88:12 mixture of isomers (**1:1'**); the major fraction being that indicated in Scheme 2.4 (**1**), while the minor fraction consists of the isomer wherein the magnesium and lithium ions have exchanged places (**1'**). Given the similarity in the ionic radii of Li^+ and Mg^{2+} , the solution stability of BuLi and the propensity of s-block metals to undergo Schlenk-type equilibria, this disorder is unsurprising. Furthermore, although extensive debate still exists as to the degree of covalency in lithium organometallics calculations have indicated that such covalency is accessible [21]. This is similar to magnesium wherein Mg–C bonds have a significant degree of covalency but contrasts with the heavier alkali metals wherein M–C bonds are entirely ionic. In contrast, both **2** and **3** crystallise with magnesium solely in the 3-coordinate position, while the alkali metal displays a 2-coordinate geometry; a potential reflection of the distinct ionic radii of the cations and the insolubility of the relevant MBu compounds. In the case of **3**, the asymmetric unit was disordered 50:50 with regards to its orientation, and furthermore an evident undetermined systematic issue with the data was apparent from the high residuals after refinement ($R1 = 0.1637$ $wR2 = 0.4190$). The connectivity, however, was unambiguous and, while the bond length and angle data must be treated with caution, a number of structural trends are evident. The crystallographically defined structures of these species are shown in Figs. 2.2, 2.3 and 2.4 and relevant bond length and angle data shown in Table 2.2. During the course of the preparation of this thesis, compound **2** was independently described by O'Hara and co-workers. Crystallographic data for both compounds

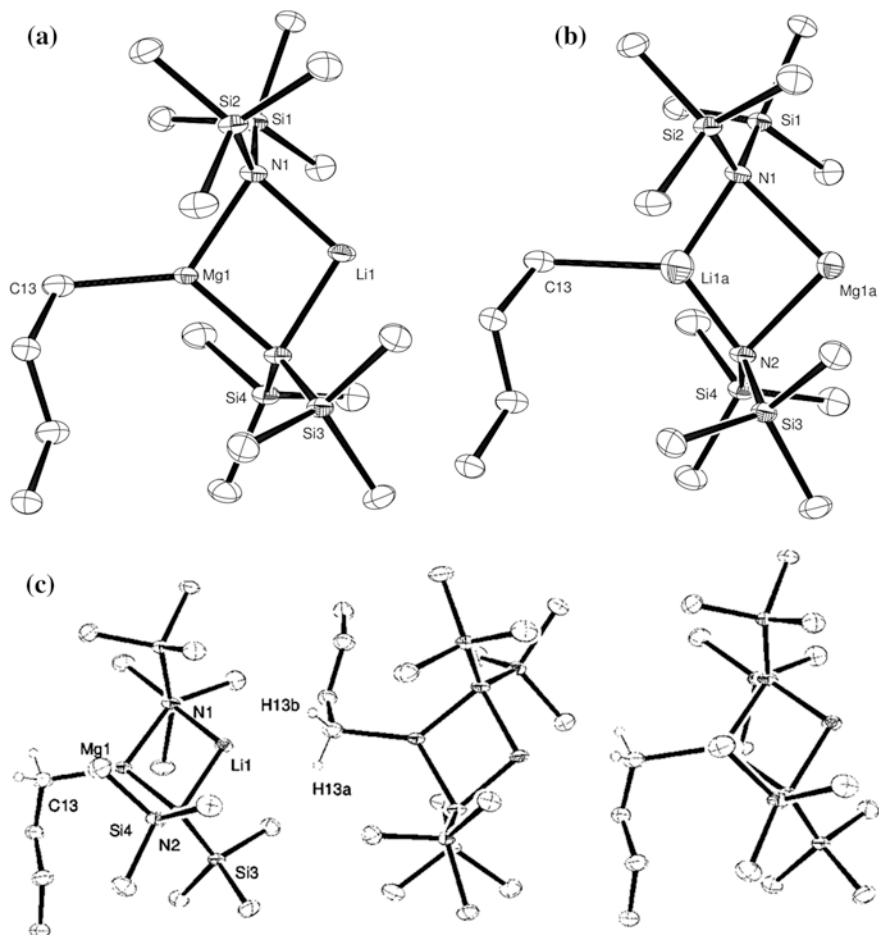


Fig. 2.2 **a** ORTEP representation of **1**, ellipsoids set to 30 %, hydrogen atoms omitted for clarity. **b** ORTEP representation of **1'**, ellipsoids set to 30 %, hydrogen atoms omitted for clarity. **c** ORTEP representation of the repeating unit of **1** in the solid state, ellipsoids set to 30 %, hydrogen atoms except those attached to C13 omitted for clarity

are identical however all analysis and data contained herein was independently collected for this thesis [22].

As shown in Figs. 2.2, 2.3 and 2.4, the isostructural complexes **1-3** crystallise as linear arrays with alternating orientations of the *n*-butyl chains, in a manner reminiscent of the amidopyridine-alkyl species reported by Kays and coworkers [4]. The authors note therein the novelty of the observed bridging butyl groups wherein an Mg-C...Li contact is observable. In contrast, no significant interaction between the independent molecules in **1** is readily observable. This can likely be attributed to the far larger hexamethyldisilazide ligands in contrast to the

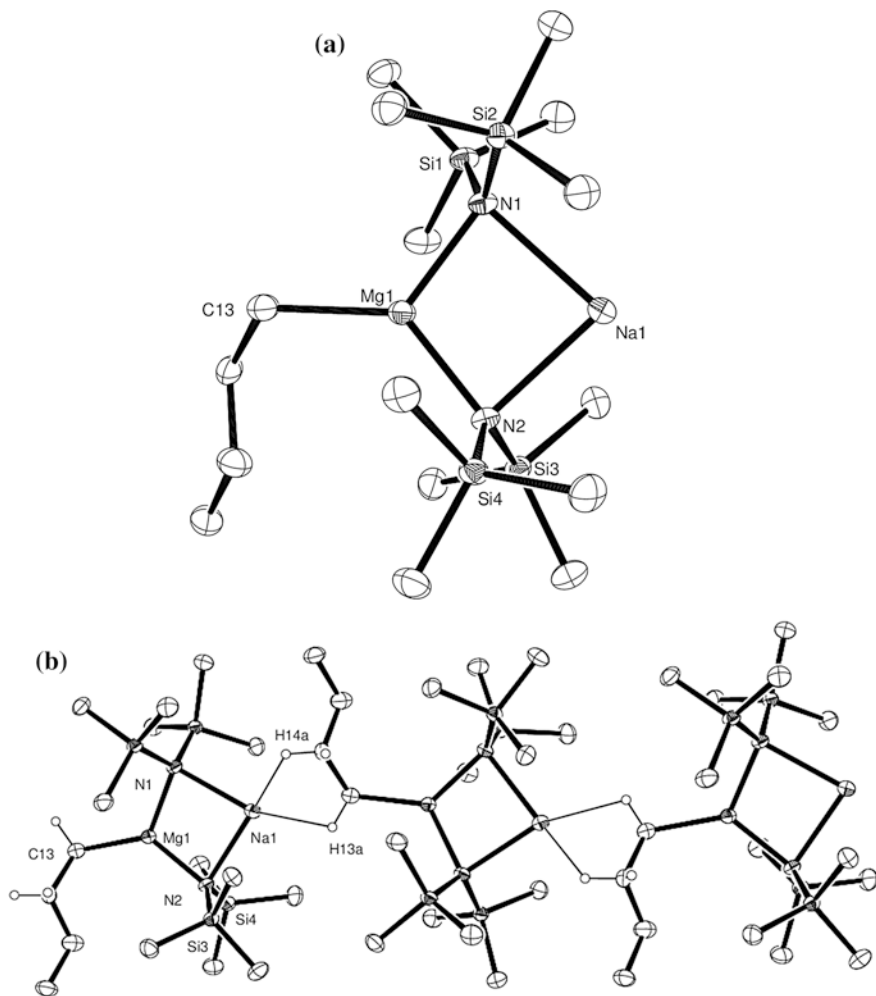


Fig. 2.3 **a** ORTEP representation of **2**, ellipsoids set to 30 %, hydrogen atoms omitted for clarity. **b** ORTEP representation of the repeating unit of **2** in the solid state, ellipsoids set to 30 %, hydrogen atoms except those attached to C13 and C14 omitted for clarity

amidopyridines in this previous report. In contrast, however, both **2** and **3** show significant intermolecular interactions as a result of the increased alkali metal cation size. In contrast to the interactions observed by Kays and co-workers, however these are not of the form $\text{Mg-C}\cdots\text{M}$ but instead appear to comprise $\text{Mg-CH}\cdots\text{M}$ and $\text{Mg-C(H)}_2\text{-CH}\cdots\text{M}$ contacts to yield a solid state polymer bound by anagostic interactions. As noted, no significant $\text{H}\cdots\text{Li}$ contact is discernible in **1**, while in **2** and **3** the $\text{H}\cdots\text{M}$ contact is evident. Two notable variations between **2** and **3** can be further observed. **2** shows a significant anagostic interaction with not only H13a,

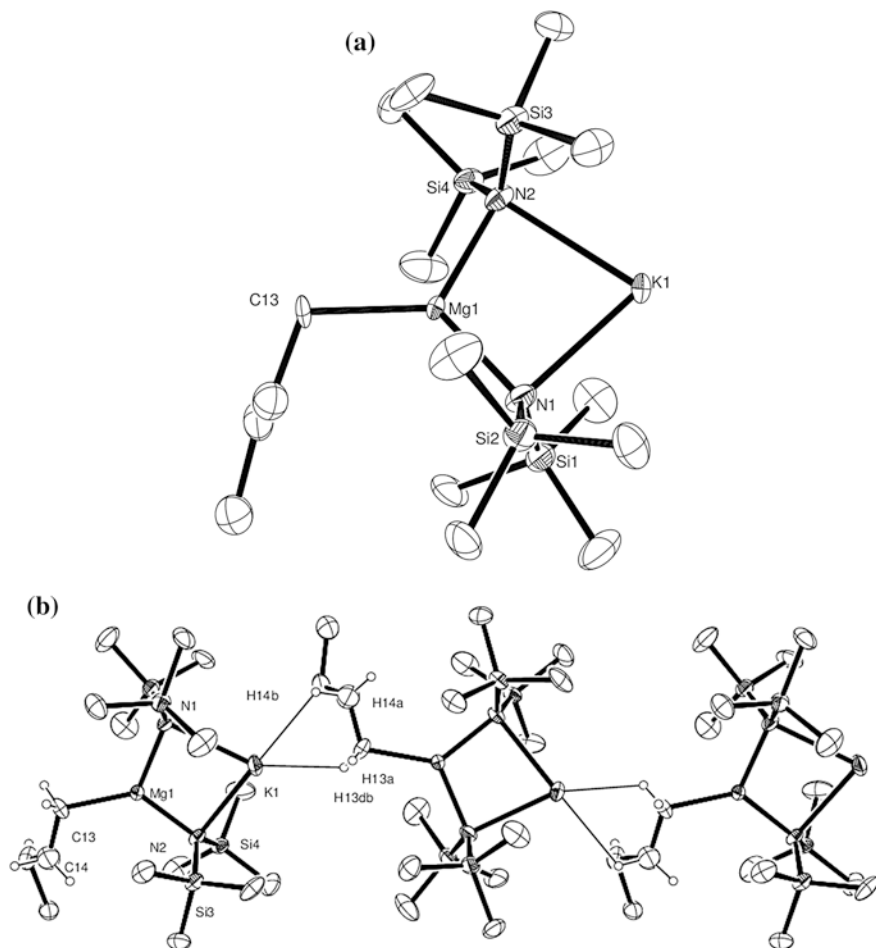


Fig. 2.4 **a** ORTEP representation of **3**, ellipsoids set to 30 %, hydrogen atoms omitted for clarity. **b** ORTEP representation of the repeating unit of **2** in the solid state, ellipsoids set to 30 %, hydrogen atoms except those attached to C13 and C14 omitted for clarity

projecting from the α -methylene of the *n*-butyl chain but also H14a which projects from the β -methylene. This second interaction, although also present in **3** appears to be significantly weaker. In contrast, the H13a \cdots K interaction in **3** appears to be stronger than the corresponding interaction for its lighter congener, **2**, as reflected in the elongation of the H13a \cdots M interaction being less than the change in ionic radius from Na⁺ to K⁺.

These interactions appear to have significant structural consequences, with Mg1-C13 bond of **2** being shorter than that of **1** while both are exceeded by the analogous measurement in **3**. Correspondingly, an increase in the Mg-C13-C14

Table 2.2 Selected bond lengths and bond angles for **1–3**

	1	2	3
M1-N1	2.054(18)	2.466(2)	2.767(9)
M1-N2	2.073(16)	2.436(2)	2.755(9)
Mg1-N1	2.097(3)	2.095(2)	2.175(10)
Mg1-N2	2.089(3)	2.0798(1)	2.118(9)
Mg1-C13	2.181(4)	2.152(3)	2.19(2)
H13a-M1'	2.165	2.443	2.532
H14a-M1'	2.572	2.213	2.705
M1-N1-Mg1	81.6(5)	84.34(7)	87.8(3)
M1-N2-Mg1	81.3(5)	85.43(7)	89.2(3)
N1-M1-N2	99.4(8)	85.03(7)	76.5(2)
N1-Mg1-N2	97.49(13)	105.05(8)	105.5(4)
N1-Mg1-C13	127.95(14)	124.44(9)	123.0(7)
N2-Mg1-C13	134.51(13)	130.44(9)	131.2(7)
Mg1-C13-C14	112.9(2)	114.90(17)	114.2(17)

angles of **2** and **3** in contrast to **1**, is observed which could be attributed to the decrease in the N(1,2)-Mg-C13 angles. Given the clear interactions within the unit cell and the limited change between **2** and **3**, however, as well as the influence of H14a-Na interactions in **2**, it is more likely that this angle is rendered more obtuse by the interactions between the butyl chain and the Group 1 cation of a neighbouring molecule.

Although these data may be affected by both the poor quality of the crystallographic data for **3** and the constraints utilised to separate the modelling of the isomers in **1**, it is notable that this trend of **1** may be consistently differentiated from **2** and **3** for other means of analysis as well as the crystallography (*vide infra*). It is thus suggested that these observed variations can be attributed to the species occupying two classes—those which have significant anagostic interactions (**2** and **3**) and those which do not (complex **1**). This observation can be used to rationalise the subsequent structural and spectroscopic variations seen for complexes **1–3**, as well as the existence of an alternate, crystallographically defined isomer **1'**, wherein the lack of stabilising anagostic interactions reduce the drive towards the major isomer, **1**.

In all three complexes the magnesium centre remains trigonal planar with the angles around Mg adding up to $\sim 360^\circ$. However, unsurprisingly, the move from the smaller Li to the larger K cation via the intermediate Na leads to an elongation in the M–N bond. Notably, the increase in M–N bond length from **1** to **2** is significantly larger than the variation in the ionic radius of lithium versus sodium. This is not, however, true of the increase in bond length from **2** to **3** which is of a similar magnitude to the ionic radii. This increase in bond length occurs concurrently with an increase in the M–N–Mg angle and a corresponding decrease in the N–M–N angle, with the increasingly acute angles at the Group 1 centre leading to an increasing planarization of the MgN₂M fragment. Consequently the N–Li–N plane in **1** sits 5.26° from the N–Mg–N plane, while **2** is closer at 4.52° and **3** is

Table 2.3 Selected NMR spectroscopic data (ppm) for compounds **1–3**

	1	2	3
M-CH ₂ δ _{1H}	0.01	-0.07	-0.40
M-CH ₂ δ _{13C}	11.2	12.1	14.0
N(SiMe ₃) ₂ δ _{1H}	0.17	0.19	0.22
N(SiMe ₃) ₂ δ _{13C}	5.1	6.0	6.3
N(SiMe ₃) ₂ δ _{15N}	47.3	47.0	49.7

closer still at 2.63°, possibly a reflection of the increased coordinative flexibility of the alkali metals down Group 1 or as a result of increasing potential for the formation of anagostic interactions. Also notable is the effect of the increasing Group 1 cation size on the geometry of the magnesium centre, with the N-Mg-N angle being forced to be increasingly obtuse by the increasingly dominant size of the Group 1 centre.

Although these solid-state structural parameters noted hint to the effects of the variation in alkali metal upon complexes **1–3**, the ¹H, ¹³C and ¹⁵N NMR data, as summarised in Table 2.3, provide clearer electronic discrimination.

The aforementioned elongation of the N–M bond lengths between Li and K leads to a corresponding deshielding of the silylmethyl carbon centre and protons present on the hexamethyldisilazide ligand. The trend in the ¹⁵N NMR spectroscopic shifts is more complex, however, suggesting that increasing N–M length does not simply yield a deshielding of the nitrogen nucleus. This increase in shielding between **1** to **2** but significant decrease from **2** to **3** appears to mirror the trends observed for the M–N and Mg–C bond lengths and indicate a significant structural shift from **1** to **2** followed by a less profound variation from **2** to **3**. However, the unreferenced nature of the ¹⁵N NMR spectroscopy performed here renders these conclusions tentative at best.

Perhaps of most significance is the variation in the ¹³C and ¹H NMR spectroscopic chemical shifts for the α-methylene of the butyl chain. In contrast to the observed variation in Mg–C bond length, a smooth progression in deshielding of the ¹³C NMR resonance attributed to C13 from **1** to **3** is observed, suggesting an interplay of stereoelectronic factors. The α-methylene ¹H NMR signal once again provided a smooth progression in chemical shift; perversely however this occurred as an increased shielding of these protons from **1** to **3**. This counterintuitive trend could be a simple reflection of the paramagnetic contribution to the ¹³C NMR chemical shifts, it could also be a direct result of the persistence of intermolecular interactions occurring in solution in a similar manner to those observed in the solid state for **2** and **3**. Further evidence for the persistence of interactions of this form can be provided by analysing the effect of concentration upon the ¹H NMR shift of the α-CH₂ protons which shows almost no concentration dependence for **1** but a small dependence for **2** and **3**. The increasing shielding of the α-CH₂ protons versus deshielding of the carbon centre is thus a reflection of a balance between the Mg–C13 and H13···M bond strengths in which the latter interaction is increasingly augmented at the expense of the former as the size of the Group 1 cation increases.

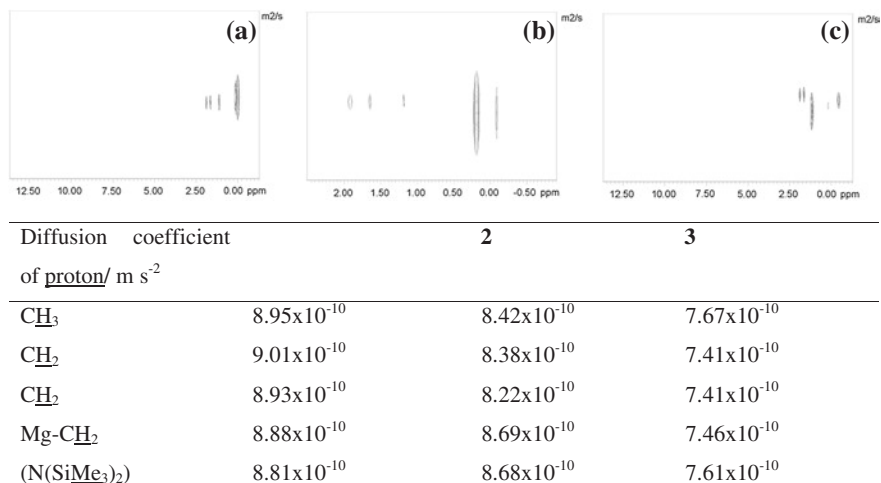


Fig. 2.5 The DOSY spectra and diffusion coefficients for compounds **1–3**

To further probe the possibility of solution intermolecular interactions, these species were subjected to DOSY analysis as summarised in Fig. 2.5.

As shown, visual inspection of the DOSY parameters suggested each compound retained its solid state structure in solution, with the hexamethyldisilazide and *n*-butyl resonances all sharing very similar diffusion coefficients.

Complexes **1** and **3** were further subjected to variable temperature NMR experiments which showed these species to be stable up to 95 °C. This stability contrasts with the previously observed reactivity for di-*iso*-propylamide-ligated structures **Xa-c** (vide supra).

Previously reported mixed metal clusters bound by hexamethyldisilazide ligands, such as $[(\text{Me}_3\text{Si})_2\text{N}]\text{Ca}\{\mu\text{-N}(\text{SiMe}_3)_2\}_2\text{Mg}\{\text{N}(\text{SiMe}_3)_2\}$ as well as the parent $[\text{Mg}\{\text{N}(\text{SiMe}_3)_2\}_2]$ show extensive solution fluxionality reflecting the Schlenk-like equilibria to which these species are prone [2]. Indeed, in the former case ¹H NMR analysis reflects the presence of all possible hexamethyldisilazide-bound Group 2 complexes comprising of either the homoleptic Mg and Ca diamide species, as well as the bimetallic species in solution. Gratifyingly, in the case of **1–3** the major peaks observable in ¹H NMR spectrum could be attributed to compounds possessed of a solution structure corresponding to that observed in the solid state as defined by crystallography. Notable, however, were the presence of minor peaks in the region characteristic of hexamethyldisilazide silylmethyl resonances observed in the ¹H NMR spectra of **1–3** which would appear to indicate some solution equilibria occurring faster than the NMR timescale. Although minor peaks tentatively attributed to the butyl resonances of alternative solution isomers were also identifiable, these could not be rationally integrated and matched to any of the observed silylmethyl resonances. The extreme relative intensity of the hexamethyldisilazide peak corresponding to the crystallographically defined structures of **1–3** may be responsible for masking the corresponding resonances, thus complicating this analysis. Notably, the observed disorder in the crystallographically

defined structure of **1/1'** and reactivity of **2** with donor molecules observed by O'Hara and co-workers were also liable to be reflections of these equilibration processes (vide supra).

2.3 s-Block Mixed Metal Hydrides

Although β -hydride elimination has previously yielded bimetallic s-block hydrides supported by amide ligands, approaches towards these species utilising σ -bond metathesis have remained hitherto unreported. This contrasts with the common routes to both homometallic Group 1 and Group 2 species which have predominantly relied upon the activity of hydridic silanes with relevant metal amides or alkyls. It was thus speculated that σ -bond metathesis with silanes would take place selectively with the relatively unbulky and reactive alkyl groups borne by **1–3** could yield a variety of novel heterobimetallic hydrides structurally related to **Xa-c**. Furthermore, these reactions were investigated for the relevance of such a step to dehydrocoupling, particularly of silanes and amines.

To assess this possibility, solutions of **1–3** were reacted with equimolar quantities of phenylsilane in *d*₈-toluene on an NMR scale. The ¹H NMR spectrum resulting from the reaction of compound **3** under these conditions suggested the formation of PhSi(H)₂*n*-Bu and three broad, metal-bound hexamethyldisilazide environments between 0.16–0.36 ppm indicative of Mg-C/Si-H σ -bond metathesis as well as a new signal at 3.66 ppm which corresponded to a single proton by integration.

Preparative scale repetition of this reaction in toluene yielded crystals of compound **4**, a heterobimetallic hydride of the formula [K{N(SiMe₃)₂}₂MgH]₂, suitable for single crystal X-ray diffraction analysis, the results of which are shown in Fig. 2.6. Although this species is structurally analogous to the previously reported hydride, **V**, its synthesis is, as hoped, the result of selective Mg-C/Si-H σ -bond metathesis of the more reactive and less sterically encumbered alkyl group of compound **3**. The bond length and angle data of **4** are also similar to those observed for the analogous di-*iso*-propylamide analogue **V** with some notable elongation of bonds as a consequence of the more sterically encumbered hexamethyldisilazide ligands. The previously unattributed peak at 3.66 ppm in the ¹H NMR spectrum of **4** also corresponded to the chemical shift of the hydride peak of **V** and was, thus, assigned as the bridging hydride resonance. The persistence of the solid state structure in aromatic solvents was corroborated by the observation of a single diffusion coefficient in the ¹H DOSY NMR spectrum for both the hydride and silylmethyl signals, while no evidence for fluxional behaviour was observed in variable temperature experiments.

In contrast to this straightforward behaviour, an analogous reaction of **2** with phenylsilane in *d*₈-toluene provided a considerably more complex ¹H NMR spectrum with two notable peaks at 4.44 and 5.12 ppm attributed to the hydride resonances of PhSi(H)₂*n*-Bu and PhSi(H)₂N(SiMe₃)₂ respectively. This latter observation is suggestive of not only Mg-C/Si-H but also M-N/Si-H σ -bond metathesis. Also notable were the complex signals associated with the metal-bound-N(SiMe₃)₂ region, which consisted of overlapping peaks between 0.32

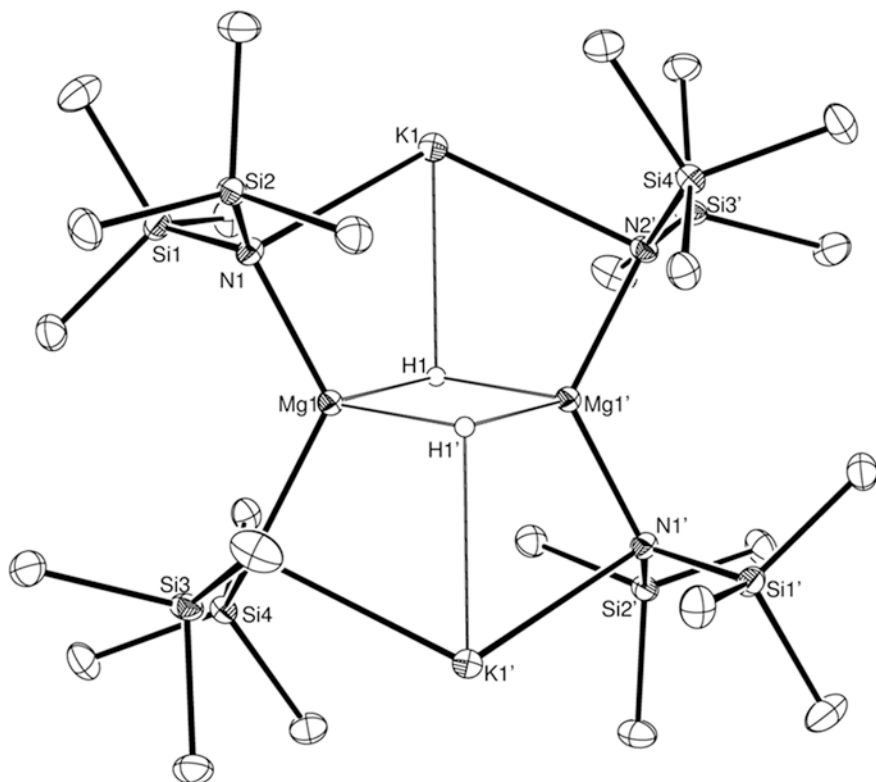


Fig. 2.6 ORTEP plot of **4** (30 % probability ellipsoids). H atoms apart from metal-bound hydrides omitted for clarity. Selected bond lengths (Å) and angles (°): Mg1-N1 2.0742(13), K1'-N2 2.9283(13), Mg1-H1 1.89(2), K1-H1 2.86(2), N1-Mg1-N2 124.97(5), N1-K1-N2' 113.50(4), Mg1-H1-Mg1' 106(1). Symmetry transformations used to generate equivalent atoms: $x-1/2, -y + 1/2, z + 1/2, -x, -y + 1, -z + 1$

and 0.47 ppm alongside a pair of broad overlapping signals centred on 3.87 and 3.69 ppm which integrated in a 144:4:6 ratio. In order to elucidate the origin of these observations, a preparative scale reaction undertaken in toluene provided compound **5**, a heterobimetallic hydride of the form $[\text{Na}_6\text{Mg}_6\{\text{N}(\text{SiMe}_3)_2\}_8\text{H}_{10}]$, as crystals suitable for X-ray crystallographic analysis. The results of this analysis are shown in Fig. 2.7.

Compound **5** is a heterododecametallic species ligated by eight hexamethyldisilazide and ten hydride ligands with a formula of $[\text{Mg}_6\text{Na}_6\{\text{N}(\text{SiMe}_3)_2\}_8\text{H}_{10}]$. Its formation and the side-product peaks observed in the in situ ^1H NMR experiments are rationalised by the stoichiometry shown in Eq. 1. Indeed, a repeat of the in situ NMR scale experiment with this stoichiometry yielded a stoichiometric quantity of compound **5**.

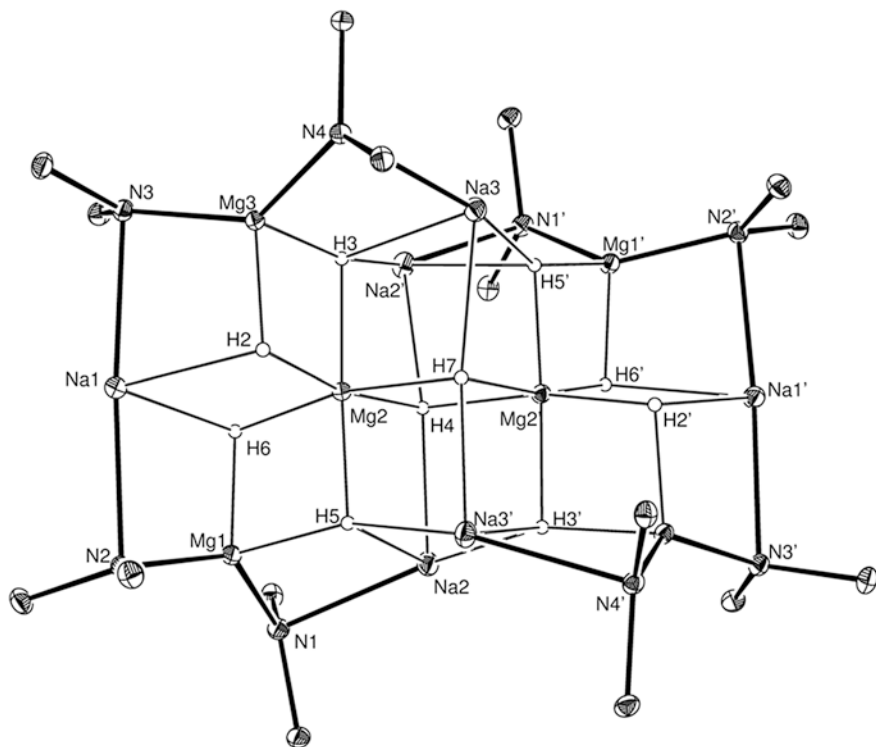
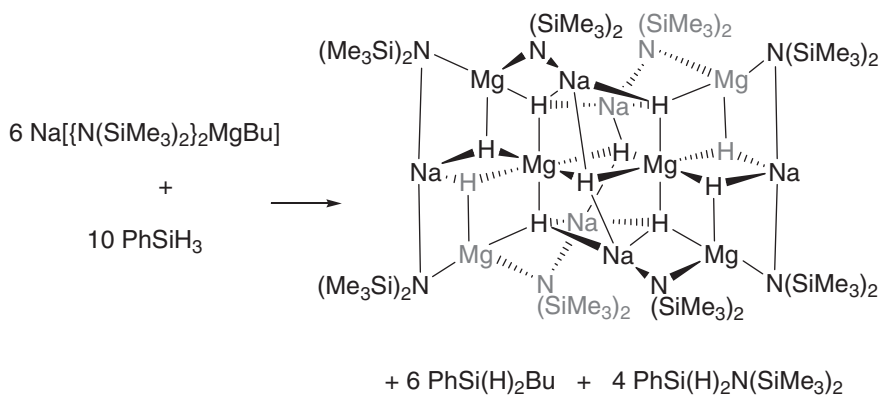


Fig. 2.7 ORTEP plot of **5** (30 % probability ellipsoids). H atoms apart from metal-bound hydrides and carbon atoms omitted for clarity. Selected bond lengths (Å) and angles (°): Na1-N2 2.6093(17), Na1-H2 2.34(2), Mg1-N2 2.0627(16), Mg2-H2 1.89(2), Mg2-H3 2.01(2), Mg2-H4 2.01(2), Na2-N1 2.5169(17), Na2-H4 2.385(7), Na2-H5 2.46(2), Mg1-N1 2.0534(16), Mg1-N2 2.0627(16), Mg2-H2-Na1 104(1), N2-Na1-N3 175.72(6), Mg2-H7-Mg2' 103(1). Symmetry transformations used to generate equivalent atoms: $-x + 2, y, -z + 3/2$



Equation 1 The proposed stoichiometry necessary to achieve compound **5**.

The formation of **5** constitutes a synthetic route which, although evidently selective for a specific compound, is not discriminating for the less bulky and more nucleophilic alkyl substituent over the present hexamethyldisilazides. Given the observed solution equilibria to which **2** appears to be subject it is therefore reasonable to speculate that the selective formation of **5** is in fact more a reflection of these equilibria than of the reactivity of substituents around the crystallographically defined structure of **2**.

The structure of **5** possesses a C_2 symmetry element running through the 2 central hydrides (H4 and H7), which bridge between two 6-coordinate magnesium centres (Mg2, Mg2') ligated only by hydrides in a structural core reminiscent of magnesium dihydride. Perhaps imposed by the imperfect octahedral geometry of its $[Mg_2H_{10}]$ core, the Mg-H bonds of **5** are elongated in comparison to those observed in bulk MgH_2 (1.718 Å) [1]. The remaining four magnesium centres (Mg1, Mg3, Mg1' and Mg3') exist in identical coordination environments wherein the presence of two bulky hexamethyldisilazide ligands lowers their coordination number to four, with the other two sites occupied by hydrides bridging to the $[Mg_2H_{10}]$ core. The terminal sites of the potentially polymeric $[Mg_2H_{10}]$ core are capped by sodium atoms, Na1 and Na1', which exist in a sawhorse conformation ligated axially by two amides. These ligands bridge to the tetracoordinate magnesium ions while two of the equatorial sites share hydrides, H2, H6, H2' and H6', with the $[Mg_2H_{10}]$ core. The residual sodium atoms (Na2, Na3, Na2' and Na3') are located in distorted tetrahedral sites which bridge, via hydrides H3, H5, H3' and H5', the central magnesium ions and are capped by amides shared with the tetracoordinate magnesium centres. These latter sodium ions form the vertices of cubic $[(NaMgH_2)_2]^{2+}$ clusters reminiscent of those observed by Stasch for the $[(LiH)_4]$ core of the structurally characterised lithium hydride, $[\{(DippNPPH_2)Li\}_4(LiH)_4]$ [14].

DOSY experiments (Fig. 2.8) performed on a crude sample of **5** suggested a single diffusion coefficient for the silylmethyl and hydride regions, corroborating the proposed peak attributions and suggesting that the solid state structure is retained in aromatic solvents (Table 2.4).

Although the crystallographically defined structure is suggestive of three hydride environments in a 2:4:4 ratio and two hexamethyldisilazide environments in a 1:1 ratio, the 1H NMR spectrum at room temperature comprised only 2 broad, complex signals in a 4:6 ratio for the hydrides and a series of overlapping, second order peaks in the silylmethyl region. The more downfield hydride shift is suggested to be the 3-coordinate hydrides H2 and H6, with the six remaining, 4-coordinate hydrides providing the upfield signal at 3.87 ppm (Fig. 2.9).

Cooling the sample evidenced a fluxional process as a result of exchange of the tetracoordinate hydrides within the $[Mg_2H_{10}]$ core. At 267 K (calibrated utilising 4 % MeOH in MeOD) the 6H peak at 3.69 ppm was observed to split yielding two broad singlet resonances in a 2:4 ratio at 3.68 (H_a) and 3.59 ppm (H_b) respectively and a free energy of activation (ΔG^\ddagger) for this process of 56 kJ mol⁻¹ (Fig. 2.10).

The silylmethyl region at 248 K was split into two doublets at 0.32 and 0.48 ppm which can be attributed to the two observed hexamethyldisilazide environments each further split by the diastereotopic disposition imposed by the

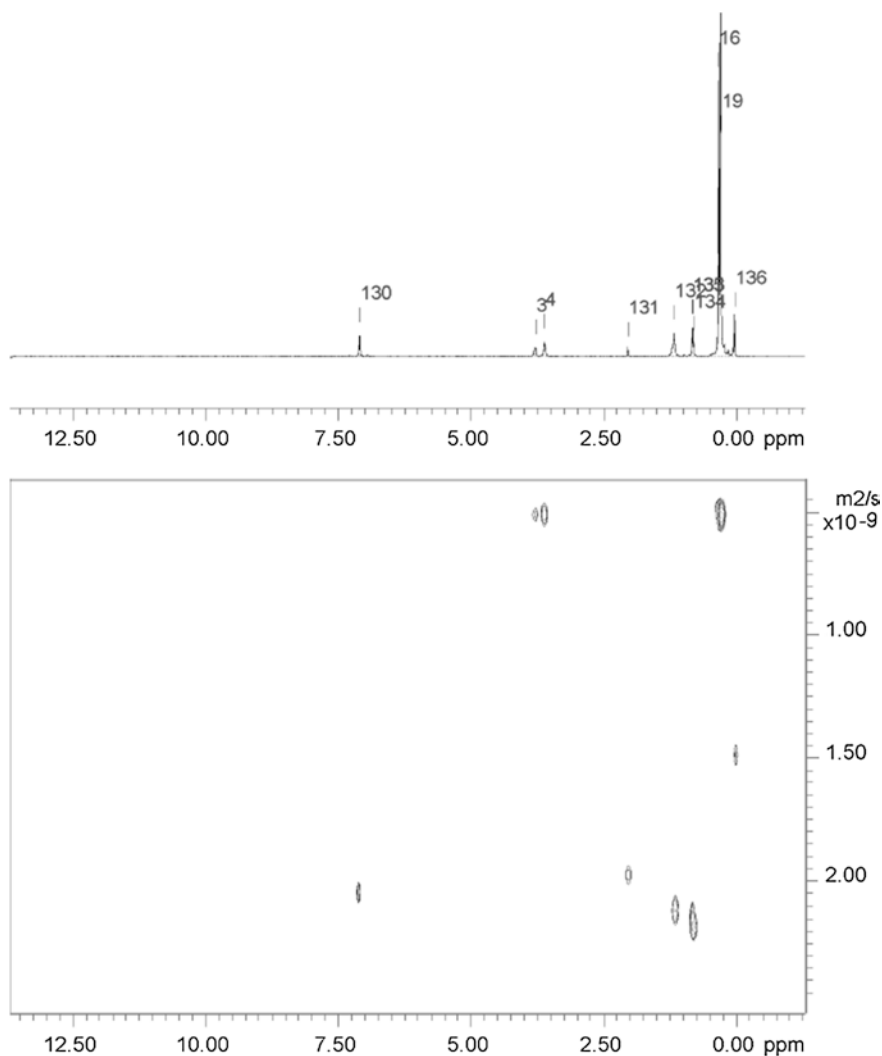


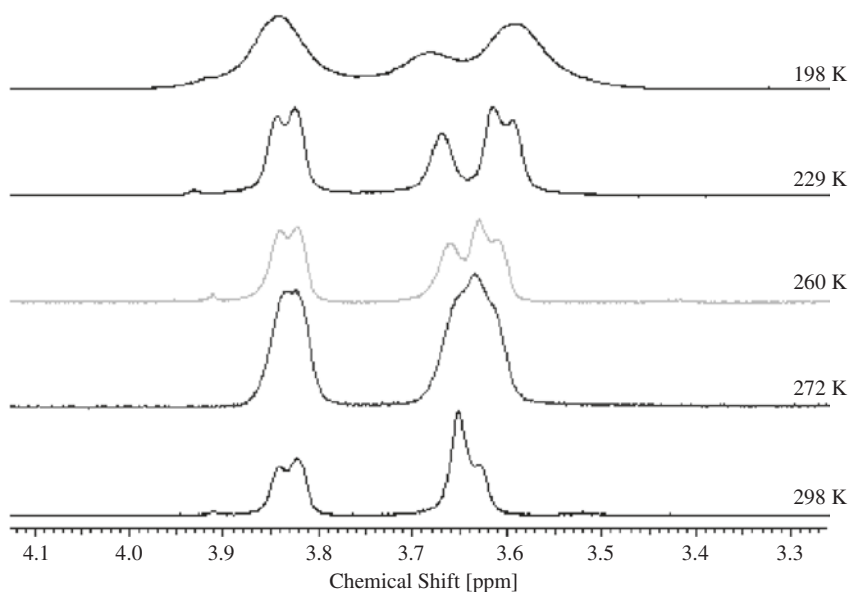
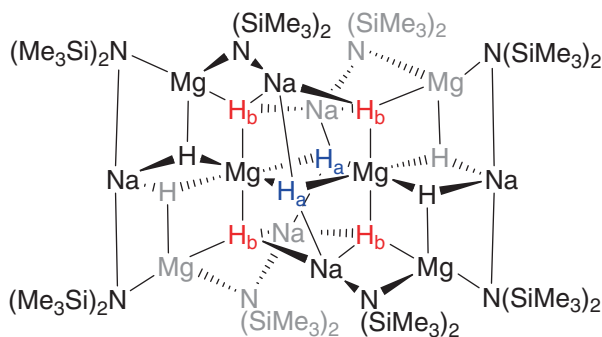
Fig. 2.8 The ^1H NMR and DOSY plots for a crude sample of compound **5**

rigidity of the cage structure. No coalescence temperature for the exchange of each separate hexamethyldisilazide environment, however, could be attained, even to the boiling point of the d_8 -toluene solvent.

Attempts to extend this reactivity to the lightest congeneric analogue, **1**, yielded immediate precipitation of a fine, insoluble, colourless solid, thought to be various metal hydrides. NMR analysis suggested consumption of the PhSiH_3 and formation of $\text{PhSi}(\text{H})_2\text{Bu}$ and $\text{PhSi}(\text{H})_2\text{N}(\text{SiMe}_3)_2$ as well as silanes with higher alkyl and amide incorporation indicative of Mg-C/Si-H and Mg-N/Si-H σ -bond metathesis respectively. Repetition of this reaction in the more coordinating

Table 2.4 The diffusion coefficients, with relevant errors for the component ^1H NMR peaks of compound **5** as measured by DOSY

Proton	Peak	Chemical shift/ppm	Diffusion coefficient/ $\text{m}^2 \text{s}^{-1}$	Error
Mg-H	3	3.781	5.27×10^{-10}	8.901×10^{-12}
Mg-H	4	3.610	5.29×10^{-10}	4.992×10^{-12}
(N(SiMe ₃) ₂)	16	0.328	5.26×10^{-10}	5.310×10^{-12}
(N(SiMe ₃) ₂)	17	0.301	5.29×10^{-10}	5.088×10^{-12}
(N(SiMe ₃) ₂)	18	0.292	5.31×10^{-10}	3.582×10^{-12}
(N(SiMe ₃) ₂)	19	0.284	5.29×10^{-10}	5.153×10^{-12}

**Fig. 2.9** The hydride region of the ^1H NMR of **5** below, at and above the coalescence temperature (uncalibrated temperatures)**Fig. 2.10** The proposed fluxional hydrides (H_a and H_b) in complex **5**

solvent THF yielded an identical result, suggesting that extension to complex s-block polyhydrides of the lightest alkali metal is not possible with a hexamethyldisilazide co-ligand set under these conditions.

This chapter describes a novel series of s-block mixed metal amidoalkyls encapsulating a range of alkali metal cations with magnesium. These species show fascinating structural variation contingent on the identity of the Group 1 cation and resultant intermolecular interactions both in the solid state and solution. Further explored is the formation of heterobimetallic magnesium-alkali metal hydride clusters may be prepared by a σ -bond metathesis route from the corresponding s-block amidoalkyls bearing only simple ligands of catalytic relevance. While the formation of compound **4** suggests selective metathesis at the more reactive alkyl substituent, the formation of **5** requires less discriminative metathesis of both alkyl and amide ligands of **2**, and may, alongside the inaccessibility of a lithium analogue, represent a reflection of the solution equilibria which **1–3** are subject to. Nevertheless, this chapter indicates the under-represented utility of heteroleptic s-block clusters for metathesis chemistry and a novel approach to higher metal hydride clusters wherein the coordinative flexibility of a mixture of s-block elements allows them to act as both corner and edge occupying species. Work to extend this reactivity to the lightest alkali metal ion is ongoing, alongside studies into the reactivity of these novel and structurally interesting s-block species.

2.4 Experimental Data

[Li{N(SiMe₃)₂MgBu}, **1**

To a toluene solution (2 mL) of di-*n*-butylmagnesium in heptanes (1 mmol, 2 mL) was added hexamethyldisilazane (1 mmol, 0.210 mL). The resultant solution bubbled and was stirred overnight after which time lithium hexamethyldisilazide (1 mmol, 167 mg) was added. Stirring was continued for 1 hour and the resultant suspension filtered, the solution was then used as is. Material suitable for crystallographic characterisation was procured by reducing this solution in vacuo to incipient crystallisation then cooling to $-18\text{ }^{\circ}\text{C}$ (265 mg, 67 %).

¹H NMR (300 MHz, d₈-Tol) δ ppm 0.01 (m, 2 H, MgCH₂CH₂CH₂CH₃) 0.17 (s, 36 H, N(SiMe₃)₂) 1.15 (t, 3 H, MgCH₂CH₂CH₂CH₃) 1.64 (m, 2 H, MgCH₂CH₂CH₂CH₃) 1.90 (m, 2 H, MgCH₂CH₂CH₂CH₃). ¹³C NMR (75 MHz, d₈-Tol) δ ppm 5.1 (N(SiMe₃)₂), 11.2 (MgCH₂CH₂CH₂CH₃) 14.4 (MgCH₂CH₂CH₂CH₃) 31.8 (MgCH₂CH₂CH₂CH₃) 32.5 (MgCH₂CH₂CH₂CH₃).

In spite of repeated attempts, no consistent elemental analysis data could be obtained.

[Na{N(SiMe₃)₂MgBu], 2

To a toluene solution (2 mL) of di-*n*-butylmagnesium in heptanes (1 mmol, 2 mL) was added hexamethyldisilazane (1 mmol, 0.210 mL). The resultant solution bubbled and was stirred overnight after which time sodium hexamethyldisilazide (1 mmol, 183 mg) was added. Stirring was continued for 1 h and the resultant suspension filtered, the solution was then used as is. Material suitable for crystallographic characterisation was procured by reducing this solution *in vacuo* to incipient crystallisation then cooling to -18°C (218 mg, 53 %).

¹H NMR (400 MHz, d₈-Tol) δ ppm -0.07 (m, 2 H, MgCH₂CH₂CH₂CH₃) 0.19 (s, 36 H, N(SiMe₃)₂) 1.18 (t, 3 H, MgCH₂CH₂CH₂CH₃) 1.68 (m, 2 H, MgCH₂CH₂CH₂CH₃) 1.92 (m, 2 H, MgCH₂CH₂CH₂CH₃). ¹³C NMR (100 MHz, d₈-Tol) δ ppm 6.0 (N(SiMe₃)₂), 12.1 (MgCH₂CH₂CH₂CH₃) 14.5 (MgCH₂CH₂CH₂CH₃) 32.0 (MgCH₂CH₂CH₂CH₃) 33.0 (MgCH₂CH₂CH₂CH₃).

In spite of repeated attempts, no consistent elemental analysis data could be obtained.

[K{N(SiMe₃)₂MgBu], 3

To a toluene solution (2 mL) of di-*n*-butylmagnesium in heptanes (1 mmol, 2 mL) was added hexamethyldisilazane (1 mmol, 0.210 mL). The resultant solution bubbled and was stirred overnight after which time potassium hexamethyldisilazide (1 mmol, 199 mg) was added. Stirring was continued for 1 hour and the resultant suspension filtered, the solution was then used as is. Material suitable for crystallographic characterisation was procured by reducing this solution *in vacuo* to incipient crystallisation then cooling to -18°C (303 mg, 71 %).

¹H NMR (300 MHz, d₈-Tol) δ ppm -0.40 (m, 2 H, MgCH₂CH₂CH₂CH₃) 0.22 (s, 36 H, N(SiMe₃)₂) 1.20 (t, 3 H, MgCH₂CH₂CH₂CH₃) 1.67 (m, 2 H, MgCH₂CH₂CH₂CH₃) 1.92 (m, 2 H, MgCH₂CH₂CH₂CH₃). ¹³C NMR (75 MHz, d₈-Tol) δ ppm 6.3 (N(SiMe₃)₂), 14.0 (MgCH₂CH₂CH₂CH₃) 14.6 (MgCH₂CH₂CH₂CH₃) 32.0 (MgCH₂CH₂CH₂CH₃) 33.0 (MgCH₂CH₂CH₂CH₃).

Anal. calc'd for C₁₅H₄₃KMgN₂Si₄ C, 42.17; H, 10.14; N, 6.56 %. Found C, 43.32; H, 10.15; N, 6.26 %.

[K{N(SiMe₃)₂MgH]₂, 4

To a toluene solution (3 mL) of **2** (1 mmol in 4 mL 1:1 toluene:heptanes) was added phenylsilane (1 mmol, 0.123 mL) and the resultant solution stirred overnight. Subsequent filtration followed by concentration to incipient crystallisation and chilling to -35°C yielded colourless blocks suitable for X-ray analysis (262 mg, 68 %).

¹H NMR (400 MHz, d₈-Tol) δ ppm 0.19–0.31 (m, 36 H, N(SiMe₃)₂) 3.66 (s, 1 H, Mg-H). ¹³C NMR (75 MHz, d₈-Tol) δ ppm 6.1 (N(SiMe₃)₂) 6.2 (N(SiMe₃)₂) 6.8 (N(SiMe₃)₂).

Anal. calc'd for C₂₄H₇₄K₂Mg₂N₄Si₈.C₆H₅CH₃: C, 43.17; H, 9.58; N, 6.50 %. Found: C, 42.81; H, 9.98; N, 6.17 %.

[Na₆Mg₆{N(SiMe₃)₂}₈H₁₀], 5

To a toluene solution (3 mL) of **2** (1 mmol in 4 mL 1:1 toluene:heptanes) was added phenylsilane (1.66 mmol, 0.204 mL) and the resultant solution stirred overnight. Subsequent filtration followed by concentration to incipient crystallisation and chilling to $-35\text{ }^{\circ}\text{C}$ yielded colourless blocks suitable for X-ray analysis (139 mg, 53 %).

¹H NMR (400 MHz, d₈-Tol) δ ppm 0.28–0.48 (m, 144 H, N(SiMe₃)₂) 3.54–3.75 (m, 6 H, Mg-H), 3.75–3.93 (m, 4 H, Mg-H). ¹³C NMR (100 MHz, d₈-Tol) δ ppm 7.0 (N(SiMe₃)₂), 7.3 (N(SiMe₃)₂), 7.4 (N(SiMe₃)₂).

Anal. calc'd for C₄₈H₁₅₄Mg₆N₈Na₆Si₁₆: C, 36.56; H, 9.84; N, 7.11 %. Found: C, 36.44; H, 9.68; N, 6.95 %.

M. p. 162–~200 °C (dec.)

	1	2	3	4	5
Empirical formula	C ₁₆ H ₄₅ LiMgN ₂ Si ₄	C ₁₆ H ₄₅ NaMgN ₂ Si ₄	C ₁₆ H ₄₅ KMgN ₂ Si ₄	C ₁₂ H ₃₇ KMgN ₂ Si ₄	C _{27.50} H ₈₁ Mg 3Na ₄ Na ₃ Si ₈
Formula weight (g mol ⁻¹)	409.15	425.20	441.31	385.21	834.58
Crystal system	Monoclinic	Monoclinic	Monoclinic	Monoclinic	Monoclinic
Space group	P2 ₁ /n	P2 ₁ /n	P2 ₁ /n	P2 ₁ /n	C ₂ /c
<i>a</i> (Å)	a = 9.2930(1) Å alpha = 90°	9.3020(2)	9.2520(2)	9.4600(1)	25.2680(2)
<i>b</i> (Å)	20.3790(4)	20.6500(4)	20.5140(4)	14.8070(2)	17.8740(2)
<i>c</i> (Å)	13.8580(3)	13.9670(3)	14.6960(3)	16.5070(3)	24.3340(3)
α (°)	90	90	90	90	90
β (°)	98.2550(10)	96.493(1)	93.112(1)	90.168(1)	104.234(1)
γ (°)	90	90	90	90	90
<i>V</i> (Å ³)	2597.26(8) Å ³	2665.66(10) Å ³	2785.12(10) Å ³	2312.20(6) Å ³	10652.8(2) Å ³
<i>Z</i>	4	4	4	4	8
ρ (g cm ⁻³)	1.046 Mg/m ³	1.059 Mg/m ³	1.052 Mg/m ³	1.107 Mg/m ³	1.041 Mg/m ³
μ (mm ⁻¹)	0.255	0.266	0.389	0.459	0.283
θ range (°)	3.73–27.49	3.60–27.49	4.66–27.49	3.56–27.46	3.52–27.50
Measured/independent reflections/ <i>R</i> _{int}	30373/ 5873/ 0.0580	48709/ 6100/ 0.0746	45366/ 6345/ 0.0632	30880/ 5256/ 0.1116	73776/ 12160/ 0.0460
Data/restraints/parameters	5873/1/238	6100/0/230	6345/48/287	5256/0/197	12160/ 36/466

Goodness-of-fit on F^2	1.249	1.104	1.154	1.075	1.084
R_1, wR_2 [$I > 2\sigma(I)$]	0.0574, 0.1402	0.0480, 0.1026	0.1518, 0.4129	0.0362, 0.0942	0.0399, 0.1044
R_1, wR_2 (all data)	0.0673, 0.1446	0.0788, 0.1135	0.1637, 0.4190	0.0401, 0.0978	0.0550, 0.1141

Notes on crystal refinement

1 Mg1 and Li1 were seen to be closely disordered with each other in an 88:12 ratio. The minor disordered fractional occupancy atoms have been denoted with labels Mg1A and Li1A and they were treated isotropically in order to assist convergence. An additional distance restraint was also included, namely, to maintain a distance of 0.3 Å between Mg1 and Li1A. Unsurprisingly, the latter 12 % fractional-occupancy alkali metal benefited from the stability that this restraint imposed

3 Potassium, and *n*-butyl group based on C13 disordered over 2 sites in a 50:50 ratio. Some ADP restraints added in the disordered butyl group to assist convergence

4 Asymmetric unit comprises 1 potassium cation plus ½ of a dimer anion. The latter straddles a crystallographic inversion centre which serves to generate the remainder of this species. The hydride (H1) was located and refined without restraints

5 The asymmetric unit comprises half of a molecule and a toluene solvent entity with half site occupancy. The remainder of the former is generated via a 2-fold rotation axis implicit in the space group symmetry. The solvent moiety also straddles this rotation axis and, as such is disordered about same in the gross structure. In addition, the methyl group could not be reliably located in the solvent, which probably reflects positional disorder between the 6 ring carbon positions. In effect, the solvent was treated as a benzene in the refinement, with account of the missing, half-occupancy solvent methyl group is accounted for in the formula herein. The phenyl ring was treated as a regular hexagon during refinement, and the ADPs therein were restrained to assist convergence

References

1. R.E. Mulvey, *Acc. Chem. Res.* **42**, 743 (2009); R.E. Mulvey, *Dalton Trans.* **42**, 6676 (2013)
2. L.T. Wendell, J. Bender, X. He, B.C. Noll, K.W. Henderson, *Organometallics* **25**, 4953 (2006)
3. A.J. Martinez-Martinez, D.R. Armstrong, B. Conway, B.J. Fleming, J. Klett, A.R. Kennedy, R.E. Mulvey, S.D. Robertson, C.T. O'Hara, *Chem. Sci.* **5**, 771 (2014)
4. F. Ortu, G.J. Moxey, A.J. Blake, W. Lewis, D.L. Kays, *Inorg. Chem.* **52**, 12429 (2013)
5. S. Aldridge, A.J. Downs, *Chem. Rev.* **101**, 3305 (2001)
6. F. Buch, H. Brettar, S. Harder, *Angew. Chem.-Int. Ed.* **45**, 2741 (2006); F. Buch, S. Harder, *Organometallics* **26**, 5132 (2007); *Z. Naturforsch., B: Chem. Sci.* **63**, 169 (2008); M. Arrowsmith, M.S. Hill, T. Hadlington, G. Kociok-Köhn, C. Weetman, *Organometallics* **30**, 5556 (2011); M. Arrowsmith, T.J. Hadlington, M.S. Hill, G. Kociok-Köhn, *Chem. Commun.* **48**, 4567 (2012)
7. J.F. Dunne, S.R. Neal, J. Engelkemier, A. Ellern, A.D. Sadow, *J. Am. Chem. Soc.* **133**, 16782 (2011); M.S. Hill, D.J. Liptrot, D.J. MacDougall, M.F. Mahon, T.P. Robinson, *Chem. Sci.* **4**, 4212 (2013)
8. M.S. Hill, M.F. Mahon, T.P. Robinson, *Chem. Commun.* **46**, 2498 (2010)
9. A.G.M. Barrett, M.R. Crimmin, M.S. Hill, P.B. Hitchcock, P.A. Procopiou, *Organometallics* **26**, 4076 (2007); D.J. Liptrot, M.S. Hill, M.F. Mahon, D.J. MacDougall, *Chem. Eur. J.* **16**, 8508 (2010)
10. M. Kelly, in *Fuel Cells and Hydrogen Storage*, vol. 141, eds. by A. Bocarsly, D. M. P. Mingos (Springer, Berlin Heidelberg, 2011)

11. F. Schuth, B. Bogdanovic, M. Felderhoff, *Chem. Commun.* **20**, 2249 (2004); M. Dornheim, S. Doppiu, G. Barkhordarian, U. Boesenberg, T. Klassen, O. Gutfleisch, R. Bormann, *Scripta Materialia* **56**, 841 (2007); K.-F. Aguey-Zinsou, J.-R. Ares-Fernandez, *Energy Environ. Sci.* **3**, 526 (2010); I.P. Jain, C. Lal, A. Jain, *Int. J. Hydrogen Energy* **35**, 5133 (2010)
12. S. Harder, *Chem. Commun.* **48**, 11165 (2012); R.W.P. Wagemans, J.H. van Lenthe, P.E. de Jongh, A.J. van Dillen, K.P. de Jong, *J. Am. Chem. Soc.* **127**, 16675 (2005)
13. M. Arrowsmith, M. S. Hill, D.J. MacDougall, M.F. Mahon, *Angew. Chem.-Int. Ed.* **48**, 4013 (2009)
14. Harder, J. Spielmann, J. Intemann, H. Bandmann, *Angew. Chem.-Int. Ed.* **50**, 4156 (2011)
15. J. Intemann, J. Spielmann, P. Sirsch, S. Harder, *Chem.-Eur. J.* **19**, 8478 (2013)
16. Hoffmann, T. Kottke, R.J. Lagow, R.D. Thomas, *Angew. Chem.-Int. Ed.* **37**, 1537 (1998)
17. A. Stasch, *Angew. Chem.-Int. Ed.* **51**, 1930 (2012)
18. A. Stasch, *Angew. Chem.-Int. Ed.* **53**, 1338 (2014)
19. D.J. Gallagher, K.W. Henderson, A.R. Kennedy, C.T. O'Hara, R.E. Mulvey, R.B. Rowlings, *Chem. Commun.* 376 (2002); D.V. Graham, A.R. Kennedy, R. E. Mulvey, C.T. O'Hara, *Acta Crystallogr. Sect. C* **62**, m366 (2006)
20. P.C. Andrikopoulos, D.R. Armstrong, A.R. Kennedy, R.E. Mulvey, C.T. O'Hara, R.B. Rowlings, *Eur. J. Inorg. Chem.* **2003**, 3354 (2003)
21. A. Streitwieser, *Acc. Chem. Res.* **17**, 353 (1984); R. Benn, A. Ruffńska, *Angew. Chem.-Int. Ed.* **25**, 861 (1986); N.N. Greenwood, A. Earnshaw, *Chemistry of the Elements*, 2nd edn. (Elsevier, New York, 1997), pp. 102–105, 127
22. J. Francos, B.J. Fleming, P. Garcia-Alvarez, A.R. Kennedy, K. Reilly, G.M. Robertson, S.D. Robertson, C.T. O'Hara, *Dalton Trans.* **43**, 14424 (2014)

Chapter 3

Silicon–Nitrogen Dehydrocoupling

3.1 Introduction

Silicon–nitrogen coupling is a reaction of significant interest. Compounds containing Si–N bonds are utilised as silylating agents [1], bases [2], ligands and ceramic precursors [3] and furthermore silanes act as protecting groups for amides, and vice versa [4]. Current synthetic routes to these compounds rely on the atom uneconomical aminolysis of chlorosilanes yielding the desired product and HCl, which creates highly acidic reaction conditions, reducing functional group tolerance and acts as a waste stream [5]. Dehydrocoupling approaches to these groups have been reported with a range of homogeneous metal catalysts including titanium(IV) [6], chromium(III) [7], copper(I) [8], rhodium(I) [9, 10], ruthenium(0) [11], ytterbium(II) [12] and samarium(II) [12], and uranium(IV) [13]. Finally a range of catalysts for germane and stannane dehydrocoupling have been reported [9]. Many of these metals are expensive, toxic or environmentally problematic and hence a Group 2 metal mediated dehydrocoupling would be a useful synthetic tool.

Initial work in this area was reported by Harder and co-workers, who reported an efficient, high yielding coupling of a variety of amines with silanes mediated by a calcium azametallacyclopropane [14]. More recently, Sadow et al. have described a dehydrocoupling between silanes and amines mediated by the trisoxazolanylborate magnesium precatalyst **VII** [15]. This work revealed a nuanced mechanistic framework and is summarised in Sect. 1.3.5.

Silicon–nitrogen dehydrocoupling has been reported with a range of metals (vide supra), the vast majority of which have relatively low abundance and accordingly high costs. Although limited reports of Group 2-catalysed silicon–nitrogen dehydrocoupling have been made, these are isolated to magnesium and calcium and, in the latter case, were the subject of only a very limited study. In order to explore the reactivity of the heavier Group 2 congeners the congeneric series of Group 2 bis(hexamethyldisilazides) $[M(N\{SiMe_3\}_2)_2]_2$ ($M = Mg, Ca, Sr$; **IIa–c**) were selected as precatalysts. An approach utilising catalytic, crystallographic and mechanistic studies is reported herein.

3.2 Catalytic Scope

An initial NMR investigation was undertaken into the substrate scope with regards to silanes and amines as shown in Table 3.1. On addition of the precatalyst to a mixture of the amine and silane in C₆D₆ a pronounced bubbling was observed for many of the reactions.

A number of notable general trends can be identified. Primarily, each of the precatalysts is active for a wide range of both amine and silane coupling partners. Qualitatively, strontium and calcium appear to be more active for dehydrocoupling than magnesium. Furthermore, the bulkiest silane, triphenylsilane is almost entirely inactive with magnesium (Table 3.1, entries 13–18), with only a modest yield with the least bulky amines, benzylamine (Table 3.1, entry 13) and pyrrolidine (Table 3.1, entry 16) being achieved.

Table 3.1 The results of the scope study into silicon–nitrogen dehydrocoupling catalysed by complexes **Ila-c** (0.05 mmol) with amine (0.1 mmol) and silane (0.1 mmol) in C₆D₆ (0.5 mL)

$$\begin{array}{c}
 \text{R}_2\text{NH} \\
 + \\
 \text{R}'_3\text{SiH}
 \end{array}
 \xrightarrow[\text{C}_6\text{D}_6, \text{RT}]{\text{Ila-c}}
 \text{R}_2\text{N}-\text{SiR}_3$$

Entry	Catalyst ^c	Silane	Amine	Product	Time/ days	Conversion (%)
1	Ila	PhSiH ₃	BnNH ₂	Intractable mixture	1 ^a	99
2			<i>t</i> BuNH ₂	PhSiH ₂ NH <i>t</i> Bu + PhSiH(NH <i>t</i> Bu) ₂	1 ^a	99 (86:14)
3			DippNH ₂	PhSiH ₂ NHDipp + PhSiH(NHDipp) ₂	1 ^a	99 (39:61)
4			(CH ₂) ₄ NH	PhSiH ₂ (N(CH ₂) ₄) + PhSiH(N(CH ₂) ₄) ₂	1 ^a	99 (29:71)
5			Et ₂ NH	PhSiH ₂ NEt ₂ + PhSiH(NEt ₂) ₂	1 ^a	99 (99:trace)
6			(Me ₃ Si) ₂ NH	PhSiH ₂ N(SiMe ₃) ₂	7 ^a	71
7			Ph ₂ SiH ₂	BnNH ₂	Ph ₂ SiHNHBn + Ph ₂ Si(NHBn) ₂	1 ^a
8	<i>t</i> BuNH ₂	Ph ₂ SiHNH <i>t</i> Bu			1 ^b	95
9	DippNH ₂	Ph ₂ SiHNHDipp			4 ^a	99
10	(CH ₂) ₄ NH	Ph ₂ SiHN(CH ₂) ₄			2 ^a	99
11	Et ₂ NH	Ph ₂ SiHNEt ₂			1 ^a	99
12	(Me ₃ Si) ₂ NH	No reaction			1 ^b	0
13	Ph ₃ SiH	BnNH ₂	Ph ₃ SiNHBn	5 ^b	25	
14			<i>t</i> BuNH ₂	Ph ₃ SiNH <i>t</i> Bu	2 ^b	0
15			DippNH ₂	No reaction	2 ^b	0
16			(CH ₂) ₄ NH	Ph ₃ SiN(CH ₂) ₄	5 ^b	7
17			Et ₂ NH	Ph ₃ SiNEt ₂	2 ^b	0
18			(Me ₃ Si) ₂ NH	No reaction	2 ^b	0

(continued)

Table 3.1 (continued)

Entry	Catalyst ^c	Silane	Amine	Product	Time/ days	Conversion (%)	
19	I Ib	PhSiH ₃	BnNH ₂	Intractable mixture	1 ^a	99	
20			<i>t</i> BuNH ₂	PhSiH ₂ NH <i>t</i> Bu + PhSiH(NH <i>t</i> Bu) ₂ + (PhSiH ₂) ₂ N <i>t</i> Bu	1 ^a	99 (78:10:12)	
21			DippNH ₂	PhSiH ₂ NHDipp + PhSiH(NHDipp) ₂ + (PhSiH ₂) ₂ NDipp	1 ^a	99 (12:20:68)	
22			(CH ₂) ₄ NH	PhSiH(N(CH ₂) ₄) ₂	1 ^a	99	
23			Et ₂ NH	PhSiH ₂ NEt ₂ + PhSiH(NEt ₂) ₂	1 ^a	99 (87:13)	
24			(Me ₃ Si) ₂ NH	PhSiH ₂ N(SiMe ₃) ₃	1 ^a	99	
25			Ph ₂ SiH ₂	BnNH ₂	Ph ₂ SiHNHBn + Ph ₂ Si(NHBn) ₂ + (PhSiH) ₂ NBn	1 ^a	99 (80:12:8)
26		<i>t</i> BuNH ₂		Ph ₂ SiHNH <i>t</i> Bu	1 ^a	99	
27		DippNH ₂		Ph ₂ SiHNHDipp	3 ^a	99	
28		(CH ₂) ₄ NH		Ph ₂ SiHN(CH ₂) ₄	1 ^a	94 (98:2)	
29		Et ₂ NH		Ph ₂ SiHNEt ₂	1 ^a	88	
30		(Me ₃ Si) ₂ NH		No reaction	4 ^b	0	
31		Ph ₃ SiH		BnNH ₂	Ph ₃ SiNHBn	1 ^a	99
32			<i>t</i> BuNH ₂	Ph ₃ SiNH <i>t</i> Bu	12 ^b	7	
33			DippNH ₂	No reaction	1 ^b	0	
34			(CH ₂) ₄ NH	Ph ₃ SiN(CH ₂) ₄	1 ^b	99	
35			Et ₂ NH	Ph ₃ SiNEt ₂	12 ^b	54	
36			(Me ₃ Si) ₂ NH	No reaction	4 ^b	0	
37		I Ic	PhSiH ₃	BnNH ₂	Intractable mixture	1 ^a	99
38				<i>t</i> BuNH ₂	PhSiH ₂ NH <i>t</i> Bu + PhSiH(NH <i>t</i> Bu) ₂	1 ^a	99 (58:42)
39				DippNH ₂	PhSiH ₂ NHDipp (PhSiH ₂) ₂ NDipp	1 ^a	99 (31:33)*
40				(CH ₂) ₄ NH	PhSiH ₂ (N(CH ₂) ₄) + PhSiH(N(CH ₂) ₄) ₂	1 ^a	99 (15:85)
41				Et ₂ NH	PhSiH ₂ NEt ₂ + PhSiH(NEt ₂) ₂	1 ^a	96 (89:11)
42			Ph ₂ SiH ₂	BnNH ₂	Ph ₂ SiHNHBn + Ph ₂ Si(NHBn) ₂ + (PhSiH) ₂ NBn	3 ^a	99 (5:35:55)*
43	DippNH ₂			Ph ₂ SiHNHDipp + (Ph ₂ SiH) ₂ NDipp	3 ^a	99 (77:23)	
44	Ph ₃ SiH		BnNH ₂	Ph ₃ SiNHBn	1 ^a	99	
45			<i>t</i> BuNH ₂	Ph ₃ SiNH <i>t</i> Bu	5 ^b	54	
46			DippNH ₂	No reaction	1 ^b	0	
47			(CH ₂) ₄ NH	Ph ₃ SiN(CH ₂) ₄	2 ^a	91	
48			Et ₂ NH	Ph ₃ SiNEt ₂	12 ^b	83	
49	(Me ₃ Si) ₂ NH		No reaction	1 ^b	0		

*Higher oligomers constitute the remainder of the conversion

^aRoom temperature^b60 °C

Primary amines of low to moderate bulk are readily dehydrocoupled with all three silane partners by each of the metals (Table 3.1, entries 1–3, 7–9, 19–21, 25–27, 31, 37–39, 42–44) with the exception of the aforementioned issues with magnesium. The bulkiest amine, 2,6-di-*iso*-propylaniline however fails to dehydrocouple with the bulkiest silane, triphenylsilane with any of the Group 2 precatalysts (Table 3.1, entries 15, 33, 46) although it is nevertheless very active with the less sterically congested phenylsilane, yielding doubly dehydrocoupled products in preference to single dehydrocoupling in defiance of stoichiometry (Table 3.1, entries 3, 21, 39). This suggests that both the steric demands and electronic character of the substituents have significant influences on reactivity with this far more acidic aniline coupling more readily than its aliphatic partners where the bulk of the coupling partner is insignificant. Furthermore, the very bulky *tert*-butylamine only couples in extremely poor yields with calcium and moderate yields with the heavier congener, $[\text{Sr}(\text{N}\{\text{SiMe}_3\}_2)_2]_2$ (Table 3.1, entries 32, 45).

Secondary amines of low bulk are readily dehydrocoupled, with the more basic pyrrolidine coupling far faster than its acyclic partner diethylamine with phenylsilane (Table 3.1, entries 4, 5, 23, 24, 40, 41). This results in lower selectivity, with the doubly dehydrocoupled $\text{PhSiH}(\text{N}(\text{CH}_2)_4)_2$ forming in preference to the single dehydrocoupled $\text{PhSiH}_2(\text{N}(\text{CH}_2)_4)$ when this amine is reacted with phenylsilane for all 3 precatalysts. With very bulky secondary amines such as hexamethyldisilazane, reaction is only observed readily with the least bulky phenylsilane (Table 3.1, entries 6, 24) but with more phenyl-substituted silanes no reaction is observed (Table 3.1, entries 12, 18, 30, 36, 49). With the exception of the aforementioned cases, conversions are consistently high under relatively mild conditions reflecting catalyst identity and substrate steric demands.

Finally, multiple dehydrocoupling to yield bis- and tris-aminosilanes or bis-silylamines are observed particularly for phenylsilane (Table 3.1, entries 1–5, 19–21, 23, 37–41). The least bulky pairing of phenylsilane and benzylamine rapidly and consistently yields intractable mixtures of higher oligomers suggesting that subsequent dehydrocoupling is very rapid for all metals with these substrates (Table 3.1, entries 1, 19, 37). Furthermore, strontium yields higher oligomers with phenylsilane and the very active 2,6-di-*iso*-propylaniline (Table 3.1, entries 39) and the combination of the small benzylamine with diphenylsilane (Table 3.1, entries 42). Strontium also yields multiple dehydrocoupling extensively with all dehydrocouplings of the smaller phenyl- and diphenylsilane providing this result (Table 3.1, entries 37–43).

In order to rationally access higher aminosilane oligomers, a further range of reactions were investigated by NMR spectroscopy utilising amine to silane ratios reflective of the stoichiometries of the desired heavier aminosilane oligomers. These investigations are summarised in Table 3.2.

As shown, formation of the desired higher oligomers is generally achievable, although conversion appears to occur less readily than the initial dehydrocoupling. Given the bulk-sensitive nature of these reactions seen in the first dehydrocoupling, and the effect of aminosilane formation on the hydricity of silicon-hydrogen bonds this is unsurprising. Of particular note is the reaction of benzylamine

Table 3.2 The results of the scope study into silicon–nitrogen dehydrocoupling catalysed by complexes **IIa–c** (0.05 mmol) with limiting reagent (0.1 mmol) in C₆D₆ (0.5 mL)

Entry	Cat.	Silane	Amine		Product	Time/days	Conversion (%)	
1	IIa	PhSiH ₃	BnNH ₂	1:3	(BnNH) ₃ SiPh + (BnNH) ₂ SiHPh	1 ^a	99 (91:9)	
2			<i>t</i> BuNH ₂	1:2	PhSiH ₂ NH <i>t</i> Bu + PhSiH(NH <i>t</i> Bu) ₂	7 ^a	92 (77:23)	
3			(CH ₂) ₄ NH	3:1	1:2	PhSiH ₂ (N(CH ₂) ₄) + PhSiH(N(CH ₂) ₄) ₂	1 ^b	66 (100:0)
4							1 ^a	99 (84:16)
5		Ph ₂ SiH ₂	BnNH ₂	1:2	Ph ₂ SiHNHBn + Ph ₂ Si(NHBn) ₂	3 ^a	90 (30:70)	
6				2:1		1 ^a	99 (99:trace)	
7			<i>t</i> BuNH ₂	1:2	2:1	Ph ₂ SiHNH <i>t</i> Bu	1 ^b	64
8							1 ^b	99
9			(CH ₂) ₄ NH	1:2	Ph ₂ SiHN(CH ₂) ₄ + Ph ₂ Si(N(CH ₂) ₄) ₂	7 ^b	55 (83:17)	
10	IIb	PhSiH ₃	BnNH ₂	1:3	Intractable mixture	1 ^a	99	
11			<i>t</i> BuNH ₂	1:3	1:2	PhSiH(NH <i>t</i> Bu) ₂ + (PhSiH ₂) ₂ N <i>t</i> Bu	1 ^b	66 (100:0)*
12							1 ^a	87 (93:7)
13							1 ^a	99 (0:100)
14			(CH ₂) ₄ NH	3:1	1:2	PhSiH(N(CH ₂) ₄) ₂ + PhSi(N(CH ₂) ₄) ₃	2 ^b	99 (0:100)
15		1 ^a					99 (100:0)	
16		Ph ₂ SiH ₂	BnNH ₂	1:2	Ph ₂ SiHNHBn + Ph ₂ Si(NHBn) ₂ + (Ph ₂ SiH) ₂ NBn	1 ^a	99 (0:100:0)	
17				2:1		5 ^a	99 (52:9:39)	
18			<i>t</i> BuNH ₂	1:2	2:1	Ph ₂ SiHNH <i>t</i> Bu + Ph ₂ Si(NH <i>t</i> Bu) ₂	10 ^b	99 (65:35)
19							10 ^b	99 (100:0)
20	(CH ₂) ₄ NH		1:2	Ph ₂ SiHN(CH ₂) ₄ + Ph ₂ Si(N(CH ₂) ₄) ₂	2 ^a	95 (12:88)		
21	IIc	PhSiH ₃	BnNH ₂	1:3	Intractable Mixture	1 ^a	99	
22			<i>t</i> BuNH ₂	1:3	1:2	PhSiH(NH <i>t</i> Bu) ₂	1 ^a	66*
23							1 ^a	99*
24			(CH ₂) ₄ NH	3:1	PhSi(N(CH ₂) ₄) ₃	1 ^b	99	
25		Ph ₂ SiH ₂	BnNH ₂	1:2	Ph ₂ Si(NHBn) ₂ + (Ph ₂ SiH) ₂ NBn	1 ^a	99 (88:12)	
26				2:1		1 ^a	99 (100:0)	

*Higher oligomers constitute the remainder of the conversion

^aRoom temperature^b60 °C

with phenylsilane in a 3 to 1 ratio catalysed by magnesium, which yields well defined products in contrast to the results of the 1 to 1 reaction (Table 3.2, entry 1). In contrast, the heavier congeners once again yield intractable products (Table 3.2, entries 10, 21). When utilising phenylsilane, although access to the tris-aminated product is possible via a 1:3 silane:amine ratio, this only occurs for amines with low steric demand (Table 3.2, entries 1, 14, 24), in contrast to the reaction with larger amines (Table 3.2, entries 3, 11, 22). Although bis(amino)silanes are

accessible from a 1:2 silane:amine ratio, they only form cleanly in a limited number of cases (Table 3.2, entries 11, 15, 26) and only for the heavier congeners, Ca and Sr. With larger amines the singly dehydrocoupled product is extensively favoured (Table 3.2, entries 2, 4, 9, 15, 23), irrespective of the stoichiometry. Finally, with a 2:1 silane:amine ratio the disilylamines are almost always inaccessible with a few notable exceptions (Table 3.2, entries 13, 17, 25) where they form as a small proportion of the product mixture.

On the basis of this extensive study into the scope of this reaction, a number of trends can be highlighted. Both the steric demands and the electronic character of both coupling partners have a significant influence on reactivity. The degree to which steric bulk influences the reaction is defined by the size of the metal centre; effects are smallest on strontium and largest on magnesium. This has an effect both on the reaction of bulky amines and silanes and also higher dehydrocouplings to yield bis(amino)silanes. Electronically, anilines couple more readily than their aliphatic partners and strontium and calcium appear to have far higher activity than magnesium as evidenced by both their shorter reaction times, milder conditions and, notably, their reduced selectivity. Nevertheless, this study shows that amine-silane coupling is readily catalysed by Group 2 amides under mild conditions giving moderate to excellent conversions for a broad range of coupling partners.

3.3 Stoichiometric Studies

In order to provide further insight into the mechanism of these dehydrocouplings, a range of stoichiometric reactions were undertaken. To prevent complications due to the presence of hexamethyldisilazane, metal sources ligated by basic anions which yield inert products when protonated were selected. For magnesium, the commercially available di-*n*-butylmagnesium was selected while for calcium and strontium the metal alkyls $[M(\text{CH}(\text{SiMe}_3)_2)_2(\text{THF})_2]$ **IVb–c** were utilised. Reactions were performed by the stepwise addition of amine to metal alkyl, followed by silane after 1 h.

An initial reaction between a 1:1:2 mixture of di-*n*-butylmagnesium, phenylsilane and 2,6-di-*iso*-propylaniline in heptanes yielded only the doubly dehydrocoupled species DippNHSiPh(H)NHDipp **6** and a light, colourless precipitate, thought to be magnesium hydride. A single crystal X-ray diffraction analysis was undertaken on crystals isolated from heptanes solution after filtering at room temperature. The results of this analysis are shown in Fig. 3.1.

It was proposed under the correct conditions that the dianion of this species could act as a ligand for dicationic metal centres. As such, the above reaction was reattempted in THF, in the hope that the proposed magnesium hydride by-product would remain in solution and undergo a protonolysis with the formed bis(amino)silane, **6**. This reaction yielded, by fractional crystallisation from toluene at reduced temperature, both the mono-dehydrocoupled

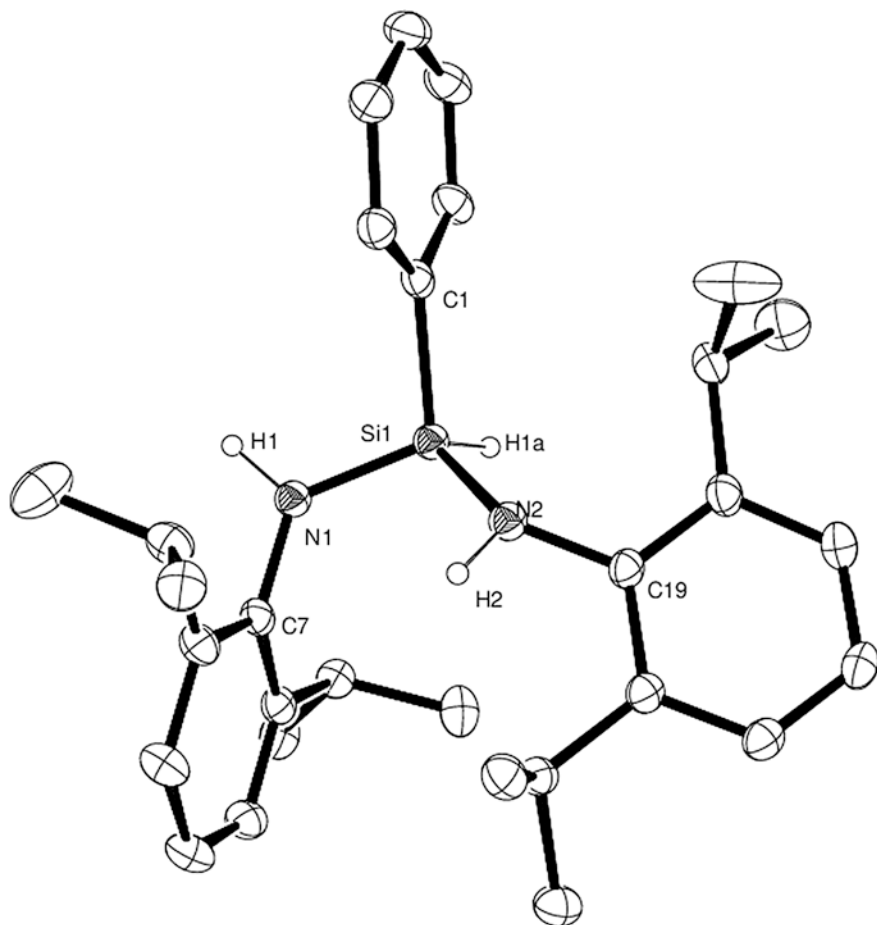


Fig. 3.1 ORTEP representation of the doubly dehydrocoupled DippNHSiPh(H)NHDipp, **6**. Thermal ellipsoids at 30 % probability. Hydrogen atoms except those attached to N1, Si1 and N2 omitted for clarity. Reproduced from Ref. II.1 with permission from The Royal Society of Chemistry

magnesium-amide-silylamide **7** and the desired magnesium bis(amido)silane **8**. The structures of these species are shown in Figs. 3.2 and 3.3.

Of note was the competitive formation of **7** and **8** which crystallised simultaneously from a single solution and were separated manually under microscopy. This suggests the formation of the DippNHSiPh(H)NHDipp ligand occurs step-wise with the magnesium-anilide-silylanilide **7** acting as an intermediate in the formation of **6**. The dehydrocoupling step which would yield the bis(amino)silane **6** from **7** also yields a magnesium hydride which can deprotonate **6** yielding **8**. In a non-polar reaction medium, **6** crystallises as the coproduced MgH_2 has insufficient solubility to deprotonate this species, however switching the solvent to the more

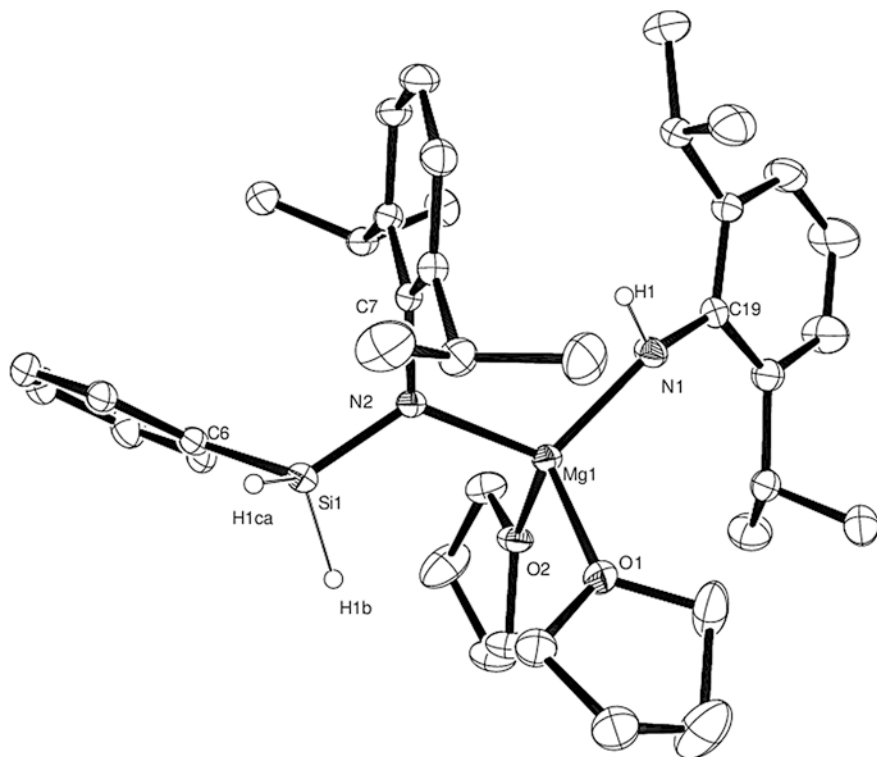


Fig. 3.2 ORTEP representation (DippNH)[DippNSi(H)Ph]Mg(THF)₂, **7**. Thermal ellipsoids at 30 % probability. Hydrogen atoms except those attached to N1, Si1 and N2 omitted for clarity. Reproduced from Ref. II.1 with permission from The Royal Society of Chemistry

polar, donor solvent THF yields an increased lifetime of this putative magnesium hydride in solution which can therefore deprotonate **6** yielding **8**. Alternatively, **7** may spontaneously convert into **8** via an intramolecular Si-H/Mg-N metathesis followed by a protonolysis of the products, a magnesium hydride and amine, yielding H₂. Further evidence for this is provided by the spontaneous conversion of **7** into **8** in an NMR tube precluding NMR analysis of **7**. Although production of any of these species, **6–8**, has not been optimized, their formation clearly underlines the viability of a stepwise silicon-nitrogen dehydrocoupling catalysed by magnesium as summarised in Scheme 3.1.

For the heavier congeners, the reactions between a 1:1:2 mixture of the Group 2 dialkyls [M{CH(SiMe₃)₂}₂(THF)₂] (M = Ca; **IVb**, Sr; **IVc**), phenylsilane and 2,6-di-*iso*-propylaniline were conducted in THF utilising the same methodology as for magnesium. A rapid exotherm and foaming was noted on mixing of the reagents. Subsequent reduced temperature crystallisation from toluene yielded crystals suitable for X-ray crystallography, which were found to be the relevant metal bis(amido)silanes of calcium and strontium, **9** and **10** respectively, as shown in

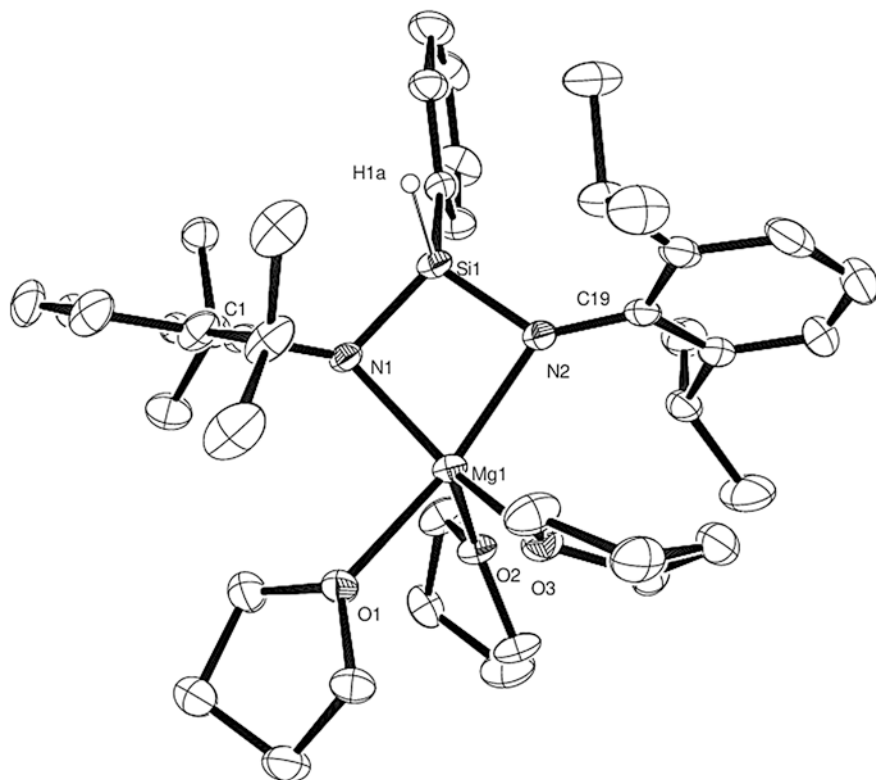
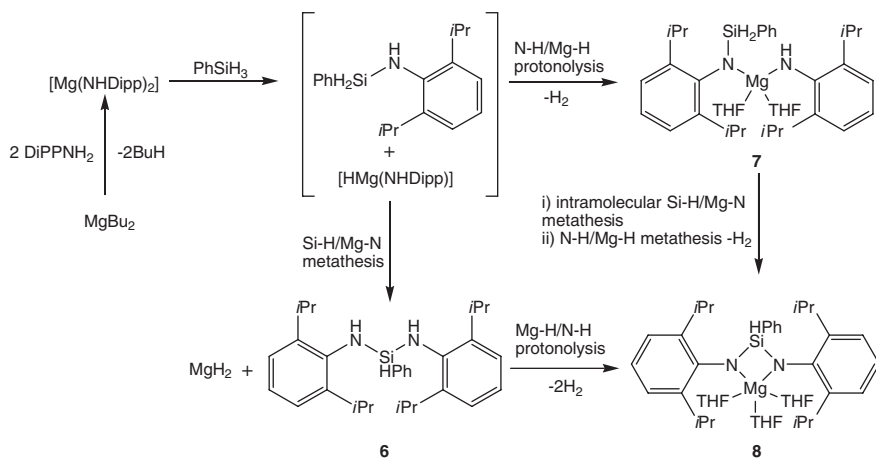


Fig. 3.3 ORTEP representation $[(\text{DippN})_2\text{Si}(\text{H})\text{Ph}]\text{Mg}(\text{THF})_2$, **8**. Thermal ellipsoids at 30 % probability. Hydrogen atoms except those attached to Si1 omitted for clarity. Reproduced from Ref. II.1 with permission from The Royal Society of Chemistry



Scheme 3.1 Summary of the stoichiometric studies into silicon–nitrogen dehydrocoupling mediated by di-butylmagnesium rationalising the crystallographically defined products

Figs. 3.4 and 3.5. Although the data collected for crystals of **10** was of poor quality ($R(\text{int}) = 0.1702$), the connectivity was nevertheless unambiguous and bond length and angle data is included for the purposes of comparison to its more well resolved congeneric analogues. The formation of these products exclusively, in contrast to the more complicated products of their lighter congener, magnesium, is a reflection of the qualitative (*vide supra*) and quantitative (*vide infra*) rate acceleration observed consistently for the heavier alkaline earths.

While the bond lengths and angles, as summarised in Tables 3.3 and 3.4, in these Group 2 metal silyl(bisamides), **8–10**, and amido-silylamide **7** are unremarkable in comparison to the variety of previously reported amide [16], silylamide [17] and bis(amido)silane [18] derivatives of Mg, Ca and Sr, the complexes

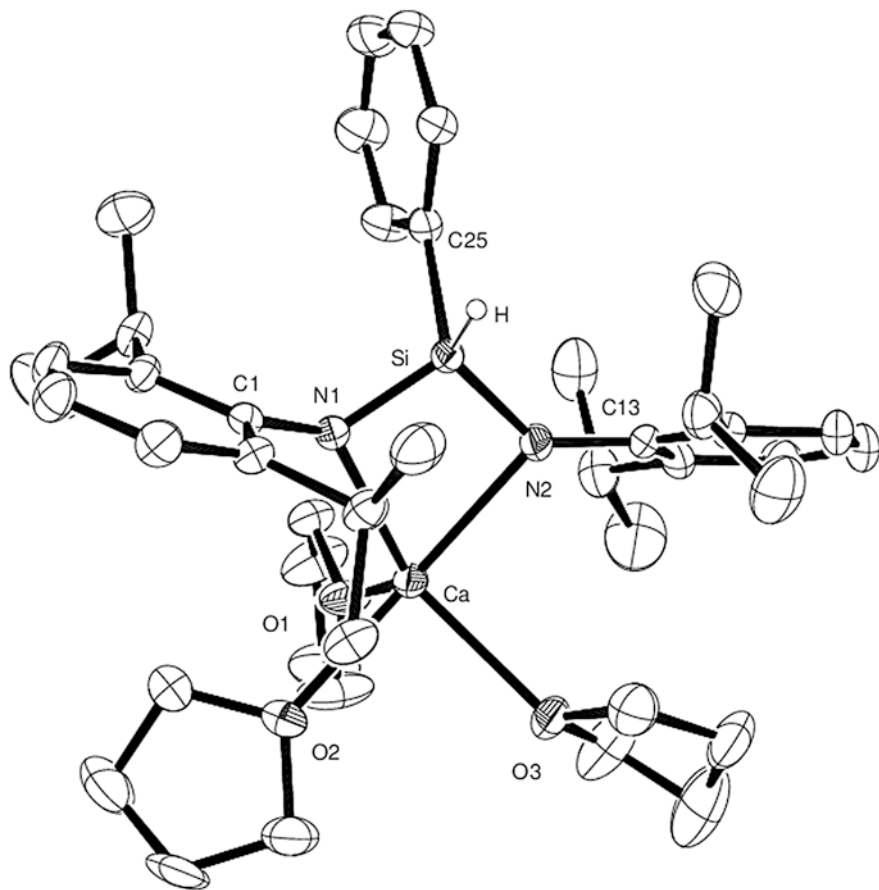


Fig. 3.4 ORTEP representation of $[(\text{H})\text{PhSi}(\text{DippN})_2]\text{Ca}(\text{THF})_3$, **9**. Thermal ellipsoids at 30 % probability. Hydrogen atoms except those attached to Si omitted for clarity. Reproduced from Ref. II.1 with permission from The Royal Society of Chemistry

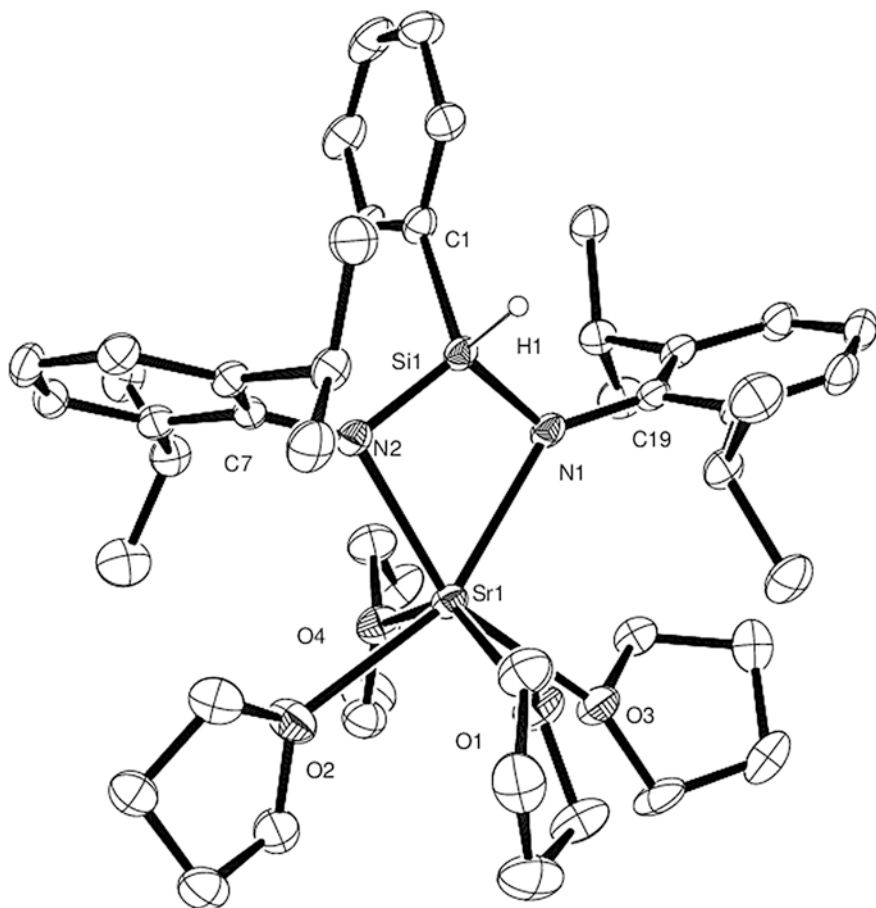


Fig. 3.5 ORTEP representation of $[(\text{H})\text{PhSi}(\text{DippN})_2]\text{Sr}(\text{THF})_4$, **10**. Thermal ellipsoids at 30 % probability. Hydrogen atoms except those attached to Si1 omitted for clarity. Reproduced from Ref. II.1 with permission from The Royal Society of Chemistry

formed of the conjugate dianion of **6** with these Group 2 dications constitute the first report of any metal complex containing a bridging Si–H functionality between two nitrogen centres. Although these bond lengths are unremarkable, a number of trends can be identified. The increase in M^{2+} radius down Group 2 is reflected by the M–N bond lengths of compounds **8** (M = Mg, 2.044(2), 2.108(3) Å), **9** (M = Ca, 2.281(3), 2.342(3) Å), and **10** (M = Sr, 2.489(4), 2.494(4) Å), and further reflected by the number of molecules of coordinated THF which raise the alkaline earth coordination number from five for **8** and **9** to six for **10**.

Table 3.3 Selected bond lengths (Å) for compounds **6–10**

	6	7	8	9	10
M1-N1	–	1.9795(19)	2.044(2)	2.281(3)	2.489(4)
M1-N2	–	2.0073(18)	2.108(3)	2.342(3)	2.494(4)
M1-O1	–	2.0341(1)	2.157(2)	2.335(3)	2.591(3)
M1-O2	–	2.0194(16)	2.057(2)	2.377(3)	2.597(3)
M1-O3	–	–	2.075(2)	2.388(3)	2.645(3)
M1-O4	–	–	–	–	2.561(4)
N1-Si1	1.7119(16)	–	1.699(3)	1.699(3)	1.704(4)
N2-Si1	1.7281(17)	1.6908(18)	1.696(2)	1.693(3)	1.693(4)

Table 3.4 Selected bond angles (°) for compounds **6–10**

	6	7	8	9	10
N1-M1-N2	–	114.07(8)	77.15(10)	69.46(12)	65.04(12)
N1-M1-O1	–	112.31(8)	96.05(10)	109.10(12)	107.00(12)
N2-M1-O1	–	110.04(8)	164.22(10)	114.58(13)	107.25(12)
N2-M1-O2	–	106.86(7)	111.61(10)	160.41(13)	87.95(12)
M1-N1-Si1	–	–	92.75(11)	95.34(15)	94.77(15)
M1-N2-Si1	–	123.18(10)	90.60(11)	93.31(15)	94.90(16)
N2-Si1-N2	104.15(8)	–	99.43(12)	101.88(16)	104.10(19)

3.4 Kinetic Analyses

A kinetic study was undertaken utilising ^1H NMR spectroscopy to help elucidate the mechanism of the σ -bond metathesis between amines and silanes, centring on the reaction of diethylamine with diphenylsilane as catalysed by the metal silylamides **IIa–c**, as shown in Scheme 3.2. These coupling partners were selected as the reaction occurs in a practicable timeframe and yields a range of well-defined products with well-defined NMR resonances which give valid integrations.

An initial study into the turnover frequency for each precatalyst, **IIa–c**, reflected the observed activity of the different congeners noted in the prior scope study (vide supra) and is summarised in Table 3.5.

This simple analysis reflects the qualitative results of the initial scope and stoichiometric studies which indicated the heavier alkaline earths, Ca and Sr, to have far higher rates for silicon-nitrogen dehydrocoupling than their lighter congener, Mg.

With this in hand, a more in-depth study was undertaken to further elucidate the reasons for this extreme congeneric divergence.

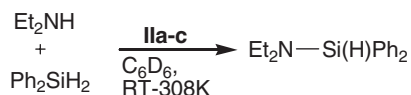
**Scheme 3.2** The reaction of diethylamine and phenylsilane mediated by **IIa–c** kinetically investigated by NMR

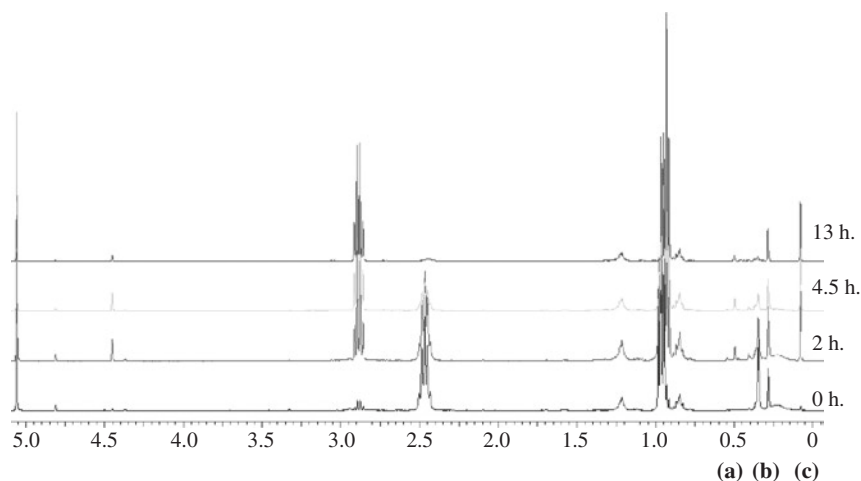
Table 3.5 Turnover frequency data for the silicon–nitrogen dehydrocoupling of diethylamine and diphenylsilane mediated by precatalysts **IIa–c**

Catalyst	TOF (h ⁻¹)
IIa	57.1(4)
IIb	2822.5(54)
IIc	125.5(22)

3.4.1 Catalyst Initiation

Initial studies suggested divergence in entry to the catalytic cycle exists between magnesium, calcium and strontium and to gain insight into this a series of reactions between a 1:1 ratio of diethylamine and diphenylsilane in the presence of 5 mol% **IIa–c** were analysed by NMR spectroscopy. Magnesium showed no initial induction period and activity is immediately observed. As spectra were performed at intervals of 30 min, it is possible that activation occurs far faster than activity and hence no activation period is discernible. Nevertheless, analysis of the trimethylsilyl region of the ¹H NMR is instructive, as shown in Fig. 3.6.

Over the course of the entire reaction the peak corresponding to hexamethyldisilazide bound to the magnesium centre slowly converts to 2 other peaks but only fully converts after complete consumption of the amine. This suggests that throughout the reaction, at least one hexamethyldisilazide group acts as a ligand for the magnesium centre. Immediate conversion to hexamethyldisilazane and a small amount of Ph₂SiHN(SiMe₃)₂ is observed. Although an increase in both protonation and silylation of hexamethyldisilazide is observed however this takes time

**Fig. 3.6** NMR spectra of the key region in the activation of **IIa** in the presence of diethylamine and diphenylsilane. **a** Mg–N(SiMe₃)₂, **b** Ph₂SiHN(SiMe₃)₂, **c** HN(SiMe₃)₂

equivalent to the lifetime of the reaction. These observations are consistent with a rate determining protonolysis for the unbulky silylamide product while with a very bulky hexamethyldisilazide the rate of Si–N bond formation is similar to that of protonolysis yielding to a mixture of protonated and silylated ligand in the reaction medium.

It is notable that amine is not initially consumed in the plots of amine concentration against time for calcium, yielding an induction period in the kinetics. NMR analysis is once again instructive as shown in Fig. 3.7.

In this case NMR spectra were performed at much shorter intervals of 1 min owing to the far higher activity of the calcium centre. In this case, the induction period is clearly indicative that the rate of induction is below the rate of reaction and hence catalyst activation is initially rate limiting. Furthermore, the NMR spectra clearly show a different mechanism of activation to that of magnesium. During this period little conversion of the amine occurs, reflecting the observed induction period. Furthermore, the peak corresponding to the hexamethyldisilazide ligand bound to calcium is completely converted before significant activity is observed. This is a notable contrast to magnesium, suggesting that calcium is not in fact ligated by hexamethyldisilazide during the catalytic reaction. Furthermore, this peak converts predominantly to the resonance corresponding to the minor product in the activation of the magnesium centre which was previously attributed to $\text{Ph}_2\text{SiHN}(\text{SiMe}_3)_2$ and almost no $\text{HN}(\text{SiMe}_3)_2$ is observed.

Finally, the heaviest congener analysed, strontium, once again showed divergent activity. Analysis at 30 min intervals evidenced a rapid conversion to the active species as shown in Fig. 3.8.

As shown, conversion of all of the strontium bound hexamethyldisilazide peaks to a resonance corresponding to the major product of magnesium activation,

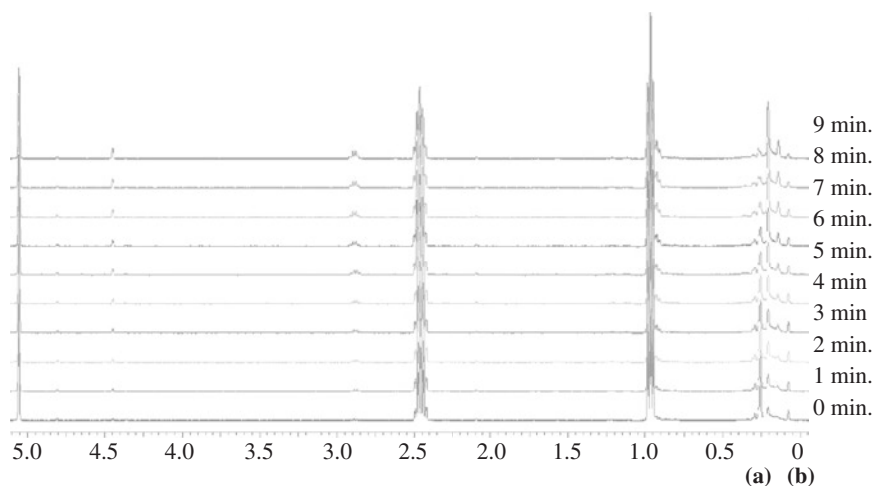


Fig. 3.7 NMR spectra of the key region in the activation of **IIb** in the presence of diethylamine and diphenylsilane. **a** $\text{Ca-N}(\text{SiMe}_3)_2$, **b** $\text{Ph}_2\text{SiHN}(\text{SiMe}_3)_2$ [19]

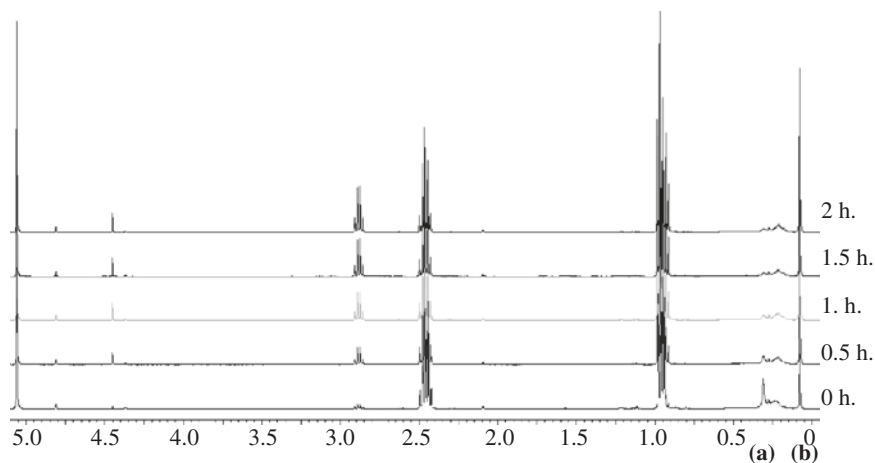


Fig. 3.8 NMR spectra of the key region in the activation of **IIc** in the presence of diethylamine and diphenylsilane. **a** $\text{Sr-N}(\text{SiMe}_3)_2$, **b** $\text{HN}(\text{SiMe}_3)_2$

$\text{HN}(\text{SiMe}_3)_2$, is observed. The complete conversion suggests no persistent ligation of the strontium centre by hexamethyldisilazide. In contrast to calcium, however the major product of the activation in the reaction medium is the protic hexamethyldisilazane.

Analysis of the products of these activation reactions is instructive. Hexamethyldisilazane is a protic amine; an equilibrium has been previously observed between Group 2 amides and hexamethyldisilazane [20, 21]. This equilibrium reduces the catalytic activity by decreasing the solution concentration of the catalytically active metal-substrate amide species. For magnesium and strontium the persistence of hexamethyldisilazane in the reaction medium is likely to have an inhibitory effect on the reaction. Owing to the rate determining nature of the protonolysis for magnesium (*vide infra*), however, this effect is likely to be small although extant as evidenced by the ongoing silylation of the hexamethyldisilazide ligand observed during activation of magnesium in Fig. 3.6. In contrast the activation of calcium which, occurring before any diethylamine-diphenylsilane dehydrocoupling, yields only the tris-silylated amine $\text{Ph}_2\text{SiHN}(\text{SiMe}_3)_2$. Lacking a proton this species does not undergo these equilibrium reactions and hence no inhibition of the calcium activity by this mechanism is observed. In the case of **IIb**, this exclusive, irreversible metathesis-based activation yields a brief induction period which initially complicated kinetic analysis. Consequently, premixing of the precatalyst, **IIb**, and diphenylsilane was utilised to deconvolute the kinetics, rendering them amenable to analysis. This may account partially for the increased activity of calcium relative to the other congeners in these reactions.

The persistence of ligation of the magnesium by hexamethyldisilazide throughout the reaction in contrast to the heavier congeners is of interest in the context of the observed reaction orders in [catalyst] (*vide infra*). The magnesium-catalysed

reaction shows a first order rate dependence on [catalyst], which would suggest a monomeric species. A large ligand, such as hexamethyldisilazide may account for this as the very small magnesium centre cannot accommodate this ligand in the form of a dimer and hence a monomeric species persists in solution. In contrast, the calcium species shows a first order dependence on [catalyst] wherein the concentration of diethylamine ensures a monomeric calcium centre while the strontium precatalyst shows a $\frac{1}{2}$ order dependence on [catalyst] which can be accounted for by a dimeric catalyst species.

3.4.2 Order of Reactants for Magnesium

To analyse the order in catalyst, a 1:1 mixture of amine and silane was reacted at a range loadings of **IIa**. These data, showing the reaction to be first order overall, were then analysed via a best fit plot of rate against loading to find the order in catalyst as shown in Figs. 3.9 and 3.10 which was found to be first order in [catalyst].

Subsequent to this, the orders in amine and silane were determined via a *pseudo*-first order methodology in which a tenfold excess of silane was reacted with a single equivalent of amine and vice versa. The consumption of the limiting reagent with time was then fitted to an order in limiting reagent, as shown in Figs. 3.11 and 3.12.

This analysis was suggestive of a first order dependence on [amine] and a zero-order dependence on [silane]. With these data in hand it is possible to formulate a rate law for this reaction as shown in Eq. 3.1.

$$\text{rate} = k[\text{cat}]^1[\text{amine}]^1[\text{silane}]^0 \quad (3.1)$$

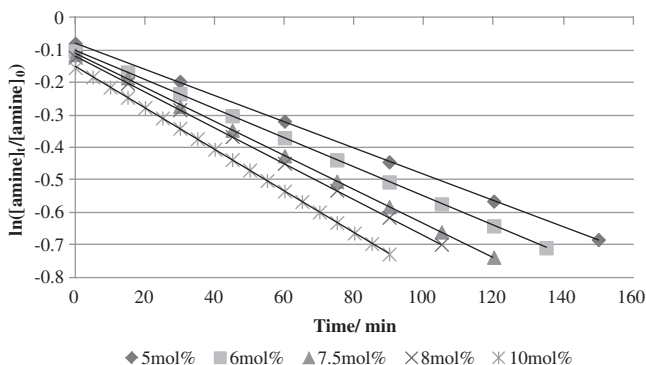


Fig. 3.9 The overall first-order plot of $\ln([\text{amine}]_t/[\text{amine}]_0)$ against time for a range of **IIa** concentrations

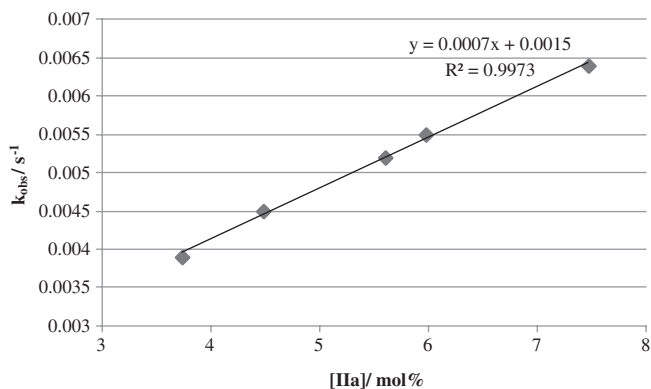


Fig. 3.10 The plot of observed rate constant against catalyst loading for a range of **IIa** concentrations

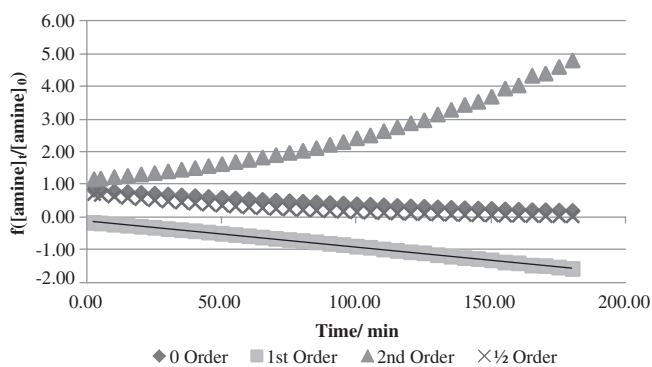


Fig. 3.11 The overall first-order plot of $f([\text{amine}]_t/[\text{amine}]_0)$ against time for a reaction with a tenfold excess of diphenylsilane

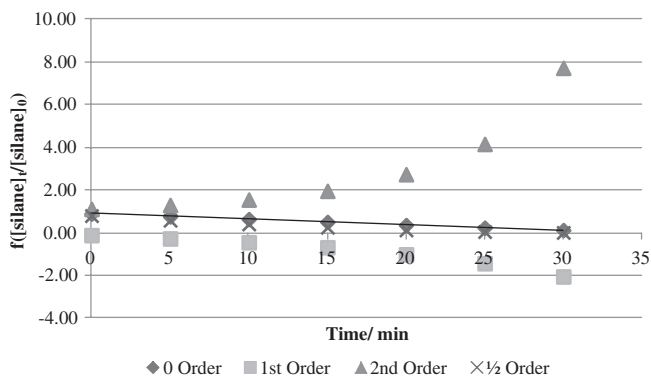


Fig. 3.12 The overall zero-order plot of $f([\text{silane}]_t/[\text{silane}]_0)$ against time for a reaction with a tenfold excess of diethylamine

3.4.3 Order of Reactants for Calcium

To analyse the order in catalyst, a 1:1 mixture of amine and silane was reacted at a range loadings of **IIb**. These data, showing the reaction to be first order overall, were then analysed via a best fit plot of rate against loading to deduce a first order dependence on [catalyst] as shown in Figs. 3.13 and 3.14.

Subsequently, the orders in amine and silane were determined via a *pseudo*-first order methodology in which a tenfold excess of silane was reacted with a single equivalent of amine and vice versa. The consumption of the limiting reagent with time was then fitted to an order in limiting reagent, as shown in Figs. 3.15 and 3.16.

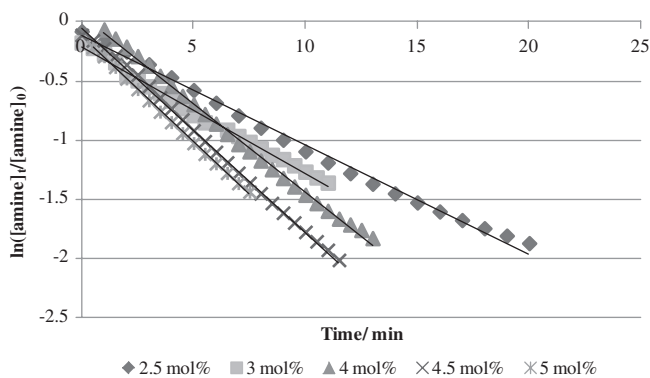


Fig. 3.13 The overall first-order plot of $\ln([\text{amine}]_t/[\text{amine}]_0)$ against time for a range of **IIb** concentrations

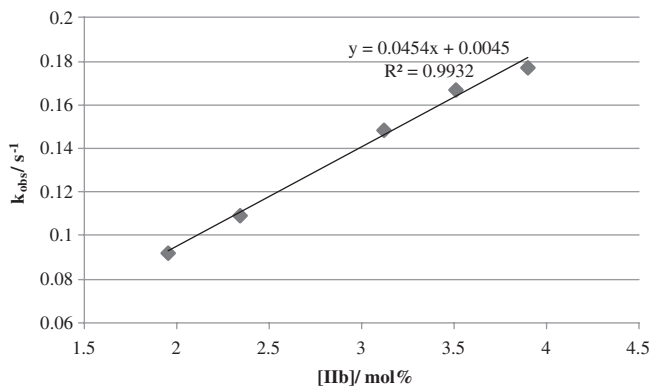


Fig. 3.14 The plot of observed rate constant against catalyst loading for a range of **IIb** concentrations

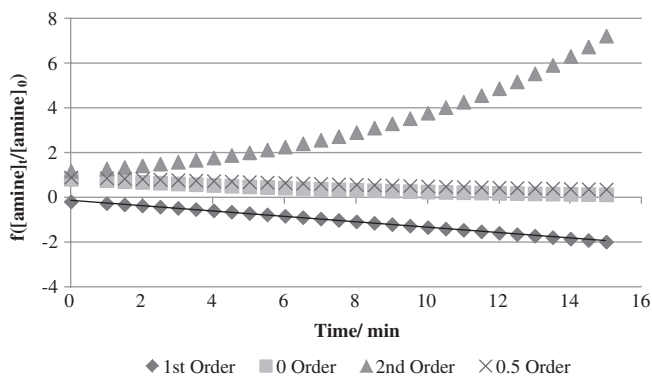


Fig. 3.15 The overall first-order plot of $f([\text{amine}]_t/[\text{amine}]_0)$ against time for a reaction with a tenfold excess of diphenylsilane

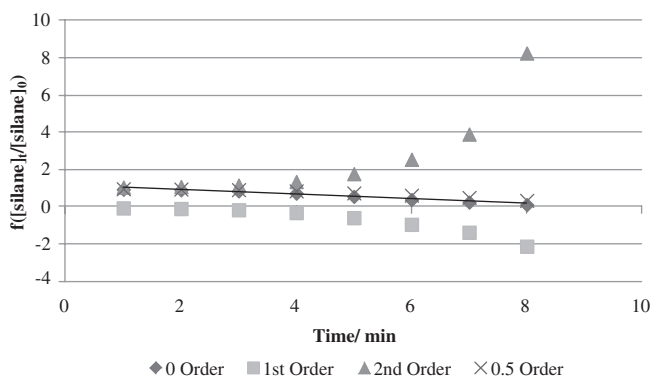


Fig. 3.16 The overall zero-order plot of $f([\text{silane}]_t/[\text{silane}]_0)$ against time for a reaction with a tenfold excess of diethylamine

This analysis was suggestive of a first order dependence on [amine] and a zero-order dependence on [silane]. With this data in hand it is possible to formulate a rate law for this reaction as shown which is identical to that formulated for magnesium, as shown in Eq. 3.1.

3.4.4 Order of Reactants for Strontium

To analyse the order in catalyst, a 1:1 mixture of amine and silane was reacted at a range loadings of **IIc**. These data, showing the reaction to be second order overall, was then analysed via a best fit plot of rate against loading to find the order in catalyst as shown in Figs. 3.17 and 3.18 which was found to be $\frac{1}{2}$ order in [catalyst].

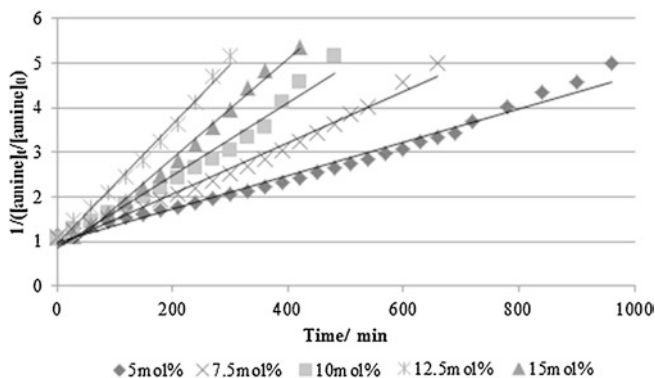


Fig. 3.17 The overall first-order plot of $\ln([\text{amine}]_t/[\text{amine}]_0)$ against time for a range of **IIc** concentrations

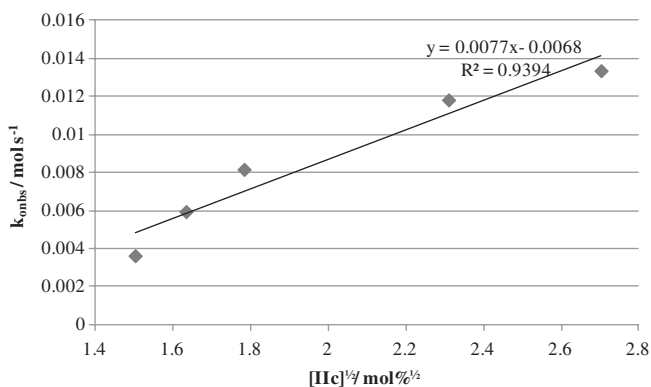


Fig. 3.18 The plot of observed rate constant against catalyst loading for a range of **IIc** concentrations

The orders in amine and silane were then determined via a *pseudo*-first order methodology in which a tenfold excess of silane was reacted with a single equivalent of amine and vice versa. The consumption of the limiting reagent with time was then fitted to an order in limiting reagent, as shown in Figs. 3.19 and 3.20.

This analysis was suggestive of a first order dependence on [amine] and a first order dependence on [silane]. With this data in hand it is possible to formulate a rate law for this reaction as shown below.

$$\text{rate} = k[\text{cat}]^{0.5}[\text{amine}]^1[\text{silane}]^1 \quad (3.2)$$

Notably, this analysis suggested two independent rate laws were operant, Eq. 3.1, operant for **IIa** and **IIb**, while Eq. 3.2 is operant for **IIc**. Assuming that Eq. 3.1 reflects an elementary reaction step which correlates with molecularity in the

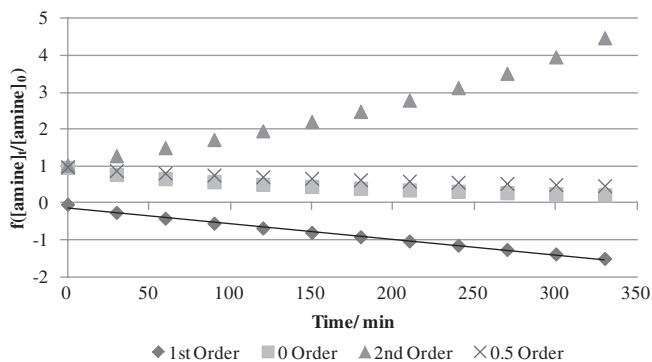


Fig. 3.19 The overall first-order plot of $f([\text{amine}]_t/[\text{amine}]_0)$ against time for a reaction with a tenfold excess of diphenylsilane

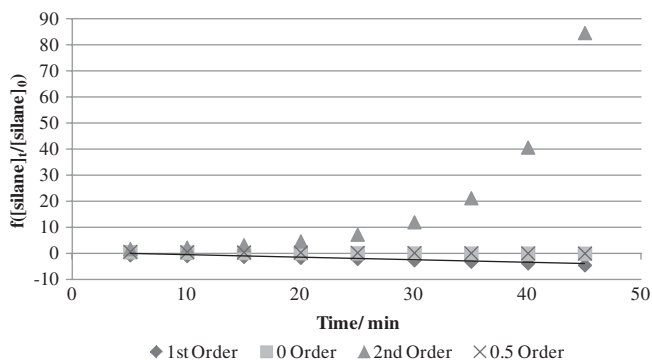


Fig. 3.20 The overall first-order plot of $\ln([\text{silane}]_t/[\text{silane}]_0)$ against time for a reaction with a tenfold excess of diethylamine

catalysis, these rate laws suggest a single magnesium or calcium centre and one molecule of amine being involved in the transition state while diphenylsilane plays no role. In contrast, Eq. 3.2 is suggestive of a transition state wherein a dimer of two strontium centres interacts with both one equivalent of amine and one equivalent of silane.

3.4.5 Eyring and Arrhenius Analyses for *Ila-c*

With these analyses in hand, a number of reactions were undertaken to assess the effect of temperature upon the rate of reaction. The results of these analyses are summarised in Figs. 3.21, 3.22, 3.23, 3.24 and 3.25.

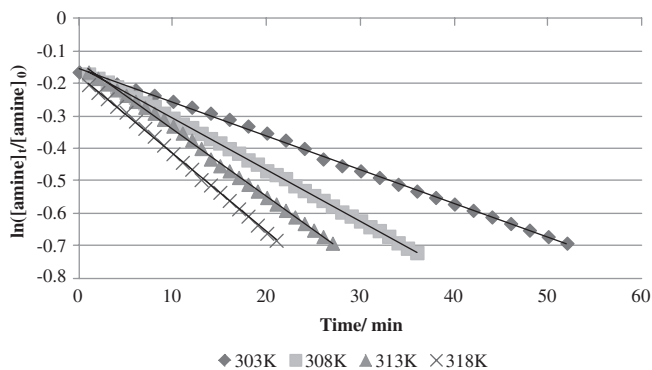


Fig. 3.21 The variable temperature plots for diethylamine-diphenylsilane coupling mediated by **IIa**

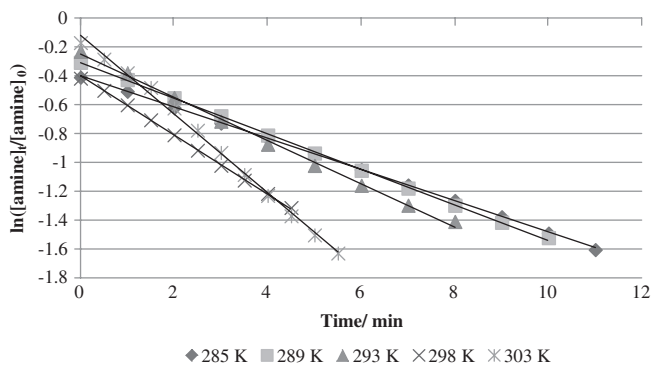


Fig. 3.22 The variable temperature plots for diethylamine-diphenylsilane coupling mediated by **IIb**

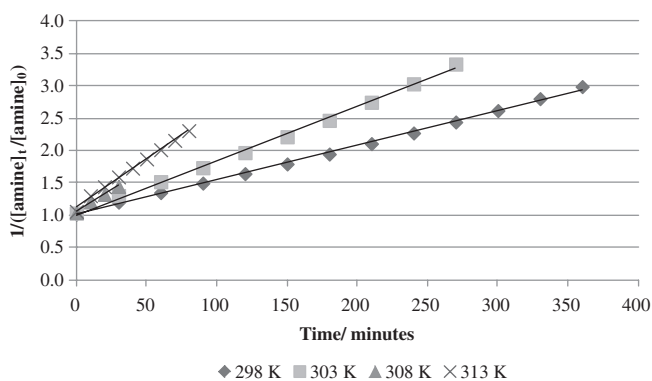


Fig. 3.23 The variable temperature plots for diethylamine-diphenylsilane coupling mediated by **IIc**

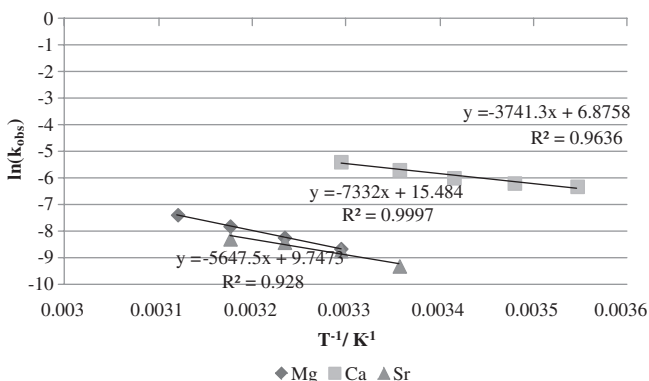


Fig. 3.24 The Arrhenius analysis to elucidate the activation energy for the rate determining step of diethylamine-diphenylsilane dehydrocoupling catalysed by **IIa-c**

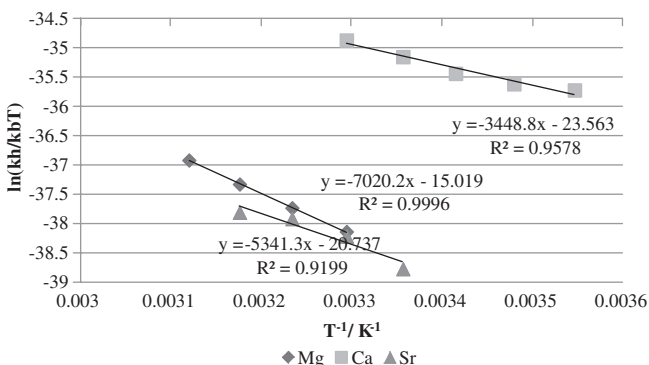


Fig. 3.25 The Eyring analysis to elucidate the activation enthalpy and entropies for the rate determining step of diethylamine-diphenylsilane dehydrocoupling catalysed by **IIa-c**

Table 3.6 Activation parameters for the catalytic dehydrocoupling of Et_2NH and Ph_2SiH_2 mediated by **IIa-c**

Catalyst	E_a (kcal mol ⁻¹)	ΔH^\ddagger (kcal mol ⁻¹)	ΔS^\ddagger (cal mol ⁻¹ K ⁻¹)	ΔG_{298}^\ddagger (kcal mol ⁻¹)
IIa	14.6(2)	13.9(2)	-29.8(6)	22.8
IIb	7.4(1)	6.8(1)	-46.8(1)	20.7
IIc	11.2(23)	10.6(23)	-41.2(81)	23.5

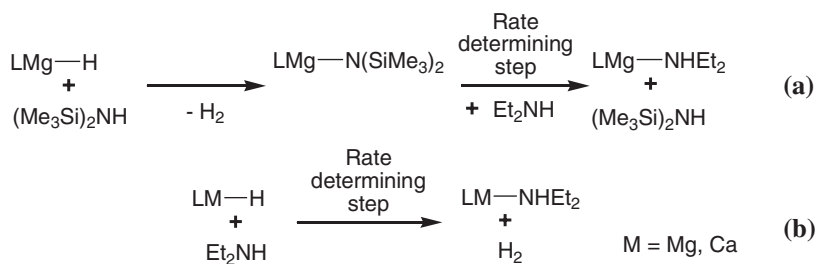
Utilising Arrhenius and Eyring analysis techniques, a number of key parameters regarding the rate determining step can be derived and are summarised in Table 3.6.

These data are consistent with the observed activity wherein **IIb** enjoys a turnover frequency an order of magnitude larger than its congeners **IIa** and **IIc** (Table 3.6). To wit, **IIb** enjoys a calculated activation energy and enthalpy of activation with a 4–8 kcal mol⁻¹ advantage over **IIa** and **IIc**.

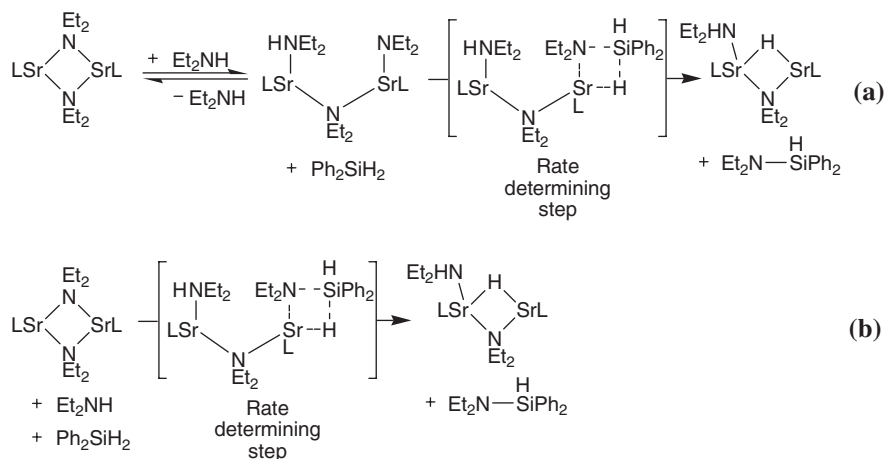
Previous hypotheses evinced by the Hill group have implicated the varying charge densities down Group 2 of the M^{2+} cations in their ability to mediate metathesis and C=C insertions, alongside amine-borane dehydrocouplings. Comparable effects may account for the distinct variations in E_a and ΔH^\ddagger displayed in Table 3.6. In contrast, the resultant ΔG_{298}^\ddagger values are less indicative of such significant discrimination. These similar values can be rationalised based upon the effect of the entropy of activation wherein the extremely negative value for calcium mitigates its energetic and enthalpic advantage. It has been previously noted that the entropic component can play a major role in the deterministic kinetic analyses of Group 2-mediated heterofunctionalisation of C–C multiple bonds.

In the current case, however, a number of secondary considerations must be taken into account when considering the observed variations. These are, most notably, catalyst solution molecularity, mode of activation and the presence of off-cycle metal amides derived from the persistent presence of the protic $\text{HN}(\text{SiMe}_3)_2$ in the reaction. It is further notable that the mechanism for **IIa** is distinct from that for the trisoxazolinyborate magnesium precatalyst **VII** derived by Sadow [15], in spite of the persistent ligation of the metal by hexamethyldisilazide throughout the reaction. This suggests that the bulky but unidentate hexamethyldisilazide does not impose a similar environment upon the magnesium centre as a more complex trisoxazolinyborate and is noteworthy as distinct ligand effects in Group 2 mediated reactions are becoming a more widely noted phenomenon and most likely reflects the observations of Sarazin and co-workers with regards to ligand denticity [22]. With these caveats in mind, a number of tentative conclusions as to the mechanism of each of these reactions can be drawn. In the case of **IIa** and **IIb**, the first order dependence on amine can be interpreted as a rate determining protonolysis. In the case of **IIb**, this must be of the metal hydride, while in the case of **IIa** this may be upon the hydride (Scheme 3.3b), or hexamethyldisilazide formed by the reaction of the hydride and persistent hexamethyldisilazane (Scheme 3.4a).

This rationale would account for the significant rate acceleration for calcium as a result of either the increased radius of the Ca^{2+} yielding a faster protonolysis of the intermediate hydride with amine or as a result of the pre-equilibrium between the magnesium diethylamide and hexamethyldisilazide. Although the former case is consistent with the calculated decrease in barrier height for protonolysis down



Scheme 3.3 The proposed possible mechanisms of the rate determining step of silicon–nitrogen dehydrocoupling mediated by **IIb** and **IIa**



Scheme 3.4 The proposed possible mechanisms of the rate determining step of silicon–nitrogen dehydrocoupling mediated by **IIc**

Group 2 [21], the latter case cannot be precluded and may account for the distinct variation in the E_a and ΔH^\ddagger .

In contrast, direct comparison with the strontium congener is complicated by its divergent rate law, as shown in Eq. 3.2. This rate law is suggestive of an alternative rate determining step reliant on activation of an inactive strontium amide, and equal involvement of Et_2NH and Ph_2SiH_2 . This suggests, in contrast to the rate determining protonolysis for **IIa** and **IIb**, a rate determining Si–H/Sr–N σ -bond metathesis step yielding a metal hydride. Given that the activation analysis of this reaction suggests a rapid protonolysis for strontium this is unsurprising as this trend in protonolysis rate reflects that previously calculated in Group 2 mediated hydroamination, but requires account for the dependence on [amine]. It has been previously suggested that Group 2 mediated hydroamination has a rate determining C=C insertion which is assisted by further coordinated protic substrate which could thus justify such an order, however an alternative justification for this observation, reliant upon a pre-equilibrium of catalyst activation mediated by an equivalent of amine is shown in Scheme 3.4.

In this rationale, the dimeric metal species is inactive to Si–H/Sr–N σ -bond metathesis, however activity mediated by the equivalent of Et_2NH observed in the rate law yields a terminal amide which is active towards σ -bond metathesis with the Si–H bond. The degree of dimer cleavage in this step is of key interest. A half-order dependence upon [**IIc**] could be interpreted a full dimer cleavage to yield the active species, however the observed ΔS^\ddagger seems insufficiently large to favour this interpretation. A hydride transfer from this species to the metal yields the observed product and a metal hydride with a coordinated amine which undergoes extremely rapid protonolysis owing to this precoordination to once again yield a strontium amide, which remains inactive until coordinated by another equivalent of amine. Whether this reaction is concerted (Scheme 3.4b) or stepwise (Scheme 3.4a),

with the $[\text{amine}]^1$ component of the rate law being derived from a pre-equilibrium cannot be conclusively determined in this analysis. Nevertheless, an equilibrium rationale justifies the limited variation in the ΔS^\ddagger between congeners **IIa**, **IIb** and **IIc** as it would be reasonable to posit that a rate determining step relying on the construction of a transition state from 3 components (the strontium, amine and silane, the concerted case, Scheme 3.4b) in contrast to two (the magnesium or calcium species and amine) would incur a far higher entropic penalty upon achieving the transition state which contrary to the observed ΔS^\ddagger values.

With this analysis in hand, a number of key conclusions can be drawn. Although these data are inconclusive, this is a result of the inherent complexity of the mechanistic surface. Distinct variations down Group 2 can be observed, with considerable effects being derived from solution molecularity, coordinative unsaturation, ancillary ligation, charge density and bond polarity. These variations not only effect efficacy and energetics of the reaction but in fact have profound influence on its mode and mechanism.

3.5 Alternative Ligands in Magnesium-Mediated σ -Bond Metathesis

Based on the substantial ligand effects observed for **IIa** versus **VII**, a new set of ligands was selected for investigation. Previous work in Group 2 chemistry has shown the utility of bulky carbenes, particularly IPr (IPr = $[\text{HCN}\{2,6\text{-}i\text{Pr}_2\text{C}_6\text{H}_3\}_2\text{C}]$), in stoichiometric studies. As such, dehydrocoupling mediated by $[\text{IPrMg}(\text{N}\{\text{SiMe}_3\}_2)]$ (**VIII**) was undertaken investigating the previously analysed reaction of diethylamine and diphenylsilane utilising a 10 mol% catalyst loading in C_6D_6 .

Dishearteningly, the principal peaks observable in the resultant ^1H NMR spectrum at the beginning of the reaction corresponded to the free carbene. As a result of this unfortunate result in catalytic studies, a preliminary stoichiometric study was undertaken. It was initially noted that although the **VIII** itself was only sparingly soluble in non-polar solvents, the addition of even small amounts of diethylamine yield a sudden increase in solubility. As such, the reaction between an equimolar mixture of **VIII** and diethylamine was undertaken. The reagents were combined neat, allowed to react for an hour then subjected to vacuum. The resultant solid was dissolved in the minimum volume of toluene and chilled to -34°C . This yielded crystals suitable for a single crystal X-ray diffraction analysis, the results of which are shown in Fig. 3.26.

This unexpected product is the abnormal carbene adduct of **IIa**. Its formation raises a number of intriguing questions, as prompting further in situ NMR analysis. Interrogation of the solution formed under analogous conditions to those from which **11** was crystallised revealed a number of notable features. Alongside the formation of **11**, peaks corresponding to both free IPr and free **IIa** were observable. Notably, reacting **VIII** with either triethylamine or hexamethyldisilazane under these conditions did not yield any sign of **11** in the ^1H NMR spectrum. With

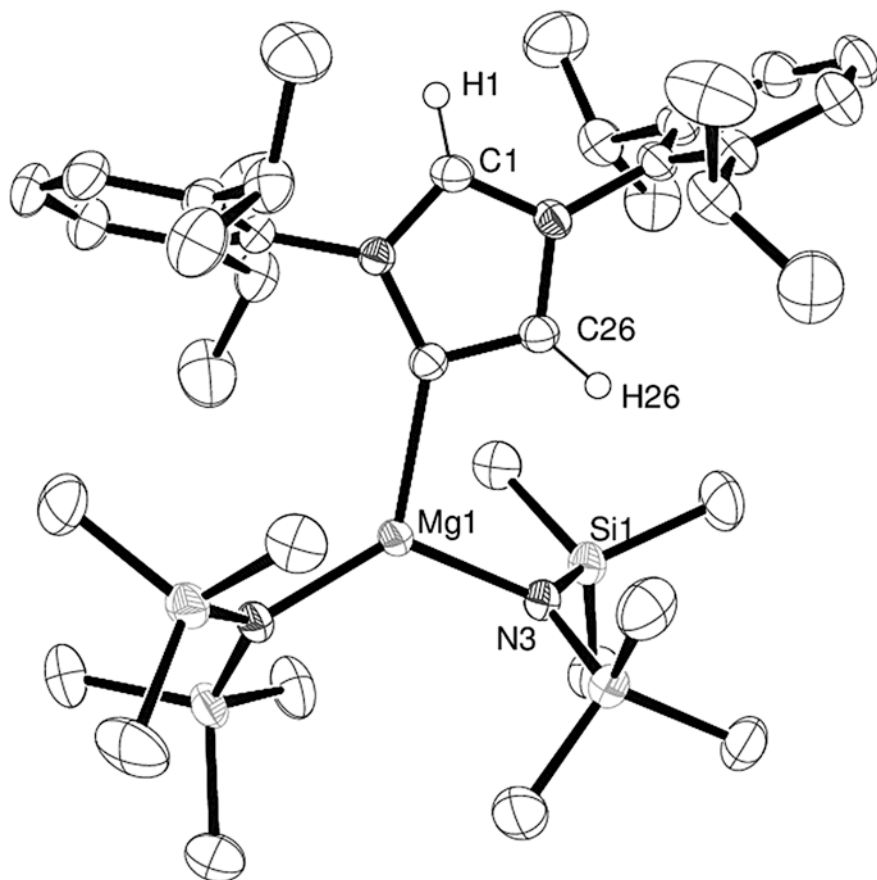
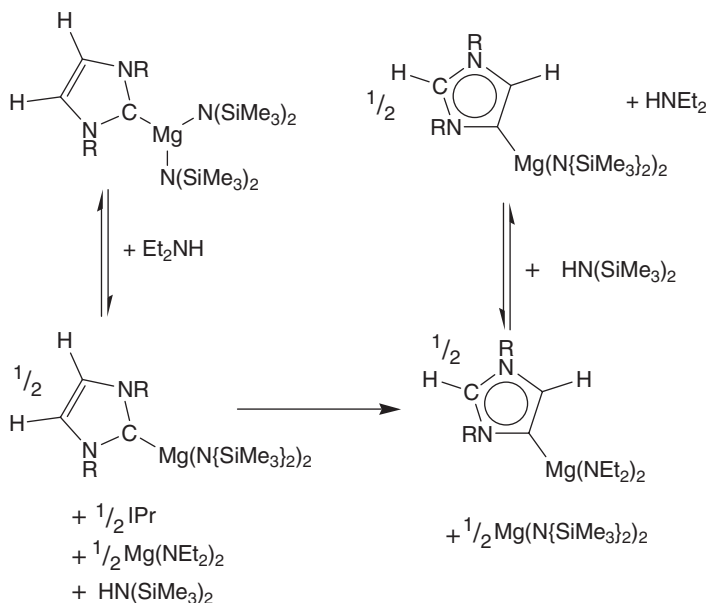


Fig. 3.26 ORTEP representation of $[\text{aIPr}]\text{Mg}(\text{N}\{\text{SiMe}_3\}_2)_2$, **11**. Thermal ellipsoids at 30 % probability. Hydrogen atoms except those attached to C1 and C26 omitted for clarity. Selected bond lengths (Å) and angles ($^\circ$): Mg1–C27 2.190(2), Mg1–N3 2.014(1), Mg1–N4 1.985(1), N3–Mg1–N4 126.54(5), N3–Mg1–C27 104.85(6), N2–C27–C26 102.1(1), N1–C1–N2 108.2(1)

these observations in hand it is possible to speculate upon the mechanism for the formation of **11**, as shown in Scheme 3.5. It is likely that the intermediate magnesium-diethylamide is sufficiently small to deprotonate one of the C–H bonds of the IPr backbone, yielding a new Mg–C bond, however the exact nature of this mechanistic step cannot be determined from these data. Whilst a dimetallated carbene could be formed, and subsequently demetallated, recent work has suggested such species to be remarkably stable, suggesting against this analysis. The deprotonation step, however, must be mediated by a metal amide, owing to the inactivity of triethylamine and cannot be simply proton assisted as the addition of excess hexamethyldisilazide gave no rearrangement.

Notably, compound **11** constitutes the first report of a structurally characterised Group 2-abnormal carbene complex.

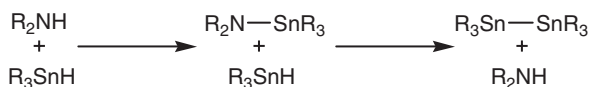


Scheme 3.5 The proposed mechanism for the formation of **11** from **VIII** mediated by diethylamine

3.6 Tin–Nitrogen Coupling

In contrast to literature precedent for silicon–nitrogen dehydrocoupling, there is a far more limited precedent for dehydrocoupling of amines with the heavier Group 14 hydrides. As a result, predominant routes to tin amides rely upon the reaction of metallated amines with tin chloride derivatives, which generates a waste stream in the form of metal salt [23]. A dehydrocoupling route to tin–nitrogen bonds is complicated by the latent reactivity of tin hydrides with stannylamides which yields tin–tin coupling and an equivalent of amine, as shown in Scheme 3.6 [24].

Although this represents an attractive route to tin–tin bonds, the complexity of synthesising tin–nitrogen bonds has precluded any wider use. Most commonly tin–tin bond synthesis is carried out via Wurtz-type couplings yielding significant waste and little functional group tolerance [24], or via the dehydrogenative coupling of tin hydrides mediated by a variety of transition metal [25] and *f*-block catalysts [26]. Ditin compounds have come to recent prominence as electrophilic tin sources in palladium-catalysed stannylation of arenes [19, 27], and



Scheme 3.6 The effect of the latent aminolysis of stannyl hydrides on the potential products of tin–nitrogen dehydrocoupling

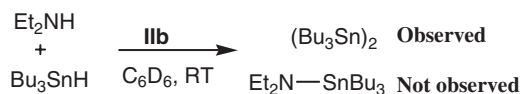
poly(stannanes) [28], synthesized via such couplings, have long been of interest for their optical-electronic properties. As such, a dehydrogenative route to tin–tin bonds from tin hydrides utilising the environmentally benign and Earth-abundant Group 2 metals would be attractive.

An initial $^{119}\text{Sn}\{^1\text{H}\}$ NMR investigation into tin-nitrogen coupling between tributylstannane and diethylamine mediated by **IIb** was undertaken (Fig. 3.27).

Initial observations readily indicated the consumption of the starting stannane ($\delta_{119\text{Sn}} = -89$) and the emergence of a new resonance at -83 ppm was initially taken to indicate successful Sn–N dehydrocoupling. However, interrogation of the ^1H NMR spectrum was telling, indicating no consumption of the diethylamine present, and, through comparison to literature values, the new peak was identified as the distannane, $(\text{Bu}_3\text{Sn})_2$ [29].

From the perspective of the results previously obtained for silicon-nitrogen dehydrocoupling this appears surprising, however as noted the aminolysis of tin-Hydrides to yield distannanes is well-precedented (*vide supra*). Given the other product of this reaction is an amine, this coupling partner should only be required in catalytic amounts and, in fact, could be added simply as the ancillary ligand of the metal precatalyst.

It is thus possible to speculate upon a manifold wherein suggests tin-nitrogen coupling occurs, however the incipient stannylamine formed is subsequently consumed (Scheme 3.7).



With this proposal in hand a scope into the qualitative effects of both metal precatalyst and amine additive was undertaken, as summarised in Table 3.7.

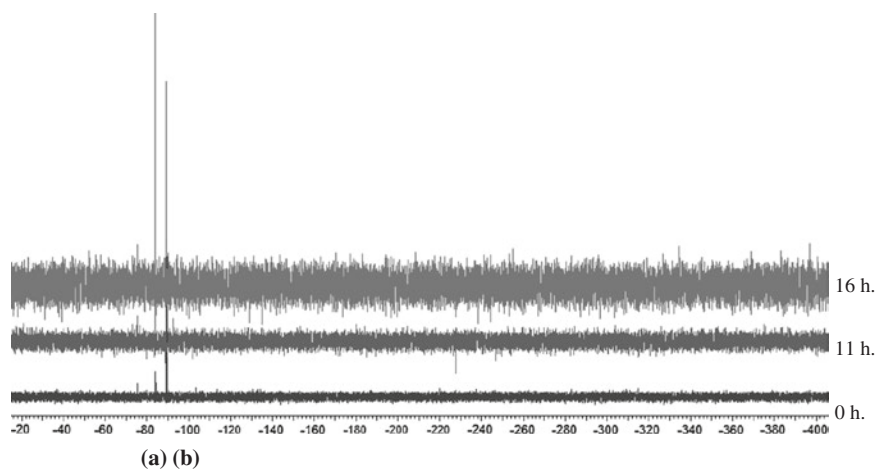
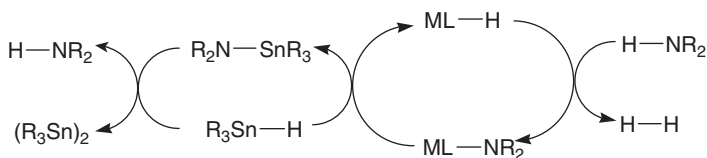


Fig. 3.27 The incomplete Group 2-mediated tin–tin coupling yielding distannanes from stannanes. **a** $\text{Bu}_3\text{SnSnBu}_3$ **b** Bu_3SnH



Scheme 3.7 The proposed mechanism for the Group 2-mediated tin–tin coupling from stannanes and amines via an intermediate stannylamide

Table 3.7 The results of the optimisation study into tin–tin dehydrocoupling catalysed by complexes **IIa–c** (0.05 mmol) with amine (0.1 mmol) and tin (0.1 mmol) in C_6D_6 (0.5 mL) at room temperature

Entry	Stannane	Amine	Catalyst	Time/days	Conversion (%)
1	Bu_3SnH	None	IIb	4	20
2	Bu_3SnH	$(CH_2)_4NH$	IIb	3	66
3	Bu_3SnH	DippNH ₂	IIb	5	Trace ^a
4	Bu_3SnH	$BuNH_2$	IIa	1	99
5	Bu_3SnH	$BuNH_2$	IIb	3	99
6	Bu_3SnH	$BuNH_2$	IIc	3	66
7	Ph_3SnH	$BuNH_2$	IIb	1	99

^aA significant proportion of DippNHSnBu₃ was identified by comparison to literature values

Although turnover was observed without additional amine (Table 3.7, entry 1), amine additives increase the rate of reaction but are not consumed (Table 3.7, entries 2, 4). Furthermore, primary amines, with low steric demands accelerated the reaction (Table 3.7, entry 4) far in excess of even very non-bulky secondary amines or bulky primary amines (Table 3.7, entries 2, 3). Utilisation of the bulky di-*iso*-propylaniline, yielded only a trace of tin–tin coupling (Table 3.7, Entry 3), however a hitherto unobserved ¹¹⁹Sn resonance at 40.1 ppm was noted which could be attributed to $Bu_3SnN(H)Dipp$ by comparison to literature values [30]. This was attributed to the bulk of the product stannylamine precluding the tin–tin coupling reaction thus allowing observation of the proposed Sn–N coupling product, providing further evidence for the scheme suggested in Scheme 3.7.

Notably, the effect of the metal precatalyst shows a distinct contrast to the trend observed for silicon–nitrogen dehydrocoupling with the rates appearing to follow the trend $Mg > Ca > Sr$. Finally, the reaction is applicable to both aliphatic and aromatic substituents on tin (Table 3.7, entries 5, 7) with a significant acceleration observed for the presence of aryl substituents.

In contrast to the trend in rate observed for the homoleptic species, β -diketiminato supported calcium systems are consistently more rapid than their magnesium analogues (Table 3.8, entries 3–6 vs. 7–9). This is unsurprising given the steric demands of the β -diketiminato which would be expected to have a more profound effect on the smaller magnesium centre. Again the presence of additional

Table 3.8 The results of the optimisation study into tin–tin dehydrocoupling catalysed by complexes **Ib**, **Id** and **If** (0.05 mmol) with amine (0.1 mmol, if utilised) and stannane (0.1 mmol) in C₆D₆ (0.5 mL) at room temperature unless otherwise stated

Entry	Stannane	Amine	Catalyst	Time/days	Conversion (%)
1	Ph ₃ SnH	None	Ib	1	0 ^{a, b}
2	Ph ₃ SnH	BuNH ₂	Ib	3	99
3	Bu ₃ SnH	None	Id	1	0 ^c
4	Bu ₃ SnH	BuNH ₂	Id	12	74 ^a
5	Ph ₃ SnH	None	Id	1	0 ^c
6	Ph ₃ SnH	BuNH ₂	Id	6	92
7	Bu ₃ SnH	None	If	15	77
8	Ph ₃ SnH	None	If	4	92
9	Ph ₃ SnH	BuNH ₂	If	2	81

^aReaction occurred at 80 °C

^bQuantitative conversion to Ph₄Sn observed

^cReaction attempted at 60 °C

amine provides an increase in reaction rate (Table 3.8, entries 1, 3, 5, 8 vs. 2, 4, 6, 9 respectively). In the absence of amine, a β-diketiminato magnesium alkyl **Ib** shows no tin–tin coupling reactivity providing further evidence for the proposed intermediacy of the stannylamine in this tin–tin coupling (Table 3.8, entry 1). Perhaps most notable is the contrast between the β-diketiminato supported magnesium alkyl and amide species **Ib** and **Id** whereupon the presence of a reversible activating group, slows the reaction considerably in contrast to an irreversible activation yielding a gaseous alkane (Table 3.8, entry 2 vs. 4). In the absence of added amine the β-diketiminato magnesium amide, **Id** (Table 3.8, entries 3 and 5) provides no activity, suggesting the bulk of the hexamethyldisilazide ligand precludes reactivity at the smaller magnesium centre. This mirrors the observations made for the silicon-nitrogen dehydrocoupling as summarised in Sect. 3.2.

Most notable was the conversion for Table 3.8, Entry 9; although the expected distannane was observed at completion of the reaction, the resonance corresponding to this species could be observed to grow-in then deplete over the course of the reaction during monitoring via ¹¹⁹Sn{¹H} NMR. Concurrent with this consumption, a number of additional resonances formed in the ¹¹⁹Sn NMR spectrum, as shown in Fig. 3.28.

By comparison to literature values, these resonances could be assigned as follows; Ph₄Sn and Ph₃SnSn(Ph)₂SnPh₃, the formation of which is summarised in Scheme 3.8.

This reaction raised a number of intriguing mechanistic possibilities. A manifold based upon a series of σ-bond metathesis steps operant upon the distannane intermediate, Ph₃SnSnPh₃ yielding a catalytic cycle as shown in Scheme 3.9a. Alternatively, given the literature precedent for α-stannylenes elimination, such a reaction could be implicated in this reactivity (Scheme 3.9b).

It is noteworthy that this result was isolated to **If** in the presence of BuNH₂, with no indications of similar reactivity for either the homoleptic

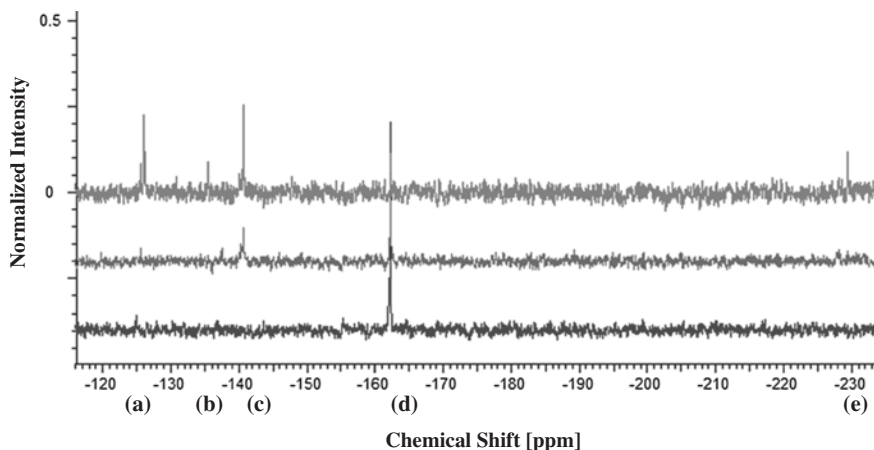


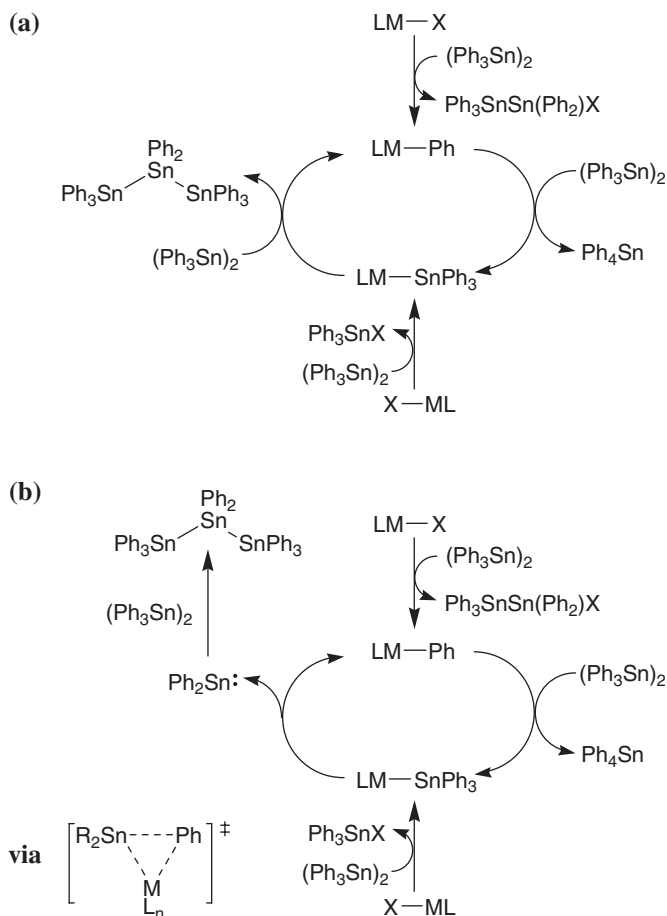
Fig. 3.28 The tin–tin coupling reaction upon Ph_3SnH mediated by **If** and BuNH_2 showing the results of a further cross-metathesis. **a** Ph_4Sn , **b** $\text{Ph}_3\text{SnSn}(\text{Ph})_2\text{SnPh}_3$, **c** $\text{Ph}_3\text{SnSnPh}_3$, **d** Ph_3SnH , **e** $\text{Ph}_3\text{SnSn}(\text{Ph})_2\text{SnPh}_3$ [29]



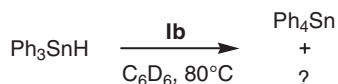
Scheme 3.8 The redistribution of ligands about $(\text{Ph}_3\text{Sn})_2$ mediated by **If**

hexamethyldisilazides (Table 3.7), the lighter congener **Ib** or **If** in the absence of added small amine. These observations are consistent with the proposed mechanism; an unligated calcium-phenyl intermediate, implicated in both mechanistic possibilities, would be precluded owing to its extreme insolubility in non-polar solvents hence the lack of activity for the homoleptic species. The lack of reactivity for the lighter congener, **Ib** and **Id**, can be accounted for in the case of pathway (a) on the basis of the proposed metal stannyl which, owing to the extreme bulk of the stannyl anion, would prevent reactivity with the bulky $\text{Ph}_3\text{SnSnPh}_3$ if bound to magnesium ligated by a large β -diketiminato. Alternatively, the small magnesium centre may be precluded from α -stannylene based reactivity if pathway (b) is operant.

Another tantalising hint of the rich chemistry accessible for stannanes is the reaction of **Ib** with triphenylstannane in the absence of additional amine. In contrast to the tin–tin coupling observed for all amine-involving reactions, the product which appears to form in quantitative yield, based on the ^{119}Sn NMR spectroscopy and unit cell of the crystalline product, is tetraphenyltin. This can be accounted for via a redistribution of the substituents around the tin as summarised in Scheme 3.10 however the side product of this reaction remained unidentified.



Scheme 3.9 The proposed mechanistic possibilities for the Group 2-mediated formation of higher tin oligomers and tetraphenyltin via a cross-metathesis mechanism **a** or α -stannylyne elimination **b**

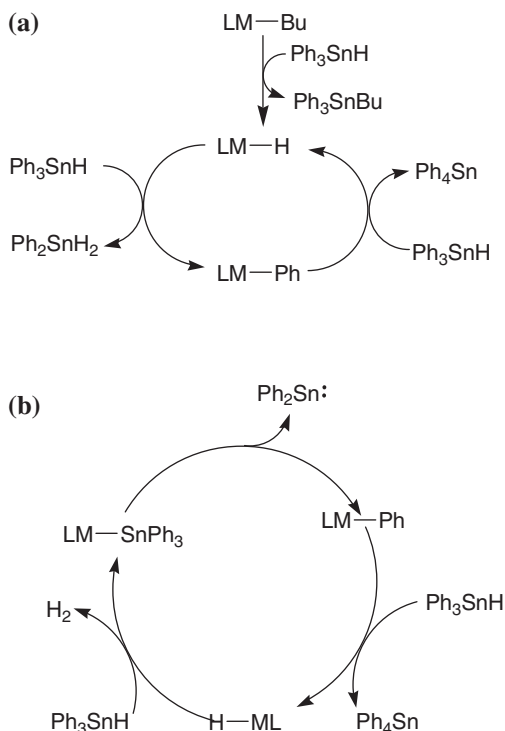


Scheme 3.10 The proposed redistribution of the substituents bound to Ph_3SnH mediated by **Ib**

Once again, it is viable to postulate a number of mechanistic possibilities for this reaction predicated upon either a series of σ -bond metathesis steps, as shown in Scheme 3.11a or a pathway implicating α -stannylyne elimination (Scheme 3.11b).

A peak corresponding to formation of Ph_3SnBu , its intensity proportionate to the loading of **Ib** was observed. Nevertheless, no mass-balance satisfying side

Scheme 3.11 The proposed mechanistic possibilities for the redistribution of the substituents bound to Ph_3SnH mediated by **Id**



product could be identified in the $^{119}\text{Sn}\{^1\text{H}\}$ NMR spectra. A hint to the possible identity of the other products of this reaction, however, can be noted from the intense brown colour which the solution in the NMR tube acquired over the course of the reaction, a colour change not observed for any of the other reactions. This colour could be attributed to the breakdown products of the postulated SnH_4 product or alternatively oligo(stannanes) formed via spontaneous coupling of the postulated diphenylstannylene.

This result represents a new tranche of Group 2 mediated reactivity with stannanes and must be pursued in future studies, furthermore these results suggest the intermediacy of a transient stannylamine to the observed tin–tin coupling as suggested in Scheme 3.7. Most notable is the distinction of this reaction to that observed for lanthanide alkyls and hydrides reacting with triarylstannanes [26]. In the latter case, tin–tin coupling is observed, proposed to be a result of stannylstannane σ -bond metathesis.

A number of notable features can be identified from this somewhat superficial analysis of the reactivity of stannanes mediated by Group 2 metals. Although tin–nitrogen dehydrocoupling is evidently accessible, this does not represent a useable route to stannylamines except, perhaps, for very bulky amines. Instead, a rapid formation of tin–tin bonds via a transient stannylamine reacting with stannane Sn–H bonds can instead be reported. This represents a rapid and novel route to ditin

compounds and may have a wide variety of applications both in the synthesis of these useful, simple compounds and in potential extension to a variety of more complex systems such as dehydrogenative polymerizations. Finally, observations as to the effect of ligation upon the metal centre do not yield any particularly surprising variations as a result of the introduction of persistent, bulky ligands. More surprisingly, however is the observation of products which can be rationalised as being a result of a number of SN-H/M-X, Sn-C/M-X and Sn-Sn/M-X σ -bond metathesis or α -stannylene elimination steps forming a hitherto unprecedented Group 2 mediated cross-metathesis which is not reliant upon the elimination of dihydrogen as an entropic drive, or perhaps even reaction mechanisms beyond traditional σ -bond metathesis.

3.7 Experimental

Synthesis of N,N'-2,6-diisopropylphenyl-diamino(phenyl)silane, **6**.

In a glovebox, to a stirring 0.5 mol dm⁻³ heptanes solution of di-butylmagnesium (1 mmol, 2 mL) was added 2,6-di-*iso*-propylaniline (2 mmol, 0.354 g). The mixture was stirred for 1 h after which time was added phenylsilane (1 mmol, 0.108 g). A rapid foaming was observed and a fine white solid precipitated. The mixture was left to stir overnight, filtered then cooled to -35 °C thus **6** crystallised as colourless blocks (76 %). ¹H NMR (300 MHz, d₈-THF) δ ppm 7.71–6.95 (10H, m, ArH), 6.58 (1H, m, ArH), 5.28 (1H, s, SiH), 4.16 (2H, s, NH), 3.31 (2H, h, CH₃CHCH₃), 2.97 (2H, h, CH₃CHCH₃), 1.21 (12H, d, CH₃CHCH₃), 1.03 (12H, dd, CH₃CHCH₃). ¹³C{¹H} NMR (75 MHz, d₈-THF) δ ppm 144.3 (C_{Ar}), 139.3 (C_{Ar}), 138.1 (C_{Ar}), 134.8 (C_{Ar}), 130.8 (C_{Ar}), 128.6 (C_{Ar}), 124.3 (C_{Ar}), 123.8 (C_{Ar}), 29.1 (CH₃CHCH₃), 24.2 (CH₃CHCH₃), 24.1 (CH₃CHCH₃).

Anal. calc'd for C₃₀H₄₂N₂Si: C, 78.54; H, 9.23; N, 6.11 %. Found: C, 78.42; H, 9.40; N, 6.15 %.

Synthesis of (DippNH)[DippNSi(H)Ph]Mg(THF)₂, **7** and [(H)PhSi(DippN)₂]Mg(THF)₃, **8**.

In a glovebox, to a stirring 0.5 mol dm⁻³ heptanes solution of di-butylmagnesium (1 mmol, 2 mL) diluted in THF (10 mL) was added 2,6-di-*iso*-propylaniline (2 mmol, 0.354 g). The mixture was stirred for 1 h after which time was added phenylsilane (1 mmol, 0.108 g). A rapid foaming was observed and the mixture was left to stir overnight during. After this time, the THF was removed in vacuo and the residue taken up in toluene (10 mL). This solution was filtered, the solvent removed to incipient crystallisation and cooled to -20 °C overnight yielding powder. This suspension was submerged in hot water and allowed to cool overnight. This yielded **7** and **8** as colourless blocks (62 %) which were separated under a microscope and subjected to X-ray analysis. (DippNH)[DippNSi(H)Ph]Mg(THF)₂, **7**.

Owing to a rapid conversion of **7–8** in solution, suitable NMR spectroscopic data could not be acquired.

Crystals of and $[(\text{H})\text{PhSi}(\text{DippN})_2]\text{Mg}(\text{THF})_3$, **8**, separated by this method were found to be of insufficient quality for full crystallographic analysis, however they were solved to yield connectivity and as such a rational synthesis of this species was undertaken, yielding material of an identical unit cell and connectivity. To a 0.5 mol dm^{-3} heptanes solution of di-*n*-butylmagnesium (1 mL, 0.5 mmol) diluted in THF (5 mL) was added *N,N'*-2,6-diisopropylphenyl-diamino(phenyl) silane (88 mg, 0.5 mmol) and the mixture allowed to stir overnight. The solvent was then removed in vacuo, and the residue dissolved in toluene. The resultant solution was concentrated to incipient crystallisation and cooled to $-18 \text{ }^\circ\text{C}$ overnight yielding colourless blocks suitable for single crystal X-ray analysis (74 %).

^1H NMR ppm (300 MHz, d_8 -THF) δ ppm 7.37–6.30 (11H, m, ArH), 5.14 (1H, s, SiH), 3.66 (2H, h, CH_3CHCH_3), 2.47 (2H, h, CH_3CHCH_3), 0.91 (24H, m, CH_3CHCH_3). $^{13}\text{C}\{^1\text{H}\}$ NMR (75 MHz, d_8 -THF) δ ppm 153.9 (C_{Ar}), 150.9 (C_{Ar}), 145.3 (C_{Ar}), 143.9 (C_{Ar}), 140.8 (C_{Ar}), 135.9 (C_{Ar}), 132.3 (C_{Ar}), 128.3 (C_{Ar}), 123.8 (C_{Ar}), 122.3 (C_{Ar}), 120.8 (C_{Ar}), 111.5 (C_{Ar}), 28.6 (CH_3CHCH_3), 28.2 (CH_3CHCH_3), 26.4 (CH_3CHCH_3), 23.9 (CH_3CHCH_3).

Anal. calc'd for $\text{C}_{42}\text{H}_{64}\text{MgN}_2\text{O}_3\text{Si}$: C, 73.00; H, 9.03; N, 4.48 %. Found: C, 72.78; H, 8.95; N, 4.56.

Synthesis $[(\text{H})\text{PhSi}(\text{DippN})_2]\text{Ca}(\text{THF})_3$, **9**.

In a glovebox, to a stirring solution of $\text{Ca}(\text{CH}(\text{SiMe}_3)_2)(\text{THF})_2$ [31] (0.15 mmol, 75 mg) in THF (10 mL) was added 2,6-di-*iso*-propylaniline (0.3 mmol, 53 mg). The mixture was stirred for 1 h after which time was added phenylsilane (0.15 mmol, 16 mg). A rapid foaming was observed and the mixture was left to stir overnight. After this time, the THF was removed in vacuo and the residue taken up in toluene (5 mL). This solution was filtered, the solvent removed to incipient crystallisation and cooled to $-20 \text{ }^\circ\text{C}$ overnight. This yielded **9**, suitable for crystallographic characterisation (67 %).

^1H NMR (300 MHz, d_8 -THF) δ ppm 7.66–6.48 (11H, m, ArH), 5.88 (1H, s, SiH), 4.51 (4H, h, CH_3CHCH_3), 1.23–1.16 (24H, m, CH_3CHCH_3). $^{13}\text{C}\{^1\text{H}\}$ NMR (100 MHz, d_8 -THF) δ ppm 156.2 (C_{Ar}), 154.9 (C_{Ar}), 150.6 (C_{Ar}), 142.9 (C_{Ar}), 142.8 (C_{Ar}), 135.2 (C_{Ar}), 134.6 (C_{Ar}), 134.1 (C_{Ar}), 130.3 (C_{Ar}), 127.1 (C_{Ar}), 122.5 (C_{Ar}), 115.0 (C_{Ar}), 67.9 ($\text{O}(\text{CH}_2\text{CH}_2)_2$), 27.5 (CH_3CHCH_3), 26.0 ($\text{O}(\text{CH}_2\text{CH}_2)_2$), 25.9 (CH_3CHCH_3), 25.2 (CH_3CHCH_3), 23.9 (CH_3CHCH_3), 23.6 (CH_3CHCH_3).

Repeated attempts to yield acceptable elemental analysis failed and the compound was observed to degrade in the solid state over time.

Synthesis $[(\text{H})\text{PhSi}(\text{DippN})_2]\text{Sr}(\text{THF})_4$, **10**.

In a glovebox, to a stirring solution of $\text{Sr}(\text{CH}(\text{SiMe}_3)_2)(\text{THF})_2$ [31] (0.15 mmol, 75 mg) in THF (10 mL) was added 2,6-di-*iso*-propylaniline (0.3 mmol, 53 mg). The mixture was stirred for 1 h after which time was added phenylsilane (0.15 mmol, 16 mg). A rapid foaming was observed and the mixture was left to stir overnight during. After this time, the THF was removed in vacuo and the residue taken up in toluene (5 mL). This solution was filtered, the solvent removed to incipient crystallisation and cooled to $-20 \text{ }^\circ\text{C}$ overnight. This yielded **10**, suitable for crystallographic characterisation (71 %).

^1H NMR (300 MHz, d_8 -THF) δ ppm 7.28–7.05 (11H, m, ArH), 5.60 (1H, m, SiH), 3.53 (3H, h, CH_3CHCH_3), 3.28 (16H, br. s, $\text{O}(\text{CH}_2\text{CH}_2)_2$), 2.64 (1H, h, CH_3CHCH_3), 2.12 (16H, br. s, $\text{O}(\text{CH}_2\text{CH}_2)_2$), 1.18–1.02 (24H, m, CH_3CHCH_3). $^{13}\text{C}\{^1\text{H}\}$ (75 MHz, d_8 -THF) δ ppm 143.2 (C_{Ar}), 138.8 (C_{Ar}), 138.2 (C_{Ar}), 137.6 (C_{Ar}), 134.4 (C_{Ar}), 129.7 (C_{Ar}), 128.9 (C_{Ar}), 128.8 (C_{Ar}), 126.0 (C_{Ar}), 124.4 (C_{Ar}), 123.4 (C_{Ar}), 119.3 (C_{Ar}), 68.9 ($\text{O}(\text{CH}_2\text{CH}_2)_2$), 29.1 (CH_3CHCH_3), 28.6 (CH_3CHCH_3), 25.9 ($\text{O}(\text{CH}_2\text{CH}_2)_2$), 24.3 (CH_3CHCH_3), 22.9 (CH_3CHCH_3), 21.7 (CH_3CHCH_3).

Anal. calc'd for $\text{C}_{46}\text{H}_{72}\text{N}_2\text{O}_3\text{SiSr}$: C, 66.34; H, 8.71; N, 3.36 %. Found: C, 66.27; H, 8.68; N, 3.42 %.

Synthesis of $[\text{aIPr}]\text{Mg}(\text{N}\{\text{SiMe}_3\}_2)_2$, **11**

In a glovebox, to solid $[\text{IPr}]\text{Mg}(\text{N}\{\text{SiMe}_3\}_2)_2$ (0.068 mmol, 50 mg) was added diethylamine (0.068 mmol, 7.0 μl). The reagents were shaken to homogeneity, then subjected to vacuum for 10 min. After this time, the residue was dissolved in the minimum volume of toluene and chilled to -34 °C overnight. This yielded **11**, suitable for crystallographic characterisation (33 %).

^1H NMR (400 MHz, d_8 -Tol) δ ppm d 0.30 (s, 36 H) 0.86 (d, $J = 6.78$ Hz, 6 H) 0.93 (d, $J = 6.97$ Hz, 6 H) 1.11 (d, $J = 6.78$ Hz, 6 H) 1.37 (d, $J = 6.78$ Hz, 6 H) 2.40 (spt, $J = 6.84$ Hz, 2 H) 2.74 (spt, $J = 6.81$ Hz, 2 H) 6.92 (m, $J = 7.70$ Hz, 2 H) 7.00–7.13 (m, 4 H) 7.22–7.26 (m, 1 H) 7.54–7.59 (m, 1 H).

	6	7	8	9	10	11
Empirical formula	$\text{C}_{30}\text{H}_{42}\text{N}_2\text{Si}$	$\text{C}_{38}\text{H}_{58}\text{MgN}_2\text{O}_2\text{Si}$	$\text{C}_{44}\text{H}_{68}\text{MgN}_2\text{O}_{3.50}\text{Si}$	$\text{C}_{49}\text{H}_{72}\text{CaN}_2\text{O}_3\text{Si}$	$\text{C}_{46}\text{H}_{71}\text{N}_2\text{O}_4\text{SiSr}$	$\text{C}_{39}\text{H}_{72}\text{MgN}_4\text{Si}_4$
Formula weight (g mol $^{-1}$)	458.75	627.26	733.40	805.26	831.76	733.68
Crystal system	Monoclinic	Triclinic	Monoclinic	Monoclinic	Monoclinic	Monoclinic
Space group	$\text{P}2_1/\text{a}$	P_1	$\text{P}2_1/\text{n}$	$\text{P}2_1/\text{n}$	$\text{P}2_1$	$\text{P}2_1/\text{n}$
a (Å)	15.1354(4)	11.2940(4)	10.0310(1)	10.2642(2)	10.3700(3)	11.8620(1)
b (Å)	9.2400(3)	12.1680(4)	30.0170(5)	22.7621(6)	18.8520(8)	16.7720(2)
c (Å)	20.1280(6)	13.6040(4)	16.5560(3)	20.7835(5)	12.6320(5)	23.5120(2)
α (°)	90	96.759(2)	90	90	90	90
β (°)	101.781(2)	90.610(2)	104.903	98.249(2)	113.607(2)	95.401(1)
γ (°)	90	90.961(2)	90	90	90	90
V (Å 3)	2755.63(14)	1856.13(10)	4817.34(13)	4805.5(2)	2262.83(15)	4656.93(8)
Z	4	2	4	4	2	4
ρ (g cm $^{-3}$)	1.106	1.122	1.011	1.113	1.221	1.046
μ (mm $^{-1}$)	0.105	0.113	0.098	0.195	1.260	0.170
θ range (°)	3.81–27.48	3.53–27.49	3.62–27.44	5.04–25.03	3.68–27.52	3.53–27.52
Measured/independent reflections/ R_{int}	35,403/6254/0.0772	25602/8357/0.0590	10,746/10,746/0.000	64,099/8386/0.1702	37,584/10,228/0.1217	64,074/10,667/0.0500
Data/restraints/parameters	6254/2/304	8357/17/435	10,746/36/481	8386/106/572	10,228/76/544	10,667/0/454
Goodness-of-fit on F^2	1.084	1.054	0.980	1.078	1.033	1.035

	6	7	8	9	10	11
R_1 , wR_2 [$I > 2\sigma(I)$]	0.0621, 0.1462	0.0612, 0.1597	0.0798, 0.2061	0.0756, 0.1990	0.0640, 0.1119	0.0417, 0.1014
R_1 , wR_2 (all data)	0.0803, 0.1582	0.0989, 0.1843	0.1594, 0.2358	0.1379, 0.2270	0.1090, 0.1238	0.0620, 0.1120

Notes on crystallographic refinement

6 H1 and H2—attached to N1 and N2, respectively, were located and refined at a distance of 0.98 Å from the relevant parent atoms. H1A, attached to Si1, was also located and refined without restraints.

7 Hydrogen atoms attached to Si1 were located and refined subject to being similar distances from the parent. H1 attached to N1 was similarly located and refined at distance of 0.98 Å from the nitrogen. C36 and C37 were found to be disordered in 1 50:50 ratio over two proximate sites. C–C distances were refined with distance restraints in the associated THF molecule to assist convergence.

8 H1a, attached to Si1 was located and refined freely. Some disorder was present. In particular, c36/37 were disordered over 2 sites in a 55:45 ratio, while C41 was similarly fragmented bit in a 60:40 ratio. The unit cell was seen to contain 2 areas of diffuse solvent which could not be modelled in any plausible manner. Hence PLATON SQUEEZE was employed to treat these regions. Based on pre-PLATON electron density and the results for the SQUEEZE analysis, guest solvent has been included in the asymmetric unit as ½ of a THF molecule.

9 The asymmetric unit contains one Ca complex and one solvent molecule of toluene. The dataset was weak with a strong decline of intensity at higher theta. This resulted in a high R(int) and unresolved disorder. There is potential disorder in the THF group with atom O2 which could not be solved. The other two THF showed disorder in the ratio 60:40 (THF with O3) and 70:30 (THF with O2). All atoms involved in the disorder had to be restrained using DFIX and or SADI and SIMU.

10 H1, attached to Si1, located and freely refined. C40 disordered over 2 sites in a 70:30 ratio, while C43–46 disordered in 50:50 ratio. Some ADP, C–O and C–C restraints used in disordered regions to assist convergence.

References

1. C.A. Roth, *Product R&D* **11**, 134 (1972); Y. Tanabe, M. Murakami, K. Kitaichi, Y. Yoshida, *Tetrahedron Lett.* **35**, 8409 (1994); Y. Tanabe, T. Misaki, M. Kurihara, A. Iida, Y. Nishii, *Chem. Commun.* 1628 (2002)
2. A.P. Smith, J.J.S. Lamba, C.L. Fraser, *Org. Synth.* **78**, 82 (2002)
3. Y.D. Blum, K.B. Schwartz, R.M. Laine, *J. Mat. Sci.* **24**, 1707 (1989)
4. P.G.M. Wuts, W. Greeneodora, T.W. Greene, in *Greene's Protective Groups in Organic Synthesis* (2006)
5. C. Eaborn, in *Organosilicon Compounds* (Butterworths, London, 1960); R. Fessenden, J.S. Fessenden, *Chem. Rev.* **61**, 361 (1961); V. Passarelli, G. Carta, G. Rossetto, P. Zanella, *Dalton Trans.* 413 (2003)
6. H.Q. Liu, J.F. Harrod, *Organometallics* **11**, 822 (1992)
7. E. Matarasso-Tchiroukhine, *J. Chem. Soc.-Chem. Commun.* 681 (1990)
8. H.Q. Liu, J.F. Harrod, *Can. J. Chem.* **70**, 107 (1992)
9. J.A. Reichl, D.H. Berry, in *Advances in Organometallic Chemistry*, ed. by F.H. Robert West and Anthony (Academic Press, 1998), pp. 197–265
10. W.D. Wang, R. Eisenberg, *Organometallics* **10**, 2222 (1991)
11. Y. Blum, R.M. Laine, *Organometallics* **5**, 2081 (1986)
12. K. Takaki, T. Kamata, Y. Miura, T. Shishido, K. Takehira, *J. Org. Chem.* **64**, 3891 (1999); K. Takaki, K. Komeyama, K. Takehira, *Tetrahedron* **59**, 10381 (2003); Y. Chen, H. Song, C. Cui, *Angew. Chem.-Int. Ed.* **49**, 8958 (2010); W. Xie, H. Hu, C. Cui, *Angew. Chem.-Int. Ed.* **51**, 11141 (2012)

13. J.X. Wang, A.K. Dash, J.C. Berthet, M. Ephritikhine, M.S. Eisen, *J. Organomet. Chem.* **610**, 49 (2000)
14. F. Buch, S. Harder, *Organometallics* **26**, 5132 (2007)
15. J.F. Dunne, S.R. Neal, J. Engelkemier, A. Ellern, A.D. Sadow, *J. Am. Chem. Soc.* **133**, 16782 (2011)
16. A. Xia, M.J. Heeg, C.H. Winter, *Organometallics* **21**, 4718 (2002); M.M. Olmstead, W.J. Grigsby, D.R. Chacon, T. Hascall, P.P. Power, *Inorg. Chim. Acta* **251**, 273; D.R. Armstrong, W. Clegg, R.E. Mulvey, R.B. Rowlings, *J. Chem. Soc.-Dalton Trans.* 409 (2001); J.R. Lachs, A.G.M. Barrett, M.R. Crimmin, G. Kociok-Köhn, M.S. Hill, M.F. Mahon, P.A. Procopiou, *Eur. J. Inorg. Chem.* 4173 (2008); A.G.M. Barrett, I.J. Casely, M.R. Crimmin, M.S. Hill, J.R. Lachs, M.F. Mahon, P.A. Procopiou, *Inorg. Chem.* **48**, 4445 (2009)
17. P.B. Hitchcock, M.F. Lappert, G.A. Lawless, B. Royo, *J. Chem. Soc.-Chem. Commun.* 1141 (1990); M. Westerhausen, *Inorg. Chem.* **30**, 96 (1991); W. Vargas, U. Englich, K. Ruhlandt-Senge, *Inorg. Chem.* **41**, 5602 (2002); L.T. Wendell, J. Bender, X. He, B.C. Noll, K.W. Henderson, *Organometallics* **25**, 4953 (2006); M.S. Hill, G. Kociok-Köhn, D.J. MacDougall, *Inorg. Chem.* **50**, 5234 (2011)
18. M. Veith, W. Frank, F. Töllner, H. Lange, *J. Organomet. Chem.* **326**, 315 (1987); C. Pi, L. Wan, Y. Gu, H. Wu, C. Wang, W. Zheng, L. Weng, Z. Chen, X. Yang, L. Wu, *Organometallics* **28**, 5281 (2009); D. Yang, Y. Ding, H. Wu, W. Zheng, *Inorg. Chem.* **50**, 7698 (2011); V.L. Blair, W. Clegg, A.R. Kennedy, Z. Livingstone, L. Russo, E. Hevia, *Angew. Chem.-Int. Ed.* **50**, 9857 (2011)
19. H. Azizian, C. Eaborn, A. Pidcock, *J. Organomet. Chem.* **215**, 49 (1981)
20. M. Arrowsmith, M.R. Crimmin, A.G.M. Barrett, M.S. Hill, G. Kociok-Köhn, P.A. Procopiou, *Organometallics* **30**, 1493 (2011); C. Brinkmann, A.G.M. Barrett, M.S. Hill, P.A. Procopiou, *J. Am. Chem. Soc.* **134**, 2193 (2012); C. Brinkmann, A.G.M. Barrett, M.S. Hill, P.A. Procopiou, S. Reid, *Organometallics* **31**, 7287 (2012)
21. A.G.M. Barrett, C. Brinkmann, M.R. Crimmin, M.S. Hill, P. Hunt, P.A. Procopiou, *J. Am. Chem. Soc.* **131**, 12906 (2009)
22. M. Arrowsmith, M.S. Hill, G. Kociok-Köhn, *Organometallics* **30**, 1291 (2011); B. Liu, T. Roisnel, J.-F. Carpentier, Y. Sarazin, *Angew. Chem.-Int. Ed.* **51**, 4943 (2012)
23. K. Jones, M.F. Lappert, *J. Chem. Soc. (Res)* 1944 (1965); I.M. Thomas, *Can. J. Chem.* **39**, 1386 (1961)
24. W.P. Neumann, B. Schneider, R. Sommer, *Justus Liebigs Ann. Chem.* **692**, 1 (1966)
25. U. Schubert, J. Pfeiffer, F. Stöhr, D. Sturmayer, S. Thompson, *J. Organomet. Chem.* **646**, 53 (2002); S.M. Thompson, U. Schubert, *Inorg. Chim. Acta* **350**, 329 (2003); T.N. Mitchell, A. Amamria, H. Killing, D. Rutschow, *J. Organomet. Chem.* **304**, 257 (1986); V.I. Dodero, T.N. Mitchell, J.C. Podestá, *Organometallics* **22**, 856 (2003); H.X. Zhang, F. Guibe, G. Balavoine, *J. Org. Chem.* **55**, 1857 (1990)
26. A.Z. Voskoboynikov, I.N. Parshina, A.K. Shestakova, K.P. Butin, I.P. Beletskaya, L.G. Kuz'mina, J.A.K. Howard, *Organometallics* **16**, 4041 (1997)
27. A. Bourderioux, S. Routier, V. Bénétteau, J.-Y. Mérour, *Tetrahedron* **63**, 9465 (2007); W. Qu, M.-P. Kung, C. Hou, T.E. Benedum, H.F. Kung, *J. Med. Chem.* **50**, 2157 (2007)
28. M. Trummer, F. Hoffat, P. Smith, W. Caseri, *Macromol. Rapid Commun.* **33**, 448 (2012)
29. B. Wrackmeyer, in *Annual Reports on NMR Spectroscopy*, ed. by G.A. Webb (Academic Press, 1999), pp. 203–264
30. Z. Padělková, A. Havlík, P. Švec, M.S. Nechaev, A. Růžička, *J. Organomet. Chem.* **695**, 2651 (2010)
31. M.R. Crimmin, A.G.M. Barrett, M.S. Hill, D.J. MacDougall, M.F. Mahon, P.A. Procopiou, *Chem.-Eur. J.* **14**, 11292–11295 (2008)

Chapter 4

Boron–Nitrogen Dehydrocoupling

4.1 Introduction

Beyond the dehydrocoupling of Group 14 elements with protic amines, the extension of such reactivity to hydridic reagents from Group 13 is attractive, most notably boranes yielding aminoboranes. Boron–nitrogen bond containing species have found recent utility in a variety of interesting transformations, including as sources of highly nucleophilic amide anions for reactions with activated alkenes, alkynes and strained lactones [1]. Further extensive work by Suginome has shown the utility of aminoboranes to give ready access to iminium cations via their reactions with ketones and aldehydes [2]. In contrast to the activity of aminoboranes on ketones, yielding iminium ions, the action of aminodi(boranes) on ketones was shown to give ready access to imines [3].

Such applications are, however, hindered by the multistep synthetic routes necessary to yield anything more than very simple aminoboranes. Although some latent reactivity exists between protic amines and highly Lewis acidic boranes, such as the parent borane or simple dialkylboranes such as 9-BBN [4, 5], especially in the presence of base [6], synthesis of aminoboranes via this route is unreliable, and requires forcing conditions. More reliably, the action of tin- [7] and silicon–nitrogen [4, 8] bonds upon boranes and haloboranes readily yields aminoboranes and the relevant E–X bond, however this latter species, in the case of tin, is a highly toxic waste stream. As a result, most popular synthetic routes to aminoboranes utilise the reaction of lithium amides with BCl_3 , and, if a ligated aminoborane is desired, protonolysis with e.g. diols [9]. A more specialised route reliant upon the generation of borylnitrenes, and their ability to activate C–H bonds has further been reported but its scope is highly limited [10]. Extensive work by a variety of groups have shown that hydroboration of imines readily yields aminoboranes, including uncatalysed reports with $\text{Me}_2\text{S}\cdot\text{BH}_3$ [11], and reports involving coinage metal [12], ruthenium [13], Lewis pair and organo-catalysis [14]. Finally, the double-hydroboration of nitriles to yield aminodi(boranes) mediated by an imido-hydrido molybdenum(IV) complex has been reported [3] and an extension of this reactivity to a magnesium precatalyst has further been devised by the Hill group. In each of the cases, the

scope of reactivity is limited by the availability of starting materials, be those silylamines, stannylamines, borylnitrenes, imines or nitriles.

With limitations in mind, a general and simple dehydrocoupling route to aminoboranes, via the reaction of a hydridic B–H and protic N–H bond would be highly desirable. Beyond limited reports of rhodium catalysed dehydrocoupling [15], the only other dehydrogenative coupling yielding aminoboranes was reported by the Hill group and summarised in Chap. 1, to wit a stoichiometric reaction between **If** and diphenylamine followed by two equivalents 9-BBN was reported to yield the relevant aminoborane and a β -diketiminato supported calcium borohydride, **II** [16].

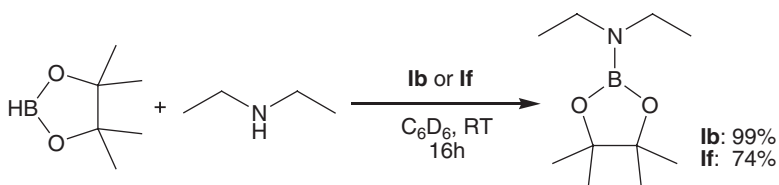
4.2 Catalytic B–N Dehydrocoupling

In spite of these disappointing preliminary results, the aforementioned utility of B–N bonds, led to an initial attempt to render this reaction catalytic. This, however, focussed on the more useful pinacolborane, as shown in Scheme 4.1. **Ib** and **If** were selected for, in the magnesium case possession of a traceless activating group and in both cases possession of a bulky ligand which might simplify solution behaviour rendering the reaction more amenable to analysis.

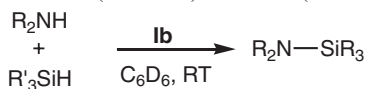
Notably, although both **If** and **Ib** catalyse this dehydrocoupling, **Ib** shows a far higher efficacy. With this highly preliminary result in mind, an investigation into boron–nitrogen dehydrocoupling catalysed by **Ib** was undertaken. In order to allow comparison with the results of Chap. 2 and to allow comparison between Groups 13 and 14 in Group 2 mediated dehydrocouplings, a simultaneous investigation into silicon–nitrogen dehydrocoupling with this precatalyst was undertaken.

4.3 Catalytic Scope

An initial NMR investigation was thus carried out into the substrate scope with regards to boranes, silanes and amines as shown in Tables 4.1, 4.2 and 4.3 utilising **Ib**. On addition of the precatalyst to a mixture of the amine and hydridic reagent in C_6D_6 , a pronounced bubbling was observed for many of the reactions.



Scheme 4.1 The initial study upon the dehydrocoupling of diethylamine and pinacol(borane) mediated by **Ib** and **If**

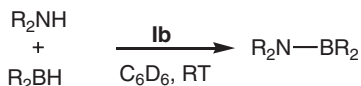
Table 4.1 The results of the scope study into silicon–nitrogen dehydrocoupling catalysed by complexes **Ib** (0.05 mmol) with amine (0.1 mmol) and silane (0.1 mmol) in C₆D₆ (0.5 mL)

Entry	Silane	Amine	Product	Time (days)	Conversion (%)
1	PhSiH ₃	BuNH ₂	PhSiH ₂ NHBu + PhSiH(NHBu) ₂ + PhSi(NHBu) ₃	1 ^a	99 (11:58:6)*
2		<i>t</i> BuNH ₂	PhSiH ₂ NH <i>t</i> Bu + PhSiH(NH <i>t</i> Bu) ₂	1 ^a	99 (70:30)
3		PhNH ₂	PhSiH ₂ NHPh + PhSiH(NHPh) ₂	1 ^a	99 (21:60)*
4		DippNH ₂	PhSiH ₂ NHDipp	3 ^b	53
5		PhN(H)Me	PhSiH ₂ N(SiMe ₃) ₂	<1 ^a	99
6		(CH ₂) ₄ NH	PhSiH ₂ (N(CH ₂) ₄) + PhSiH(N(CH ₂) ₄) ₂	1 ^a	99 (92:8)
7		Et ₂ NH	PhSiH ₂ NEt ₂ + PhSiH(NEt ₂) ₂	<1 ^a	99
8		Ph ₂ NH	PhSiH ₂ NPh ₂	3 ^b	51
9		(Me ₃ Si) ₂ NH	PhSiH ₂ N(SiMe ₃) ₂	1 ^c	6
10	Ph ₂ SiH ₂	BuNH ₂	Ph ₂ SiHNHBu + Ph ₂ Si(NHBu) ₂	1 ^a	99 (90:10)
11		<i>t</i> BuNH ₂	Ph ₂ SiHNH <i>t</i> Bu	1 ^a	99
12		PhNH ₂	Ph ₂ SiHNHPh	1 ^b	82
13		DippNH ₂	Ph ₂ SiHNHDipp	3 ^a	20
14		PhN(H)Me	Ph ₂ SiHN(Me)Ph	1 ^b	99
15		(CH ₂) ₄ NH	Ph ₂ SiHN(CH ₂) ₄	<1 ^a	99
16		Et ₂ NH	Ph ₂ SiHNEt ₂	<1 ^a	99
17		Ph ₃ SiH	BuNH ₂	Ph ₃ SiNHBu	4 ^b
18	Et ₂ NH		No reaction	6 ^c	0

*Higher oligomers constitute the remainder of the conversion

^aRoom temperature^b60 °C^c80 °C

A number of notable trends can be identified. As observed for the magnesium bisamide **IIa**, substrate bulk significantly affects the yield. Indeed, in the case of phenylsilane, coupling is significantly inhibited for hexamethyldisilazane (Table 4.1, entry 9) relative to that catalysed by **IIa** (Table 3.1, entry 6). This is unsurprising given the steric constraints imposed by the bulky β-diketiminato ligand. Although multiple couplings are once again a common characteristic of these equimolar investigations, a higher level of selectivity is observed, with disubstituted amines having a higher propensity to only couple once compared to the unligated magnesium centre (Table 4.1, entries 6 and 7 vs. Table 3.1 entries 4 and 5). This can most likely once again be attributed to the steric bulk of the β-diketiminato ligand. Moving to the larger diphenylsilane, a similar trend can be observed; the very bulky aniline, DippNH₂, couples far more reluctantly with **Ib** than **IIa** (Table 4.1, entry 13 vs. Table 3.1, entry 9) whereas smaller amines

Table 4.2 The results of the scope study into boron–nitrogen dehydrocoupling catalysed by complexes **Ib** (0.05 mmol) with amine (0.1 mmol) and borane (0.1 mmol) in C₆D₆ (0.5 mL)

Entry	Silane	Amine	Product	Time (h)	Conversion (%)
1	PinBH	BuNH ₂	PinBNHBu	<1 ^a	99
2		<i>t</i> BuNH ₂	PinBNH <i>t</i> Bu	<1 ^a	99
3		PhNH ₂	PinBNHPh	<1 ^a	99
4		DippNH ₂	PinBNHDipp	<1 ^a	99
5		PhN(H)Me	PinBN(Me)Ph	<1 ^a	99
6		(CH ₂) ₄ NH	PinBN(CH ₂) ₄	<1 ^a	99
7		Et ₂ NH	PinBNEt ₂	<1 ^a	99
8		Ph ₂ NH	PinBNPh ₂	<1 ^a	99
9		(Me ₃ Si) ₂ NH	No reaction	144 ^b	0
10	9-BBN	BuNH ₂	R ₂ BNHBu	<1 ^a	99
11		<i>t</i> BuNH ₂	R ₂ BNH <i>t</i> Bu	144 ^b	83
12		PhNH ₂	R ₂ BNHPh	12 ^a	99
13		DippNH ₂	R ₂ BNHDipp	144 ^b	80
14		PhN(H)Me	R ₂ BN(Me)Ph	–	–
15		Ph ₂ NH	R ₂ BNPh ₂	144 ^b	73

^aRoom temperature^b60 °C**Table 4.3** The results of the scope study into silicon– and boron–nitrogen dehydrocoupling catalysed **6** by complexes **Ib** (0.05 mmol) with limiting reagent (0.1 mmol) in C₆D₆ (0.5 mL)

Entry	Silane	Amine	Ratio	Product	Time (days)	Conversion (%)
1	PhSiH ₃	BuNH ₂	1:2	PhSiH ₂ NHBu + PhSiH(NHBu) ₂ +	1 ^a	99 (5:88:7)
2			1:3	PhSi(NHBu) ₃	1 ^a	99 (0:0:100)
3		(CH ₂) ₄ NH	1:2	PhSiH ₂ (N(CH ₂) ₄) + PhSiH(N(C	<1 ^a	99 (8:92)
4			1:3	H ₂) ₄) ₂	<1 ^a	99 (0:100)
5	Ph ₂ SiH ₂	BnNH ₂	1:2	Ph ₂ SiHNHBu + Ph ₂ Si(NHBu) ₂	1 ^a	99 (40:60)
6		(CH ₂) ₄ NH	1:2	Ph ₂ SiH(N(CH ₂) ₄)	<1 ^a	99
7	PinBH	BuNH ₂	2:1	(PinB) ₂ NBu	1 ^b	99
8		<i>t</i> BuNH ₂	2:1	(PinB) ₂ N <i>t</i> Bu	<1 ^a	99
9		PhNH ₂	2:1	PinBNHPh	2 ^b	99
10	9-BBN	BuNH ₂	2:1	R ₂ BHNHBu	1 ^a	99
11		PhNH ₂	2:1	R ₂ BNHPh	2 ^b	99

*Higher oligomers constitute the remainder of the conversion

^aRoom temperature^b60 °C

couple readily. Finally, moving to the bulkiest silane analysed, triphenylsilane, coupling becomes far less accessible. Only the very small butylamine couples readily (Table 4.1, entry 17), notably to a higher yield than could be achieved with **IIa** for the analogous benzylamine reaction (Table 3.1, entry 13). This is likely a consequence of the residence time of the intermediate magnesium amide in the non-polar reaction medium which is increased by the presence of the β -diketiminato ligand.

Change of the hydridic coupling partner to a borane yielded a number of other notable trends. The weakly Lewis acidic pinacolborane couples readily with a variety of aromatic and aliphatic amines of varying bulk (Table 4.2, entries 1–8), but failed to tolerate the very bulky hexamethyldisilazane (Table 4.2, entry 9). Notably, the reaction rate is far in excess of that for silanes, with all coupling partners coupling in less than a day with a pronounced bubbling. The reaction was entirely selective for monocoupling when monosubstituted amines were utilised (Table 4.2, entries 1–4) which reflects the inaccessibility of disilylation of amines noted for **IIa** (Table 3.2, entries 1, 2, 5–8). In contrast to the facile reaction between pinacolborane and a wide variety of amines, the reaction of the more Lewis acidic 9-BBN showed a much greater dependence on the identity of the amine. While the smallest amine, butylamine, couples readily (Table 4.2, entry 10), bulkier aliphatic amines couple extremely sluggishly, to the point that the introduction of **Ib** appears to induce no rate acceleration over the background reaction (Table 4.2, entries 11, and 15). In contrast, small monosubstituted and disubstituted aromatic amines couple at rates in excess of the background (Table 4.2, entries 12 and 14), while bulkier anilines revert to the uncatalysed rate (Table 4.2, entry 13). These data suggest a subtle interplay of steric and electronic effects dominate in the case of 9-BBN and, alongside the results for both silanes, and pinacolborane are indicative of a reaction which is profoundly influenced by the identity of the hydridic coupling partner. Notably, beyond the effects of bulk noted previously for variations in the silane coupling partner, the Lewis acidity of the hydridic partner also appears to be influential.

As for equimolar silicon–nitrogen couplings (Table 4.1), multiple dehydrocouplings were observed to yield silanes with higher amine incorporation. In order to rationally investigate these, a series of dehydrocouplings were attempted with amine:silane ratios reflective of the observed product of the equimolar reaction. Notably, the trend mirrors that **IIa** (Table 3.2), with subsequent dehydrocouplings to yield higher oligomers being more sluggish than the initial reactions. This is once again thought to be a consequence of both the increased steric demands of the silylamines and the effect of amine substitution on the hydridicity of the silicon–hydrogen bond. Although the smallest amine investigated, butylamine, a 1:2 silane:amine ratio did yield an increase in the proportion of the bis(amino)silane relative to the equimolar reaction, this proportion did not yield complete conversion to the persilylated product (Table 4.1, entry 1). In contrast to **IIa** (Table 3.2, entry 1) a 1:3 silane:amine ratio gave high conversion to the tris(amino)silane. In contrast to this, the secondary amine pyrrolidine gave, at best, double dehydrocoupling independent of stoichiometry, albeit for a 1:2 silane:amine ratio, with a

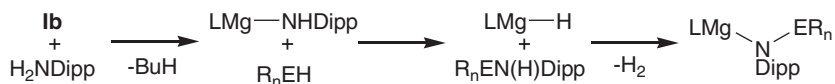
higher ratio of bis(amino)silane (Table 3.2, entries 3 and 4 vs. Table 3.2 entries 3 and 4). For the more sterically encumbered diphenylsilane, unremarkably, diaminosilane formation was inaccessible for all but the smallest amine, butylamine (Table 3.2, entry 5) and in this case in a smaller proportion than is accessible for **IIa** (Table 3.2, entry 5) which can also access the bis(pyrollidino)silane (Table 4.3, entry 6 vs. Table 3.2, entry 9), a reflection of the steric demands imposed by the β -diketiminato ligand.

Whereas higher amine incorporation into silanes was observed readily, such reactivity is inaccessible for the boranes investigated herein owing to their possession of only a single hydride. Notably, however, unlike attempts to yield aminodi(silanes) utilising **IIa** which were unsuccessful in almost all cases (Table 3.2, entries 3, 6 and 8), aminodi(boranes) were accessible. In the case of both pinacolborane and 9-BBN double dehydrocoupling with butylamine occurred (Table 4.3, entries 7 and 10), albeit with a need for gentle heating and slightly extended reaction times compared to aminoborane formation reflective of the effect of successive borylation on the electronic nature of the nitrogen. Although *tert*-butylamine also coupled twice with pinacolborane (Table 4.3, entry 8) neither borane showed any sign of multiple dehydrocoupling being with aniline (Table 4.3, entries 9 and 11). The ready coupling of the more bulky *tert*-butylamine suggest this limitation is a reflection of the electronic structure rather than bulk of the anilinoborane, most likely the deficit of electron density at the nitrogen atom as a result of the effects of both the borane and phenyl substituents.

From this in-depth scope study a number of key observations can be noted. Coupling is contingent upon both steric and electronic effects of the hydridic coupling partner, most notably the Lewis acidity at the element bound to the hydride, yielding a general rate acceleration for pinacolborane over both silanes and 9-BBN. This suggests a “Goldilocks effect” wherein moderate Lewis acidity yields a rate acceleration, but more extreme Lewis acidity has an inhibitory effect. Furthermore, stereoelectronic effects at the nitrogen centre are also striking. Finally, comparison can be drawn with **IIa** which shows the effect of the bulky β -diketiminato ligand, and yielded decreased tolerance for bulk but in some cases, increased selectivity. This study shows that dehydrocoupling is readily catalysed by **Ib** giving moderate to excellent conversions for a broad range of coupling partners and is indicative of fascinating variations contingent on hydridic substrate warranting further investigation.

4.4 Stoichiometric Studies

In order to provide further insight into the effect of hydridic coupling partner, a range of stoichiometric reactions were undertaken. The amine selected for investigation was 2,6-di-*iso*-propylaniline which, upon equimolar reaction with **Ib**, has been reported to readily form the anilide. Subsequent addition of an equivalent of hydridic reagent followed by interrogation by ^1H and, in the case of the boranes, ^{11}B NMR spectroscopy



Scheme 4.2 The proposed pathway to stoichiometrically analyse borane- and silane–dehydro-coupling with DippNH₂

was utilised to analyse the reaction. In each case crystals suitable for single crystal X-ray diffraction analysis were achieved, as summarised in Scheme 4.2.

In the case of phenylsilane, the ¹H NMR spectrum indicated the consumption of the phenylsilane partner and the emergence of a new resonance at 4.92 ppm, attributed to the silyl-hydride peak of the product (**12**) alongside a series of new *iso*-propyl resonances which were suggestive of a metal-bound anilidosilane. Crystallisation occurred from a mixture of toluene and hexane and the results of the resultant X-ray investigation are shown in Fig. 4.1.

Compound **12** is, as suggested by the ¹H NMR spectrum, is indeed a metal-bound anilidosilane which retains two silylhydrides. The bond lengths and angles in this species are unremarkable in comparison to a variety of previously reported silylamide derivatives of magnesium [17].

In the case of the reaction utilising pinacolborane, interrogation of the ¹¹B NMR spectrum ($\delta = 32.1$ ppm) suggested a new, 3-coordinate nitrogen bound boron environment. Inspection of the ¹H NMR spectrum was less informative, with a complex set of signals in the regions attributable to the pinacol-methyl and *iso*-propyl resonances. Crystallisation at -38 °C from toluene, however, yielded crystals of **13** suitable for X-ray diffraction analysis and the results of this investigation are summarised in Fig. 4.2.

Compound **13** is a heteroleptic β -diketiminato ligated magnesium bound amido(pinacol)borane and constitutes the first structurally characterised species of this class. Whilst a variety of magnesium amidoborane complexes derived from amineboranes, which contain four coordinate boron centres and B–H bonds yielding Mg...H agostic-type interactions, have been structurally characterised, those containing three coordinate boron centres are more sparse and are confined to reports of an aminoboratabenzene [18] derivative, an amineborane containing scorpionate ligand [19] and two reports of alkyldi(amino)boranes [20]. While none of these structures bear sufficient similarities to **13** for comparison to be suitable, a number of striking structural features can be highlighted, most notably the donor interaction between one of the pinacol oxygens and the magnesium centre. This interaction raises the coordination number of the magnesium to four and yields, due to the structural constraints of the amidoborane fragment, a highly distorted tetrahedral environment at the magnesium centre, most remarkably indicated by the N–Mg versus O–Mg distances (2.003(2) vs. 2.3737(18) Å respectively). The complexity of the pinacol methyl region in the ¹H NMR can be thus explained as this bond, which is evidently persistent in a solution of the non-donor deuterobenzene solvent, renders the pinacol methyls magnetically inequivalent and hence yields a variety of peaks in the pinacolmethyl region.

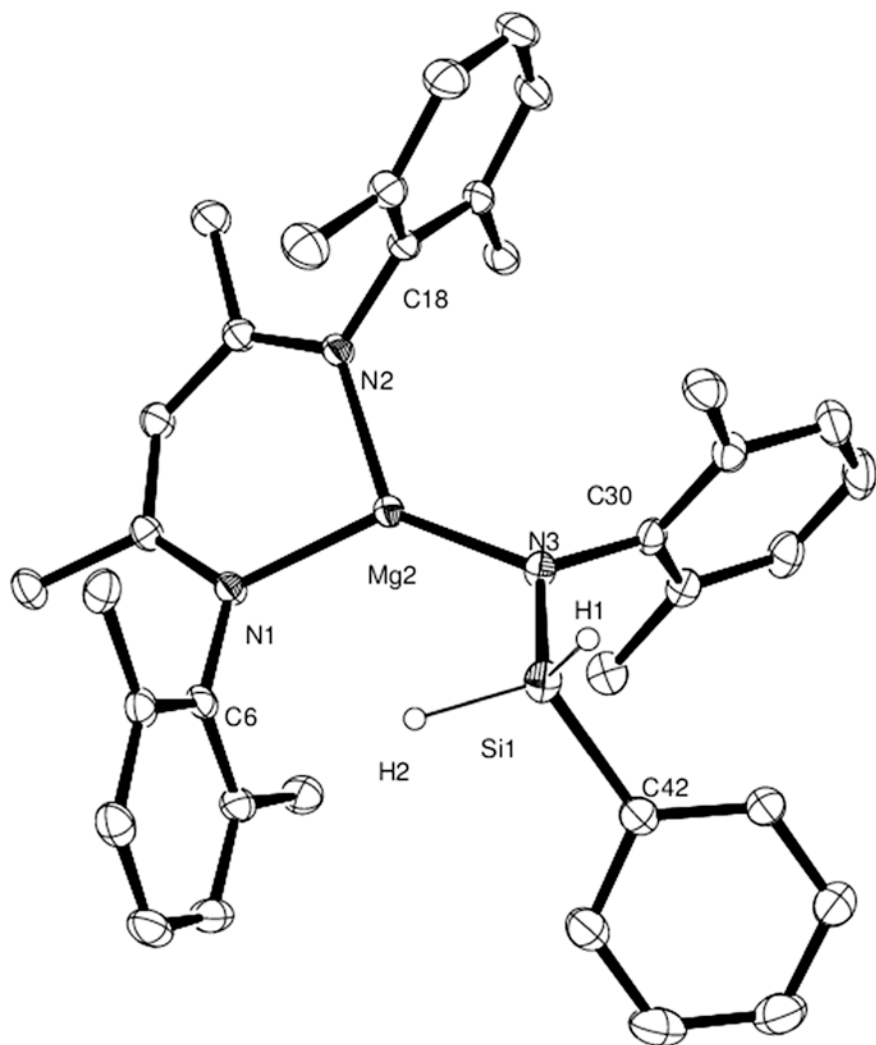


Fig. 4.1 ORTEP representation of **12** (30 % probability ellipsoids). *Iso*-propyl methyl groups and hydrogen atoms except those attached to Si1 omitted for clarity. Selected bond lengths (Å) and angles (°): Mg2–N3 1.9599(16), N3–Si1 1.7032(16), N3–C30, Si1–C42 1.872(2), Mg2–N3–Si1 120.06(8), N1–Mg2–N2 95.79(6), N1–Mg2–N3 132.54(7), C30–N3–Si1 116.93(12)

The initial ^1H NMR spectrum provided by an analogous reaction with 9-BBN was not readily amenable to interpretation owing to the complexity of the ^1H NMR resonances of the 9-BBN fragment. The ^{11}B NMR contained more useful, if surprising information. The ^{11}B NMR spectrum was indicative of two boron environments. The first at 53.6 ppm, by comparison with the catalytic scope studies (*vide supra*) could be attributed to the anilineborane DippN(H)BR_2 which

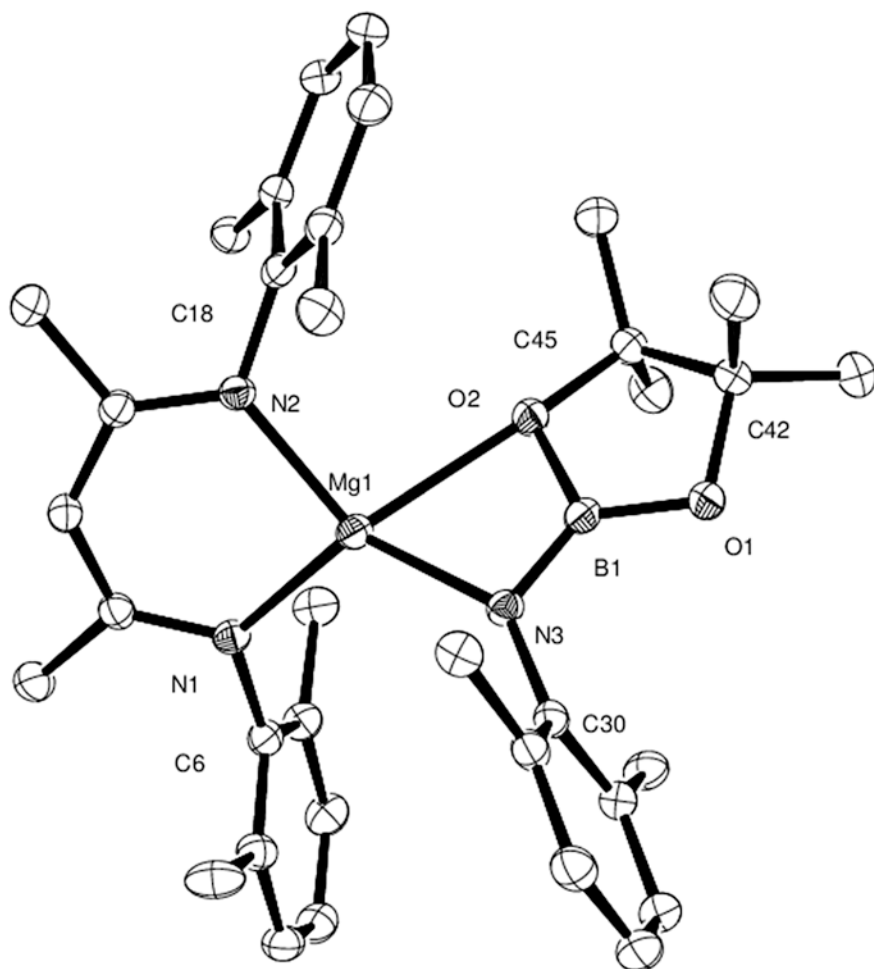


Fig. 4.2 ORTEP representation of **13** (30 % probability ellipsoids). *Iso*-propyl methyl groups and hydrogen atoms omitted for clarity. Selected bond lengths (Å) and angles (°): Mg1-O2 2.3737(18), Mg1-N3 2.003(2), O2-B1 1.418(3), B1-N3 1.379(4), N3-C30 1.423(3), N1-Mg1-N2 94.72(8), Mg1-O2-B1 80.94(14), O2-B1-N3 116.8(2), B1-N3-Mg1 96.96(15), B1-N3-C30 120.6(2)

appeared to form quantitatively, with complete consumption of aniline. The second resonance, a broadened triplet at -13.8 ppm, was suggestive, based on the higher field chemical shift and coupling pattern, of a four coordinate borohydride of the form $[R_2BH_2]^-$. Crystallisation from a mixture of THF and toluene at -38 °C yielded crystals of **14** suitable for X-ray crystallography and the results of this experiment are summarised in Fig. 4.3.

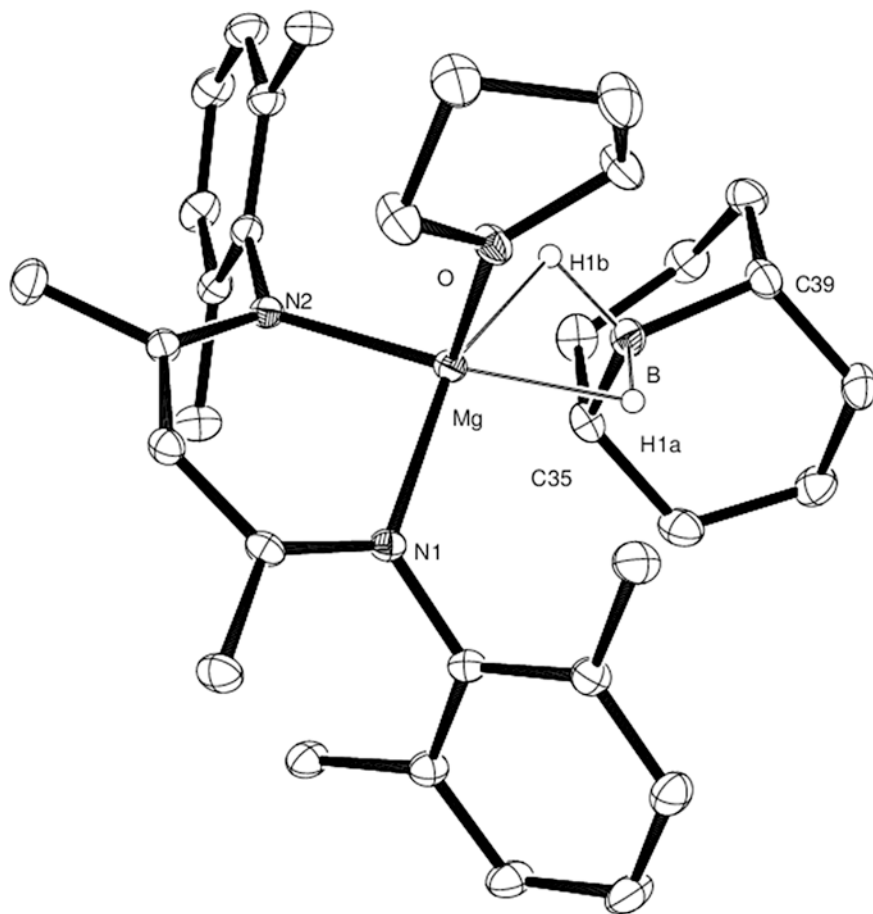


Fig. 4.3 ORTEP representation of **14** (30 % probability ellipsoids). *Iso*-propyl methyl groups and hydrogen atoms except those attached to B omitted for clarity. Selected bond lengths (Å) and angles (°): Mg–B 2.3092(15), Mg–O1 2.0555(9), Mg–H1a 1.932(14), Mg–H1b 1.929(15), B–C35 1.618(2), B–C39 1.6027(19), N1–Mg1–N2 93.48(4), N1–Mg–B 125.62(5), C35–B–C39 107.44(11). Symmetry transformations used to generate equivalent atoms: $-x + 1, -y + 1, -z + 1$

The formation of this metal borohydride, bound via $\text{H}\cdots\text{Mg}$ interactions, can be rationalised as a result of an excess of 9-BBN in solution reacting with the postulated intermediate metal hydride (Scheme 4.2). Although two magnesium dialkylborohydride complexes have been structurally characterised [21], these occupy vastly distinct coordination environments, as a result of pentafluorophenyl substitution on the boron and high magnesium coordination numbers as a result of hydroxide coligands, to **14** and are, as such, of limited relevance. On the other hand, this species is closely related to the more expansive class

of magnesium borohydrides containing $[\text{BH}_4]^-$. Indeed the direct analogue $[\text{CH}\{\text{C}(\text{Me})\text{N}(\text{Dipp})\}_2]\text{Mg}(\text{BH}_4)$ has only recently been described by Mountford and coworkers [22]. Remarkably, in spite of the significantly reduced steric demands of the $[\text{BH}_4]^-$ anion $\text{Mg}-\text{H}$ distances for this fragment are significantly elongated compared to **14** whilst the $\text{Mg}-\text{B}$ distances are similar ($\text{Mg}-\text{B}$ 2.223 vs. 2.309, $\text{Mg}-\text{H}$ 2.022 vs. 1.929(15) Å). In all other respects, these compounds show remarkably similar bond length and angle data. This data, however, must be treated with extreme caution as in the case of $[\text{CH}\{\text{C}(\text{Me})\text{N}(\text{Dipp})\}_2]\text{Mg}(\text{BH}_4)$, the hydrides were not independently located.

It was hypothesised this strong $\text{Mg}\cdots\text{H}_2\text{BR}_2$ interaction could be responsible for inhibiting the deprotonation of the anilinoborane. The reaction was reattempted with more stringent attention to stoichiometry and interrogation of the resultant ^1H and ^{11}B NMR spectra. In the latter spectrum, a single resonance previously attributed to $\text{DippN}(\text{H})\text{BR}_2$ was the only observable boron environment. Two species could be identified based on their proton resonances, however; $\text{DippN}(\text{H})\text{BR}_2$ and peaks attributable to the previously reported β -diketiminato magnesium hydride **II** could be identified. This result suggests that, when not in excess, the 9-BBN does not inhibit the deprotonation of $\text{DippN}(\text{H})\text{BR}_2$ via the formation of **14**. Rather the proposed intermediate metal hydride does indeed form but is unable to deprotonate the bulky $\text{DippN}(\text{H})\text{BR}_2$. Nevertheless, the persistence of this $\text{Mg}\cdots\text{H}_2\text{BR}_2$ species in the presence of excess borane may well be responsible for the limitations in the catalytic activity for **II** in $\text{N}-\text{B}$ dehydrocoupling with 9-BBN.

It is informative to compare **14** to the previously reported analogous β -diketiminato calcium dialkylborohydride, **II**. Although **II** was the result of a stoichiometric $\text{B}-\text{N}$ coupling which occurred via σ -bond metathesis, this species was unable to effect catalytic $\text{B}-\text{N}$ coupling. Structural comparison of **14** and **II** shows a number of contrasts; whilst **14** crystallises as a single conformer, **II** shows two conformeric forms, as shown in Fig. 4.4.

Whilst in **II(a)** the hydride ligands and nitrogen atoms of the β -diketiminato ligand are coplanar, in **II(b)** these ligands are orthogonal. A further notable feature is an agostic interaction from the hydrocarbon framework of the 9-BBN. In contrast **14** shows only one conformer, that analogous to **II(a)** and no such agostic interaction is present. Finally, comparison of the $\text{M}\cdots\text{H}_2\text{BR}_2$ distances reflects the variation in cation size between these species. Whilst in **13** the $\text{Mg}-\text{B}$ distance is

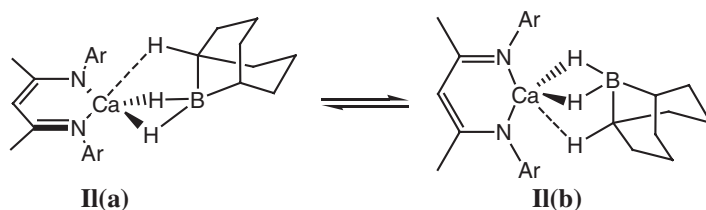


Fig. 4.4 The two conformeric forms of **II** observed crystallographically

2.309 Å and the Mg–H interactions of an identical length, in **II** the former distance is far longer (**II(a)**: 2.542 Å, **II(b)**: 2.550) and the conformation of the 9-BBN fragment indicate two different B–H–Ca bond lengths and angles. These data could be indicative of two bonding extremes; whilst the Mg⋯H₂BR₂ interaction is dominated by covalent Mg–H and B–H interactions, the Ca⋯H₂BR₂ interaction is a predominantly ionic one, wherein a tightly bound ion pair of [LCa][H₂BR₂] is present. Such a species would be precluded from the dissociation of the 9-BBN from the LMH fragment which seems to be essential for catalytic activity in **14** and may thus account for the catalytic inability of **II** in boron–nitrogen dehydrocoupling with 9-BBN. Further credence for this hypothesis is provided by the observed activity for B–N dehydrocoupling of the calcium precatalyst **If**, when utilising pinacol(borane) as a coupling partner Scheme 4.1. This latter observation can be accounted for as a consequence of the reduced Lewis acidity of the pinacol(borane) coupling partner which would render such a H⋯B interaction far more labile.

These stoichiometric investigations suggested reactivity occurring via a series of σ -bond metathesis steps: deprotonation of an amine followed by an M–N/E–H σ -bond metathesis, to yield a magnesium hydride and an E–N bond which can, but is not always, deprotonated by the hydride. Notably, under a superstoichiometric regime wherein the concentrations of hydride source and amine are in large excess, this metal hydride would deprotonate another equivalent of amine allowing catalytic turnover. Consistent with the observations from the scope study, once again a variety of steric and electronic effects can again be observed contingent both on steric bulk and Lewis acidity of the hydride source.

4.5 Kinetic Analyses

Utilising ¹H NMR spectroscopy, a kinetic study was undertaken to help elucidate the mechanism of the σ -bond metathesis between amines and silanes or boranes, centring on the reaction of *N*-methylaniline with diphenylsilane, pinacolborane and 9-BBN as catalysed by **Ib** (Scheme 4.3). These coupling partners were selected as the reaction occurs in a practicable timeframe and yields a range of well defined products with NMR resonances which give valid integrations. NMR solutions were prepared in the glovebox, immediately cooled to 193 K upon removal and allowed to warm to room temperature in the spectrometer.



Scheme 4.3 The dehydrocoupling of *N*-methylaniline and pinacol(borane), 9-BBN and diphenylsilane mediated by **Ib** investigated in this kinetic study

Table 4.4 Turnover frequency data (298 K) for the dehydrocoupling of *N*-methylaniline and 9-BBN, pinacol(borane) and diphenylsilane mediated by **Ib**

Hydride source	TOF (h ⁻¹)
9-BBN	26.4(28)
PinBH	9935(1353)
Ph ₂ SiH ₂	2.5(5)*

*Calculated via Arrhenius modelling to allow direct comparison. Data collected at 343 K

Concentrations of substrate and product were followed by integration over three half-lives.

An initial analysis of the turnover frequency for these dehydrocoupling partners was thus undertaken. Although the acquisition consistent data was somewhat complicated by the experimental requirement to perform reactions with the silane coupling partner at elevated temperature, Arrhenius analysis (vide infra) was utilised to model consistent data for 298 K.

The results of this initial study (Table 4.4) mirror the results of the scope study, with boranes far outstripping the silane in their ability to undergo dehydrocoupling with this aniline coupling partner.

4.5.1 Order of Reactants for 9-BBN

To analyse the order in catalyst, a 1:1 mixture of aniline and borane was reacted at a range of loadings of **Ib** (Fig. 4.5). This data, showing the reaction to be first order overall was then analysed via a best fit plot of rate against loading to find the order in catalyst as shown in Fig. 4.6. These analyses indicated the reaction to be ½ order in **Ib**.

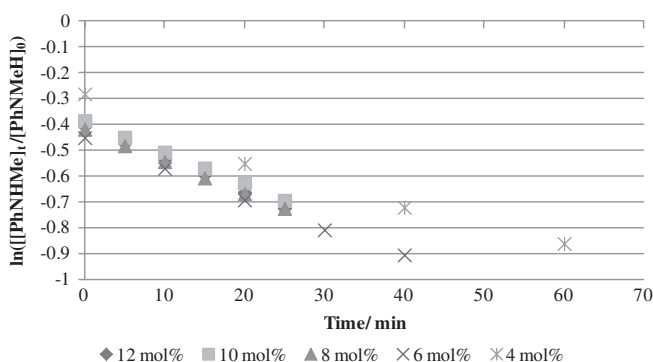


Fig. 4.5 The overall first-order plot of $\ln([\text{amine}]_t/[\text{amine}]_0)$ against time for a range of **Ib** concentrations

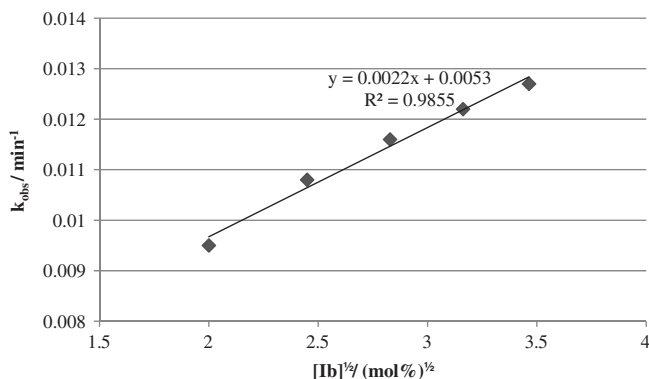


Fig. 4.6 The plot of observed rate constant (k_{obs}) against catalyst loading for a range of **Ib** concentrations

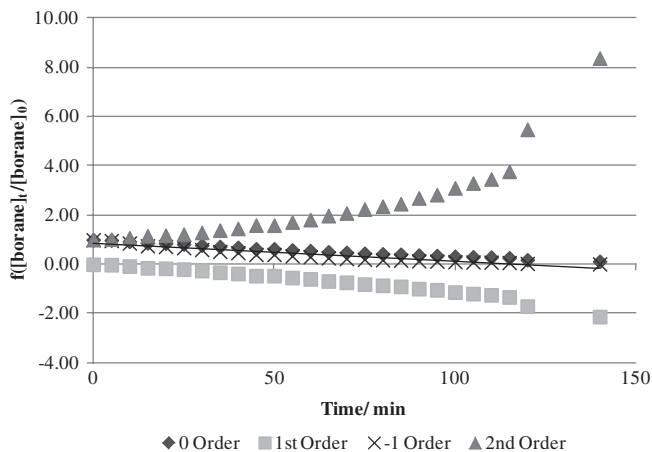


Fig. 4.7 The overall first-order plot of $f([\text{borane}]_t/[\text{borane}]_0)$ against time for a reaction with a tenfold excess of *N*-methylaniline

Subsequent to this, the orders in aniline and borane were determined via a *pseudo*-first order methodology in which a tenfold excess of aniline was reacted with a single equivalent of borane and vice versa. The consumption in limiting reagent with time was then fitted to an order, as shown in Fig. 4.7. This data, with a tenfold excess of amine, was judged to indicate a 0 order dependence on [9-BBN], assuming the first order kinetics of the overall reaction are an indicator that the reaction rate is independent of [9-BBN].

Unfortunately, the addition of a tenfold excess of borane appeared to inhibit the reaction to such an extent that no data could be acquired. This inhibition can be rationalised based upon the stoichiometric results previously observed for

this reaction wherein the presence of a excess borane was found to yield persistent formation of a β -diketiminato magnesium borohydride, which may well be catalytically inactive and present in far larger proportions when a vast excess of 9-BBN is added. It is nevertheless possible to formulate a rate law for this reaction as shown below (Eq. 4.1).

$$\text{rate} = k[\mathbf{Ib}]^{1/2}[\text{borane}]^0[\text{amine}]^1 \quad (4.1)$$

4.5.2 Order of Reactants for Pinacol(Borane)

Using an analogous methodology as that utilised for 9-BBN, the order of reagents for the dehydrocoupling of pinacol(borane) with *N*-methylaniline was assessed. The reaction was judged to be first order overall (Fig. 4.8). A best fit plot of rate against **Ib** indicated a second-order dependence on catalyst concentration (Fig. 4.9).

Experiments performed with a tenfold excess of pinacol(borane) indicated a 0 order dependence on aniline concentration, as shown in Fig. 4.10. By process of elimination, similar to that assumed in the derivation of Eq. 4.1, it is thus possible to imply the reaction is first order in [PinBH].

With these data in hand it is further possible to formulate a rate law for this process, distinct from that of its dialkylborane analogue as shown in Eq. 4.2.

$$\text{rate} = k[\mathbf{Ib}]^2[\text{borane}]^1[\text{amine}]^0 \quad (4.2)$$

4.5.3 Order of Reactants for Diphenylsilane

The reaction between diphenylsilane and *N*-methylaniline was thus investigated. An equimolar reaction was judged to show zero-order overall behaviour

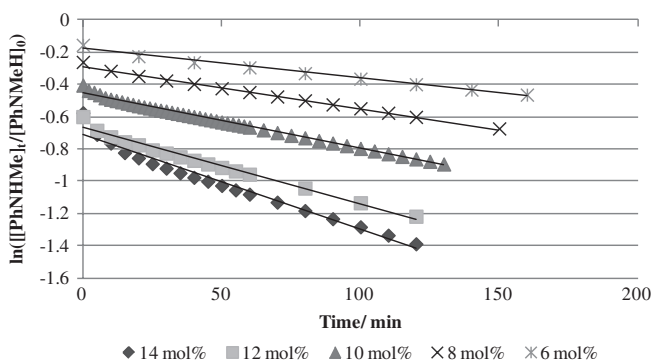


Fig. 4.8 The overall first-order plot of $\ln([\text{amine}]_t/[\text{amine}]_0)$ against time for a range of **Ib** concentrations

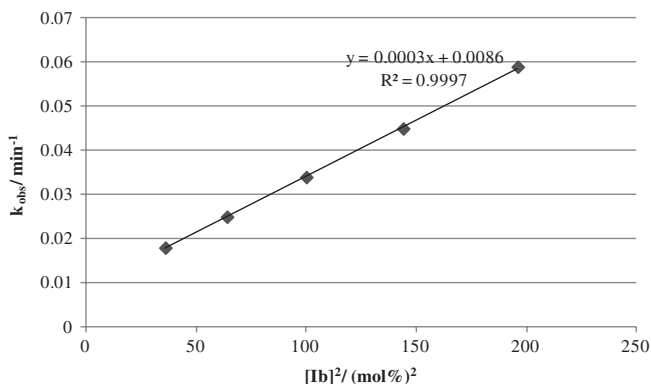


Fig. 4.9 The plot of observed rate constant against catalyst loading for a range of **Ib** concentrations

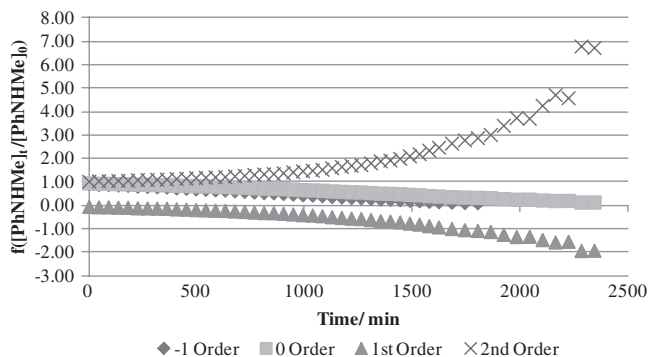


Fig. 4.10 The overall first-order plot of $f([\text{amine}]_t/[\text{amine}]_0)$ against time for a reaction with a tenfold excess of pinacol(borane)

(Fig. 4.11) and a series of catalyst loading experiments indicated a $\frac{1}{2}$ order dependence upon **Ib** as shown in Fig. 4.12.

When a tenfold excess of diphenylsilane was subsequently investigated, this indicated a -1 order dependence upon [aniline] which, by elimination, suggested a first-order dependence on [silane], as summarised in Fig. 4.13.

These analyses once again allowed the formulation of a rate law, independent of that derived for the prior reactions.

$$\text{rate} = k[\mathbf{Ib}]^{1/2}[\text{silane}]^1[\text{amine}]^{-1} \quad (4.3)$$

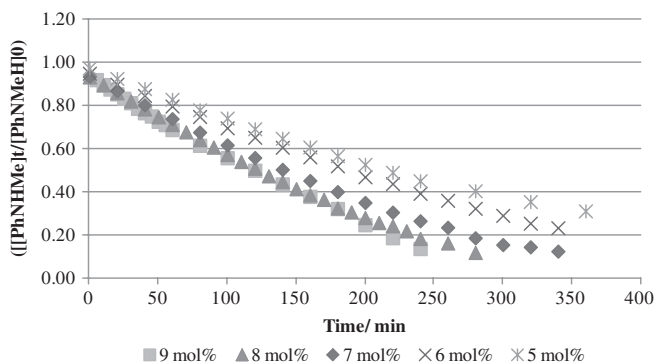


Fig. 4.11 The overall first-order plot of $\ln([\text{amine}]_t/[\text{amine}]_0)$ against time for a range of **Ib** concentrations at 343 K

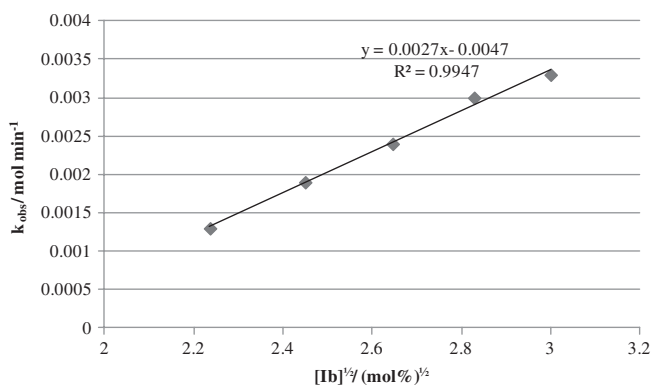


Fig. 4.12 The plot of observed rate constant against catalyst loading for a range of **Ib** concentrations at 343 K

4.5.4 Eyring and Arrhenius Analyses for 9-BBN, Pinacolborane and Diphenylsilane

Subsequently, analysis was undertaken into the effect of temperature upon these reactions, as summarised in Figs. 4.14, 4.15 and 4.16.

Utilising Arrhenius and Eyring analysis techniques, key parameters relating to the rate determining step can be derived (Figs. 4.17 and 4.18) and are thus summarised in Table 4.5.

Consideration of the activation energy for these processes shows a somewhat striking divergence from the observed turnover frequencies. Whilst pinBH enjoys a 7 kcal mol^{-1} advantage over silane, as would be suggested by the order of magnitude difference in their turnover frequencies (Table 4.4), 9-BBN would, from

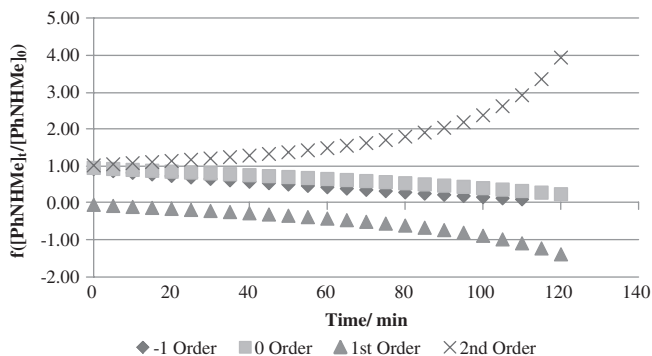


Fig. 4.13 The overall -1 order plot of $f([\text{amine}]_t/[\text{amine}]_0)$ against time for a reaction with a tenfold excess of diphenylsilane at 343 K

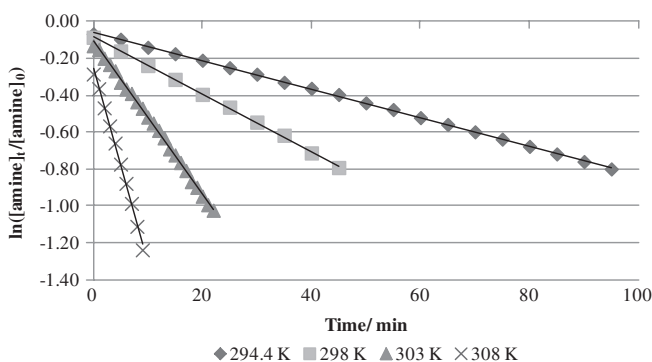


Fig. 4.14 The variable temperature plots for *N*-methylaniline-9-BBN coupling mediated by **Ib**

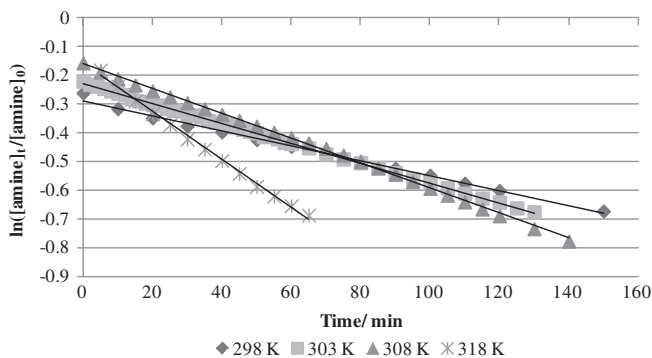


Fig. 4.15 The variable temperature plots for *N*-methylaniline-pinacol(borane) coupling mediated by **Ib**

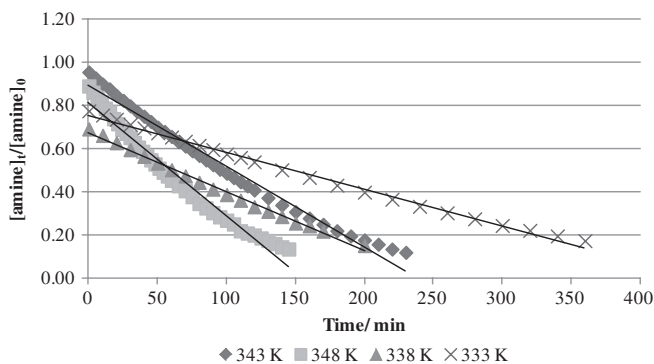


Fig. 4.16 The variable temperature plots for *N*-methylaniline-diphenylsilane coupling mediated by **Ib**

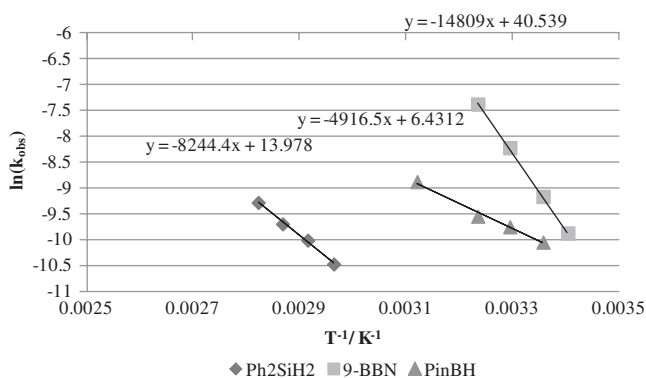


Fig. 4.17 The Arrhenius analysis to elucidate the activation energy for the rate determining step of *N*-methylaniline-hydric reagent dehydrocoupling catalysed by **Ib**

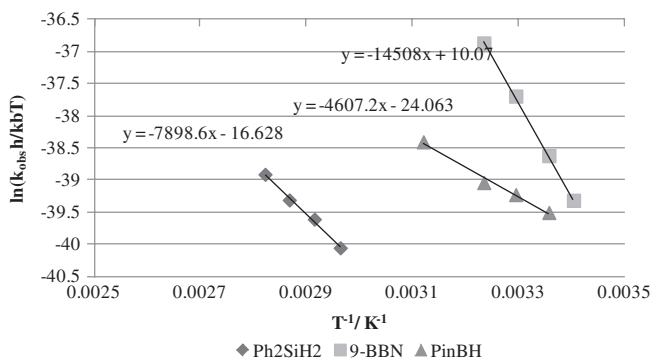


Fig. 4.18 The Eyring analysis to elucidate the activation enthalpy and entropies for the rate determining step of *N*-methylaniline-hydric reagent dehydrocoupling catalysed by **Ib**

Table 4.5 Activation parameters for the catalytic dehydrocoupling of *N*-methylaniline with a range of hydridic reagents mediated by **1b**

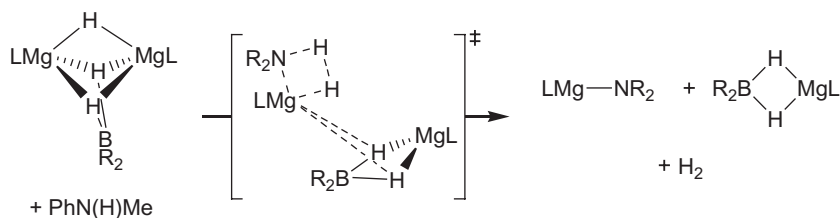
	E_a (kcal mol ⁻¹)	ΔH^\ddagger (kcal mol ⁻¹)	ΔS^\ddagger (cal mol ⁻¹ K ⁻¹)	ΔG_{298}^\ddagger (kcal mol ⁻¹)
9-BBN	29.5(7)	29.9(7)	20.0(25)	23.0
PinBH	9.8(7)	9.2(7)	-47.9(25)	23.5
Ph ₂ SiH ₂	16.4(8)	15.7(8)	-33.1(24)	25.6

consideration of the activation energies alone, be expected to be the slowest coupling partner.

In contrast to these results, consideration of the ΔG^\ddagger values is more informative. In the case of this measure the trend in endergonicity more closely mirrors that of turnover frequency. This striking divergence can be attributed to the observed values for the entropy of activation. Extensive precedent both herein and in the literature has indicated the profound effect of entropic effects in the rate determining steps of Group 2 catalysis. Whilst both phenylsilane and pinacol(borane) provide negative entropies of activation, indicative of highly ordered transition states, 9-BBN was observed to show a positive entropy of activation. The resultant inference of a strongly disordered transition state readily mitigates the distinct enthalpic penalty which the 9-BBN system suffers upon achieving the rate determining transition state.

With these data in hand, and with consideration of the previously derived rate laws for these reactions, it is possible to speculate upon the nature of the rate determining step for each of these transformations. Notably, each reaction appears to occur by a distinct mechanistic pathway.

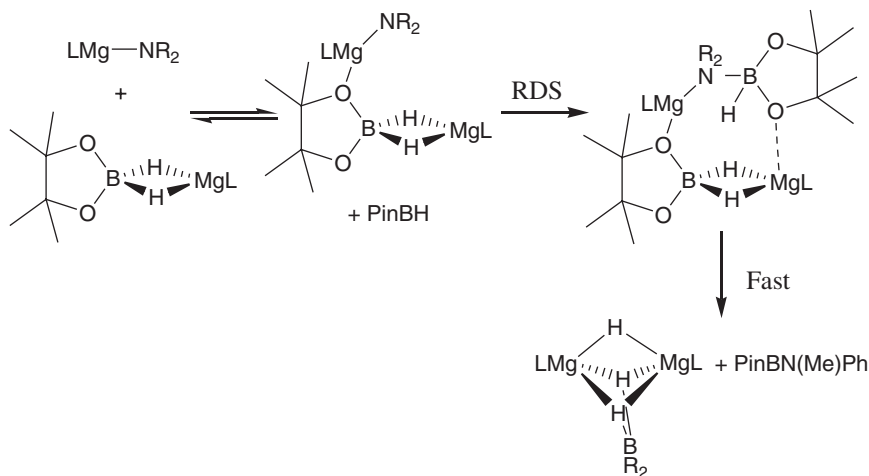
9-BBN showed a 1/2-order dependence on [**1b**], such a dependence on catalyst can be readily accounted for via a dimeric catalytic system. Given the dimeric nature of a number of the β -diketiminato magnesium hydrides and borohydrides reported in the literature, a consequence of the unique steric and electronic properties of the hydride ligand, this result is somewhat unsurprising. Such a species may be a hydride bridged dimer, similar to **1h** but is more likely, given the distinct Lewis acidity of 9-BBN, to be a dimer bridged by one borohydride and one hydride. Furthermore, the first order dependence on [amine] may be indicative of a rate determining protonolysis, in a manner reminiscent of the silicon–nitrogen dehydrocoupling mediated by **11a** described in Chap. 2. Whilst the activation parameters derived for the silicon–nitrogen dehydrocoupling of **11a** indicated a highly ordered transition state ($\Delta S^\ddagger = -29.8(6)$), with a moderate ΔH^\ddagger (13.9(2)), the dehydrocoupling of 9-BBN and *N*-methylaniline mediated by **1b** occurs via assembly of a far more disordered transition state, with the occurrence of a greater degree of bond breaking necessary to achieve this transition state. Such parameters are most readily accounted for by considering the consequences of the apparent dimeric nature of the catalyst in this reaction, and would indicate a significant degree of dimer cleavage in the transition state, as summarised in Scheme 4.4.



Scheme 4.4 The proposed rate determining step and transition state for the dehydrocoupling of *N*-methylaniline and 9-BBN mediated by **Ib**

As shown, protonolysis, occurring in a concerted fashion with dimer cleavage, yields a ligated magnesium amide and a borohydride, structurally analogous to **14**, with this transformation constituting the rate determining step. A subsequent rapid B–N coupling could be envisaged to proceed by one of two possible paths; a subsequent interaction of the magnesium amide with an equivalent of 9-BBN, which undergoes a rapid σ -bond metathesis to form the product aminoborane and a metal hydride which interacts with the magnesium borohydride produced in the rate determining step to yield the hydrido-borohydride dimer postulated to be involved in such a step may be envisaged. Alternatively, direct interaction between the products of the rate determining step, most likely via a dissociation of the 9-BBN fragment from the borohydride, might yield the B–N coupling and a hydride bridged dimer, structurally related to **Ih**. The reaction of this with 9-BBN thus once again yields the catalytic species involved in the rate determining step.

In contrast, the reaction of pinacol(borane) with *N*-methylaniline mediated by **Ib** showed both a distinct rate law and activation parameters. A second order dependence on [**Ib**] was observed, with only a first order dependence on [PinBH]. Furthermore, the ΔS^\ddagger value suggested a highly ordered transition state but only a modest ΔH^\ddagger was observed. These data were close to those derived by Sadow and co-workers for silicon–nitrogen dehydrocoupling mediated by **VII**, wherein they postulated a rate determining nucleophilic attack of a magnesium bound amide on the silane (ΔH^\ddagger : 5.9(2), ΔS^\ddagger : $-46.5(8)$ kcal mol $^{-1}$). Although it is likely that such a rate determining step is occurring here also, such a hypothesis does not account for the observed second-order dependence on [**Ib**]. This dependence, however, can be accounted for by consideration of the ligand variation between **VII** and **Ib**. **VII** is ligated by a tris(oxazoly)borate, a tridentate ligand which may be able to support a terminal magnesium hydride in solution. In contrast, with the exception of one striking example reliant on a super-bulky β -diketiminato [23], no terminal 3-coordinate magnesium species have been described. In order to stabilise the product of the subsequent N–B coupling, a metal hydride, a second equivalent of β -diketiminato magnesium borohydride could be envisioned to be required to yield an active species. In this case, the product is a dimeric magnesium hydrido-borohydride, identical to one previously structurally characterised. Protonolysis of this species with *N*-methylaniline would thus yield the magnesium amide and

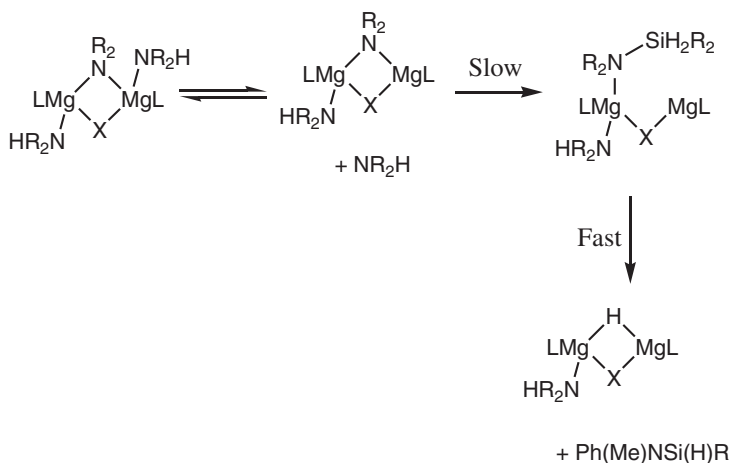


Scheme 4.5 The proposed rate determining step and transition state for the dehydrocoupling of *N*-methylaniline and PinBH mediated by **Ib**

borohydride species required to come together to access the rate determining step in a pre-equilibria which contributes the second-order dependence on catalyst to the rate law (Scheme 4.5).

Such a scheme seems somewhat contrived given the evident nucleophilicity of the monomeric β -diketiminato magnesium amide which could thus attack the pinacol(borane) and yield turnover. It is likely, however, that even if such reactivity is occurring in solution, a Curtin-Hammett effect inhibits the produced monomeric magnesium amidoborane from contributing to reactivity as the subsequent hydride transfer, which would yield an unprecedented three-coordinate magnesium hydride, is slowed to such an extent that the pathway in Scheme 4.5 instead dominates.

Finally, when considering the diphenylsilane coupling partner, a divergent rate law is once again observed. A $\frac{1}{2}$ -order dependence on [**Ib**] is once again deduced, liable to be indicative of a persistent dimer. In contrast to both borane coupling partners, however, this reaction suggested an inhibitory effect of aniline, indicating a -1 -order dependence on [amine], with a first order dependence on [silane] being thus implied. The activation parameters once again suggest a highly ordered transition state with limited bond breaking, and are comparable with both that for pinacol(borane) coupling mediated by **Ib** and silicon–nitrogen dehydrocoupling mediated by **VII**. Although these data can be again accounted for by a rate determining nucleophilic attack on the silane coupling partner, owing to the reduced Lewis acidity of the silane, it is far less likely that the catalyst dimer is held together by a bridging H–Si interaction. Thus the dimer is liable to be either hydride or anilide bridged, and structurally related to **Ij**. In the presence of excess aniline, a reversible donor interaction from the aniline to the catalyst dimer can be envisaged which, owing to the steric congestion of this species may prevent approach of the silane. As such, the observed -1 order in aniline can be readily



Scheme 4.6 The proposed rate determining step and transition state for the dehydrocoupling of *N*-methylaniline and diphenylsilane mediated by **Ib**

accounted for by a dissociative pre-equilibrium upon which the subsequent nucleophilic attack is contingent (Scheme 4.6).

With these data in hand, a number of key conclusions may thus be drawn. Boron–nitrogen dehydrocoupling can be readily mediated by **Ib**, alongside silicon–nitrogen dehydrocoupling. This reactivity shows a relatively wide range of substrate tolerance and occurs in practicable timeframes. More interesting, however, are the mechanistic nuances once again indicated by the kinetic study. Alongside effects from solution molecularity, coordinative unsaturation and ancillary ligation, in a manner reminiscent of the results described in Chap. 2, a number of other factors can now be added to considerations of dehydrocoupling activity of magnesium precatalysts. To wit, Lewis acidity of coupling partners appears to have a profound effect on not only the rate but also the mechanism of dehydrocoupling catalysis. These factors are, partially at least, a consequence of the privileged position of the hydride ligand as being both electronically and sterically unique but further being able to interact with highly Lewis acidic substrates. These observations once again build on the mechanistic complexity of Group 2 mediated dehydrocoupling catalysis, and add observations which provide essential insight to further analysis of these intriguing reactions.

4.6 Experimental

$[\text{CH}\{\text{C}(\text{Me})\text{N}(\text{Dipp})\}_2]\text{Mg}\{\text{N}(\text{Dipp})\text{Si}(\text{H})_2\text{Ph}\}$, **12**

To a toluene solution (3 mL) of **Ib** (50 mg, 0.1 mmol) was added DippNH₂ (18.85 μL, 0.1 mmol) and the resultant solution, which initially bubbled, allowed to sit for 1 h. After this time was added phenylsilane (12.3 μL, 0.1 mmol) and a

bubbling noted again. After 1 h, removal of solvent in vacuo yielded a sticky residue which was diluted with hexane (0.3 mL). The resultant suspension had toluene added dropwise until dissolution and the resultant solution was chilled to $-34\text{ }^{\circ}\text{C}$ yielding material suitable for crystallographic characterisation (34 mg, 47 %).

^1H NMR (400 MHz, Tol) δ ppm 0.86 (d, $J = 7.07$ Hz, 12 H, $\underline{\text{H}_3\text{CCHCH}_3}$) 1.05 (d, $J = 6.82$ Hz, 4 H, $\underline{\text{H}_3\text{CCHCH}_3}$) 1.09 (d, $J = 6.82$ Hz, 8 H) 1.17 (d, $J = 6.82$ Hz, 12 H, $\underline{\text{H}_3\text{CCHCH}_3}$) 1.52 (s, 6 H, $\underline{\text{H}_3\text{C}}$) 3.09 (br. spt, 4 H, $\underline{\text{H}_3\text{CCHCH}_3}$) 3.55 (spt, $J = 6.80$ Hz, 1 H, $\underline{\text{H}_3\text{CCHCH}_3}$) 4.79 (s, 1 H $\underline{\text{CH}_3\text{CCHCCH}_3}$) 4.91 (s, 2 H, $\underline{\text{SiH}}$) 6.79–7.14 (m, 14 H, ArH); ^{13}C NMR (Tol, 101 MHz): $\delta = 171.5, 147.4, 145.0, 143.7, 142.3, 138.0, 134.8, 127.4, 126.3, 124.4, 123.8, 121.5, 96.2, 29.1, 27.5, 24.8, 24.6, 24.5, 24.3$ ppm.

Anal. calc'd for $\text{C}_{47}\text{H}_{65}\text{MgN}_3\text{Si}$: C, 77.92; H, 9.04; N, 5.80 %. Found: C, 77.78; H, 9.17; N, 5.75 %.

$[\text{CH}\{\text{C}(\text{Me})\text{N}(\text{Dipp})\}_2]\text{Mg}\{\text{N}(\text{Dipp})\text{Bpin}\}$, 13

To a toluene solution (3 mL) of **Ib** (50 mg, 0.1 mmol) was added DippNH_2 (18.85 μL , 0.1 mmol) and the resultant solution, which initially bubbled, allowed to sit for 1 h. After this time was added pinacol(borane) (14.4 μL , 0.1 mmol) and a bubbling noted again. After 1 h, the resultant solution had solvent removed in vacuo to incipient crystallisation and was chilled to $-34\text{ }^{\circ}\text{C}$ yielding material suitable for crystallographic characterisation (27 mg, 34 %).

^1H NMR (300 MHz, Tol) δ ppm 0.48–0.67 (m, 12 H, $\text{OC}(\text{CH}_3)_2$) 0.70 (s, 6 H, $\underline{\text{H}_3\text{CCHCH}_3}$) 0.73–0.85 (m, 12 H, $\underline{\text{H}_3\text{CCHCH}_3}$) 0.91 (dd, $J = 6.69, 3.11$ Hz, 12 H, $\underline{\text{H}_3\text{CCHCH}_3}$) 1.05–1.15 (m, 6 H, $\underline{\text{H}_3\text{CCHCH}_3}$) 1.33 (s, 4 H) 2.89 (spt, $J = 6.80$ Hz, 4 H, $\underline{\text{H}_3\text{CCHCH}_3}$) 3.04 (spt, $J = 6.80$ Hz, 1 H, $\underline{\text{H}_3\text{CCHCH}_3}$) 4.58 (s, 1 H, $\underline{\text{CH}_3\text{CCHCCH}_3}$) 6.60–6.88 (m, 9 H, ArH); ^{13}C NMR (Tol, 75 MHz): δ ppm 170.3, 145.7, 142.9, 141.5, 140.4, 125.4, 123.4, 122.6, 120.0, 95.7, 82.7, 82.4, 31.7, 28.5, 28.1, 27.9, 24.6, 24.5, 24.4, 24.1, 23.8, 22.8, 14.0; ^{11}B NMR (96 MHz, Tol): $\delta = 32.1$ (s).

Anal. calc'd for $\text{C}_{47}\text{H}_{70}\text{BMgN}_3\text{O}_2$: C, 75.85; H, 9.48 N, 5.65 %. Found: C, 75.65; H, 9.56; N, 5.77 %.

$[\text{CH}\{\text{C}(\text{Me})\text{N}(\text{Dipp})\}_2]\text{Mg}(\text{THF})(\text{H}_2\text{B}\{\text{CHCH}_2\text{CH}_2\text{CH}_2\}_2)$, 14

To a toluene solution (3 mL) of **Ib** (50 mg, 0.1 mmol) was added DippNH_2 (18.85 μL , 0.1 mmol) and the resultant solution, which initially bubbled, allowed to sit for 1 h. After this time was added 9-BBN (12.2 mg, 0.1 mmol) and a bubbling noted again. After 1 h, the resultant solution had solvent removed in vacuo to incipient crystallisation and was chilled to $-34\text{ }^{\circ}\text{C}$ yielding a powder. Three drops of THF were thus added and chilling to $-34\text{ }^{\circ}\text{C}$ yielded material suitable for crystallographic characterisation (52 mg, 82 %).

$^1\text{H}\{^{11}\text{B}\}$ NMR (300 MHz, d_8 -THF) δ ppm 1.01 (dd, 12H, $\underline{\text{H}_3\text{CCHCH}_3}$), 0.89–1.69 (m, 12H, 9-BBN), 1.80 (s, 6H, $\underline{\text{H}_3\text{C}}$), 3.30 (sept, 2H, $\underline{\text{H}_3\text{CCHCH}_3}$), 3.39 (s, H, $\underline{\text{H}_2\text{-B}}$), 4.79 (s, 1H, $\underline{\text{CH}_3\text{CCHCCH}_3}$), 6.89–7.30 ppm (m, H, aromatic); ^{13}C NMR (benzene- d_6 , 75 MHz) δ ppm 169.4, 145.3, 142.5, 125.4, 123.9, 95.0, 67.9, 27.4, 26.0, 24.7, 24.2, 23.9, 23.2, 14.2; ^{11}B NMR (96 MHz, d_8 -THF): δ ppm -14 (d, $\text{R}_2\text{B-H}_2\text{-Mg}$).

Anal. calc'd for (%) for $C_{41}H_{65}BMgN_2O$ C, 77.30; H, 10.28; N, 4.40 %. Found: C, 79.11; H, 9.80; N, 4.89 %.

Aminoboranes were synthesised according to conditions noted in Table 4.2 and identified by comparison to literature compounds. Novel compounds are characterised hereafter.

BuN(H)Bpin

1H NMR (300 MHz, benzene- d_6) δ ppm 2.92 (q, $J = 6.8$ Hz, 2 H), 2.07 (br. s, 1 H), 1.19–1.23 (m, 4 H), 1.10–1.17 (m, 12 H), 0.81 ppm (t, $J = 7.5$ Hz, 3 H); ^{13}C NMR (benzene- d_6 , 75 MHz): δ ppm 82.1, 41.4, 36.4, 25.2, 20.3, 14.4; ^{11}B NMR (96 MHz, benzene- d_6) δ ppm 28.04 (s).

tBuN(H)Bpin

1H NMR (300 MHz, benzene- d_6) δ ppm 1.12 (s, 12 H) 1.21 (s, 9 H); ^{13}C NMR (benzene- d_6 , 75 MHz): δ ppm 81.7, 32.6, 25.3, 25.1; ^{11}B NMR (96 MHz, benzene- d_6) δ ppm 27.33 (s).

tBuN(Bpin) $_2$

1H NMR (300 MHz, benzene- d_6) δ ppm 1.20 (s, 3 H), 1.12 (s, 6 H), 1.00 (s, 24 H); ^{13}C NMR (benzene- d_6 , 75 MHz): δ ppm 83.5, 32.6, 25.3, 25.1; ^{11}B NMR (96 MHz, benzene- d_6) δ ppm 31.63 (s).

DippN(H)Bpin

1H NMR (300 MHz, benzene- d_6) δ ppm 1.15 (s, 24 H) 1.30 (d, $J = 6.78$ Hz, 24 H) 3.49 (m, $J = 6.88$ Hz, 4 H) 7.10–7.22 (m, 3 H); ^{13}C NMR (benzene- d_6 , 75 MHz): δ ppm 145.8, 136.4, 126.3, 123.6, 82.8, 29.0, 25.0, 24.2; ^{11}B NMR (96 MHz, benzene- d_6) δ ppm 27.52 (s).

	12	13	14
Empirical formula	$C_{47}H_{65}MgN_3Si$	$C_{47}H_{70}BMgN_3O_2$	$C_{96}H_{146}B_2Mg_2N_4O_2$
Formula weight (g mol $^{-1}$)	724.42	744.18	1457.40
Crystal system	Monoclinic	Triclinic	Triclinic
Space group	$P2_1/n$	P_{-1}	P_{-1}
a (Å)	12.0310(2)	10.4810(4)	10.6157(2)
b (Å)	21.6920(3)	12.1080(4)	11.7803(3)
c (Å)	17.0200(3)	18.7980(5)	11.7803(3)
α (°)	90	94.881(2)	84.5660(10)
β (°)	94.632(1)	103.832(2)	84.3360(10)
γ (°)	90	104.473(2)	84.3360(10)
V (Å 3)	4427.31(12)	2216.08(13)	2228.54(8)
Z	4	2	1
ρ (g cm $^{-3}$)	1.087	1.115	1.086
μ (mm $^{-1}$)	0.101	0.079	0.075
θ range (°)	3.70–27.42	5.39–25.05	3.07–30.07
Measured/independent reflections/ R_{int}	69316/10038/0.0786	7761/5250/0.0918	43046/12947/0.0595

	12	13	14
Data/restraints/ parameters	10038/0/491	7761/0/505	12947/0/531
Goodness-of-fit on F^2	1.049	1.030	1.019
R_1, wR_2 [$I > 2\sigma(I)$]	0.0523, 0.1123	0.0565, 0.1249	0.0514, 0.1182
R_1, wR_2 (all data)	0.0923, 0.1306	0.0960, 0.1488	0.0837, 0.1356

Notes on crystallographic refinement

12 H1 and H2 (attached to Si1) were located and refined without restraints.

13 Data truncated to a Bragg angle of 25° because of a consequent fall-off in diffracting ability that reflects a very small crystal size.

14 The asymmetric unit consists of one Mg complex and solvent molecules of toluene. The THF ligand in the Mg complex shows disorder in the ratio 80:20 with the minor part refined isotropically. Both solvent molecules are located about a centre of inversion. One molecule is complete with 50 % occupation factor and the other is half a molecule with full occupation.

References

1. C. Solé and E. Fernández, *Angew. Chem.-Int. Ed.* **52**, 11351 (2013)
2. M. Sugimoto, L. Uehlin M. Murakami, *J. Am. Chem. Soc.* **126**, 13196 (2004); M. Sugimoto, in *Pure and Applied Chemistry*, 2006, p. 1377; M. Sugimoto, Y. Tanaka, T. Hasui, *Synlett* 1047 (2006)
3. A.Y. Khalimon, P. Farha, L.G. Kuzmina, G.I. Nikonov, *Chem. Commun.* **48**, 455 (2012)
4. B. Wrackmeyer, H.E. Maisel, M. Herberhold, *J. Organomet. Chem.* **637**, 727 (2001)
5. M. Yalpani, R. Boese, R. Köster, *Chem. Ber.* **123**, 1275 (1990); M. Yalpani, R. Köster, R. Boese, W.A. Brett, *Angew. Chem.-Int. Ed.* **29**, 302 (1990); B. Singaram, *Heteroat. Chem.* **3**, 245 (1992)
6. H.-B. Zhou, K.W. Nettles, J.B. Bruning, Y. Kim, A. Joachimiak, S. Sharma, K.E. Carlson, F. Stossi, B.S. Katzenellenbogen, G.L. Greene, J.A. Katzenellenbogen, *Chem. Biol.* **14**, 659 (2007)
7. Seifert, W. Storch, M. Vosteen, *Eur. J. Inorg. Chem.* **1998**, 1343 (1998); T. Gasparis-Ebeling, H. Nöth, *Chem. Ber.* **123**, 261 (1990); H. Nöth, P. Otto, W. Storch, *Chem. Ber.* **119**, 2517 (1986)
8. J.F. Janik, C.K. Narula, E.G. Gulliver, E.N. Duesler, R.T. Paine, *Inorg. Chem.* **27**, 1222 (1988); B. Wrackmeyer, B. Schwarze, W. Milius, *J. Organomet. Chem.* **489**, 201 (1995); B. Wrackmeyer, G. Kehr, S. Ali, *Z. Naturforsch. B: Chem. Sci.* **53**, 393 (1998)
9. T. Yijun, L. Xiao, CN 101440101 (2009); G. Zhinong, L. Xiao, CN 102093399 (2011)
10. H.F. Bettinger, M. Filthaus, *Org. Biomol. Chem.* **8**, 5477 (2010); M. Muller, C. Maichle-Mossmar, H.F. Bettinger, *Chem. Commun.* **49**, 11773 (2013)
11. M. Tokizane, K. Sato, Y. Sakami, Y. Imori, C. Matsuo, T. Ohta, Y. Ito, *Synthesis* 36 (2010)
12. R.T. Baker, J.C. Calabrese, S.A. Westcott, *J. Organomet. Chem.* **498**, 109 (1995)
13. L. Koren-Selfridge, H.N. Londino, J.K. Vellucci, B.J. Simmons, C.P. Casey, T.B. Clark, *Organometallics* **28**, 2085 (2009)
14. E.H.M. Kirton, G. Tughan, R.E. Morris, R.A. Field, *Tetrahedron Lett.* **45**, 853 (2004)
15. C.M. Vogels, P.E. O'Connor, T.E. Phillips, K.J. Watson, M.P. Shaver, P.G. Hayes, S.A. Westcott, *Can. J. Chem.* **2001**, 79 (1898)
16. A.G.M. Barrett, M.R. Crimmin, M.S. Hill, P.B. Hitchcock, P.A. Procopiou, *Organometallics* **26**, 4076 (2007)

17. P.B. Hitchcock, M.F. Lappert, G.A. Lawless, B. Royo, *J. Chem. Soc.-Chem. Commun.* 1141 (1990); W. Vargas, U. English, K. Ruhlandt-Senge, *Inorg. Chem.* **41**, 5602 (2002); L.T. Wendell, J. Bender, X. He, B.C. Noll, K.W. Henderson, *Organometallics* **25**, 4953 (2006); M.S. Hill, G. Kociok-Köhn, D.J. MacDougall, *Inorg. Chem.* **50**, 5234 (2011)
18. X. Zheng, U. Englert, G.E. Herberich, J. Rosenplänter, *Inorg. Chem.* **39**, 5579 (2000)
19. E.V. Mutseneck, S. Bieller, M. Bolte, H.-W. Lerner, M. Wagner, *Inorg. Chem.* **49**, 3540 (2010)
20. A. Reichert, J. Schmidt, M. Bolte, M. Wagner, H.-W. Lerner, *Z. Anorg. Allg. Chem.* **639**, 1083 (2013); A. Kawachi, S. Nagae, Y. Onoue, O. Harada, Y. Yamamoto, *Chem.- Eur. J.* **17**, 8005 (2011)
21. A. Schnurr, K. Samigullin, J.M. Breunig, M. Bolte, H.-W. Lerner, M. Wagner, *Organometallics* **30**, 2838 (2011)
22. R.A. Collins, J. Unruangsri, P. Mountford, *Dalton Trans.* **42**, 759 (2013)
23. M. Arrowsmith, B. Maitland, G. Kociok-Köhn, A. Stasch, C. Jones, M.S. Hill, *Inorg. Chem.* **53**, 10543 (2014)

Chapter 5

Single Electron Transfer Steps in Group 2 Catalysis

5.1 Introduction

The stable nitroxyl radical, TEMPO (2,2,6,6-tetramethyl-1-piperidinyloxy) [1], has attracted widespread interest since its first synthesis in 1960. Much of this attention has centred on its utility in polymer synthesis [2], organic oxidation reactions [3] and, due to its persistent radical character, in molecular magnetism [4]. Although the use of TEMPO as a radical donor ligand is dominated by reports of redox active *d*-block complexes [5], there is also more limited precedent for the use of TEMPO in d^0 *f*- [6] and *s*-block complex chemistry [7–10]. Mulvey and co-workers reported the first Group 1 and 2 complexes of TEMPO in 2001, [7] noting not only its coordination as a neutral two electron donor but also its ability to adopt an anionic electron configuration when ligating Group 2 cations in complexes of the form $[(\text{Me}_3\text{Si})_2\text{N}\text{Mg}\{\mu\text{-TEMPO}\}]_2$ (XI). A subsequent, elegant report from this group of single electron transfer (SET) from elemental Group 1 metals to TEMPO yielded a structurally diverse series of $[\text{L}_n\text{M}\{\text{OTEMP}\}]$ compounds ($\text{M} = \text{Li}, \text{Na}, \text{K}, \text{Rb}, \text{Cs}, \text{L} = \text{THF}, \text{Me}_2\text{NCH}_2\text{CH}_2\text{NMe}_2$) once again containing TEMPO anions (hereafter referred to as TEMPOxide) [8].

A demonstration of TEMPO reactivity with Group 2 reagents has also been observed by Fedushkin et al. who reported SET with a magnesium complex mediated by a redox active 1,2-bis(arylimino)acenaphthene (BIAN) ligand [10]. Furthermore, stoichiometric SET to a variety of organomagnesium reagents is well precedented yielding a variety of C–C and C–N coupled products [11]. Although this reactivity has not yet been extended to magnesium hydride species, it is notable that Jones et al. have described the stoichiometric reaction of TEMPO with a range of Group 13 hydrides yielding molecular dihydrogen alongside the formation of TEMPOxide ligated to the relevant Group 13 centre [12]. Similarly, Stephan and co-workers have described the effect of TEMPO upon $[\text{Zn}\{\text{C}_5\text{Me}_5\}_2]$, yielding $[\text{Zn}\{\text{OTEMP}\}_2]_6$ and the radical coupling product derived from the C_5Me_5^- ligands. [13] In contrast to these SET-derived products, a number of f^0d^0 or *p*-block metal containing adducts of the TEMPO radical are also known, including $[\{\text{TEMPO}\}\text{MX}_3]$ ($\text{M} = \text{B}, \text{X} = \text{Br}; \text{M} = \text{Al}, \text{X} = \text{Cl}, \text{Br}$) [14] and $[\text{RE}^{\text{III}}(\text{hfa}$

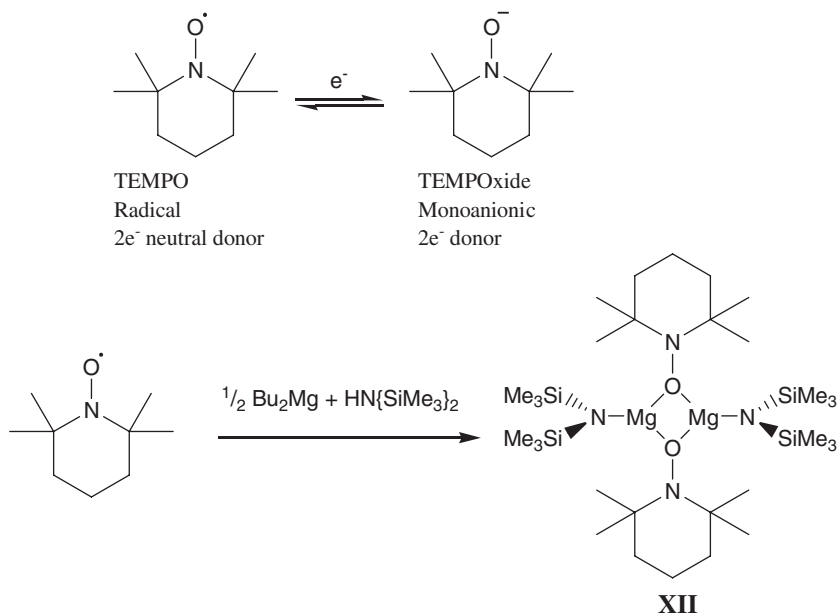


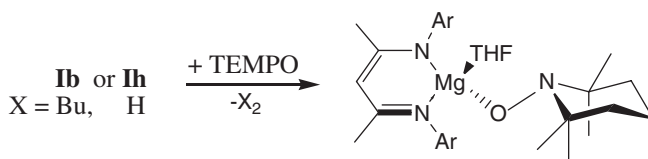
Fig. 5.1 The “chameleonic” nature of the TEMPO/TEMPOoxide ligand set as exemplified by its SET activity on MgBu_2

$\text{c}_3(\text{TEMPO})_2$ (RE = Y, Ln, Gd) [15] alongside those described by Mulvey and co-workers [7].

While reductive processes, based on Group 2 hydride intermediates generated by metathesis of silane and borane reagents at amide- and alkoxide-ligated centres, have dominated recent progress, as shown in Chaps. 1–4 [17], all previous work in Group 2 catalysis has been contingent on 2-electron processes. As a result, introduction of single electron transfer steps into Group 2 mediated manifolds would be an attractive goal. Thus, an investigation into the activity of the stable radical TEMPO upon Group 2, inspired by previous stoichiometric reports, was undertaken (Fig. 5.1).

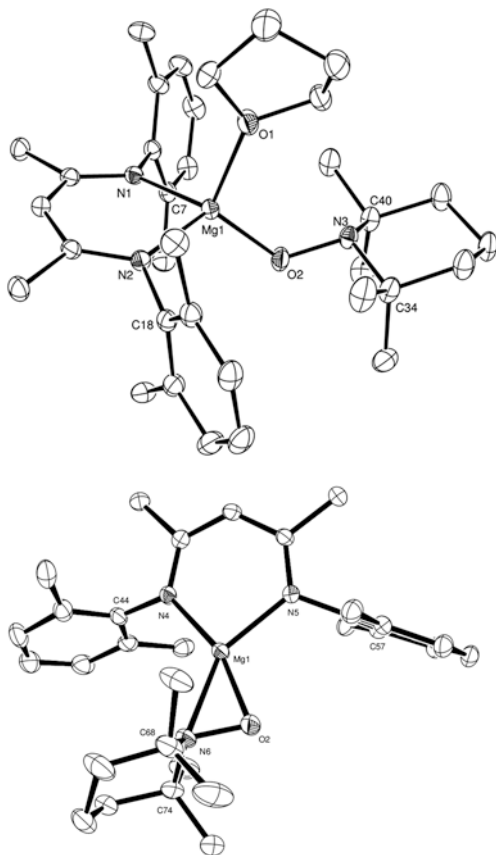
5.2 Stoichiometric Reactivity of TEMPO with Magnesium Species

Our initial investigation centred upon β -diketiminate complexes of magnesium [$\text{CH}\{\text{C}(\text{Me})\text{NDipp}\}_2\text{Mg}^n\text{Bu}$] (**Ib**) [18] and [$\text{CH}\{\text{C}(\text{Me})\text{NDipp}\}_2\text{MgH}$]₂ (**Ih**) [19]. Gratifyingly, the action of TEMPO upon both these species evidenced SET characteristics with almost instantaneous extinction of the red colour associated with TEMPO. Monitoring by ^1H NMR spectroscopy revealed that compound **Ib**



Scheme 5.1 The reaction between a series of β -diketiminato magnesium complexes and TEMPO yielding a TEMPOxide and radical coupling product

Fig. 5.2 ORTEP representation of **15** and **15'** (30 % probability ellipsoids). *Isopropyl* methyl groups and hydrogen atoms omitted for clarity. Selected bond lengths (\AA) and angles ($^\circ$) for **15**: Mg1-N1 2.0915(15), Mg1-O2 1.8887(13), O2-N3 1.4423(1), Mg1-O2-N3 125.60(11), N1-Mg1-N2 92.65(6), C34-N3-C40 117.1(1). Repetition of the reaction in toluene omitting THF yielded **15'** in which *pseudo*-merohedral twinning prevented complete refinement, nevertheless the compound is presented as connectivity was unambiguous



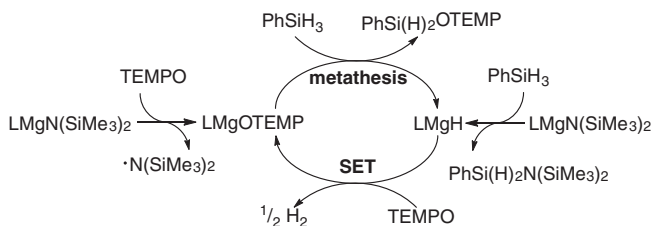
had undergone a well-precedented alkyl coupling to form *n*-octane, while compound **Ih**, in reactivity reminiscent of that reported Group 13 hydrides, provided a pronounced bubbling of molecular dihydrogen (Scheme 5.1). Alongside the desired small molecule product of this reaction, a magnesium complex (**15**) was isolated and characterised by NMR spectroscopy and single crystal X-ray diffraction analysis (Fig. 5.2).

Although the coordination environment of compound **15** is otherwise comparable to Fedushkin's BIAN derivative, [10] wherein the nitroxide displays significant pyramidalisation indicative of single electron reduction of the radical starting material, the two compounds differ significantly in the mode of binding of the TEMPO_x ligand. Whereas the TEMPO_x binds in an unambiguous η^1 coordination mode through the terminal oxygen centre in **15**, coordination to the BIAN-coordinated magnesium occurs through both of the nitroxide nitrogen and oxygen centres [10] and repeating the reaction which yielded **15** yielded a THF free analogue, **15'**, which contained a magnesium centre in a similar coordination environment. **15'**, however, was of poor crystalline quality and thus only connectivity could be established and no meaningful comparisons on bond length or angle data can thus be made. It is, however, clear that the coordination variation of the TEMPO_x fragment between **15** and the BIAN complex is a direct result of the presence of the THF atom, and this adjustment results in a significant shortening of the Mg–O distance within compound **15** (1.8887(13) vs. 1.9061(10) Å).

Attempts to extend this reactivity to a catalytic manifold, reliant upon the conversion **15** into **1h** via σ -bond metathesis, were undertaken utilising phenylsilane as a hydride source. Unfortunately no reactivity between **15** and PhSiH₃ was observed which was attributed to the steric demands of the various substituents surrounding the magnesium centre and precluding approach of the silane reagent.

Consequently, attention turned to the homoleptic magnesium amide **IIa** due to the reduced steric congestion of the magnesium centre. Gratifyingly, the reaction between phenylsilane and TEMPO in the presence of 10 mol% **IIa** in C₆D₆ induced an observable bubbling and the decolourisation of the solution over the course of days. Analysis of the resultant solution by NMR spectroscopy also confirmed the formation of a new silane containing species, proposed to be TEMPOSi(H)₂Ph, forming via a catalytic manifold reliant upon both SET and σ -bond metathesis (Scheme 5.2). The reaction was optimized with respect to a small range of solvents, with the donor solvent *d*₈-THF showing a vast superiority in reaction rate to both aromatic solvents investigated, C₆D₆ and *d*₈-toluene.

In order to elucidate the intermediate species participating in this reaction, a series of stoichiometric investigations were undertaken. Reaction of di-butylmagnesium with two equivalents of TEMPO in THF yielded stepwise activation of the magnesium bound butyl groups giving rise to a crystallographically characterised



Scheme 5.2 The proposed catalytic cycle predicated on σ -bond metathesis and SET steps to yield an oxidative coupling of H₂ and a TEMPO-silylether

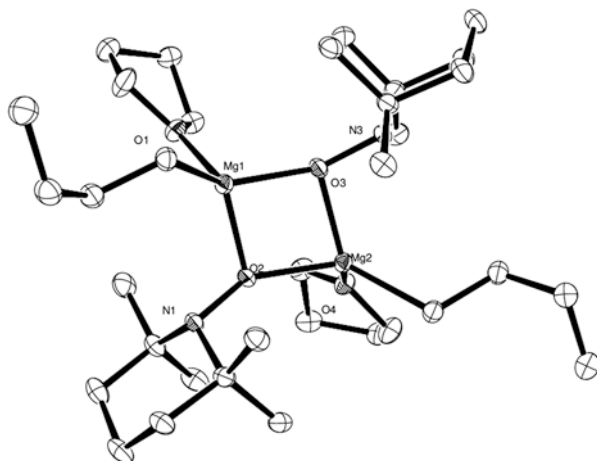


Fig. 5.3 ORTEP representation of **16** (30 % probability ellipsoids). Hydrogen atoms omitted for clarity. Selected bond lengths (Å) and angles (°): Mg1-C4 1.9909(16), Mg1-O2 1.9883(16), O2-N1 1.451(2), Mg1-O2-N1 106.81(11), C9-N1-C15 117.88(17), C9-N1-O2 108.59(15), C15-N1-O2 110.34(15), Mg1-O2-Mg2 97.46(7)

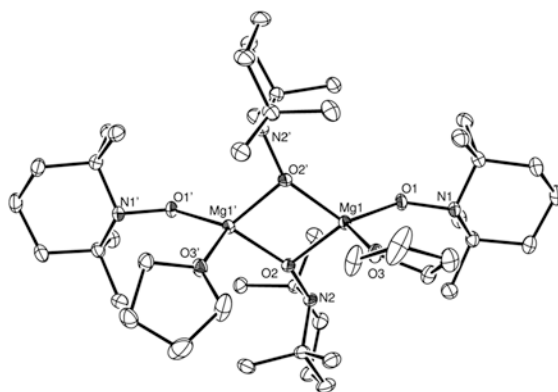


Fig. 5.4 ORTEP representation of **17** (30 % probability ellipsoids). Hydrogen atoms omitted for clarity. Selected bond lengths (Å) and angles (°): Mg1-O1 1.8848(11), Mg1-O2 1.9869(11), O1-N1 1.4420(15), O2-N2 1.4551(15), Mg1-O1-N1 130.91(9), C1-N1-C7 109.97(11), Mg1-O2-Mg1' 100.20(5), Mg1-O2-N2 106.85(8), C10-N2-C16 118.3(1). Symmetry transformations used to generate equivalent atoms: (') $-x, y, -z + 1/2$

heteroleptic TEMPO₂oxide-alkyl [(THF)Mg(OTEMP)(Bu)]₂ (**16**) (Fig. 5.3) and the desired homoleptic magnesium TEMPO₂oxide complex, [(THF)Mg(OTEMP)₂]₂ (**17**), which was isolated and characterised by NMR spectroscopy and a further single crystal X-ray diffraction analysis (Fig. 5.4).

Both species are dimeric with bridging TEMPOxide ligands. In the case of **16** the butyl ligands adopt a terminal arrangement, analogous to the hexamethyldisilazide ligands in Mulvey's structurally related complex, **XII** [7]. In contrast to this species, however, the coordination sphere of the magnesium is completed by a THF ligand. This seems, however, to have a limited effect upon the Mg–O bond lengths of the bridging TEMPOxides, which are in the range of those reported by Mulvey. Finally, pyramidalisation of the TEMPOxide nitrogens, an indication of a loss of radical character, further confirms the TEMPOxide ligands to be binding in a reduced, anionic form.

Similarly, the dimeric structure of compound **17** comprises terminal and bridging TEMPOxide ligands. Once again, the bridging Mg–O interactions within the structure of **17** [1.9869(11), 1.9891(1) Å] are similar to those of **XII** [7], but are significantly elongated in comparison to both the terminal distances within the dimeric unit itself [1.8848(11) Å] and the unique TEMPOxide ligand of compound **15**. Notably, the pyramidalisation of the TEMPO nitrogens is again present, indicative of the anionic character of the TEMPOxide ligands.

Gratifyingly, the reaction of **17** with an excess of phenylsilane did indeed induce the appearance of peaks corresponding to the proposed silane containing product, TEMPOSi(H)₂Ph, in the ¹H NMR spectrum. Although the corresponding magnesium hydride intermediate implicated in the proposed mechanism was not observed by ¹H NMR spectroscopy, an intractable white solid was seen to be deposited from solution. This was proposed to be bulk magnesium hydride which, under such stoichiometric conditions was not intercepted and thus precipitated.

5.3 Catalytic TEMPO Induced Silane Dehydrogenation

The influence of substitution of the silane coupling partner was then assessed via a limited scope study (Table 5.1).

A number of notable trends can be identified from this study—a significant dependence on substrate bulk was notable with a primary silane (Table 5.1, entry 1)

Table 5.1 The results of the scope study into silane (0.1 mmol) coupling partners with TEMPO mediated by Mg{N(SiMe₃)₂}(THF)₂ (0.01 mmol) in 4:1 THF:C₆D₆ (0.5 mL)

	Silane	Silane:TEMPO	Product	Time (d)	Temp. (°C)	Conversion (%)
1	PhSiH ₃	1:1	PhSi(H) ₂ OTEMP	1	60	99
2		1:2	PhSi(H)OTEMP ₂	6	80	96
3	Ph ₂ SiH ₂	1:1	Ph ₂ Si(H)OTEMP	3	60	97
4		1:2	Ph ₂ Si(H)OTEMP	4	80	99
5	Ph(Me)SiH ₂	1:1	Ph(Me)Si(H)OTEMP	1	80	77
6	Et ₃ SiH	1:1	N/A	3	80	0
7	Ph ₃ SiH	1:1	N/A	3	80	0

reacting far faster than secondary silanes (Table 5.1, entries 2, 3 and 5). Tertiary silanes were found to be too bulky to couple even at elevated temperatures and extended reaction times (Table 5.1, entries 4, 6 and 7). These data are consistent with limitations previously observed for the magnesium-mediated coupling of amines with silanes. Finally, subsequent further TEMPO substitution upon the silane substrate was accessible, but only once and for the smallest of the silane coupling partners, PhSiH₃.

To give further mechanistic insight into this reaction an initial, limited, kinetic study was undertaken focussing on ¹H NMR analysis of the reaction between PhSiH₃ and TEMPO mediated by **IIIa**. After an initial induction period, consistent with the formation of an intermediate magnesium TEMPOxide, structurally related to **17**, the reaction was judged to be second-order overall as shown in Fig. 5.5. The corresponding product of this initiation was attributed to HN(SiMe₃)₂ the formation of which was tentatively ascribed to the coupling of a hexamethyldisilazyl and hydrogen radical species. Such an activation mechanism is unsurprising given the recalcitrance for **IIa** to induce hexamethyldisilazane-silane coupling, as shown in Chap. 3.

A *pseudo*-first order study with a tenfold excess of phenylsilane, however, indicated a first-order dependence on [TEMPO] as shown in Fig. 5.6 and a rate determining process predicated upon the presence of one equivalent of phenylsilane and one equivalent of TEMPO at the catalytic reaction centre. The latter deduction is suggestive of a rate determining step in which one molecule of silane is transformed to the silyl TEMPOxide and one molecule of TEMPO facilitates the assembly of the requisite polarised transition states in a manner broadly reminiscent of frustrated Lewis pair behaviour and the proton-assisted pathways integral to successful turnover of Group 2-centred olefin hydroamination catalysis. Further studies to more fully elucidate the nature of the rate determining process are ongoing.

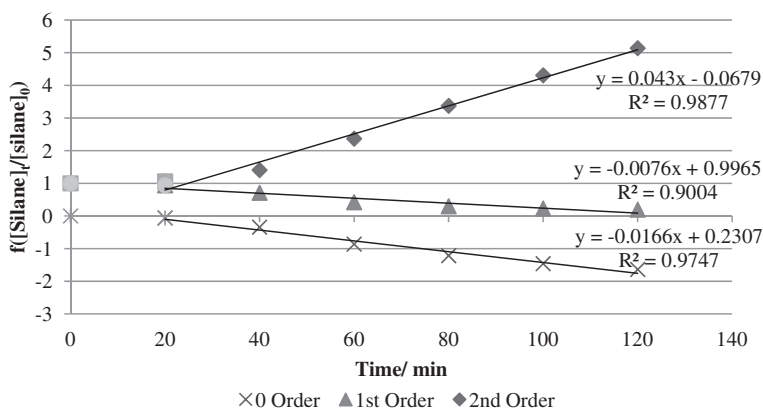


Fig. 5.5 The graph of $f([silane]_t/[silane]_0)$ against time for an equimolar reaction between silane and TEMPO indicative of the overall reaction order

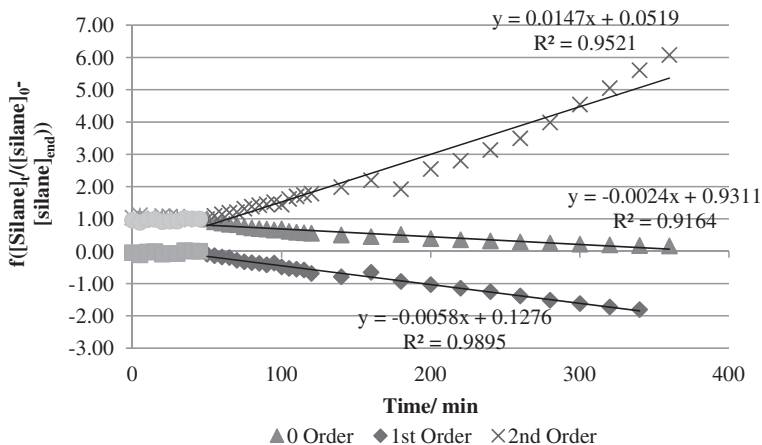


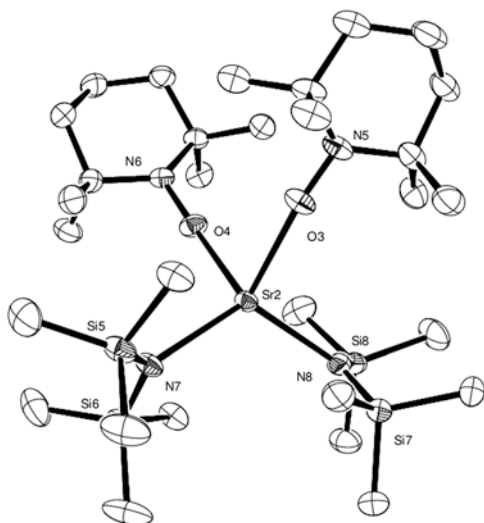
Fig. 5.6 The *pseudo*-first order graph of $f([\text{silane}]_0/[\text{silane}]_{\text{used}}) - [\text{silane}]_{\text{used}}$ against time for a 10:1 ratio of reaction between silane and TEMPO indicative of the reaction order in TEMPO

5.4 Reactivity of TEMPO with Calcium and Strontium Amides

With this investigation into the reactivity of magnesium undertaken attention was turned to the heavier congeners, calcium and strontium. Initial stoichiometric investigations into the reaction of a 2:1 ratio of TEMPO with **IIb** and **IIc** were undertaken on an NMR scale in C_6D_6 . In contrast to the rapid decolourisation and resultant spectrum observed for **IIIa**, these solutions retained the characteristic red colour of the TEMPO radical and NMR spectra which were uninterpretable and heavily broadened as a result of the radical character of TEMPO, suggesting no SET process has occurred. Notably, however, the reaction of **IIc** with TEMPO under these conditions was observed to precipitate a microcrystalline material. Although crystals suitable for a single crystal X-ray diffractometry experiment could not be grown directly from the NMR sample, a repeat on a preparative scale yielded crystals suitable for such an experiment, the results of which are summarised in Fig. 5.7.

The product of this reaction is a simple adduct of the TEMPO radical and the starting material, **IIc**, wherein two neutral TEMPO ligands, acting as 2 electron donors, complete the coordination sphere of the strontium yielding a distorted tetrahedral arrangement. There is extensive precedent in Groups 1–3 and 13 complexes for TEMPO to act as a 2 electron donor while retaining its radical character as evidenced by the trigonal arrangement around the TEMPO nitrogen atom and the N–O bond length, reflective of the partial double bond between the nitrogen and oxygen atoms [14, 15]. Notably, the N5–O3 bond length, C31–N5–C3 bond angle and Sr2–O3 bond lengths strongly mirror the corresponding bonds in the $[\text{Ln}(\text{hfac})_3(\text{TEMPO})_2]$ complex described by Ishida and co-workers which was

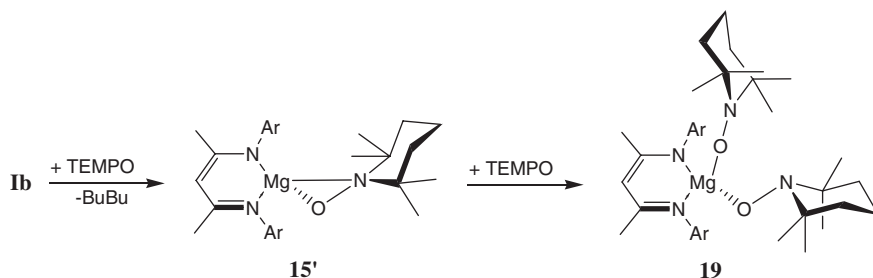
Fig. 5.7 ORTEP representation of **18** (30 % probability ellipsoids). Hydrogen atoms omitted for clarity. Selected bond lengths (Å) and angles (°): Sr2-N7 2.493(3), Sr2-O3 2.478(3), O3-N5 1.293(4), Sr2-O3-N5 162.6(3), C31-N5-C37 125.0(4). Symmetry transformations used to generate equivalent atoms: $-x, -y + 1, -z$



found to have persistent, TEMPO-centred radical character and no super-exchange between TEMPO ligands via the metal [15]. Unfortunately, attempts to yield tractable material under these conditions with **IIb** and **If** yielded only red oils which were not readily amenable to ^1H NMR spectroscopic analysis. Given the recalcitrance of the heavier congeners of **IIa** to undergo SET steps under stoichiometric conditions, no further investigation into their catalytic ability was undertaken.

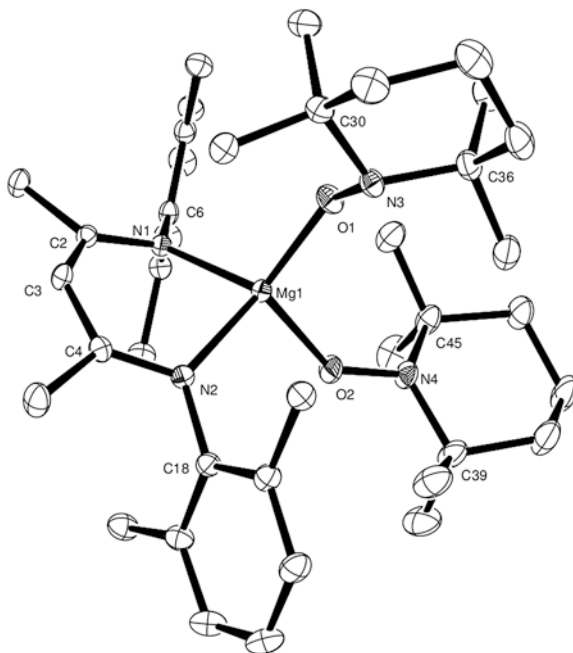
In order to elucidate the mechanism of the SET operant upon **IIb**, a number of subsequent studies were undertaken. It was noted that when TEMPO was added to **IIb**, the initial red colour associated with the TEMPO radical was instantaneously replaced by a deep black colour. Within a minute, this colour was observed to discharge to yield a colourless solution. In attempt to identify the source of this colour, the addition of a second equivalent of TEMPO was added **15**, synthesized in situ via the reaction of **IIb** and TEMPO. The resultant solution maintained the intense black colour previously only noted transiently and cooling this solution to $-34\text{ }^\circ\text{C}$ yielded material suitable for crystallographic analysis, as summarised in Scheme 5.3 and Fig. 5.8.

This species is superficially similar to **15**, albeit with a TEMPO radical acting as a neutral 2-electron donor in place of the THF. The TEMPOxide and TEMPO ligands are crystallographically distinct. The TEMPOxide ligand can be identified by its pyramidalised nitrogen, N3 which sits 0.455 \AA out of the plane made by C30–C36–O1, furthermore the N–O bond length of $1.4394(16)$, these data are remarkably similar to those described for the TEMPOxide ligand of **14** (N3 to C34–O2–C40 plane 0.437 \AA , O2–N3 $1.4423(1)\text{ \AA}$). The neutral TEMPO donor, in contrast shows data far closer to the simple adduct **18** with a shortened O2–N4 bond length of $1.2952(17)\text{ \AA}$ and a N4 to C39–C45–O2 distance of just 0.144 \AA (**18**: N6 to C40–C46–O4 plane 0.142 \AA O3–N5, $1.293(4)\text{ \AA}$). Finally, a contrast between the coordination of these distinct ligands can be drawn from their variation in



Scheme 5.3 The reactivity between TEMPO and **15'** and TEMPO to yield **19**

Fig. 5.8 ORTEP representation of **19** (30 % probability ellipsoids). *Isopropyl methyl groups and hydrogen atoms omitted for clarity.* Selected bond lengths (Å) and angles (°) for **18**: Mg1-N1 2.0882(12), Mg1-O1 1.8873(11), Mg1-O2 2.0297(12), O1-N3 1.4394(16), O2-N4 1.2952(17), Mg1-O1-N3 131.76(9), Mg1-O2-N4 137.53(10), N1-Mg1-N2 93.60(5), C30-N3-C46 116.75(12) C39-N4-C45 124.17(13)



Mg1–O bond length, in the TEMPOxide this is close to that of **15** (1.8873(11) vs. 1.8887(13) Å) whilst the TEMPO neutral donor is more distant at 2.0297(12) Å.

In spite of this analysis suggesting a simple complex of a β -diketiminato magnesium bound to a TEMPOxide with TEMPO acting as a simple adduct and the radical nature of this species localised thereon, this fails to account for a number of characteristics of **19**. Notably, **19** was crystallised as black crystals from a black solution, this colour is highly distinct from both **18** and the parent TEMPO suggesting perturbation of the electronic structure of the TEMPO radical. Furthermore, the puckering of the β -diketiminate ring, readily analysed by comparison of the N1-N2-C2-C4 plane compared to the C2-C3-C4 plane is distinct on **19** compared to **15** (14.08

vs. 8.49°). Although this could be a simple consequence of the steric constraints imposed by the TEMPO ligand in contrast to the smaller THF, however one alternative explanation could be partial delocalization of the radical from the TEMPO ligand to the β -diketiminato backbone. Such non-innocence has some precedent in magnesium chemistry [20] and thus further analysis of the electronic structure of **19** must be undertaken. Furthermore, **19** represents a metal-bound mixed valence oxygen compound, an intriguing class of compounds worthy of further study.

In summary, this chapter has described the first process involving a SET step which is catalytic in an s-block metal. This oxidative coupling yields dihydrogen and a series of novel TEMPO silylethers mediated by a magnesium(II) centre. Catalytic turnover most likely proceeds via a catalytically active magnesium TEMPOxide which undergoes Si-H/Mg-O σ -bond metathesis yielding a magnesium hydride species and the aforementioned silylether. The action of TEMPO upon this magnesium hydride can be considered a SET step and, to the best of our knowledge, constitutes the first example of the action of TEMPO on a Group 2 hydride. In contrast, the heavier alkaline earths appear to be far more reluctant to engage in SET steps, and work to elucidate the reasons behind this is ongoing. Furthermore, the chameleonic nature of the TEMPO ligand has been explored with its ability to act as both a 2-electron neutral donor in its radical form and as an anion explored. The combination of these forms on a single molecule, as in **18** raises intriguing possibilities for bonding and possible reactivity in these novel structural motifs.

5.5 Experimental Details

[CH{C(Me)N(Dipp)}₂Mg{ON{C(CH₃)₂CH₂}₂CH₂}{THF}], **15**

To a stirring toluene solution (4 mL) of **Ib** (100 mg, 0.2 mmol) was added TEMPO (31 mg, 0.2 mmol). The resultant red solution rapidly turned black before decolourising to yield a precipitate, drops of THF were added to yield redissolution, thus a colourless solution which was filtered. The filtrate was concentrated to incipient crystallisation and cooled to -35 °C yielding colourless blocks (76 %) suitable for single crystal X-ray diffractometry.

¹H NMR (300 MHz, d₈-Tol) δ ppm 1.02 (d, 12H, O-NC(Me)₂), 1.10–1.35 (m, 30H, H₃CCHCH₃, ON(C(Me)2CH₂)CH₃), 1.46 (s, 6H, H₃C), 3.76 (m, 4H, H₃CCHCH₃), 4.55 (s, 1H, CH₃CCHCH₃), 6.92 (s, 6H, ArH); ¹³C NMR (75 MHz, C₆D₆) δ ppm ¹³C NMR (75 MHz, benzene-*d*₆) δ ppm 21.1, 23.8, 24.1, 24.8, 25.1, 25.7, 29.0 41.1, 70. 6, 94.7, 123.9, 125.6, 143.1, 147.3, 169.1.

Anal. calc'd for C₄₂H₆₇MgN₃O₂: C, 75.26; H, 10.08; N, 6.27 %. Found: C, 76.16; H, 9.88; N, 6.90 %.

[CH{C(Me)N(Dipp)}₂Mg{ON{C(CH₃)₂CH₂}₂CH₂}], **15'**

To a stirring toluene solution (15 mL) of **Ib** (100 mg, 0.2 mmol) was added TEMPO (31 mg, 0.2 mmol). The resultant red solution rapidly turned black before decolourising to yield a colourless solution which was filtered. The filtrate was concentrated to incipient crystallisation and cooled to -35 °C yielding colourless

blocks (25 %) suitable for single crystal X-ray diffractometry. Full refinement of this data, however, was hindered due to *pseudo*-merohedral twinning of the crystal.

^1H NMR (300 MHz, d_8 -Tol) δ ppm 1.06–1.51 (m, 18 H, $\text{ON}\{\text{C}(\text{CH}_3)_2\text{CH}_2\}_2\text{CH}_2$) 1.17 (d, $J = 6.78$ Hz, 12 H, H_3CCHCH_3) 1.37 (d, $J = 6.97$ Hz, 12 H, H_3CCHCH_3) 1.68 (s, 6 H, H_3C) 3.19 (spt, $J = 6.70$ Hz, 4 H, H_3CCHCH_3) 4.89 (s, 1 H, $\text{CH}_3\text{CCHCCH}_3$) 6.92–7.19 (m, 6 H, ArH); ^{13}C NMR (d_8 -Tol, 75 MHz): δ ppm 24.3, 24.5, 24.9, 95.3, 124.0, 125.7, 142.4, 145.9, 170.2.

Despite repeated attempts, no suitable elemental analysis data for **15'** could be obtained.

$[(\text{THF})\text{Mg}(\text{OTEMP})(\text{Bu})_2]$ (16) and $[(\text{THF})\text{Mg}(\text{OTEMP})_2]_2$ (17)

To a stirring heptanes solution of 0.5 mol dm^{-3} di-butyilmagnesium in heptanes (1 mL, 0.5 mmol) was added TEMPO (156 mg, 1 mmol). The resultant red solution rapidly decolourised and precipitated polycrystalline solid. THF was added to yield a solution which was filtered, the filtrate was concentrated to incipient crystallisation and cooled to -35 °C yielding colourless blocks (67 %) suitable for single crystal X-ray diffractometry. Subsequent recrystallization of the solution that yielded **16** yielded only **17** of analytical purity precluding the full characterisation of **16**.

$[(\text{THF})\text{Mg}(\text{OTEMP})_2]_2$, 17

^1H NMR (300 MHz, C_6D_6) δ ppm 1.22 (br. s., 8 H) 1.31–1.54 (m, 20 H) 1.54–1.68 (m, 8 H) 1.68–1.84 (m, 4 H) 3.54–3.73 (m, 4 H); ^{13}C NMR (75 MHz, d_8 -Tol) δ ppm 19.6, 25.6 ($\text{O}(\text{CH}_2\text{CH}_2)_2$), 33.1, 35.6, 38.7, 40.9, 68.4 ($\text{O}(\text{CH}_2\text{CH}_2)_2$).

Despite repeated attempts, no suitable elemental analysis data for **17** could be obtained.

$\text{PhSi}(\text{H})_2\text{OTEMP}$

^1H NMR (300 MHz, THF) δ ppm 1.13 (br. s., 12 H, $\text{C}(\text{CH}_3)_2$) 1.49 (br. m., 6 H, CH_2) 5.09 (s, 2 H, SiH) 7.28–7.41 (m, 3 H, CH_{Ar}) 7.58–7.65 (m, 2 H, CH_{Ar}); ^{13}C NMR (75 MHz, C_6D_6) δ ppm 17.7, 32.3, 40.4, 61.3, 128.8, 130.9, 135.2, 136.5.

$\text{PhSi}(\text{H})\text{OTEMP}_2$

^1H NMR (300 MHz, C_6D_6) δ ppm 0.69–1.38 (br. m., 24 H, $\text{C}(\text{CH}_3)_2$) 1.32 (br. m., 12 H, CH_2) 5.30 (s, 1 H, SiH) 7.19 (br. s., 3 H, CH_{Ar}) 7.69 (br. s., 2 H, CH_{Ar}); ^{13}C NMR (75 MHz, C_6D_6) δ ppm 17.0, 32.3, 40.5, 60.9, 128.0, 130.4, 135.6, 135.9.

$\text{Ph}_2\text{Si}(\text{H})\text{OTEMP}$

^1H NMR (300 MHz, THF) δ ppm 0.91–1.16 (m, 12 H, $\text{C}(\text{CH}_3)_2$) 1.43 (br. s., 6 H, CH_2) 5.53 (s, 1 H, SiH) 7.21–7.41 (m, 6 H, CH_{Ar}) 7.59 (m, 4 H, CH_{Ar}); ^{13}C NMR (75 MHz, THF) δ ppm 17.9, 26.4, 40.8, 61.2, 128.6, 130.7, 135.8, 136.6.

$\text{PhSi}(\text{Me})(\text{H})\text{OTEMP}$

^1H NMR (300 MHz, C_6D_6) δ ppm 0.36 (d, $J = 3.01$ Hz, 3 H, SiCH_3) 1.00 (s, 12 H, $\text{C}(\text{CH}_3)_2$) 1.33 (br. s., 6 H, CH_2) 5.08 (q, $J = 3.01$ Hz, 1 H, SiH) 7.16–7.20 (m, 3 H, CH_{Ar}) 7.50 (m, 2 H, CH_{Ar}); ^{13}C NMR (75 MHz, C_6D_6) δ ppm 4.0, 19.1, 33.5, 41.9, 62.1, 129.8, 131.7, 135.9, 136.8.

[{(Me₃Si)₂N)₂Sr{ON{C(CH₃)₂CH₂}₂CH₂}₂], 18

To toluene solution (3 mL) of **Ic** (82 mg, 0.2 mmol) was added TEMPO (62.4 mg, 0.4 mmol). The resultant red solution was filtered. The filtrate was concentrated to incipient crystallisation, cooled to $-35\text{ }^{\circ}\text{C}$ yielding orange blocks (73 %) for X-ray diffractometry.

Owing to the paramagnetic nature of this compound, suitable NMR data was inaccessible. Despite repeated attempts, no suitable elemental analysis data for **18** could be obtained.

[CH{C(Me)N(Dipp)}₂]Mg{ON{C(CH₃)₂CH₂}₂CH₂}₂, 19

To toluene solution (3 mL) of **Ib** (300 mg, 0.6 mmol) was added portionwise TEMPO (18.7 mg, 1.2 mmol). The resultant red solution rapidly turned black before decolourising during the course of the reaction until >1 equivalent of TEMPO was added, whereupon the black colour persisted. After complete addition, this yielded a black solution which was filtered. The filtrate was concentrated to incipient crystallisation and cooled to $-35\text{ }^{\circ}\text{C}$ yielding black blocks (54 %) suitable for single crystal X-ray diffractometry.

Owing to the paramagnetic nature of this compound, suitable NMR data was inaccessible. Despite repeated attempts, no suitable elemental analysis data for **19** could be obtained.

	15	16	17	18	19
Empirical formula	C ₄₂ H ₆₇ MgN ₃ O ₂	C ₃₄ H ₇₀ Mg ₂ N ₂ O ₄	C ₂₅ H ₄₇ MgN ₂ O ₃	C _{98.10} H _{224.10} N ₁₂ O ₆ Si ₁₂ Sr ₃	C ₅₀ H ₈₄ MgN ₄ O ₂
Formula weight (g mol ⁻¹)	670.30	619.54	447.96	2268.13	797.52
Crystal system	Orthorhombic	Monoclinic	Monoclinic	Monoclinic	Triclinic
Space group	P2 ₁ 2 ₁ 2 ₁	P2 ₁ /n	C ₂ /c	P2 ₁ /a	P ₋₁
<i>a</i> (Å)	12.0740(2)	8.6460(1)	28.5730(4)	23.0180(1)	11.4460(1)
<i>b</i> (Å)	17.2770(2)	19.6870(4)	9.61200(10)	19.6290(1)	11.6220(1)
<i>c</i> (Å)	19.0950(3)	21.9880(5)	21.3920(3)	30.7790(2)	20.1630(3)
α (°)	90	90	90	90	94.442(1)
β (°)	90	90.633(1)	117.690(1)	100.192(1)	94.775(1)
γ (°)	90	90	90	90	115.786(1)
<i>V</i> (Å ³)	3983.26(10)	3742.43(12)	5202.32(12)	13687.09(13)	2387.34(5)
<i>Z</i>	4	4	8	4	2
ρ (g cm ⁻³)	1.118	1.100	1.144	1.101	1.109
μ (mm ⁻¹)	0.082	0.100	0.095	1.316	0.078
θ range (°)	5.01 to 27.50	3.63 to 27.47	3.67 to 27.48	3.52 to 27.46	3.53 to 27.50
Measured/independent reflections/ <i>R</i> _{int}	54,893/9060/ 0.0713	53,641/ 8553/ 0.0919	5946/ 5946/0.0000	177754/ 31145/ 0.0902	37,987 / 7854/ 0.0423

Data/restraints / parameters	9060/0 /447	8553/12/407	5946/0/262	31,145/36/1418	10,813 / 0/505
Goodness-of-fit on F^2	1.032	1.030	1.046	1.019	1.044
R_1 , wR_2 [$I > 2\sigma(I)$]	0.0413, 0.0983	0.0582, 0.1133	0.0500, 0.1410	0.0670, 0.1355	0.0529, 0.1382
R_1 , wR_2 (all data)	0.0534, 0.1065	0.1156, 0.1347	0.0630, 0.1486	0.1414, 0.1661	0.0781, 0.1517

Notes on crystallographic refinement

1. C31 and C32 disordered over 2 sites in a 75:25 ratio. Hydrogen atoms attached to C33 are included on the basis of the major component of C32.
2. Asymmetric unit comprises $\frac{1}{2}$ of a dimer molecule and a region of disordered electron density (proximate to a crystallographic inversion centre) that has been attributed to $\frac{1}{2}$ of a benzene of recrystallization. Such was the disorder that it defeated the crystallographers to model it and—hence—the SQUEEZE algorithm was (reluctantly) deployed.
3. Asymmetric unit consists of 3 molecules of the strontium complex, $\frac{1}{2}$ of a molecule of benzene located proximate to a crystallographic inversion centre and a full molecule of benzene at 85 % occupancy. The carbon atoms in the ligands based on N1 and N2 were disordered in a 60:40 ratio, and all fractional occupancy atoms were refined anisotropically with constraints. There was some evidence of a similar disorder in relation to the ligands based on N9 and N10. However, preliminary attempts to model this indicated that the minor component occupancies were relatively small. Balancing this information against the number of restraints necessary to achieve a satisfactory model convergence in region of the map tended towards over parameterisation—and hence the disorder model was abandoned. Distance and ADP restraints were applied within the fractional occupancy solvent moiety.

References

1. O.L. Lebedev, S.N. Kazarnovskii, *Tr. Khim. Khim. Tekhnol.* **2**, 649 (1959); *Chem. Abstr.* **56**, 15479f (1962)
2. E.E. Malmström, C.J. Hawker, *Macromol. Chem. Phys.* **199**, 923 (1998)
3. J.M. Hoover, B.L. Ryland and, S.S. Stahl, *J. Am. Chem. Soc.* **135**, 2357 (2013); T. Vogler, A. Studer, *Synthesis* 1979 (2008)
4. Y. Yonekuta, K. Susuki, K. Oyaizu, K. Honda, *J. Am. Chem. Soc.* **129**, 14128 (2007)
5. S.S. Eaton, G.R. Eaton, *Coord. Chem. Rev.* **26**, 207 (1978); M.H. Dickman, R.J. Doedens, *Inorg. Chem.* **21**, 682 (1982); J. Laugier, J.M. Latour, A. Caneschi, P. Rey, *Inorg. Chem.* **30**, 4474 (1991); M.K. Mahanthappa, K.-W. Huang, A.P. Cole, R.M. Waymouth, *Chem. Commun.* 502 (2002); D.J. Mindiola, R. Waterman, D.M. Jenkins, G.L. Hillhouse, *Inorg. Chim. Acta.* **345**, 299 (2003)
6. W.J. Evans, J.M. Perotti, R.J. Doedens, J.W. Ziller, *Chem. Commun.* 2326 (2001)
7. G.C. Forbes, A.R. Kennedy, R.E. Mulvey, P.J.A. Rodger, *Chem. Commun.* 1400 (2001)
8. L. Balloch, A.M. Drummond, P. García-Álvarez, D.V. Graham, A.R. Kennedy, J. Klett, R.E. Mulvey, C.T. O'Hara, P.J.A. Rodger, I.D. Rushworth, *Inorg. Chem.* **48**, 6934 (2009)
9. D.R. Armstrong, L. Balloch, J.J. Crawford, B.J. Fleming, L.M. Hogg, A.R. Kennedy, J. Klett, R.E. Mulvey, C.T. O'Hara, S.A. Orr, S.D. Robertson, *Chem. Commun.* **48**, 1541 (2012)
10. I.L. Fedushkin, A.G. Morozov, V.A. Chudakova, G.K. Fukin, V.K. Cherkasov, *Eur. J. Inorg. Chem.* **2009**, 4995 (2009)

11. R.G. Lopez, C. Boisson, F. D'Agosto, R. Spitz, F. Boisson, D. Gigmes, D. Bertin, J. Polym. Sci. A-Polym. Chem. **45**, 2705 (2007); M.S. Maji, T. Pfeifer, A. Studer, Angew. Chem.-Int. Ed. **47**, 9547 (2008); M.S. Maji, A. Studer, Synthesis-Stuttgart 2467 (2009); M.S. Maji, S. Murarka, A. Studer, Organic Lett. **12**, 3878 (2010); M.S. Maji, T. Pfeifer, A. Studer, Chem. Eur. J. **16**, 5872 (2010); S. Murarka, A. Studer, Adv. Synth. Cat. **353**, 2708 (2011); Angew. Chem.-Int. Ed. **51**, 12362 (2012); S. Murarka, S. Wertz, A. Studer, Chimia **66**, 413 (2012); O.G. Mancheno, T. Stopka, Synthesis-Stuttgart **45**, 1602 (2013)
12. C. Jones, R.P. Rose, New J. Chem. **31**, 1484 (2007)
13. P. Jochmann, D.W. Stephan, Chem. Commun. 8295 (2014)
14. J.J. Scepaniak, A.M. Wright, R.A. Lewis, G. Wu, T. W. Hayton, J. Am. Chem. Soc. **134**, 19350 (2012); A.M. Wright, J.S. Page, J.J. Scepaniak, G. Wu, T. W. Hayton, Eur. J. Inorg. Chem. **2013**, 3817 (2013)
15. R. Murakami, T. Nakamura, T. Ishida, Dalton Trans. **43**, 5893 (2014)
16. A.G.M. Barrett, M.R. Crimmin, M.S. Hill, P. A. Procopiou, Proc. Roy. Soc. A. **466**, 927 (2010); S. Harder, Chem. Rev. **110**, 3852 (2010)
17. F. Buch, H. Brettar, S. Harder, Angew. Chem.-Int. Ed. **45**, 2741 (2006); F. Buch, S. Harder, Organometallics **26**, 5132 (2007); F. Buch, S. Harder, Z. Naturforsch, B: Chem. Sci. **63**, 169 (2008); M. Arrowsmith, M.S. Hill, T. Hadlington, G. Kociok-Köhn, C. Weetman, Organometallics **30**, 5556 (2011); M. Arrowsmith, T.J. Hadlington, M.S. Hill, G. Kociok-Köhn, Chem. Commun. **48**, 4567 (2012); J.F. Dunne, S.R. Neal, J. Engelkemier, A. Ellern, A.D. Sadow, J. Am. Chem. Soc. **133**, 16782 (2011); M.S. Hill, D.J. Liptrot, D.J. MacDougall, M.F. Mahon, T.P. Robinson, Chem. Sci. **4**, 4212 (2013); D.J. Liptrot, M.S. Hill, M.F. Mahon, D.J. MacDougall, Chem. Eur. J. **16**, 8508 (2010)
18. A.P. Dove, V.C. Gibson, P. Hornmiron, E.L. Marshall, J.A. Segal, A.J.P. White, D.J. Williams, Dalton Trans. 3088 (2003)
19. S.J. Bonyhady, C. Jones, S. Nembenna, A. Stasch, A.J. Edwards, G.J. McIntyre, Chem.-Eur. J. **16**, 938 (2010)
20. D.M. Murphy, L.E. McDyre, E. Carter, A. Stasch, C. Jones, Mag. Res. Chem. **49**, 159 (2011)

Chapter 6

Summary

In summary, this thesis describes a variety of investigations into the utility of Group 2-mediated σ -bond metathesis, both for synthetic stoichiometric reactions and, further, for catalytic dehydrocouplings.

As a result of these investigations, a number of key conclusions can be drawn. Chapter 2, via the synthesis of mixed Group 1-Group 2 amidoalkyls **1-3**, and their resultant reactivity with phenylsilane indicates the utility of Group 1 metals in higher hydride clusters such as **4** and **5**. This utility is a result of the coordinative flexibility of the Group 1 cations which allows them to occupy a range of positions in clusters such as **5**, a dodecaheterobimetallic decahydrido octaamide.

The catalytic utility of Group 2 reagents in dehydrocouplings was investigated in Chaps. 3 and 4. These investigations, trivially, indicated the utility of Group 2 precatalysts such as **IIa-c** and **IIb** in dehydrocoupling of amines with silanes, stannanes and boranes. The former coupling partner yielded fascinating congeneric variation when considering **IIa-c** and this study draws attention to the importance of ancillary ligation, solution molecularity and congener identity in dehydrocoupling. Stannane-amine dehydrocoupling, as investigated in Chap. 3 indicated both the potential for cascade reactivity reliant on dehydrocouplings and, more intriguingly, the potential for further Group 2 mediated mechanisms in dehydrocoupling. Finally, the consideration of borane-nitrogen dehydrocoupling mediated by **IIb** suggested the importance of substrate Lewis acidity, alongside the aforementioned ligation and molecularity effects.

Finally, the activity of the stable radical TEMPO, as exemplified in Chap. 5, gave intriguing hints as to the inclusion of SET steps in Group 2 mediated catalytic manifolds. Furthermore, these investigations indicated the synthetic potential of TEMPO to yield novel and structurally unique Group 2 species.

Chapter 7

Future Work

Although extensive studies are herein described, a number of aspects of future work are necessary in order to gain greater insight into both Group 2 mediated dehydrocoupling, the synthetic utility of σ -bond metathesis in the synthesis of novel s-block compounds and the use of single electron transfer steps in Group 2 mediated reactivity.

7.1 Chapter 2

Further investigations into the synthetic utility of the reactivity outlined in Chap. 2 is essential. The ability of alkali metal cations to act as a variety of structural elements in higher hydride clusters, a consequence of their coordination flexibility is key, and the potential indicated by the synthesis of **4** must be investigated. Furthermore, the reactivity of the described compounds with other hydride sources is of interest, particularly with a focus upon **1** with the aim of generating higher hydride species without the issues of redistribution and precipitation herein described.

7.2 Chapter 3

Whilst the data described for the silicon-nitrogen dehydrocoupling gives useful insight into the effects of congeneric variation on this reaction, computational investigations could provide key insight into transition state structure which could be correlated with the observed kinetic data. Furthermore, a number of other observations warrant further investigation. The formation of the abnormal carbene in **11** is a step of significant interest that requires mechanistic insight. Furthermore, the unusual results in the tin-nitrogen dehydrocoupling which hint at the accessibility of α -elimination of low valent p-block species from Group 2 complexes is fascinating and requires authentication and interrogation.

7.3 Chapter 5

Whilst Chap. 5 successfully describes the inclusion of single electron transfer steps into Group 2 mediated catalysis, the results described are highly preliminary. The electronic structure of both the TEMPOxides **15-17** and the TEMPO adduct **19** requires interrogation by both EPR and magnetic methods. Furthermore, the application of single electron transfer steps to more productive element-element bond forming reactions is of key interest.

Appendix A

General Experimental Procedures

A.1 General Synthetic Notes

All manipulations were carried out under an inert atmosphere of argon utilising standard glovebox and Schlenk line techniques. J. Youngs tap NMR tubes sealed in a glovebox were utilised for NMR analysis. NMR spectroscopy was performed utilising a Bruker AV-300 spectrometer at 96.3 MHz (^{11}B), 75.5 MHz (^{13}C) or 111.9 MHz (^{119}Sn) or a Bruker AV-400 spectrometer and spectra were referenced to residual solvent peaks. ^{15}N NMR (40.6 MHz) was performed utilising an HMQC method via coupling to the HMDS protons and are reported un referenced. Spectra were recorded at 298 K unless stated otherwise and calibration of temperatures was performed utilising 80 % ethylene glycol in methanol for temperatures above 298 K, and 4 % MeOH in MeOD for temperatures below. Diffusion spectra were acquired on a Bruker AV400 operating at 400.13 MHz for ^1H . Spectra were obtained using a stimulated echo pulse sequence utilizing bipolar gradients, sine-shaped gradients and a longitudinal eddy current delay. Gradients were incremented in sixteen steps from 1.74 to 3.11 G cm^{-1} , with Δ and δ of 50 and 2.4 ms respectively. Spectra were processed using standard Bruker software. Elemental analysis was performed externally by London Metropolitan University Elemental Analysis Services, UK. Solvents were dried utilising an Innovative Solutions Pure Solv MD SPS (hexane, toluene) or utilising potassium/benzophenone (diethyl ether, THF) and stored over 4 Å molecular sieves and potassium. Hexadeuterobenzene and octadeuterotoluene were purchased from Goss Scientific Instruments Ltd. and dried over molten potassium then distilled under nitrogen. Metal iodides, di-*n*-butylmagnesium, amines, silanes, stannanes, boranes, and TEMPO were purchased from Sigma-Aldrich. Liquids were dried over CaH_2 then distilled while solids were subjected to vacuum overnight before use. Silylamines, distannanes and aminoboranes were identified by comparison to literature data unless otherwise denoted. Precatalysts were synthesized according to literature conditions (see Chap. 1, and references contained therein).

A.2 Crystallographic Analysis

Diffraction data for compounds **1-19** were collected on a Nonius Kappa CCD with a low temperature device at 150 K, utilising Mo-K α radiation monochromated with graphite ($\lambda = 0.71070 \text{ \AA}$). Processing utilised the Nonius software,¹ with structure solution and refinement using WINGX 1.6, SHELXS and SHELXL² and visualised utilising Ortep 3.³

A.3 Synthetic Procedures

NMR Scale investigations into the synthesis of silylamines, distannanes, aminoboranes (Tables 3.1, 2, 8; 3.7, 8; 4.1–3) and TEMPO-silyl ethers (Table 5.1) mediated by Ia, If IIa-c (Chapter 3), Ib (Chapter 4) and IIa (Chapter 5).

In a glovebox, to a vial containing precatalyst (loading as denoted on a 0.1 mmol scale) was added solvent (0.5 mL, as denoted) followed by reagents (proportions as denoted, limiting reagent on a 0.1 mmol scale). The resultant solution was transferred to a NMR tube equipped with a Youngs tap which was sealed and the tube removed from the glovebox. NMR analysis was performed at regular intervals and conversions were analysed by ratios of starting material to product, with products identified by comparison to literature values.

General method for kinetic investigation into the order in catalyst (Figures 3.9, 10, 13, 14, 17, 18; 4.5, 6, 8, 9, 11, 12)

In a glovebox, to a vial containing metal precatalyst (concentrations noted, **IIa-c** loading measured as monomer) was added C₆D₆ (Chaps. 3 and 4) or d₈-THF (Chap. 5) (0.5 mL) followed by reagents as noted (0.1 mmol). The resultant solution was transferred to a NMR tube equipped with a Youngs tap which was sealed, removed from the glovebox and frozen in liquid nitrogen. The tube was then thawed and immediately transferred to the spectrometer and subjected to NMR analysis at regular intervals. The data found herein was utilised to calculate turnover frequencies (Tables 3.5 and 4.4) with standard deviations derived from degree of variation over these 5 data points.

General method for kinetic investigation into the order in reagents (Figures 3.11, 12, 15, 16; 4.7, 10, 13; 5.6)

In a glovebox, to a vial containing metal precatalyst (loading as denoted, for **IIa-c** as monomers) was added C₆D₆ (0.5 mL) followed by reagents in a 10:1 ratio

¹ A. Altomare, M.C. Burla, M. Camalli, G.L. Cascarano, C. Giacovazzo, A. Guagliardi, A.G.G. Moliterni, G. Polidori and R. Spagna, *Journal of Applied Crystallography*, 1999, **32**, 115–119.

² Z. Otwinowski and W. Minor, *DENZO-SMN Manual*, University of Texas Southwestern Medical Centre, Dallas, USA, 1996; G.M. Sheldrick, *SHELXL97-2, Program for Crystal Structure Refinement*, Universität Göttingen, Göttingen, Germany, 1998.

³ C. Barnes, *Journal of Applied Crystallography*, 1997, **30**, 568.

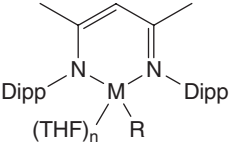
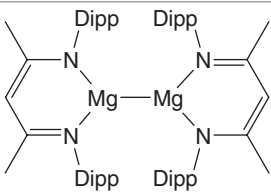
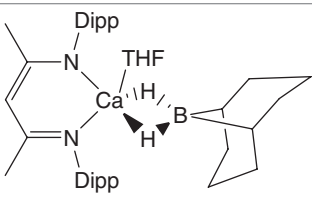
as noted (0.1 mmol of limiting reagent). The resultant solution was transferred to a NMR tube equipped with a Youngs tap which was sealed, removed from the glovebox and frozen in liquid nitrogen. The tube was then thawed and immediately transferred to the spectrometer and subjected to NMR analysis at regular intervals. Plots of $f(\text{starting material:product})$ (hereafter, x) against time were used to define order. Zero-order dependence was assessed by direct plotting of x against time, 1st order via a plot of $\ln(x)$ against time, 2nd order via a plot of x^{-1} against time and $\frac{1}{2}$ order via a plot of $x^{1/2}$ versus time.

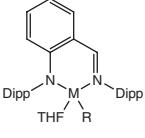
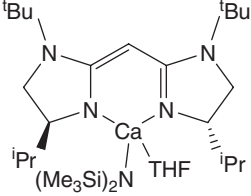
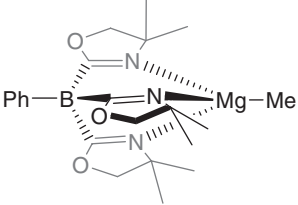
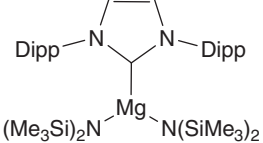
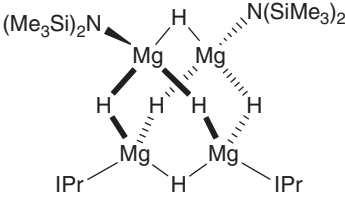
General method for Eyring and Arrhenius studies (Figures 3.21–25; 4.14–18)

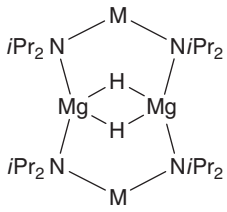
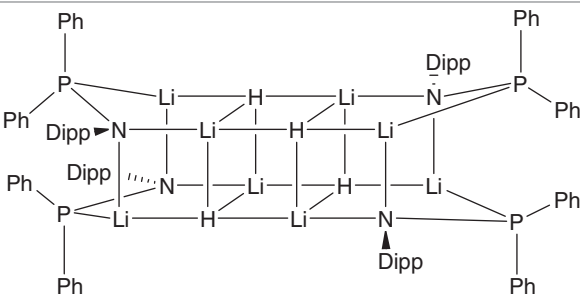
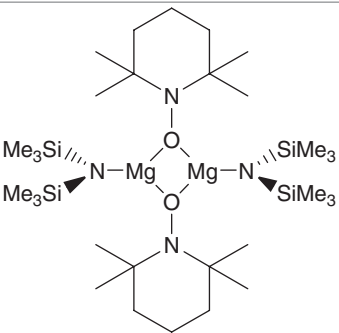
In a glovebox, to a vial containing metal precatalyst (concentrations noted, for **IIa-c** as monomers) was added C_6D_6 (0.5 mL) followed by silane or borane (0.1 mmol) then amine (0.1 mmol). The resultant solution was transferred to a NMR tube equipped with a Youngs tap which was sealed, removed from the glovebox and frozen in liquid nitrogen. The tube was then thawed and immediately transferred to the spectrometer which had been allowed equilibrate at the noted temperature for at least 20 min to and subjected to NMR analysis at regular intervals. This was then repeated at the range of temperatures noted and Arrhenius and Eyring analyses utilised to derive activation parameters (Tables 3.6 and 4.5)

Appendix B

Literature Compounds Described Herein

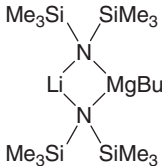
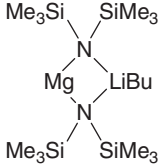
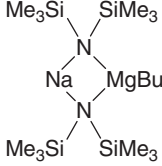
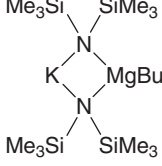
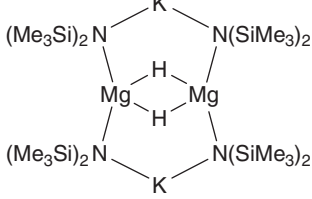
I	 <p style="text-align: center;"> a b c d e f g h i j M = Mg, Mg Mg Mg Ca, Ca, Sr, Mg, Mg, Ca R = Me, Bu, Bu, N(SiMe₃)₂ H H H n = 0, 0, 1, 0, 0, 1, 1, 0, 1, 1 </p>
	 <p style="text-align: center;">k</p>
	 <p style="text-align: center;">l</p>
II	<p style="text-align: center;">[M(N{SiMe₃})₂]₂</p> <p style="text-align: center;"> a b c d M = Mg, Ca, Sr, Ba </p>

III	$[M(N\{\text{SiMe}_3\}_2)_2(\text{THF})_2]$ a b c d M = Mg, Ca, Sr, Ba
IV	$[M(\text{CH}\{\text{SiMe}_3\}_2)_2(\text{THF})_2]$ a b c d M = Mg, Ca, Sr, Ba
V	 a b c M = Ca, Sr, Ba R = N(SiMe ₃) ₂ n = 1, 2, 2
VI	
VII	
VIII	
IX	

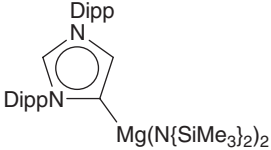
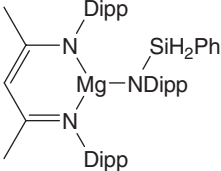
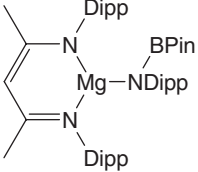
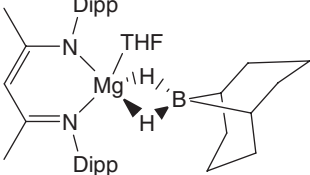
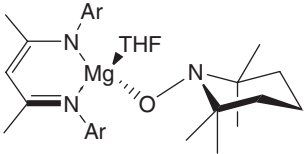
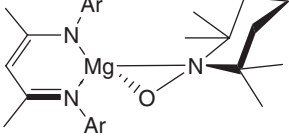
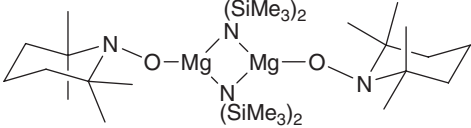
X	 <p style="text-align: center;">a b c</p> <p>M = Na(C₇H₈), Na, K(C₇H₈)</p>
XI	
XII	

Appendix C

Novel Compounds Described Herein

1	
1'	
2	
3	
4	

5	
6	
7	
8	
9	
10	

11	
12	
13	
14	
15	
15'	
16	
17	